Understanding the mechanisms that control the release of a soluble crystalline agrichemical extruded with biopolymers

Ian Christopher Levett

Masters and Bachelor of Chemical and Biological Engineering

0000-0002-5164-686X

A thesis submitted for the degree of Doctor of Philosophy at The University of Queensland in 2020

School of Chemical Engineering

Abstract

Nitrogen (N) is an essential element to sustain all life on Earth, yet it also wreaks havoc when in excess. The production of synthetic N fertilisers through the Haber-Bosch process began in the early 1900s and initiated the 'green revolution', seeing agricultural productivity soar. These productivity gains support roughly half of the current global population. Yet while heavy application of synthetic N fertilisers ensures crop success, it also leads to harmful environmental losses of 50-70% of the N applied. Such losses damage fresh and coastal aquatic ecosystems through eutrophication and biodiversity loss, reduce air quality, accelerate climate change and lead to numerous human health implications. The human race has doubled the cycling of N through the environment leading to a global challenge.

To reduce these environmental nutrient losses, enhanced efficiency fertilisers were developed, including slow- and controlled-release fertilisers and stabilised N fertilisers. These products aim to increase the proportion of N taken up by the crop relative to the amount added, meaning that less fertiliser is required. Slow- and controlled-release products specifically aim to deliver N at a rate to match the crop N uptake curve, while N stabilisers are chemical additives that inhibit urease and nitrification in the soil, reducing leaching of highly mobile nitrate-N and lowering denitrification to gaseous nitrogen oxides (NO_x) and nitrous oxide (N_2O) - a potent greenhouse gas. Dicyandiamide (DCD) is a commercial nitrification inhibitor that effectively reduces N losses and can improve crop productivity in temperate climates. However, in tropical soils, microbial metabolism of this molecule results in limited efficacy.

This project aimed to improve the efficacy of DCD for tropical agriculture through encapsulation and controlled-release of this soluble, crystalline agrichemical using biodegradable and environmentally friendly polymers. The principle is to protect the DCD from degradation and extend the duration of effective concentration in the soil. Controlled-release DCD pellets were produced through extrusion processing, as a simple, cost-effective, commercially relevant fabrication technique. The polymers tested include thermo-plastic wheat starch (TPS), the bacterial polyester poly(3-hydroxybutyrate-*co*-3-hydroxyvalerate) (PHBV) and synthetic polycaprolactone (PCL) as well as blends of PHBV with PCL. DCD was distributed in these polymers through extrusion melt compounding to produce ~3×3 mm cylindrical pellets. The release kinetics were studied and, importantly, the underlying mechanisms that control release were identified and modelled. Much of the mechanistic understanding was developed through advanced imaging of the materials before and after release, using scanning electron microscopy (SEM), mapping with Raman spectroscopy, and high-resolution X-ray micro-computed tomography (μ-CT). The release kinetics were modelled using

empirical and mechanistic models.

From the outcomes of these studies, this thesis builds an understanding of the key material design parameters, including:

(1) Polymer(s) selection. The physical and chemical properties of the polymer determined the time for release, ranging from 1 day (for TPS) to 6+ months (for PHBV), and the mechanisms controlling release. Release from TPS occurred by rapid diffusion through and swelling of the hydrophilic polymer matrix. By contrast, PHBV shows promise for long-term release profiles (6+ months), but diffusion through this polymer is so slow that release occurs via other mechanisms. Initially, the release was rapid via the dissolution of surface exposed DCD crystals, confirmed through SEM, resulting in ~20 wt.% release within the first 5 h. Between 5 h and 8 weeks, a further 25 wt.% of the DCD was mobilized as water accessed connected DCD crystals or entered via micro-cracks in the matrix, as determined through high-resolution μ-CT and Raman mapping. A large portion (~50%) of the agrichemical remained encapsulated until the PHBV matrix degraded in soil environments. To increase the rate of matrix diffusion, blending with a more hydrophilic polymer, PCL, were studied. However, the higher affinity between DCD and PCL counter-intuitively resulted in less interconnected DCD crystals, which lead to slower release with increasing PCL content in the blend.

(2) The DCD loading. This determined the degree of percolation within the matrix, with a threshold at between 200 and 400 g.kg^{-1} for DCD-PHBV. Below the percolation threshold, this parameter controls the thickness of the polymer between agrichemical crystals.

(3) DCD crystal size. Below the percolation threshold, the fractional release from the surface of the pellet was modulated through the grind size of the agrichemical.

(4) DCD pellet size. As identified through mathematical modelling, this parameter can control the fractional release rate and has important consequences on the distribution of pellets within the soil.

Understanding these key parameters and the mechanisms that control release allows cost-effective, environmentally friendly material design to increase the effectiveness of nitrogen stabilisers in tropical climates and reduce N pollution. Moreover, the knowledge gained here is relevant for the controlled-release of any soluble, crystalline agrichemical and could be applied for the design of controlled-release fertilisers, herbicides and pesticides.

Declaration by author

This thesis is composed of my original work, and contains no material previously published or written by another person except where due reference has been made in the text. I have clearly stated the contribution by others to jointly-authored works that I have included in my thesis.

I have clearly stated the contribution of others to my thesis as a whole, including statistical assistance, survey design, data analysis, significant technical procedures, professional editorial advice, financial support and any other original research work used or reported in my thesis. The content of my thesis is the result of work I have carried out since the commencement of my higher degree by research candidature and does not include a substantial part of work that has been submitted to qualify for the award of any other degree or diploma in any university or other tertiary institution. I have clearly stated which parts of my thesis, if any, have been submitted to qualify for another award.

I acknowledge that an electronic copy of my thesis must be lodged with the University Library and, subject to the policy and procedures of The University of Queensland, the thesis be made available for research and study in accordance with the Copyright Act 1968 unless a period of embargo has been approved by the Dean of the Graduate School.

I acknowledge that copyright of all material contained in my thesis resides with the copyright holder(s) of that material. Where appropriate I have obtained copyright permission from the copyright holder to reproduce material in this thesis and have sought permission from co-authors for any jointly authored works included in the thesis.

Publications included in this thesis

Levett, I., Pratt, S., Donose, B. C., Brackin, R., Pratt, C., Redding, M. & Laycock, B. 2019. Understanding the Mobilization of a Nitrification Inhibitor from Novel Slow Release Pellets, Fabricated through Extrusion Processing with PHBV Biopolymer. *Journal of Agricultural and Food Chemistry*, 67, 2449-2458.

Incorporated as **Chapter 5**

Contributor	Statement of contribution		
	Research design	Data acquisition	Data interpretation and writing/reviewing
Ian Levett	65%	80%	60%
Steven Pratt	10%		10%
Bogdan Donose	5%	10%	5%
Richard Brackin		10%	5%
Chris Pratt	5%		5%
Matthew Redding	5%		5%
Bronwyn Laycock	10%		10%

Levett, I.; Liao, M.; Pratt, C.; Redding, M.; Laycock, B.; Pratt, S., Designing for effective controlled release in agricultural products: new insights into the complex nature of the polymer–active agent relationship and implications for use. *Journal of the science of food and agriculture* 2020.

Incorporated as **Chapter 7**

Contributor	Statement of contribution		
	Research design	Data acquisition	Data interpretation and writing/reviewing
Ian Levett	80%	70%	70%
Minjie Liao	5%	30%	5%
Chris Pratt	2.5%		5%
Matt Redding	2.5%		5%
Bronwyn Laycock	5%		7.5%
Steven Pratt	5%		7.5%

Submitted manuscripts included in this thesis

Levett, I.; Donose, B. C.; Laycock, B.; Pratt, S., High-resolution µ-CT reveals crazing in a hydrophobic composite - a new mechanism for mobilization in controlled release applications. Submitted to *Biosystems Engineering* 2020.

Incorporated as **Chapter 6**

Contributor	Statement of contribution		
	Research design	Data acquisition	Data interpretation and writing/reviewing
Ian Levett	70%	50%	70%
Bogdan Donose	10%	50%	10%
Bronwyn Laycock	10%		10%
Steven Pratt	10%		10%

Other publications during candidature

Peer-reviewed papers

Dilkes-Hoffman, L. S., Pratt, S., Lant, P. A., **Levett, I.** & Laycock, B. 2018. *Polyhydroxyalkanoate coatings restrict moisture uptake and associated loss of barrier properties of thermoplastic starch films.* Journal of Applied Polymer Science, 135, 46379.

Pratt, C.; Kingston, K.; Laycock, B.; **Levett, I.**; Pratt, S. *Geo-Agriculture: Reviewing Opportunities through which the Geosphere Can Help Address Emerging Crop Production Challenges.* Agronomy 2020, 10, 971.

Redding, M. R.; Phillips, I.; Pratt, C.; Paungfoo-Lonhienne, C.; **Levett, I**.; Hill, J.; Mehta, C.; Bailey, T.; Brackin, R.; McAuley, J.; Pratt, S.; Laycock, B.; Mayer, D. G., *Can Nitrogen Source and Nitrification Inhibitors Affect In-Season Nitrogen Supply?* Communications in Soil Science and Plant Analysis 2020, 51 (16), 2189-2204.

Conference abstracts

Levett, I., Pratt, S. and Laycock, B. An engineering approach to fertiliser design for increased nutrient update efficiency, *International Workshop on Nutrient Stewardship & Next-generation fertilisers*, Heron Island, QLD Australia, Heron Island, QLD Australia, 2016.

Levett, I., Pratt, S. and Laycock, B. Engineering novel controlled release agrichemical formulations, *The University of Queensland EAIT Postgraduate Conference*, Brisbane, Australia, 2017

Levett, I., Pratt, S. and Laycock, B. Engineering novel controlled release agrichemical formulations, *The University of Queensland EAIT Postgraduate Conference*, Brisbane, Australia, 2017

Levett, I., Pratt, S., Donose, B. C., Brackin, R., Pratt, C., Redding, M. and Laycock, B., Fabrication and Characterisation of a Novel Slow Release Nitrification Inhibitor Formulation, *The University of Queensland EAIT Postgraduate Conference*, Brisbane, Australia, 2018

Levett, I., Pratt, S., Donose, B. C., Brackin, R., Pratt, C., Redding, M. and Laycock, B., Using PHA for the controlled release of crystalline agrichemicals, *BIOPOL*, Stockholm, Sweden, 2019

Levett, I., Donose, B. C., Pratt, C., Redding, M., Laycock, B. and Pratt, S., Slow-release NIs: material design, fabrication and testing, *More Profit from Nitrogen Forum*, Online, 2020

Contributions by others to the thesis

A/Prof. Bronwyn Laycock, A/Prof. Steven Pratt, Dr. Matt Redding and Dr. Chris Pratt formed the advisory team for this PhD project and contributed significantly to project management, experimental design, data interpretation, editing and proof reading of this thesis.

Dr. Bogdan Donose was instrumental for the physical characterisation of the materials developed through this project, including scanning and backscattered electron microscopy, Raman mapping, and micro-computer tomography. Dr. Clement Chan assisted with electron microscopy and micro-analysis data collection and analysis.

Dr. Paul Luckman assisted with extrusion processing of materials and Dr. Brenton Fletcher helped to design the releases experiments and ultra-violet and visible light spectroscopy. Dr. Richard Brackin developed an Ultra-pressure Liquid Chromatography method for the quantification of DCD is soil leachate.

Statement of parts of the thesis submitted to qualify for the award of another degree

No works submitted towards another degree have been included in this thesis.

Research involving human or animal subjects

No animal or human subjects were involved in this research.

Acknowledgments

It is unlikely I would have ever begun this degree without the tremendous examples laid first by my family. Dad completed his doctorate in nutrient cycling within various New Zealand forests. While my eldest brother, Peter, developed hydrogel scaffolds for cartilage regeneration and my other brother, Alan, discovered the role of microbes in ferruginous duricrusts formation during their respective PhDs. Thank you for being a constant source of inspiration, support and encouragement. To my mother and my sister, you are both so strong, intelligent and hardworking. Without your guidance, love and enthusiasm, this journey would have been much, much harder. Much of my motivation came from my amazing fiancée, Amelia. You kept me going when things got overwhelming, listened when experiments failed and celebrated with me as I went through the various milestones. Thank you for being the wonderful person you are and making my life so fulfilled.

Of course, my supervisors have been instrumental throughout this project. Known as the 'dream team' within translational polymer research group (TPRG), Bronwyn and Steven, you bring contrasting, yet highly complementary, approaches to research, leadership and project management. Thank you for the wisdom, patience and excitement that you both bring to your research and student supervision. I owe my every success over the last few years to you both. Your strength in building positive collaborations provided this opportunity for me. This collaboration with the Department of Agriculture and Fisheries has been a great success and I hope it leads to further knowledge and product development. Thank you Matt for your guidance, constructive and productive meetings and overall support throughout this project. To Chris, thank you for your inputs and feedback on my work. You intrinsically bring a positivity and encouragement to the team, along with an amazing understanding of soil science and nutrient stewardship. I hope this productive collaboration can continue to exploit the differing expertise between the members. To Bogdan, thank you for always having time for me. Your hard work substantially improved this thesis through your broad knowledge of characterisation techniques.

To all members of the TPRG, thank you all for the support, engaging conversations and positivity. In particular, I would like to thank Clement and Leela. You have had to endure all the highs and lows of my project alongside me. On a daily basis, you provided advice, encouragement and support, and I am forever grateful to have friends as kind, intelligent and conscientious as you both. Similarly, I would like to thank Rhys and Alan for the coffee break chats and Friday night drinks, bringing laughter and joy to my every day.

Financial support

Keywords

Controlled-release, biopolymers, polyhydroxyalkanoates, nitrification inhibitors, extrusion, modelling

Australian and New Zealand Standard Research Classifications (ANZSRC)

ANZSRC code: 080205, Numerical computation, 40%

ANZSRC code: 091205, Functional materials, 40%

ANZSRC code: 079902, Fertilisers and agrochemicals, 20%

Fields of Research (FoR) Classification

FoR code: 0102, Applied mathematics, 40%

FoR code: 0799, Other agricultural and veterinary sciences, 40%

FoR code: 0912, Materials engineering, 20%

Contents

List of figures

List of tables

List of abbreviations

Abbreviations

AMO	*Ammonium monooxygenase*
AOA	*Ammonium oxidising archaea*
AOB	*Ammonium oxidising bacteria*
BNF	*Biological nitrogen fixation*
CRF	*Controlled release fertiliser*
COTS	*Crown-of-thorns starfish*
DCD	*Dicyandiamide*
DIN	*Dissolved inorganic nitrogen*
DMPP	*3,4-Dimethyl pyrazole phosphate*
EEF	*Enhanced efficiency fertilisers*
EDX	*Energy dispersive X-ray spectroscopy*
ESN	*Environmentally smart nitrogen*
FTIR	*Fourier transform infrared spectroscopy*
GBR	*Great Barrier Reef*
^{1}H NMR	*Proton nuclear magnetic resonance*
Nr	*Reactive nitrogen*
NUE	*Nitrogen uptake efficiency*
PM	*Particulate matter*
SEM	*Scanning electron microscopy*
SRF	*Slow release fertiliser*
SCF	*Sulfur coated fertiliser*
UV-Vis	*Ultra-violet spectroscopy*

Chemical formulas

Al	*Aluminium*
$CHCl_3$/ $CDCl_3$	*Chloroform/deuterated chloroform*
N/N_2	*Nitrogen/Dinitrogen (gas)*
N_2O	*Nitrous oxide*
NH_3/NH_4^+	*Ammonia/ammonium*
NO	*Nitric oxide*
NO^{2-}	*Nitrite*
NO^{3-}	*Nitrate*
O_3	*Ozone*

CHAPTER 1

Introduction

1.1   Defining the problem

Nutrient pollution due to anthropological perturbations of biogeochemical flows is a leading global concern. Rockstrom et al.[1] identified nitrogen (N) and phosphorus (P) biochemical flows as beyond the zone of uncertainty (high-risk) of substantially altering the Earth system, with flows greater than double their estimated planetary boundaries (Table 1.1). Nitrogen is an essential element for all forms of life, particularly for synthesis of amino acids – the building blocks of proteins and enzymes. In nature, nitrogen is scarce and often growth limiting. As a result, when N becomes available, many organisms thrive, including the crops that feed us. However, increased N availability in aquatic systems also allows microorganisms to thrive, particularly phototrophs such as cyanobacteria and algae leading to blooms that can secrete toxins, block sunlight and, upon subsequent decay, deplete the water systems of oxygen, suffocating higher trophic level organisms. Nitrogen pollution is the cause of a further myriad of local environmental and human health problems, and plays a role in major global challenges, such as loss of genetic diversity, eutrophication leading to hypoxia in riverine and coastal waters, stratospheric ozone depletion, ocean acidification and climate change.[2]

Table 1.1: Current estimates of global N and P flows and their planetary boundaries as developed by Steffen et al.[3].

Biogeochemical Flow	Current Estimate	Planetary Boundary
Global Nitrogen	~150 Tg N yr^{-1}	62 Tg N yr^{-1}
Global Phosphorus	~22 Tg P yr^{-1}	11 Tg P yr^{-1}

The increased demand for food and energy, along with the increased consumption of meat, particularly in developed countries, contribute to a significantly increased cycling of nitrogen in the global ecosystem, with predictions of exponential growth in the coming decades. Nitrogen has historically been a crop yield-limiting nutrient, which led to the industrial fixation of atmospheric dinitrogen (N_2) through the Haber-Bosch process to produce synthetic nitrogen fertilisers, such as urea and ammonium nitrate. In 2010, anthropogenic fixation of atmospheric N_2 through the Haber-Bosch process reached 120 Tg N.yr^{-1}, predominantly for N fertiliser synthesis, with small contributions for other industrial uses, such as explosives production.[4] The total anthropogenic atmospheric nitrogen fixation, through the Haber Bosch process, biological nitrogen fixation by leguminous crops, and the combustion of fossil fuels, has reached 210 Tg N.yr^{-1}, exceeding natural fixation (203 Tg N.yr^{-1}). Therefore, the development of anthropogenic fixation of N_2 has doubled the global cycling of nitrogen. Unfortunately, when N fertiliser is applied to agriculture lands <50% is taken up by the plant, with the majority of N fertiliser lost to the environment, with a cascade of consequences.[5]

The heavy use of rapidly soluble and mobile synthetic fertiliser in cropping systems is largely responsible for environmental losses, through the direct volatilisation of urea and ammonia (NH_3); microbial transformations to gaseous nitrogen oxides (NO_x) and nitrous oxide (N_2O) - a potent greenhouse gas; and through the leaching and runoff as ammonium (NH_4^+), nitrite (NO_2^-) and nitrate (NO_3^-).[6]

One method to lessen N losses is through the application of inhibitors alongside N fertilisers that can slow enzyme catalysed N transformations. Synthetic nitrification inhibitors (NIs) bind to and inhibit the ammonium monooxygenase (AMO) enzyme of various bacteria and archaea that catalyse the oxidation of NH_4^+ to NO_3^- in the soil. Inhibiting this transformation is generally beneficial due to the net negative charge of most soils, which allows ammonia to electrostatically bind to soil particles. Dicyandiamide (DCD) is a commercial NI that has shown efficacy for the inhibition of AMO, reducing leaching and denitrification losses and improving crop performance.[6-7] Unfortunately, however, DCD degrades in the soil, with its half-life decreasing exponentially with increasing soil temperature,[8] rendering it ineffective in tropical cropping systems.

1.2   Project scope

This project investigated ways to prolong the activity of the nitrification inhibitor dicyandiamide (DCD) for tropical agricultural applications. The studies herein investigate the controlled-release of DCD from biodegradable and environmentally friendly polymers as a method of protecting the inhibitor from degradation, allowing the potential extension of effective AMO inhibition. Specifically, thermoplastic wheat starch (TPS), the bacterial polyester poly(3-hydroxybutyrate-*co*-3-hydroxyvalerate) (PHBV) and synthetic polycaprolactone (PCL) were explored as matrices for controlled-release that can be fully metabolised by soil microbes. Pellets of crystalline DCD distributed in biodegradable polymers were fabricated using industrially relevant extrusion processing, as a drop-in technology of commercial relevance. Importantly, a key aim of this project was to gain a deeper understanding of the mechanisms governing the release kinetics of soluble crystalline materials distributed in hydrophilic and hydrophobic biodegradable polymers, using DCD as a model agrichemical.

This doctorate was completed as part of the *New technologies and managements: transforming nitrogen use efficiency in cane production* project led by Dr. Matthew Redding at the Queensland Department of Agriculture and Fisheries (QDAF). This project is a branch under the large*r More Profit from Nitrogen* umbrella project funded by Cotton Research Development Corporation (CRDC), Dairy Australia, Sugar Research Australia and Hort Innovation. Here, the scope was limited to the fabrication and release testing of novel controlled-release nitrification inhibitors. The efficacy

of these materials at inhibiting nitrification and the resulting impact on plant growth and environmental N loss was tested at pot, plot and field-scale by QDAF. These results will be reported elsewhere when the outcomes have been finalised. Those studies are investigating a wider range of NI-polymer combinations than reported here and the results will isolate which materials work best in tropical cropping systems.

1.3   Thesis structure

This report consists of nine chapters, where Chapters 5-8 present the primary research outcomes from the project. **Chapter 2** provides a holistic overview of the global dilemma surrounding nitrogen pollution and a review of enhanced efficiency fertilisers to minimise N losses, the degradation of inhibitors in the soil, biodegradable polymers studied for controlled-release applications and the mathematical modelling of controlled-release systems. In **Chapter 3**, the research gaps identified from the literature review are presented along with the overall project aims and focussed research questions pertinent to the project. **Chapter 4** is a collation of the common experimental methods used throughout Chapters 5-8, including details on the extrusion fabrication of the controlled-release pellets, testing of release kinetics in various media and the analytical and characterisation techniques used. Finally, **Chapter 9** synthesises the outcomes presented in Chapters 5-8 and discusses the outstanding research.

The research chapters report the development of the extrusion processing fabrication technique, testing of release kinetics, and high-resolution characterisation of the controlled-release DCD pellets.

Chapter 5 presents the first account of the fabrication of controlled-release DCD-PHBV produced through extrusion processing, loaded at 250 g.kg^{-1} DCD, with 250 g.kg^{-1} DCD-TPS fabricated as a positive control. Release was studied in water, sand, soil, sand/soil mixtures (1:3, 1:1 and 3:1) and sterilised soil over ~6 months to determine the contribution and timing of surface release versus matrix diffusion versus polymer degradation on DCD release. Importantly, this study identified that release did not occur via a moving front within the pellet, with small DCD crystals remaining encapsulated near the surface of the pellet after ~50 wt.% release and large crystals being preferentially mobilised. From these results the research plans for Chapter 6 and Chapter 7 were developed.

Chapter 6 details the 3-D high-resolution characterisation of DCD-PHBV (250 g.kg^{-1}) before and after release into sand using micro-computed X-ray tomography (μ-CT) at 0.5 μm and 4 μm resolution. Here, the presence of cracks through the matrix was identified and postulated as a key mechanism for the access of larger crystals further into the pellet. The lack of cracks leading to the smaller crystals explained why they remain encapsulated until the polymer degrades.

Chapter 7 explores the role of DCD crystal size further and assesses the conditions leading to onset of complete interconnectivity between DCD crystals, triggering rapid mobilisation, i.e., the percolation threshold. New DCD-PHBV materials were extruded with 0-106 µm, 106-250 µm and 250-420 µm DCD crystal sizes at DCD loadings of 200, 400, 600 and 800 g.kg^{-1} and release kinetics were monitored over 8 weeks in water. The threshold was identified to lie between 200 and 400 g.kg^{-1}, independent of crystal size, with the DCD crystal size significantly affecting release from the surface of the pellet at 200 g.kg^{-1}.

Chapter 8 investigates the effect of blending PHBV with PCL at 1:0, 3:1, 1:1, 1:3 and 0:1 PHBV:PCL ratios. Release from each material was studied in water over 12 weeks at 10 °C, 23 °C and 40 °C, with the release kinetics being fitted to a diffusion model to determine the Arrhenius parameters for the temperature dependence of diffusivity. Counter-intuitively, release kinetics decreased with the polymer matrix hydrophilicity, highlighting the importance of the DCD-polymer interactions during fabrication.

CHAPTER 2

A review of the global nitrogen challenge

and strategies for loss mitigation

2.1 The "green revolution"

Nitrogen is an essential element for the biosynthesis of proteins and enzymes in all living organisms. In plants, nitrogen is also critical for the synthesis of chlorophyll, the pigment within the chloroplasts of leaves that makes them green. This pigment gives plants the ability to convert sunlight into chemical energy to ultimately drive the biosynthesis of carbohydrates from atmospheric carbon dioxide and water. This unique pigment consists of tetrapyrrole with a central magnesium (Mg) ion, requiring four moles of nitrogen (N) per mole of chlorophyll. As such, chlorophyll production within plants is typically limited by Mg and N availability. Nitrogen is absorbed by roots from the soil, mostly as dissolved inorganic nitrate (NO_3^-) or ammonium (NH_4^+), and less commonly as organic N. The scarcity of plant available N in natural ecosystems limits the rate of plant growth due largely to restricted chlorophyll biosynthesis. Limited natural N_2 fixation has led to diverse ecosystems that effectively conserve and recycle nitrogen.[4] Similarly, cropping systems historically utilised organic N fertiliser sources and growth was commonly limited by ammonification, which controls the concentration of plant available N in the soil. This was until, in the early 1900's, the Haber-Bosch process was developed, kicking off the "green revolution". This high temperature and high pressure catalytic hydrogenation of atmospheric nitrogen (N_2) to ammonia allowed, for the first time, the efficient production of synthetic nitrogenous fertilisers at massive scale. In 2018, the world synthesised 175 million tonnes of ammonia using the Haber-Bosch process.[9] Consequently, N is no longer the major limitation for crop yield in most cropping systems, closing yield gaps and sustaining ~48% of our ever expanding population.[10]

2.2 Nitrogen transformations and environmental losses

Today, synthetic N fertiliser is a relatively low cost agrichemical input that ensures crop success. As such, farmers heavily apply N, in the form of anhydrous ammonia, urea, ammonium nitrate, ammonium phosphate, among others. All of which are highly soluble, reactive and mobile, allowing rapid uptake by crop roots, but also leading to harmful environmental losses of 50-70% of the N applied.[11] These losses are significant and undermine the short-term gains from the Haber-Bosch "green revolution", causing long-term damage to our Earth's system, affecting fresh and coastal aquatic ecosystems through eutrophication and biodiversity loss, reducing air quality, accelerating climate change and leading to numerous human health implications.[4, 12-13] Fertiliser N is predominantly lost through direct volatilisation of urea and NH_3, leaching of NH_4^+ and particularly NO_3^-, and through the denitrification of nitrate to gaseous nitrous oxide (N_2O), nitric oxides (NO_x) and N_2.
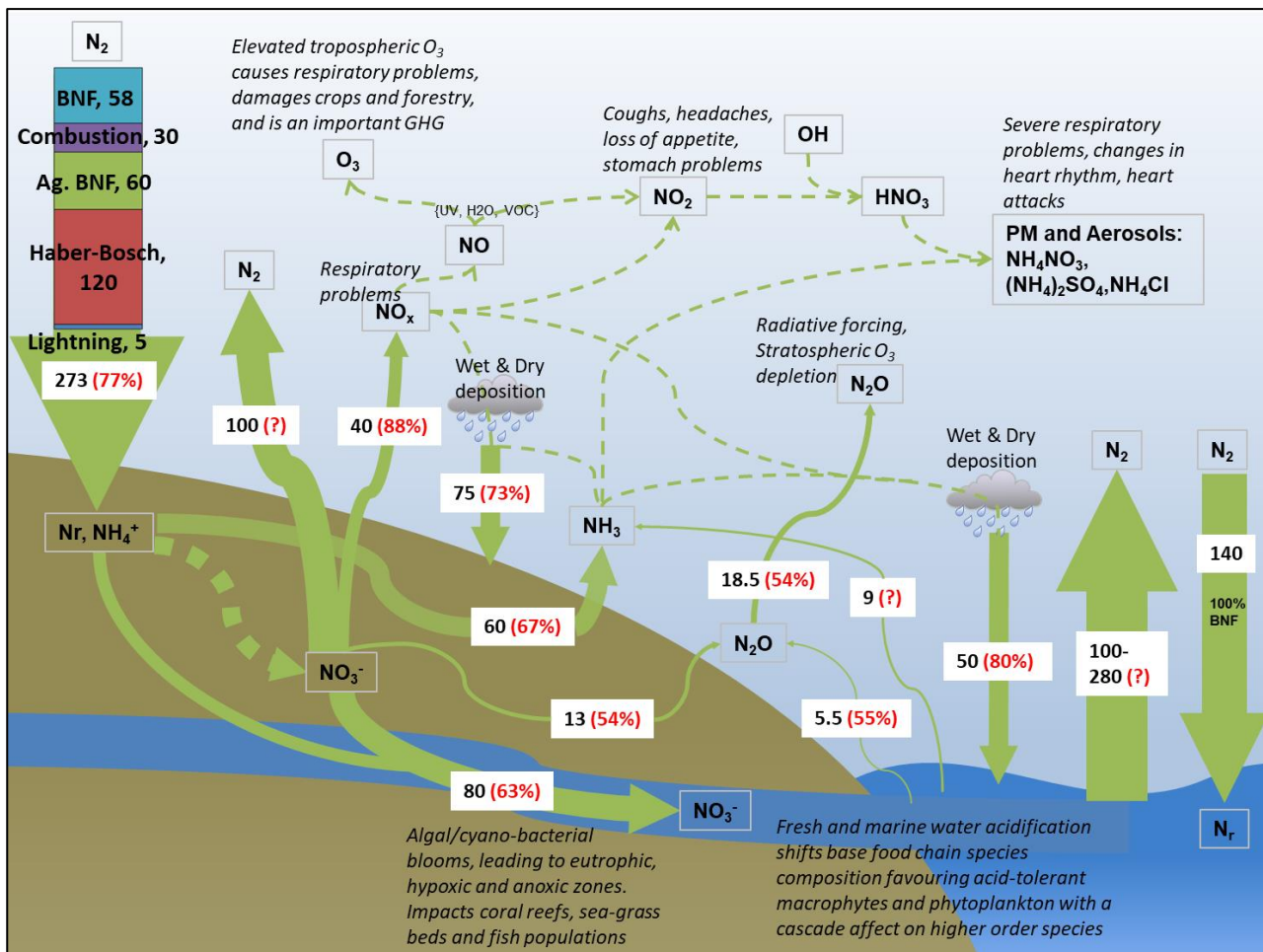
Figure 2.1: Diagram representing the global N cycle and the impacts of reactive nitrogen (Nr) in terrestrial and marine systems and exchange with the atmosphere (Tg N.yr⁻¹). Red values in brackets show anthropogenic contribution to each flow. The bar graph built into terrestrial nitrogen fixation flux arrow shows the relative global contribution of natural biological nitrification fixation (BNF), combustion of fossil fuels, agricultural BNF, Haber-Bosch N fixation and lighting. The values for N flows were sourced from Fowler et al.[4], Galloway et al.[14] and Erisman et al.[2].

Figure 2.1 highlights the major flows and transformations within the global N cycle. This diagram, which was synthesised as a platform for this work, shows a collation of literature on i) global flows and transformations of N, with the width of the arrows proportional to the flow, ii) the human contribution to each N flow, as shown by the percentage in red within parentheses, and iii) some of the key environmental and human health effects from the massive anthropogenic perturbation to global N cycling. Natural and anthropogenic N_2 fixation produces organic and inorganic reactive N forms (N_r) which are readily converted into other N_r species, including, but not limited to, organic N, soluble N forms (NH_4^+/NH_3, NO_3^-, hydroxylamine (NH_2OH), and nitrite (NO_2^-)), gaseous N forms

(NH$_3$, nitric oxides (NO, NO$_2$), N$_2$O, and nitric acid (HNO$_3$)), and particulate matter (PM)/aerosols (ammonium nitrate (NH$_4$NO$_3$), ammonium sulfate ((NH$_4$)$_2$SO$_4$ and ammonium chloride (NH$_4$Cl)). Nitrogen enters both terrestrial and aquatic ecosystems naturally through biological nitrogen fixation (BNF), natural fires, lightning and wet and dry atmospheric deposition. Microbes fix N$_2$ into organic N forms for the synthesis of amino acids, to produce proteins. Anthropogenic nitrogen fixation is not a modern perturbation to the N cycle, with agricultural BNF from the cropping of legumes dating back to the start of agriculture. Today, however, agricultural BNF represents just 29% of the ~210 Tg of N anthropologically fixed per year, with combustion contributing 14% and the majority (57%) fixed through the Haber-Bosch process. The latter is an important source of N for industrial chemicals, such as explosives, plastics, resins, glues, melamine, and animal feed supplements[15] and is required to feed ~48% of the human population through the production of N fertilisers.[10] Unfortunately, inefficiencies of N fertiliser uptake by crops, and the unintentional emissions from the combustion of fossil fuels, cause the release of immense quantities of nitrogen pollutants globally.

The inefficiencies of N fertilisers arise from the rapid transformation and high mobility of various reactive inorganic N species. When urea (CH$_4$N$_2$O) is applied to the soil it rapidly dissolves and is quickly hydrolysed to ammonia (NH$_3$) and CO$_2$ (Eq. 2.1) in a process catalysed by ureases, a ubiquitous family of enzymes synthesised by bacteria, fungi, algae and plants.[16] The ammonia exists as a dissolved species in equilibrium with ammonium (NH$_4^+$), Eq. 2.2. Due to the net negative charge of organic matter and some clays, most soils have some capacity to electrostatically bind NH$_4^+$ to soil particles.

$$CH_4N_2O + H_2O \xrightarrow{Urease} 2NH_3 + CO_2 \qquad \textbf{Eq. 2.1}$$

$$NH_3 + H_2O \rightleftharpoons NH_4^+ + OH^- \qquad \textbf{Eq. 2.2}$$
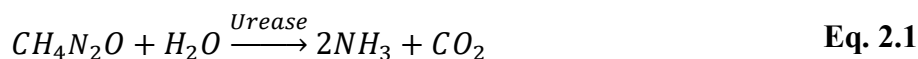
Ammonia oxidising bacteria and archaea (AOB and AOA, respectively) are also abundant in the soil, and catalyse the oxidation of ammonia to hydroxylamine (NH$_2$OH) by the ammonia monooxygenase (AMO) enzyme.

$$NH_3 + O_2 + 2H^+ + 2\bar{e} \xrightarrow{AMO} NH_2OH + H_2O \qquad \textbf{Eq. 2.3}$$
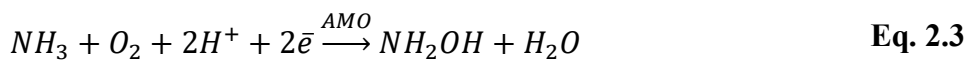
The conversion of hydroxylamine to nitrite (NO$_2^-$) is rapidly catalysed by hydroxylamine oxidoreductase (HAO), which is subsequently oxidised to nitrate by nitrite oxidoreductase (NXR).[17]

$$NH_2OH + H_2O \xrightarrow{HAO} NO_2^- + 5H^+ + 4\bar{e} \qquad \textbf{Eq. 2.4}$$

$$NO_2^- + H_2O \xrightarrow{NXR} NO_3^- + 2H^+ + 2\bar{e} \qquad \textbf{Eq. 2.5}$$
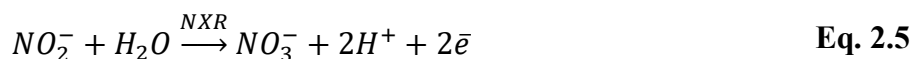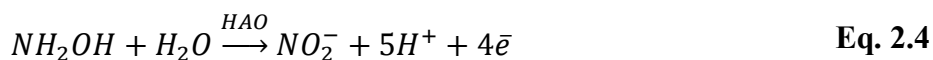
Since soils are typically net negatively charged, anions, such as nitrate and nitrite, have a high mobility and are especially susceptible to leaching into groundwater or loss through runoff in high rainfall events or irrigation, ultimately migrating into freshwater ecosystems. Furthermore, NO_3^- is vulnerable to denitrification to nitrous oxide (N_2O), nitric oxides (NO, NO_2) and N_2 (as shown in Figure 2.1), particularly in saturated soils and high temperature conditions.

Liu et al.[18] conducted a high-resolution assessment of global nitrogen flows in croplands. They estimate total global nitrogen input to croplands in 2000 was 136.6 $Tg.yr^{-1}$, of which 67.8 $Tg.yr^{-1}$ was synthetic fertiliser application, representing the single greatest contributor and almost half of the total nitrogen input. However, the contribution of synthetic N fertiliser was found to be highly region dependent. In Africa and South America, where a third of the nitrogen input is fixed biologically, fertiliser contributed only 25-29% compared to 45-48% in Europe, Asia, Oceania and North America. Manure application accounted for 20% of the N applied in South America, but less than 15% in all other continents. Intensive fertiliser application (>100 kg $N.ha^{-1}.yr^{-1}$) predominantly occurred in China, Western Europe, United States Midwest and western coastal states, Pakistan, Saudi Arabia, Iran, Uzbekistan and Egypt. By contrast, many countries in Africa showed regions with application rates lower than 10 kg $N.ha^{-1}.yr^{-1}$. This highlights the state-by-state approach required to address this global issue. Yet, the consequences disturb the Earth system as a whole, affecting the atmosphere, fresh waterways, oceans and biodiversity. These effects are detrimental to both human and ecosystem health. Furthermore, the impact is amplified through the 'nitrogen cascade' where recycling of nitrogen triggers sequential detrimental environmental impacts.[2]

2.2.1   Environmental implications

Impact on Aquatic Systems

The use of synthetic fertilisers in modern agriculture is the primary source of anthropogenic N_r inputs to the environment. Approximately 30% of all nitrogen fixed by human activities is eventually transported through watersheds into coastal oceans.[19] It is generally accepted that anthropogenic contributions have a negligible impact on nitrogen fluxes within the open oceans.[13] However, denitrification in freshwater systems represents nearly half of the total global terrestrial N_2 emissions. This indicates dominant lateral terrestrial transport of nitrogen from land into rivers and lakes, where the majority of reactive nitrogen input is removed and a significantly reduced flux enters coastal oceans.[13] Still, riverine transport contributes 40-70 Tg $N-NO_3^-.yr^{-1}$ to coastal waters[4] causing acidification, low diversity algal and cyano-bacterial blooms, and plankton outbreaks.

Eutrophication in fresh and coastal waters leads to the formation of hypoxic and anoxic zones and the release of toxic compounds.[2] Over the last 50 years, documented global hypoxic zones have

increased from 10 to 169, with a total 415 eutrophic and hypoxic regions.[20] These figures are likely underestimates, particularly in Asia where relatively few numbers of eutrophic and anoxic zones have been documented despite widespread extensification and intensification of agriculture, industrialisation and population growth over the last 20 years.

Eutrophication leads to a cascade of environmental impacts. Growth of subaquatic vegetation is limited by the reduction in light penetration, while coral larvae are outcompeted by the over-abundance of algal species for surface sites to bind and grow.[20] Biomass sedimentation and decay from excessive growth of phytoplankton and algae deplete dissolved oxygen levels at the sea floor, limiting growth of benthic communities to species tolerant of the reduced oxygen levels,[2] reducing diversity, and typically favouring gelatinous organisms such as jellyfish.[20] This alters the cycling of nutrients, limiting food availability for aquatic ecosystems as a whole.

Impacts of Gaseous Emissions

Gaseous reactive nitrogen emissions (see Figure 2.1) play a key role in atmospheric composition and chemistry, and contribute significantly to climate change. Although N_2O losses are small in terms of the agricultural N mass balance, these emissions represent 46% of agricultural greenhouse gas emissions, with one molecule of N_2O producing 300 times the radiative forcing of CO_2.[21] In 2004, agriculture contributed 14% of the global greenhouse gas emissions.[21]

Also, the transfer of gases to the atmosphere is temperature dependent and NH_3 is particularly sensitive. Rising global temperatures by 2-4 °C by 2100 are predicted to increase NH_3 volatilisation to 130 Tg N.yr^{-1}, more than double the current estimates.[22]

2.2.2   *Effects on human health*

The Haber-Bosch 'green revolution' has eliminated N as the limiting nutrient on many farmlands globally since the 1960s. Due to the cost of synthetic fertilisers, this impact has been most prominent in developed countries.[23] Still, synthetic N fertiliser has seen dramatic increases in global food supply, reducing widespread malnutrition and starvation, particularly in Asia, despite a concurrent exponential global population growth.[24] Moderate increases in N fertiliser application in developing countries will continue to offer human health benefits due to the potential increases in food and nutrition.[12] It is hypothesised that these benefits will plateau as anthropogenic N fixation increases further, while direct and indirect health implications increase exponentially and diversify, ultimately outweighing the positive implications.[12]

Consumption of meat has doubled in developing countries over the last 50 years, and increased exponentially in wealthier countries such as the United States.[12] While there are recognised health

benefits of meat consumption, excessive meat consumption has been linked with health problems such as heart disease.[25] The application of synthetic N fertilisers to animal feed crops, such as grains and corn, has allowed for this exponential growth in meat consumption. In the US, more than half the grain is currently grown for animal feed. This has led to widespread, intensively concentrated animal raising, with a cascade of environmental impacts and meat with reduced nutritional value.[12]

Atmospheric emission of NO_x, from fossil fuel combustion, burning of biomass and high nitrate concentrations in the soil, can be oxidised and generate ozone (O_3). Accumulation of O_3 in the troposphere initiates and exacerbates lung inflammation, coughs and asthma.[26] High NO_x levels are directly linked to impaired immune response to common viral infections. Chronic exposure to elevated levels of NO_2 causes coughs, headaches, asthma and reduced breathing efficiencies.[2] Hydrolysis of NO_2 to nitric acid (HNO_3) and subsequent reaction with NH_3 leads to ammonium nitrate (NH_4NO_3) particulate matter (PM) formation. Due to its alkalinity, NH_3 readily reacts with any acidic gases in the troposphere, such as sulfuric and hydrochloric acid, forming the aerosol of the respective ammonium salts. Chronic exposure to airborne PM and aerosols has been linked to cardiovascular diseases, asthma and reduced lung function.[12]

2.3   Enhanced efficiency fertilisers (EEFs)

Since the introduction of N fertilisers synthesised through the Haber-Bosch process over 100 years ago, very little has changed in fertiliser formulations and technologies. However, over the last 20-30 years, new technologies have emerged to improve the nitrogen uptake efficiency of applied N, such as foliar fertilisers, slow- and controlled-release fertilisers and stabilised fertilisers.

Enhanced efficiency fertilisers (EEFs) are broadly defined as any fertiliser that offers an agronomic, environmental or economic benefit over their conventional equivalent,[27-28] and are comprised of slow- and controlled-release fertilisers (SRF and CRFs) and stabilised fertilisers. These materials are designed to increase the nitrogen uptake efficiency (NUE) by the crop, meaning less N fertiliser is required. Several authors have comprehensively reviewed EEFs. Among them, Trenkle[28] reviewed the commercial state-of-the-art for slow- and controlled-release fertilisers and stabilised fertilisers, providing detail on the manufacture, characteristics, consumption, and environmental and economic pros and cons of commercialised EEFs. Shaviv[29] and Timilsena et al.[27] reviewed EEF formulations, their nutrient release patterns, and the implications on material selection for coated formulations. Controlled release fertilisers and release patterns were also reviewed by Sempeho et al.[30]. Further, research on the use of biodegradable polymers and their blends in CRF formulations was comprehensively reviewed by Majeed et al.[31]. As such, a condensed overview of EEFs is provided here for brevity.

2.3.1 Nitrogen stabilisers

Stabilised fertilisers offer a more economically attractive option for improved N fertilisation efficiency. These N fertilisers contain either a urease inhibitor (UI) or a nitrification inhibitor (NI) to maintain the N as urea or ammonium, respectively, adding ~20-30% to the fertiliser price. Urease inhibitors reduce ammonia volatilisation losses by delaying the enzymatic hydrolysis of urea to ammonia (Eq. 2.1), whereas, nitrification inhibitors bind to and block ammonia monooxygenases (AMO), limiting the oxidation of ammonium (Eq. 2.3). Ultimately, both reduce the concentration of nitrate in the soil. Since NH_4^+ has a higher affinity to soil surface particles in most soils than NO_3^-, both urease and nitrification inhibitors have been shown to effectively reduce nitrate leaching and denitrification N losses.[32] The inhibition of AMO has also been shown to suppress methane emissions.[33-36] Further, the assimilation and incorporation of NH_4^+ into plant proteins has a lower energy requirement than that of nitrate.[37] Furthermore, the transport of protons from root cells during NH_4^+ assimilation to balance the charges, results in rhizosphere acidification. This reduction in pH helps solubilise and mobilise other nutrients in the soil, such as phosphorus and zinc, improving nutrient availability.[38]

Urease inhibitors

N-(n-butyl)-thiophosphoric triamide (NBPT – Agrotain®) is the widely recognised UI of commercial importance. The urease inhibition is actually caused by a NBPT derivative, N-(n-butyl) phosphoric triamide.[39] Hydroquinone has been used in parts of China, while natural urease inhibitors in neem cake extracts have been used in India.[28] Several natural chemicals have shown urease inhibiting potential. For example, polyphenolic alkaloids extracted from the bark of green wattle and inknut seed coat showed effective inhibition of urease and decreased NH_3 volatilisation.[40] Neem seed kernel powder has been shown to inhibit both urease and nitrification under varying moisture and temperature conditions.[41] The reduction in urease and nitrification activity by *Pinus radiata* bark extracts was attributed to the high phenolic content of the extracts, however, the exact mechanism has not been established.[42]

Nitrification inhibitors

The most studied NIs include 2-chloro-6-(trichoromethyl)pyridine (nitrapyrin), 2-amino-4-chloro-6-methylpyrimidine (AM), dicyandiamide (DCD), 3,4-dimethylpyrazole phosphate (DMPP), carbon disulphide (CS_2), thiourea, allylthiourea, acetylene, allylsulfide, thiosemicarbazide, thioacetamide, potassium ethylxanthate, diethyldithiocarbamate, and trichloroethane (TCE). In fact, hundreds of chemicals have been studied, and many patented, for their nitrification inhibitory effects.

However, only a few synthetic NIs have commercial significance, including nitrapyrin, AM, DCD and DMPP, due to their low toxicity and strong evidence of efficacy in many soils.[28, 43]

Synthetic NIs act via various mechanisms to deactivate AMO, including chelation, allosteric and mechanism-based inhibition. Nitrapyrin inactivates AMO by chelating with the copper (Cu) reaction centre within the AMO complex.[44] Carbon disulphide, CS_2, reacts with nucleophiles to produce metal complexing compounds such as di- and tri-thiocarbamates and xanthogenates.[45] In particular, the reaction of CS_2 with amino acids near a Cu co-factor in the AMO complex is likely to result in non-competitive inhibition.[45] Like CS_2, thiourea, allylthiourea, thiosemicarbazide, thioacetamide, potassium ethylxanthate, and diethyldithiocarbamate all contain C=S bonds. While it has been argued that this functional group largely imposes the mechanism of inhibition,[46] the mechanism of CS_2 and thiourea in AMO inhibition may differ. CS_2 derivatives may form true bidentate chelates, whereas thiourea and related compounds serve as mono-dentate ligands.[45] ^{14}C-labelled acetylene was the first molecule shown to covalently bind a peptide within the AMO, resulting in mechanism-based irreversible inhibition.[47] Subsequent studies have shown mechanism-based inhibition of AMO by allylsulfide and TCE. DCD blocks the electron transport chain in the cytochrome of AMO, whereas DMPP binds indiscriminately to the membrane-bound AMO.[48]

While they have not yet received commercial interest, natural nitrification inhibitors (NNIs) have been studied extensively. Upadhyay et al.[49] and Subbarao et al.[50] reviewed the identification and efficacy of plant-derived NIs. Well known NNIs include neem oil (neem seed extract), karajin (karajin seed extract), dementholated oil (mint leaf extract), limonene, α-pinene, β-pinene, myrcenea, α-phellandrene (pine leaf extracts), sorgoleone, sakuranetin, methyl 3-(4-hydroxyphenyl) propionate (sorghum root extract), linoleic and linolenic fatty acids, brachialactone, methyl-p-coumarate and methyl ferulate.[49-50] Plants can actively suppress nitrification through the synthesis and exudation of NNIs from the roots into the rhizosphere. Monoterpenoids play a key role in biological nitrification inhibition (BNI) in forest ecosystems, particularly in ponderosa pine forests.[51-56] It was found that tropical pasture grasses that have been adapted to the low-N environments showed the highest level of BNI activity, and that NNIs were only secreted when NH_4^+ was present.[57] Unlike synthetic NIs that only target the AMO enzyme, several NNIs, such as sorgoleone, sakuranetin, and brachialactone inhibit both AMO and HAO.[17]

Inhibitor degradation in soil

UIs and NIs degrade naturally in soils through abiotic and biotic mechanisms. Here, degradation of the three inhibitors of the most commercial significance, NBPT, DMPP and DCD, are described. NBPT is degraded by both acid and base catalysis. Base-catalysis produces phenol and

diamidophosphoric acid, while acid catalyses deamination, producing phenyl phosphoramidate. Degradation is enhanced by the presence of ammonium and carbonate ions, and follows first-order reaction kinetics.[58]

The mechanisms mediating DMPP degradation are less well understood. Barth et al.[59] suggest that the extended activity of DMPP is due to adsorption to inorganic soil constituents, protecting it from microbial attack. However, the authors did not reference any literature indicating that DMPP is microbially degraded. This is in contrast with several studies that attribute reduced DMPP efficacy in high organic matter and clay content soils to DMPP adsorption to these soil constituents, likely due to the increased cation exchange capacity binding the $3,4\text{-DMP}^+$ cation.[60-61] DMPP adsorption is known to decline with increasing metal concentration in the soil due to the competition for available sites and increases in more acidic soils, possibly due to increased dissociation of the weakly basic organic salt.[62] Zhao et al.[63] found that the DMPP follows a first order decay in soil, which is accelerated at high temperature and by the presence of heavy metals, Cu^{2+} and Cd^{2+}, reducing the half-life by 58-86%. The period of DMPP efficacy thus drops off with increasing soil temperature. Merino et al.[64] found significantly higher NH_4^+ concentrations with DMPP application to manure slurry for the first 22 days in Autumn (mean 11.4 °C), compared to 7-14 days in Spring (mean 16.7 °C). In an alkaline calcareous soil, Mahmood et al.[65] found that both DCD and DMPP were effective for at least 2 weeks at 25 °C, while at 35 °C <87% of the applied N was nitrified after 1 week.

The hydrolysis of DCD is better understood, shown in Eq. 2.6. The catalytic hydration of DCD to guanylurea occurs on the surface of metal oxides; this then undergoes further microbial hydrolysis, deamination and decarboxylation to produce first guanidine, then urea.[66] Urease rapidly hydrolyses urea to ultimately produce CO_2, H_2O and NH_3.
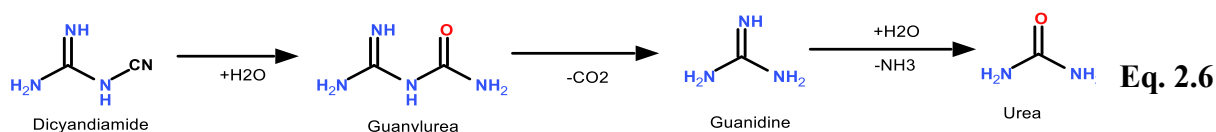
The half-life of DCD was considered to be >70 d for T<10 °C, and consequently application timing is critical to maximise effectiveness. Several studies have investigated the temperature dependence of DCD biodegradation.[8, 67-69] Kelliher et al.[8] investigated literature data on the temperature dependence of DCD degradation in soils, and found the half-life of DCD ($t_{1/2}$ in days) exponentially decays with temperature (T in °C) (Eq. 2.7). As such, the $t_{1/2}$ is reduced from 73 days at 10 °C (e.g., temperate soils), to 21 days at 25 °C (e.g., sub-tropical soils), to just 14 days at 30 °C (e.g., tropical soils).

$$t_{1/2} = 168 \times e^{-0.084T}$$
Eq. 2.7

2.3.2   Slow- and controlled-release fertilisers

Most conventional synthetic N fertilisers dissolve when applied to the soil and are therefore vulnerable to all the loss pathways described in Section 2.2. Since fertilisation typically occurs at the start of the cropping cycle, the plants initially do not assimilate N rapidly, resulting in a massive mismatch between N availability and demand. The objective of slow-release ferilisers (SRFs) and controlled-release ferilisers (CRFs) is to better synchronise N availability with N uptake by the crop. Fertilisers that best match nutrient availability with crop demand have the greatest likelihood of maximising the nutrient uptake efficiency, as shown in Figure 2.2.[70] There is no official difference between slow- and controlled-release fertilisers and the terms are commonly used interchangeably. Shaviv[29] defines SRFs as fertilisers that have a slower release profile than their conventional counterparts, but with release rates and profiles that are not well controlled due to strong dependence on soil moisture content, rainfall events, and biological activity. Whereas CRFs have been defined as products that have a well-defined release rate and profile, typically dependent on soil temperature, but not soil properties. All slow- and controlled-release products are designed to increase the fraction of nutrient uptake by plants, reducing N fertiliser requirements and protecting the environment from nutrient loading. A further advantage is the reduction in osmotic stress and burning of roots and leaves that occurs when soils are loaded with high concentrations of N fertiliser at the start of the season.[27] These benefits have been shown to increase crop yield.[27, 71] In addition to reduced fertiliser requirements, SRFs and CRFs may also allow a single application of fertiliser at the beginning of the growing season, rather than split applications, saving time, labour, and spreading equipment expenses.[72]
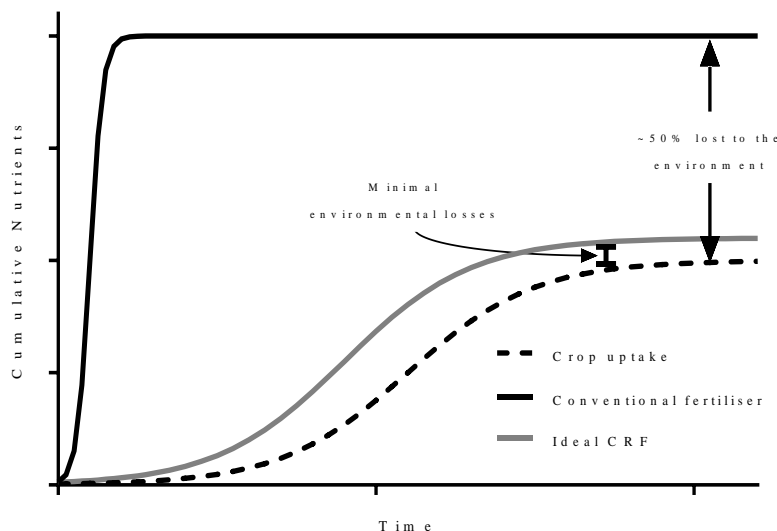
Figure 2.2: The 'ideal fertiliser' where the nutrient release is matched to the nutrient uptake from the crop. Adapted from Lammel[70].

Examples of common SRFs include urea-aldehyde condensation products, such as urea-formaldehyde (UF), urea-isobutyraldehyde (IBDU®), and urea-alcetaldehyde (IBDU®), sulfur-coated urea (SCU), urea supergranules and melamine. CRFs are typically polymer coated urea (PCU) products, and release profiles can be tailored by varying the coating thickness. Common polymers in use include alkyd-resins (Osmocote®), polyurethane (ESN®, Polyon®, Multicote®, Plantacote), ethylene-vinyl-acetate, polyethylene, and blends of the latter two (Nutricote®).[28] Note the prominent use of non-degradable polymers, which will fragment into potentially hazardous microplastics over time and accumulate in the soil.

The widespread use of any of these SRF and CRF products is limited by their high cost, which is typically more than double the cost of urea per unit N, with up to 12 times the cost reported for polymer coated urea products.[70] These costs restrict use to high-value crops, such as vegetables, and limits use for broad-acre cropping.

2.3.3 *Efficacy of enhanced efficiency fertilisers (EEFs)*

Studies on the efficacy of slow- and controlled-release and stabilised fertilisers for specific crops, soils and climates have been reviewed extensively,[6-7, 28, 43, 73-75] predominantly focussing on polymer coated fertilisers, NBPT urease inhibitor and DCD and DMPP nitrification inhibitors.

Akiyama et al.[7] evaluated the effectiveness of EEFs to reduce emissions of N_2O. From the meta-data analysis, they reported that polymer coated fertilisers reduced N_2O emissions by 14-58% compared to the equivalent conventional fertiliser. Similarly, an overall reduction of 31-44% was found for all NI studies, with DMPP outperforming DCD by an additional 20% N_2O reduction on

average. Statistically, by contrast, urease inhibitors did not show significant N_2O emission reduction over the conventional fertiliser. Interestingly, NIs significantly outperformed polymer coated fertilisers when applied to upland crops, with statistically similar reductions in N_2O emissions in grassland applications.

An additional benefit of NIs over SRFs and CRFs is the ability to reduce N losses from natural and organic soil amendments, such as urine, manures, composts etc. Globally, excreta from grazing animals accounts for ~40% of the total N_2O emissions from animal production.[76] Cai and Akiyama[75] collated data from 44 studies on the effect of UI (NBPT), NIs (a pyrazole derivative and DCD) and biochar on N_2O emissions, NO_3^- leaching and plant N uptake, concluding that NBPT, the pyrazole derivate and biochar were not effective in N_2O reduction, but NBPT did show an improvement in plant N uptake and yield. By comparison, DCD was highly effective in mitigating N_2O emissions, with a 46-55% (bias-corrected 95% confidence interval) overall reduction, but only effective on dairy cattle urine, with no benefit for beef cattle urine patches, likely due to lower cattle density. Overall, nitrate leaching was reduced by 39-51% with DCD amended urine, along with improved plant N uptake by 8-20%. Interestingly, coating the DCD with zeolites showed similar N_2O and NO_3^- loss reductions as for dissolved DCD, but improved plant N uptake by 6-59%. DCD used in conjunction with NBPT was also effective, with 43-53% reduction in N_2O overall and 35-50% reduction in NO_3^- leaching.

Abalos et al.[6] conducted a detailed meta-analysis on the effect of DCD, DMPP and NBPT and the combination of NBPT and DCD on crop productivity and nitrogen use efficiency (Figure 2.3). Inhibitors were shown to be most effective in low pH soils with medium to coarse grain size. The greatest increase in productivity was reported for the urease inhibitor, NBPT, with up to 12% increase in productivity. Nitrogen uptake efficiency was increased most by the combination of NBPT and DCD, with up to 28% increase in N uptake.

Results in the literature need to be interpreted with caution, as negative results are rarely reported, and testing conditions are often optimised to show the greatest effect of the EEFs. Furthermore, testing is almost exclusively conducted under temperate climatic conditions, due to the rapid breakdown of inhibitors at elevated temperatures (>25 °C), as described in Section 2.3.1.
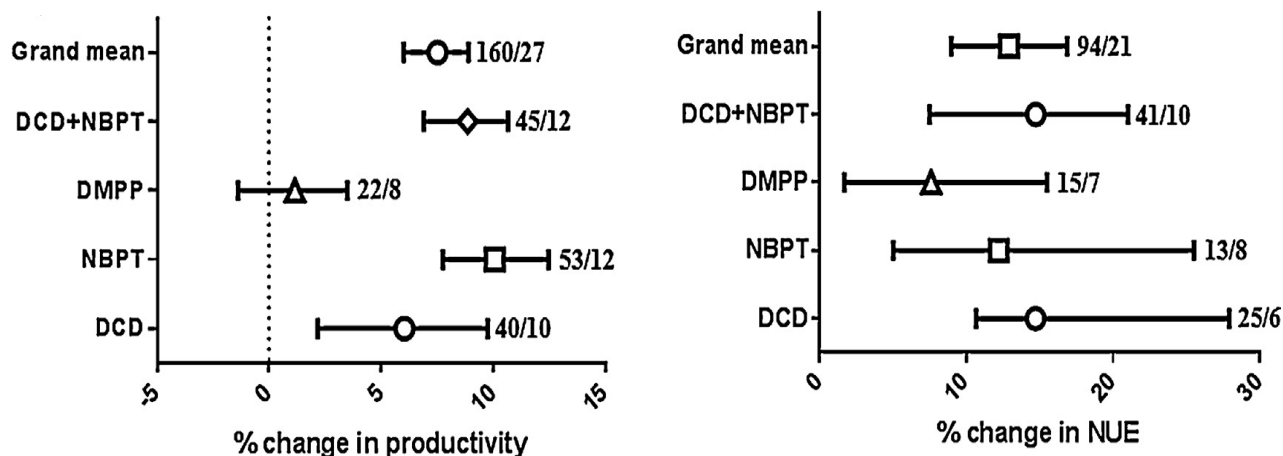
Figure 2.3: The effect of NBPT, DCD and DMPP and both NBPT and DCD on crop productivity and nutrient uptake efficiency (NUE) as a percentage of the control as reported by Abalos et al.[6]. Mean effect and 95% confidence intervals are shown. Sample sizes (i.e., the number of control–treatment pairs) are shown on the right of the confidence intervals, followed by the number of studies from which the comparisons were derived. Figure reproduced with permission from Elsevier.

2.3.4   Controlled-release of inhibitors

Controlled delivery of NIs is scarce in the literature, with no studies to date on controlled delivery of UIs. To my knowledge, the first account of the fabrication of a controlled-release NI was reported by Otey et al.[77] for the encapsulation of urea and nitrapyrin in a corn flour-based gel and a starch-based gel. Results show both slow release as the N stabilising agent and reduced volatilisation. Two fabrication methods were developed:

i)   Gelatinisation followed by granulation: pre-gelatinised corn flour or starch was mixed with a urea solution (which easily gelatinised the starch) followed by an ammonium hydroxide solution. To this, a chloroform solution of nitrapyrin was mixed, before boric acid, a cross-linking agent, was added to produce a rubbery material. Finally, dry corn starch was mixed through to granulise the rubbery mass.

ii) Extrusion processing technique: starch was gelatinised in a urea and KOH (if used) solution at 60-80 °C with minimal water in Brabender mixer. Once cooled, crystalline nitrapyrin was added and the mixture was extruded cold with a 1 mm die, and cut into 2-3 mm lengths.

Minet et al.[78] reported the slow delivery of DCD using a chitosan hydrogel. DCD-loaded chitosan microbeads were formed by precipitation of an acidified chitosan gelling solution that was cross-linked with glyoxal. Two methods of preparation were evaluated: the first involved washing the beads

with aqueous DCD solution to partly remove glyoxal (C beads), and the second method allowed the glyoxal to dry (GC beads). Rapid dissolution of DCD occurred from the C beads in water, with 84% release after a 9 h incubation. However, GC beads released just 19% after 9 h in water, and 33% in soil after 7 days under high rainfall simulated conditions.

To my knowledge, Bishop[79] was the first to produce a coated DCD formulation. First, DCD crystals were agglomerated with 10 wt% carboxyl methyl cellulose (CMC), and the micro-granules were then coated with castor oil/poly bisohenyl methyl diisocyanate (MDI) resin at 60 °C. The effect of coating thickness was investigated, with three layers (PDCD3) of polymer coatings compared to four (PDCD4). Significant differences were reported, with the PDCD3 releasing over 80% of DCD almost immediately, while PDCD 4 released ~60% after 60 days, with ~25% burst release in the first few days.

2.4 Biodegradable polymers for controlled release

The use of non-degradable polymers for the controlled-release of agrichemicals has been widely recognised as a non-sustainable option, with polymer accumulation rates in cropping soils as high as 50 kg.ha^{-1}.yr^{-1}.[28] Consequently, there is an abundance of literature on the use of biodegradable polymers and their blends in the fabrication of controlled-release fertilisers, pesticides and herbicides. There is no clear definition for a biodegradable polymer. According to Göpferich[80], a 'biodegradable' polymer is any polymer that degrades within the duration of its application. ASTM standard D-5488-94d defines the term "biodegradation" as materials "capable of undergoing decomposition into carbon dioxide, methane, water, inorganic compounds or microbial biomass in which the predominant mechanism is the enzymatic action of microorganisms". They can be grouped as natural, synthetic, or blends thereof and have a wide range of physical properties, from hydrophilic hydrogels, such as starch-based gels that can retain water to 500 times their own mass, to highly hydrophobic polymers such as waxes and polyhydroxyalkanoates (PHAs).

Biodegradable polymers studied for the fabrication of controlled-release fertilisers were reviewed by Majeed et al.[31], Naz Muhammad and Sulaiman Shaharin[81] and Chen et al.[82]. Commonly studied natural polymers include starch, chitosan, lignin, sodium alginate cellulose, gelatin, rubber, gluten and PHAs, while common synthetic biodegradable polymers include polylactic acid (PLA), polyurethanes, polycaprolactone (PCL), poly(aspartic acid) and polysulfone.[31] Starch has been also been extensively tested for the encapsulation of nitrogen and phosphorus fertilisers[83-85], coating urea[86-87] and encapsulating pesticides.[88] Many of these polymers, including starch, offer multifunctionality. Hydrogels can improve the water holding capacity of soils, reduce oxidative stress, and minimise soil erosion through soil particle aggregation.[89-92] Most biodegradable polymers

are also a carbon source that can support soil microbe growth and diversity. Volova et al.[93] found that delivery of urea cold-pressed with PHA resulted in a microbial population with 70% more nitrogen fixing bacteria over urea alone. A further benefit of degradability is the guarantee of complete release; up to 30% of fertiliser can remain inaccessible in the core of some polymer coated fertiliser product due to lack of a concentration gradient across the polymer film.[31]

There is a significant amount of literature on the use of natural hydrophilic polymers for controlled-release. While these have advantages of mild-processing conditions, water retention and low cost, the rate of water migration through these materials can limit the duration of release, often showing complete release within days of exposure to water. As such, there has been a recent shift towards more hydrophobic polymers, such as PLA, PCL and PHA.

Polyhydroxyalkanoates (PHAs) are an extensive family of polyesters that are naturally synthesised by over 300 strains of bacteria and archaea and stored as intracellular granules for carbon and/or energy storage, particularly under growth-limiting conditions in the presence of an external carbon source. This polymer consists of β-hydroxy fatty acids monomers, where the pendent group varies from methyl (C1) to tri-decyl (C13). The biological synthesis of this polymer allows incorporation of a variety of monomeric units and wide ranges of molecular weights. However, commercial production of PHAs has focussed on the synthesis of high molecular weight homopolymer poly(3-hydroxybutyrate) (PHB) through pure culture fermentation of sugars and vegetable oil. Incorporation of valerate or propionate in the broth leads to the synthesis of the co-polymer of poly(3-hydroxybutyrate-*co*-3-hydroxyvalerate) (PHBV). Equipment sterilisation and downstream extraction and purification of the polymer results in the relatively high cost of commercial PHA.

Despite its high cost, several groups have evaluated PHA-based matrices for the controlled-release of agrichemicals to improve their efficacy and uptake by the target organism.[94-97] However, this space is largely dominated by Volova et. al., with studies on the use of PHB as an encapsulating material for pesticides,[98-99] herbicides,[100-102] fungicides[103-104] and fertilisers[93, 105]. In Volova et al.[93], cold-pressed pellets and films loaded with urea at 10, 20 and 30 wt.% of the polymer content and PHB-coated urea granules were tested in water and soil release experiments.[93] All formulations showed excellent controlled release properties, releasing no more than 50 wt.% of the urea after 30 days, with release attributed to the microbial degradation of the PHB. The growth of creeping bentgrass and lettuce were significantly improved by the 20 wt.% urea loaded PHB film over the urea positive control, with a 14% increase in biomass of bentgrass and 38% increase in lettuce biomass.[93] In a similar subsequent study, Boyandin et al.[105] fabricated slow-release ammonium nitrate (AN) tablets (250 g.kg^{-1} AN, 10 mm in diameter, 1.5 mm thick) with matrices composed of PHB or 50:50

blends of PHB with PCL and PHB with sawdust, evaluating the release profiles in water and soil. To further slow the release kinetics, some AN-PHB and AN-PHB/wood flour tablets were coated with PHB by dipping the tablet into a 5 w/v% solution of PHB in chloroform between one and six times. Each dipping added 8-11 wt.% to the formulation, with calculated coating thickness of 4-5 µm per dipping. Since the different formulations were fabricated through cold pressed powders, the release profiles from uncoated matrices were unsurprisingly similar, with ~40 wt.% release in the first day in water and complete release within 7 days. In soil, uncoated matrices released ~50 wt.% AN in 14 days. By contrast, the coated formulations dipped six times (>50% weight gain and calculated coating thickness of >25 µm) released <25 wt.% AN after 7 days in water and <10 wt.% after 14 days in soil, with the majority of release in soil occurring between 6 and 12 weeks. In a pot trial, the PHB-coated PHB-AN tablet resulted in the highest growth of soft wheat (*Triticum aestivum L.*), outperforming the AN positive control by almost 30%.

While there has been significant development in the identification of suitable biodegradable polymers and fabrication techniques for controlled-release materials, there is still a lack of understanding of the mechanisms involved in the mobilisation of agrichemicals from biodegradable matrices. Many studies measure the mass loss of polymer along with the agrichemical release kinetics and conclude that matrix degradation drives release. However, correlation is not causation, and further detailed assessments and definitive evidence is still needed to fully understand the complex nature of release from these materials.

The erosion of biodegradable polymers in soils is complex and has been reviewed meticulously by Laycock et al.[106] Polymer degradation in this context is typically driven by abiotic and biotic hydrolysis of vulnerable linkages (such as polyesters, polyamides, polyurethanes and polyureas, poly(amide-enamine)s or polyanhydride linkages) or less commonly through oxidative degradation. For hydrolysable polymers, the rate of water migration through the matrices dictates the mode of polymer degradation, as depicted in Figure 2.4.[106] When diffusion (D) in the polymer matrix is rapid compared to the rate of polymer chain scission (λ), the matrix degrades throughout the bulk. However, if $D \ll \lambda$, the hydrolysis predominantly occurs at the material surface, while the bulk of the matrix remains largely unchanged. This results in a low rate of change in polymer molecular weight ($\overline{M}_n$) and mechanical properties. Such polymers surface erode until the thickness of the polymer is less than a critical thickness (L_{crit}). At this point, the mode of degradation shifts to bulk erosion, and $\overline{M}_n$ and mechanical properties begin to decline more rapidly, until a critical molecular weight is reached, ($\overline{M}_e$). From there, the polymer depolymerises into water-soluble oligomers and monomers that can be endocytosed by soil microbes for biomass building blocks or mineralised to CO_2, H_2O, CH_4 and other metabolic products for energy production.

In the context of controlled-release agrichemical applications, understanding the mode of polymer degradation is important to identify the implications of long-term use, but also helps to understand and predict release profiles, assisting product design. For example, bulk hydrolysis will increase the rate of agrichemical diffusion through the matrix, often following a first order acceleration. Whereas if the polymer surface erodes, the diffusivity remains constant, while the path length for diffusion will be reduced, often via zero order kinetics. Further, these mechanisms may determine failure release modes. For example in the context of coated products, polymer mechanical properties will determine the point at which the osmotic differential across the membrane results in rupture, leading to a burst release of the agrichemical.
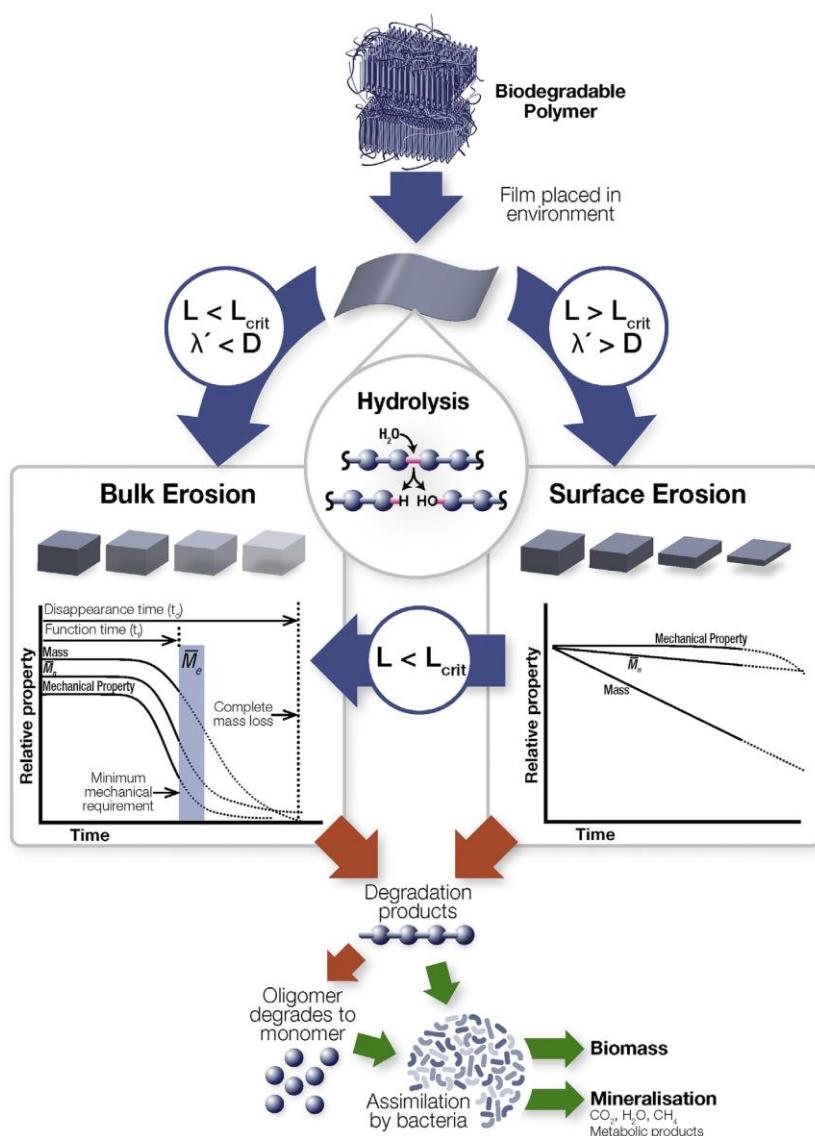
Figure 2.4: Diagram showing the mechanisms of biopolymer degradation from Laycock et al.[106]. L = thickness of the polymer film, L_crit = the thickness of the film at which the mode of degradation switches from surface to bulk erosion, λ = rate of polymer chain hydrolysis, D = rate of diffusion in the polymer. Reproduced with permission from Elsevier.

2.5 Modelling release

Depending on their application, controlled release agrichemicals can be formulated very differently. Before a model can be developed, it is necessary to understand the materials being studied. Firstly, the chemicals that make up the materials and their properties need to be defined. The next step is to describe the geometry of the materials, outlining the dimensions, shape and configuration of the formulation.

2.5.1 Design considerations for controlled-release materials

1. <u>The components</u>

For most controlled release agrichemicals, there are only two types of components:

1.   the agrichemical(s) that is/are being released;
2.   the encapsulating material(s) that allows the gradual mobilisation of the agrichemical.

The dominant physical and chemical properties of these components that influence release kinetics are listed in Table 2.1. The interaction between the encapsulating material and the agrichemical being released can also influence the release rate.[107-108] The chemistry of the components will determine the intermolecular forces between them, whether these comprise van der Waals interactions and hydrogen bonding or ionic attractions/repulsions or, less commonly, covalent linkages. The physical state of the agrichemical, whether it is solid, liquid or gas, dramatically affects the intermolecular interactions between encapsulating material and agrichemical, the distribution within material and the resulting release profile. This review considers crystalline agrichemicals only, with liquid and gaseous formulations being out of scope.

Table 2.1: Key physical and chemical characteristics for the design and modelling of controllled release agrichemical formulations

	Agrichemical	Encapsulating material
Physical properties	Water solubility	Porosity/channelling
	Density	Swellability
	Volatility	Density
	Melting/boiling points	Molecular weight
	Molecular weight	Chain length
	Crystallinity/crystal structure	Crystallinity/crystal structure
Chemical properties	Polarity	Water diffusivity/polarity
	Toxicity	Biodegradability
	Reactivity/stability	Ion exchange potential
	Intra and intermolecular bonding	

A variety of materials have been investigated for encapsulating agrichemicals. The physical and chemical properties of the components determines the mechanism that controls release. The release kinetics from highly hydrophilic matrices, such as hydrogels, are likely controlled by the degree of matrix swelling, which increases porosity and the spacing between polymer chains. Hydrophilic matrices that do not swell are typically controlled by the rate of agrichemical diffusion through the matrix. Where the rate of diffusion is comparable to the rate of matrix degradation, the release may be controlled by both mechanisms. Whereas if diffusion is extremely slow, surface or bulk erosion of the matrix will likely control the release rate.[109]

As mentioned, many controlled-release products use non-degradable polymers, while much of the recent literature focusses on biodegradable and natural polymers. However, very few attempts have been made to integrate biodegradation models to characterise release profiles for agrichemical formulations.[110] Likely, the complexity of the mechanisms involved make this challenging. However, a significant effort has been made for controlled-release drug delivery, as reviewed by Siepmann and Göpferich[111], Siepmann and Siepmann[112] and Ford Versypt et al.[109]. The mechanistic models reviewed aim to account for: polymer chain cleavage and the resulting acceleration of diffusion through the polymer; polymer erosion, which reduces the diffusion path length through the polymer and increases matrix porosity; and the breakdown of the polymeric structure entirely. These models require an understanding of the nature and rate of polymer degradation, whether it degrades via bulk or surface erosion, the rate of chain cleavage, and the potential and effect of autocatalysed chain cleavage through the formation of acidic end groups.[109, 111] For agrichemical formulations, further

complexity arises due to differing soil properties (texture, pH, aeration, microbial communities etc.), and climatic conditions (temperature, rainfall, etc.) which affect the rate of polymer degradation.

2. <u>Geometry and size</u>

The size, shape and configuration of formulations vary significantly in the literature and in commercial products. In general, formulations are approximated to be either spherical or cylindrical, ranging from nanoscale powders to pellets several millimetres in size. The particle size will affect the mode of field application, where nano-scale emulsions can be sprayed, while millimetre size granules need to be mechanically spread.

The configuration of agrichemicals and encapsulating materials form either coated formulations, where the encapsulating material coats the agrichemical, or distributed/matrix materials, also known as monolithic dispersions, where the chemical is dispersed through the encapsulating material (Figure 2.5). The manufacturing method determines the resulting formulation configuration. Emulsion precipitation, extrusion, cold pressed tablets, solvent casting, among other techniques, all produce distributed materials, while spray coating is generally the only method for coated formulation production.
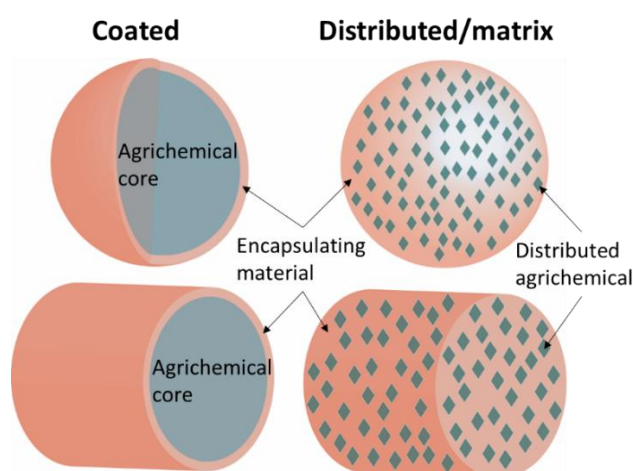
Figure 2.5: Classification of controlled release devices as defined by Siepmann and Siepmann[113] based on the i) component configuration ii) the ratio of initial loading concentration to solubility and iii) shape.

Typically, the most economical products are coated materials, since they have the highest agrichemical loading and use minimal material to control the release. These products have a permeable membrane that allows gradual dissolution and mobilisation of an agrichemical core. Matrix systems are less common for commercial controlled release fertilisers (CRFs), but are frequently presented in the literature since they are easier to produce in the laboratory. Matrix systems

are, however, more commonly used for the controlled delivery of pesticides and herbicides due to their extended release times (up to several years), lower application rates (reducing pressure on the required agrichemical loading), and the use of nanoscale emulsions.[114]

3. <u>Agrichemical loading</u>

The loading defines the agrichemical to polymer ratio. For coated materials, this ratio changes the coating thickness, increasing the diffusion path length and/or the mechanical properties and/or the time for degradation of the coating. Trinh et al.[115] investigated the effect of coating thickness by fitting a diffusion model to release data from Shaviv et al.[116] for modified polyolefin (MPO) coated urea granules. The linear release rate was shown to be proportional to the inner core radius squared over the thickness of the polymer coating (R_0^2/l):

$$Release\ rate = \left(1.6 + 1.33\left(\frac{R_0^2}{l}\right)\right) \times 10^{-12}\ mol/s$$

This is in agreement with diffusion theory. In theory, the diffusive flux during the constant release stage should be independent of the particle size, but inversely dependent of the thickness of the coating. Since the release rate is the flux multiplied by the area available for release, it is expected that the release rate will be dependent of the square of the radius.

For distributed materials, the loading defines the average distance between agrichemical particles, so increasing loadings typically accelerates release. When the loading becomes sufficiently high, particles will contact each other, producing a continuous network and resulting in rapid mobilisation. This loading is known as the lower percolation threshold.[117] However, few authors have identified this threshold. Bajpai and Giri[118] studied the effect of potassium nitrate (KNO_3) loading on release from an interpenetrating polymer network of carboxymethyl cellulose, plyethylene glycol and crosslinked polyacrylamide. Increasing KNO_3 loading from 23 wt.% to 33 wt.% increased mass of KNO_3 release after 16 days by 18%, with a further 13% release at 43 wt.% loading. Volova et al.[119] compared a 10 wt.% loading of the fungicide tebuconazole in PHB solvent cast films, cold-pressed pellets and solvent precipitated granules to 50 wt.% loading. The increased loading dramatically accelerated the release kinetics, with a >4 fold increase in fungicide release after 63 days in soil for all materials studied. Again, controlled-release drug research has studied this effect in more detail.

Siegel et al.[120] studied the effect of loading on the release of bovine serum albumin (BSA) from solvent cast ethylene acetate copolymer films. For materials with loadings at and above 450 g.kg^{-1}, rapid and complete release was realised. At loadings below 450 g.kg^{-1}, the amount of BSA entrapped in the polymer matrix increases, following a sigmoidal response with loading. Some studies have investigated the influence of drug particle size on the release kinetics and the percolation threshold.

Millán et al.[121] studied KCl release from Eudragit® RS PM with five KCl particle size fractions with at least eight different drug loadings for each particle size. A positive linear relation was found between the drug percolation threshold and the drug particle size. This indicates that for larger particles, a higher loading is required to generate connected clusters.

It is important to have a clear understanding of the effect of these design considerations because the upfront material design will determine the mechanisms that control release. When the mechanisms are clear, mathematical models can be developed to quantify and compare release rates and to aid formulation design.

2.5.2   *Mechanistic models*

Mechanistic mathematical modelling of controlled-release agrichemicals has largely been limited to the prediction of release kinetics from coated formulations, with empirical and semi-empirical modelling deployed for matrix-type formulations.[110] Solving the mass balance and transport equations varies in complexity depending on key assumptions about the conditions of the release media (finite or infinite) and initial and boundary conditions considered. The simplest models for coated formulations assume:

1. a perfect shape and size: sphere, cylinder, plane
2. perfect sink conditions, i.e., the concentration of the agrichemical outside the controlled-release material is negligible
3. coatings have a consistent thickness and uniform properties
4. dissolution in the core is rapid compared to the transport processes and a complete layer of dissolved agrichemical is created

Transport processes are commonly predicted using Fick's first and second law of diffusion. The release from sulfur-coated urea (SCU) is driven by the formation of cracks and pores in the sulfur coating. Jarrell and Boersma[122] describe the two-stage release profile (Eq. 2.8 and Eq. 2.9) using Fick's first law of diffusion to simulate the transport of urea along the cracks in the coating. During the first phase, the solid urea core is dissolving, resulting in a saturated urea solution in the core, with perfect sink conditions assumed outside the pellet. In the second phase, the urea has completely dissolved and the urea concentration in the core declines relative to the mass release, with the rate of release defined by:

$$\frac{d(M_t/M_\infty)}{dt} = \left(\frac{D}{M_0}\right)\left(\frac{A_p}{\Delta x_p}\right)C_{sat} \qquad \text{Eq. 2.8}$$

for the constant release rate phase, and

$$\frac{d(M_t/M_\infty)}{dt} = \left(\frac{D}{M_0}\right)\left(\frac{A_p}{\Delta x_p}\right)(1 - M_t)\rho_s \qquad \textbf{Eq. 2.9}$$

for the falling rate period,

where M_∞ and M_t denote the starting urea mass and the absolute cumulative amount of urea released at time t, respectively, D is the diffusivity of urea in water, C_{sat} is the solubility of urea, ρ_s is the density of urea, A_p is the cross-sectional area of the pore and Δx_p is the length of the pore.

Similarly, Fick's law of diffusion applies for the modelling of polymer-coated materials. In this case, the diffusivity relates to the migration of the agrichemical through the polymer, rather than via openings. A lag time (t_L) is included to account for the time for water to permeate the polymer coating, resulting in a three-phase model.[116] The lag time here (Eq. 2.10) only accounts for the time for water to permeate the coating and does not account for the time for the reverse diffusion of the agrichemical back through the coating. As such, the fractional release for the constant release rate phase (Eq. 2.11) and the decaying release rate (Eq. 2.12) predict the fraction of the agrichemical released from the core, as opposed to the fraction released from the pellet to the soil.

$$\frac{M_t}{M_\infty} = \begin{cases} 0, & 0 < t < t_L & where\ t_L = \dfrac{\varepsilon_g r_0 l_0}{3P_w \Delta p_{wv}} & \textbf{Eq. 2.10} \\[2mm] \dfrac{3P_s C_{sat}}{r_0 \rho_s l_0}(t - t') & t_L < t < t^* & where\ t^* = t' + \left(1 - \dfrac{C_{sat}}{\rho_s}\right)\left(\dfrac{r_0 l_0 \rho_s}{3P_s C_{sat}}\right) & \textbf{Eq. 2.11} \\[2mm] 1 - \dfrac{C_{sat}}{\rho_s}\exp\left[-\dfrac{3P_s}{r_0 l_0}(t - t^*)\right] & t \le t^* & & \textbf{Eq. 2.12} \end{cases}$$

where ε_g is the void fraction in the granule, r_0 is the radius of the core and l_0 is the coating thickness Δp_{wv} is the differential water vapour pressure between the ambient and saturated soil solution, P_w and P_s are the permeability coefficients of water and agrichemical solute through the polymer coating, C_{sat} and ρ_s are the saturation concentration and density of the agrichemical.

For a non-swelling distributed system, Higuchi[123] derived release kinetic models for the release of drugs distributed in ointments. The models combine a simple mass balance with the one-dimensional Fickian diffusion rate law, assuming a linear concentration profile (quasi-steady state) from the moving drug dissolution front (saturation concentration) to the surface of the material (assumed zero). These assumptions are valid when the loading concentration is much greater than the active agent solubility and near perfect sink conditions. The classic Higuchi equation (Eq. 2.13) models diffusive release from a distributed slab geometry assuming pseudo-steady state:

$$M_t = A\sqrt{Dt(2C_0 - C_s)C_s} \qquad \textbf{Eq. 2.13}$$

where M_t is the amount released, A is the surface area, C_0 initial active agent loading and Cs is the solubility. This equation was extended to account for the generation of pores as a result of the diffusion of dissolved agent:[124]

$$M_t = A \sqrt{\frac{D\varepsilon}{\tau} t (2C_0 - \varepsilon C_s) C_s}$$

Eq. 2.14

$$\varepsilon = \varepsilon_0 + \frac{C_0}{\rho}$$

Eq. 2.15

where ε is the porosity of the matrix and τ is a tortuosity factor. The change in porosity can be described as the initial porosity plus the volume previously occupied by the released substance (Eq. 2.15). This theory has been applied to develop 1-D models for release from cylindrical[125] (Eq. 2.16) and spherical[126] (Eq. 2.17) distributed matrices, accounting only for radial diffusion.

Cylindrical
$$M_t/M_\infty - \frac{3}{2}[1 - (1 - M_t/M_\infty)^{\frac{2}{3}}] = -\frac{3D}{R^2}\frac{C_s}{C_0}t$$

Eq. 2.16

Spherical
$$M_t/M_\infty + \left(1 - M_t/M_\infty\right) \times ln\left[1 - M_t/M_\infty\right] = \frac{4D}{R^2}\frac{C_s}{C_0}t$$

Eq. 2.17

These equations have been widely applied in the application of diffusion-controlled drug delivery[113], but are rarely used to model the controlled release of agrichemicals from distributed/matrix type materials. Authors have preferred the simpler and more broadly applicable semi-empirical models (see Section 2.5.2) of Peppas[127] and Ritger and Peppas[128] derived from the Higuchi equation.

To account for diffusion driven release in both the radial and axial directions, Fick's second law of diffusion (Eq. 2.20) can be used:

$$\frac{\partial c}{\partial t} = \frac{1}{r}\left\{\frac{\partial}{\partial r}\left(rD\frac{\partial c}{\partial r}\right) + \frac{\partial}{\partial z}\left(rD\frac{\partial c}{\partial z}\right)\right\}$$

Eq. 2.18

where c is the concentration of the agrichemical in the polymer at time (t), as a function of the radial (r) and axial (z) position from the centre of the cylinder and D denotes the diffusion coefficient of the agrichemical in the polymer. An analytical solution to this partial differential equation for the fractional release as a function of time was derived by Vergnaud[129] as an infinite series of exponential decay terms (Eq. 2.21). Fick's second law is solved according to the initial and boundary conditions of initially homogeneous distribution and perfect sink conditions, giving:[129]

$$\frac{M_t}{M_\infty} = 1 - \frac{32}{\pi^2} \sum_{n=1}^{\infty} \frac{1}{q_n^2} exp\left(-\frac{q_n^2}{R^2}Dt\right) \sum_{p=0}^{\infty} \frac{1}{(2p-1)^2} \times exp\left(-\frac{(2p+1)^2\pi^2}{L^2}Dt\right)$$

Eq. 2.19

where q_n are the zero order roots of the Bessel function of the first kind, and R and L are the radius and length of the cylindrical pellet, respectively.

2.5.3   Semi-empirical and empirical modelling

Semi-empirical and empirical modelling is helpful to parameterise data sets and make statistical comparisons between release profiles. Peppas[127] generalised the Higuchi equation to characterise Fickian and non-Fickian diffusion controlled materials. The Peppas equation (Eq. 2.20) provides a short-time approximation of Fick's 2nd law with initial agent loading less than its solubility:

Eq. 2.20

$$M_t/M_\infty = kt^n$$

where k is a kinetic constant and the exponent n indicates the mechanism controlling release, as described in Table 2.2.[112]

Table 2.2: Peppas equation exponent for various release mechanisms and device geometries.[112]

Release Mechanism	Exponent, n		
	Thin film	Cylinder	Sphere
Fickian Diffusion	0.5	0.45	0.43
Anomalous transport	0.5<n<1.0	0.45<n<0.89	0.43<n<0.85
Polymer swelling	1.0	0.89	0.85

Hundreds of authors in the controlled release agrichemical space have used the Peppas equation. The simplicity of the model makes it a rapid tool to gain preliminary understanding of the controlling mechanism(s) and provides a quantitative comparison between experimental runs. Other commonly used empirical models are listed below, with their use simply dependent on best fit to parameterise the release profiles.

Zero order kinetics	$M_t = M_\infty - kt$	**Eq. 2.21**
First order kinetics	$\frac{M_t}{M_\infty} = a - b \times e^{-kt}$	**Eq. 2.22**
Weibull model	$\log[-\ln(1-m)] = b \times log(t-T_L) - \log(a)$	**Eq. 2.23**
Hixson-Crowell model	$M_\infty^{1/3} - M_t^{1/3} = kt$	**Eq. 2.24**

where k is a kinetic constant, and a, b, m are other constants.

2.6   Identified gaps in the current state of knowledge

From reviewing the published literature, a number of key research gaps were identified:

1. *Limited research investigating the viability of extrusion processing for the fabrication of controlled-release agrichemicals*

Commonly, solvent-based approaches are utilised for laboratory-scale fabrication of the controlled-release agrichemical formulations, particularly for micro-encapsulation. Cold-pressed pellets have also been reported. Rarely are the materials melt compounded, and rarer still are they extruded. Yet, extrusion processing is a simple, industrially relevant, high throughput fabrication technique, with very little to no materials preparation, nor hazardous and expensive solvents required. One limitation is the high melt temperature of some polymers, leading to thermal decomposition of the agrichemical. However, this has been underexplored, as some agrichemicals have high thermal stability, while several biodegradable polymers have very low melting temperatures. To my knowledge, there are no studies to date on the extrusion fabrication of controlled-release NIs.

To my knowledge, Otey et al.[77], Minet et al.[78] and Bishop[79] are the only studies that consider controlled-release NIs. However, the complexity of the fabrication processes used and the resulting release profiles limit the applicability of these studies for product development. These studies aimed to extend the lifetime of DCD, but not within tropical agricultural settings. Further, there are no studies to date that report extrusion fabrication of controlled-release nitrification inhibitors.

2. *The mechanisms that control release of agrichemicals from biodegradable polymeric matrices into soil largely remain unclear*

The use of non-degradable polymers for the controlled-release of agrichemicals is widely recognised as unsustainable. This has fuelled extensive research on developing biodegradable materials, which range widely in physical and chemical properties. Consequently, the mechanisms controlling the agrichemical mobilisation will differ depending on the material selection. However, clarity of these mechanisms is still lacking. Many authors rely on the exponent of the Peppas equation (Eq. 2.20) to postulate the release mechanism, following the rules described in Table 2.2, without any physical evidence to support that mechanism proposed. In the case of long-term release profiles, many authors correlate polymer degradation with release, but lack clear evidence to support causation. Further detailed assessments and definitive evidence is still needed to fully understand the complex nature of release from these materials.

*3. **A lack of understanding of how key material properties and processing parameters affect release kinetics.***

Few authors have investigated processing parameters on release. Some of the most obvious include the grind size of the crystalline agrichemical, the agrichemical loading, and the matrix hydrophilicity.

.

CHAPTER 3

Project aims & objectives

3.1 Overall project objectives

From reviewing the literature, DCD was identified as an effective nitrification inhibitor to reduce nitrogen losses through reduced nitrate leaching, runoff and lower denitrification to nitrous oxide, a potent greenhouse gas, and increased nitrogen uptake efficiency and crop yield. However, since the half-life of DCD in soil decreases exponentially with temperature, the efficacy of DCD in tropical agriculture has not been realised.

The primary aim of this project was to increase the duration of effective DCD concentration to inhibit nitrification in tropical soils through controlled-release. However, the lessons from this thesis are relevant for the controlled-release of any soluble, crystalline agrichemical, with DCD used here as a model compound to develop understanding of the mechanisms and kinetics of release. The bacterial polyester, poly(3-hydroxybutyrate-*co*-3-hydroxyvalerate) (PHBV) was identified as a biodegradable, hydrophobic polymer that can achieve long-term release. Furthermore, this polymer is commercially produced and is the cheapest and most available polymer within the PHA family. As such, this polymer was a focus point of this project. The secondary aim of this work was to develop detailed mechanistic understanding of the release of soluble, crystalline agrichemicals from hydrophobic, biodegradable polymer matrices fabricated through extrusion processing.

3.2 Core research questions

Research question 1

Is extrusion processing a feasible technique for the fabrication of controlled-release DCD pellets?

While extrusion is a commercially relevant technique for large-scale fabrication of controlled-release pellets, it is limited by the thermal decomposition of the agrichemical in question. As such, the first step was to access the thermal stability of DCD. From there, suitable biodegradable polymers that could be processed at temperatures lower than the thermal decomposition temperature of DCD were selected. Finally, the processing conditions were optimised to achieve complete melting of the polymer (or gelatinisation in the case of thermoplastic starch), good mixing and consistent strand size.

Research question 2

What is the rate of release of DCD from different biodegradable polymer matrices and what are the contributions and timing of the different mechanisms that control the mobilisation?

With the feasibility of extrusion processing confirmed, controlled-release DCD pellets were fabricated. The release kinetics were then monitored in a number of different release media, including water in specimen containers and sand/soil mixtures with ratios of 1:0, 3:1, 1:1, 1:3 and 0:1 and

sterilised soil using leaching columns. By studying release in these media the contribution and timing of the different mechanisms (surface release, diffusion through the polymer, degradation of the polymer etc.) could be separated out, since there should be no polymer degradation in water, sand or sterilised soil. Further, the effect of release into a tortuous media such as sand or soil was compared to water.

Research question 3

Where does the percolation threshold lie and how is it affected by the grind size of the DCD crystals?

By studying the release at different DCD loadings, a threshold can be determined at which DCD crystals become interconnected resulting in rapid release, known as the percolation threshold. The outcomes from Chapter 5 and 6 highlighted the importance of DCD crystal size. As such, DCD was ground and sieved into different size fractions to investigate whether smaller crystals were better encapsulated in the PHBV matrix, thus affecting the release profiles and mechanisms.

Research question 4

How does the hydrophilicity of the biodegradable polymer matrix influence release kinetics and does release follow an Arrhenius dependence on temperature?

From Chapter 5, the release from the hydrophilic thermoplastic starch occurs rapidly, with complete release within 1 day in water. In contrast, PHBV released ~50% after 140 days in water. The objective behind this research question was to increase the rate of release from PHBV, but still achieve an extended release profile. As such, polycaprolactone, another semi-crystalline, hydrophobic polyester, was selected to blend with PHBV. While still hydrophobic, the diffusivity of water in PCL is ~15 times higher than for PHBV. By studying release from different ratios of PHBV and PCL, the effect of matrix hydrophilicity could be investigated. Due to the increased water diffusivity in PCL, it was hypothesised that diffusion through the polymer matrix would increase, and as such a diffusion model could be fit to the release data. To determine if the diffusivity followed an Arrhenius dependence on temperature, release was studied at three different temperatures. Answering this research question steps us closer to tailoring release kinetics through material design.

CHAPTER 4

Experimental methods

4.1 Overall methodology

To address the core research questions outlined in Chapter 3, tightly controlled experiments were designed. Firstly, the fabrication of materials through extrusion processing was an important decision to align the knowledge gained from the results with industrial techniques. Further, this simple technique allowed rapid fabrication of material for the experimentation reported here, as well as enabling the production of sufficient quantities for pot, plot and field trials to be conducted by the Queensland Department of Agriculture and Fisheries.

To tease apart the contribution of polymer degradation to the release kinetics, leaching columns were constructed and rate of DCD release was quantified in various media, including biologically active soil, sterilized soil, sand and sand:soil mixtures (Chapter 5). From this work, water release was realized as the best method to rapidly characterize a wide range of controlled-release materials. Water release studies were used to understand the effect of particle size and loading of DCD in a PHBV matrix (Chapter 7), as well as the effect of temperature on DCD release from PHBV/PCL blends (Chapter 8). To improve our understanding of the controlling mechanisms, several imaging techniques were employed, including electron microscopy, Raman mapping and, in particular, micro-computed X-ray tomography (μ-CT). High-resolution μ-CT (0.4 μm resolution) allowed 3-D characterization of the microstructure of the matrices, revealing the complexity of the controlling mechanism (Chapter 6).

The following sections provide details on the materials and experimental methods used through the project. Experimental details that pertain to individual studies are presented within the relevant chapter.

4.2 Materials

Dicyandiamide (DCD), 99%, and polycaprolactone (PCL), with weight-average molecular weight (M_w) of 120,000 g.mol^{-1}, were purchased from Sigma Aldrich, Australia. Poly(3-hydroxybutyrate-*co*-3-valerate) (PHBV) with ~1 mol% HV content (as determined by ^{1}H NMR analysis), 68% crystallinity[130] and a weight-average molecular weight of 590 kDa was supplied by TianAn Biopolymer, China, under the trade name of ENMAT Y1000. Wheat starch was purchased from New Zealand Starch Ltd. Deuterated water (99.9% D_2O) was purchased from Novachem Pty. Ltd., Australia.

A 20 kg soil sample was supplied from a sugarcane field in Wangan, QLD, Australia, and screened through a 2 mm sieve. The soil was analysed by SWEP Laboratories, Keysborough, VIC, Australia, see Table S1 for details. Briefly, the soil pH was 5.5-6.0, with a cation exchange capacity

(CEC) of 14.2-14.6 meq/100 g. The clay content, organic carbon content and total organic matter were 31.7 ± 1.7%, 2.2-2.3% and 4.4-4.6%, respectively.

4.3   Extrusion fabrication of controlled-release NIs

Formulations were melt compounded at 80-180 °C using a 40/1 L/D Eurolab (Thermo-Scientific) co-rotating twin-screw extruder (straight screw profile) with a 3 mm circular die. Crystalline DCD was ground and mixed with biopolymer(s) to produce the desired inhibitor loading. The DCD-biopolymer mixture was then flood fed into the extruder at a rate of ~5 g/min. Extruded strands were left to crystallise at room temperature for >2 h. Strands were then pelletised with a Labtech LZ-80 Pelletiser into roughly 3×3 mm cylindrical pellets. A schematic of the extruder is shown in Appendix A, Figure A-1.

4.4   Testing release kinetics

4.4.1   Water release

The release kinetics of DCD into water from the biopolymer matrices was monitored at temperatures of 10 °C (in a temperature-controlled refrigerator), 23 ± 1 °C (room temperature, benchtop) or 40 °C (temperature-controlled, heated chamber). One to five pellets (~30-40 mg each) were selected at random and photographed with a 0.5 mm graduated ruler for measuring the length and diameter of each pellet in ImageJ, which was required for modelling the release kinetics in Chapter 8. The pellets were added to 50 mL of distilled water in a 70 mL plastic specimen container, with experiments conducted in triplicate. Samples were taken at several time points, depending on the study, and the DCD was quantified using ultraviolet-visible (UV-Vis) spectroscopy (see Section 4.5.3).

To check the mass balance, the DCD remaining in the pellet(s) at the end of the experiment was quantified. The pellets were dissolved in 3 mL of chloroform at 70 °C for two to four hours. The DCD was then extracted from this solution with 5 mL of water by vortexing the mixture for 30 s. DCD in the water phase was then quantified using UV-Vis spectroscopy.

4.4.2   Leaching columns

Incubation columns were constructed following a similar approach to Medina et al.[131] to study the effect of polymer degradation on release kinetics. To achieve this, various media were used with differing degrees of biological activity, including sand, soil, sterilised soil and sand:soil mixtures (1:3, 1:1 and 3:1). The leaching columns (Figure 4.1) were constructed using 20 cm lengths Holman 50

mm polyvinyl chloride (PVC) pressure pipe, with two 50 mm PVC pressure caps. The bottom cap was connected to a threaded ¼" male brass fitting with a straight 7 mm barbed tailpiece. Circles of 0.5 mm stainless steel woven wire mesh, with 2 mm holes, were cut and placed in the bottom cap. The woven mesh was used to suspend a 90-mesh T316 stainless steel wire cloth off the bottom of the column. The wire cloth was used to prevent excessive loss of sand and soil out the bottom of the column during leaching events.

Each column was connected to a 500 mL filtering flask to collect leachate. Initially, 200 g of sand was added to the base of each column. Seven DCD-PHBV pellets (200-235 mg) were mixed through 100 g of the release media and added onto the sand. Above this, a final 50 g aliquot of release media was added. Water was then added to achieve 80% of the saturation moisture content (SMC). The SMC of the various release media were determined using a hydrostatic funnel system and calculated using Equation 4.1:

$$SMC = \frac{m(saturated\ sand/soil) - m(dry\ sand/soil)}{m(dry\ sand/soil)} \qquad \text{Eq. 4.1}$$

where m is the mass in grams.

An intensive leaching regime was used to maximise the recovery of DCD. Leaching of the columns was conducted with two aliquots of leachate, totalling 150 mL. Firstly, the caps were removed and the tubing connecting the columns to filtering flasks were pinched to prevent flow. The first aliquot of 100 mL of leachate was added to the headspace of the column and left for 5 min to extract the DCD. The clips were then removed from the tubing to allow the leachate to flow from the columns to the flasks. The filtering flasks were connected to the vacuum line and the columns were drained until the leachate stopped flowing. The second aliquot of 50 mL of leachate was then added, left for a further 5 min and pulled through with the vacuum. The total leachate volume was measured and a 20 mL sample was filtered through a 0.45 µm syringe filter. Finally, the columns were weighed and topped back up to 80% of SMC. DI water was used as the leachate for sand and γ-irradiated soil to minimise biological activity. All other columns contained biologically active soil. For these, a nitrate mineral salts nutrient media was used, at a 1:100 dilution with DI water, to support biological activity. See Table A-2 in Appendix A for details on the nutrient media used. DCD in the leachate was quantified with ultra-pressure liquid chromatography (UPLC), see Section 4.5.4.
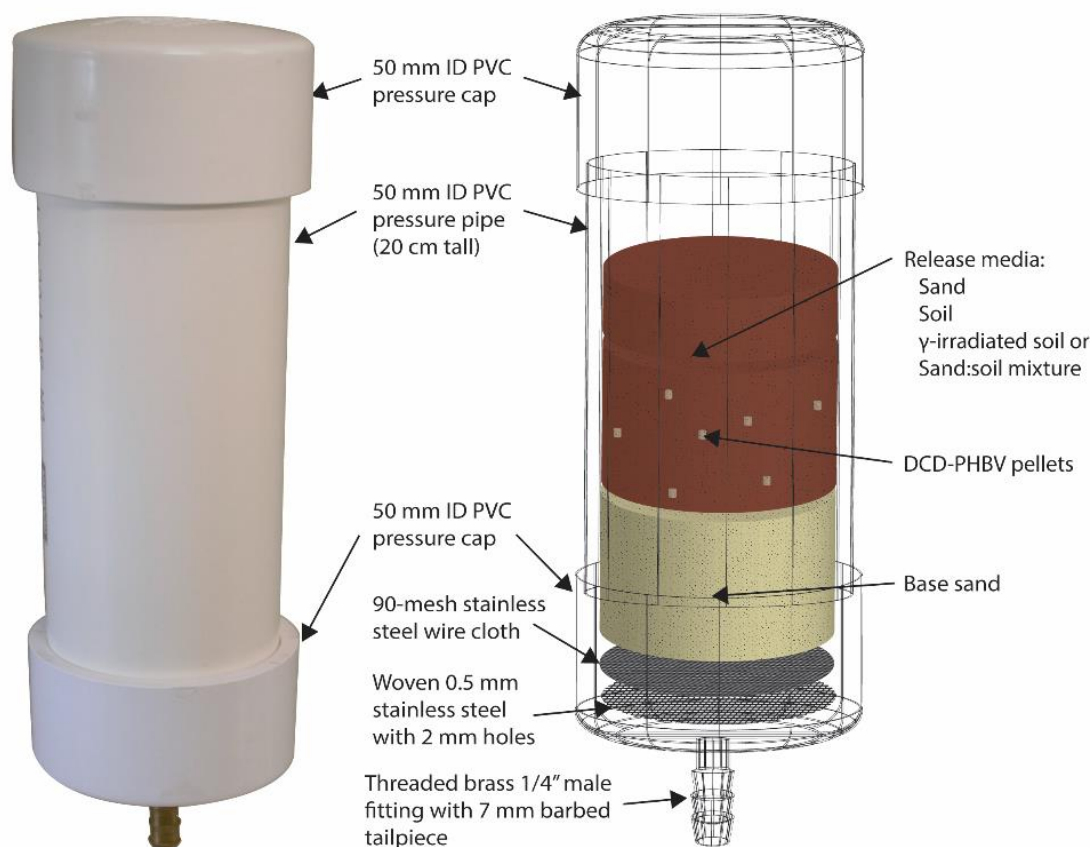
Figure 4.1: Photograph (left) and schematic of the incubation column (right) built to study the release of DCD from PHBV pellets into sand, soil, γ-irradiated soil and sand:soil mixtures.

After 26 weeks, the columns were decommissioned. The release media was washed through a 2 mm sieve to recover the pellets. Where not all the pellets were recovered, the soil was further filtered and manually sorted to find any fragments of pellets <2 mm. The recovered pellets were washed with DI water, dried in a vacuum oven overnight at 45 ℃, and weighed. The DCD was extracted from four pellets from each column individually, as described in Section 4.4.1, and quantified with UPLC.

4.5   Analysis and quantification of DCD

4.5.1   Thermogravimetric analysis (TGA)

For the thermogravimetric analysis (TGA) of DCD a Mettler-Toledo TGA/SDTA 851e under N_2 atmosphere was employed. DCD powder (~5 mg) was analysed in a standard 40 µL Al crucible, with the cap punched with a small pin. Samples were heated from room temperature to 300 ℃ at a rate of 10 ℃ per min, pausing at 100 ℃ for 3 min to remove any residual water.

4.5.2   Nuclear magnetic resonance (NMR)

The thermal stability of DCD during the high temperature extrusion processing was determined

with carbon nuclear magnetic resonance (^{13}C-NMR) spectroscopy. The pure DCD spectra was compared to DCD extracted from an extruded DCD-PHBV pellet. First, 20 mg of as received DCD was dissolved in 2 mL deuterated water (D_2O). For the extruded sample, 60 mg of DCD-PHBV (~2 pellets) was dissolved in 3 mL of chloroform at 70 °C over ~3 h. The DCD was then extracted by adding 2 mL D_2O and vortexing for 30 s. Samples were analysed on a Bruker Avance 500 MHz high-resolution NMR spectrometer at a constant temperature of 298 K. The spectra were acquired with a pulse program of zgpg30 over a spectral width of 230 ppm for ~16 h. The spectra were acquired and processed with Bruker TopSpin 3.5 software package.

4.5.3   *Ultraviolet-visible light (UV-Vis) spectroscopy*

For water release studies, aqueous DCD samples were quantified using UV-Vis spectroscopy. 200 µL samples were loaded into a Greiner UV Star 96 well plate and read at 230 nm with a Biotek Powerwave XS plate reader. A linear calibration curve was obtained from reference samples with concentration ranging between 0 and 100 mg DCD.L^{-1}.

4.5.4   *Ultra-pressure liquid chromatography (UPLC)*

Due to the complex chemistry of the soil solution, DCD in the leachate from the leaching columns was quantified using a separation technique. A UPLC method modified from Ge et al.[132] as developed to separate and quantify the DCD in the leachate. The UPLC (Waters, Milford USA) was equipped with a BEH HILIC 1.7 µm 2.1 x 100 mm analytical column maintained at 30°C and a tuneable UV detector at 220 nm. The flow rate was 0.4 mL/min. Separation was achieved by a solvent gradient from H_2O to 4% acetonitrile (HPLC grade, Merck KGaA, Darmstadt, Germany) during a 7 min run. Retention time for DCD was 0.71 minutes. 2 µL of sample or DCD standard was injected for analysis.

4.6   Imaging techniques

4.6.1   *Scanning electron microscopy (SEM) couple with energy dispersive X-ray spectroscopy (EDX) mapping*

A JEOL6460 scanning electron microscope coupled with energy dispersive X-ray (SEM/EDX) spectroscopy provided surface morphology micrographs and surface inhibitor distribution maps for the transverse and longitudinal surfaces of a fresh DCD-PHBV pellet. Samples were mounted to a metal stub, carbon coated to 30 nm thickness and imaged at 10 kV accelerating voltage and 10 mm working distance.

4.6.2   Mapping with Raman spectroscopy

Raman spectroscopy was used to map DCD, PHBV and PCL. The DCD-biopolymer pellets were cross-sectioned and Raman maps (30x30 µm, 100x100 pixels, 100x objective) acquired at 50 ms integration time/pixel, using an Alpha 300 Raman/AFM (WITec GmbH, Ulm, Germany), equipped with a frequency-doubled continuous-wave Nd:YAG laser to obtain a 532 nm excitation line. The stretching vibration of the CN bond in DCD at 2156 cm^{-1} was used to create the map for DCD. PHA signal was binned around 846 cm^{-1} (-C-CH out-plane bending) vibration and PCL data was collected around the 2920 cm^{-1} CH stretching vibration. The Raman signal was processed to remove cosmic rays; the data was Savitzky-Golay smoothed and background subtracted using Project FOUR software.

4.6.3   Micro-computed X-ray tomography (µ-CT)

For Chapter 6, high-resolution (down to 0.5 µm) µ-CT data was attained using a ZEISS Xradia 520 Versa (ZEISS microscopy customer center, Shanghai). For Chapters 7 and 8, µ-CT images were acquired over 360° with a Skyscan 1272 (Skyscan, Bruker, Belgium), using an accelerating voltage of 40-50 kV and a current of 200-250 mA. The following acquisition parameters were used, varying slightly depending on the X-ray transmittance through the sample: voxel size of 5-7 µm, exposure time of 150-225 ms, rotation step of 0.4°, no filter, 4×4 binning, and averaging of 3. NRecon Reconstruction Software (using Feldkamp algorithm) was used for reconstruction. All µ-CT data was processed with CTan software (Skyscan, Bruker, Belgium), conducting 2-D and 3-D analyses of the void space.

4.7   Polymer characterization

4.7.1   Differential scanning calorimetry (DSC)

A differential scanning calorimeter, Q2000 (TA Instruments), under a constant nitrogen flow of 50 mL.min^{-1} was used to determine the thermal properties of the DCD-biopolymer composites. Samples of 4.0 to 8.0 mg were placed in a sealed aluminium pan and were analysed using standard DSC heating and cooling scans. Each sample was heated from 25 °C to 185 °C at 10 °C.min^{-1} and kept isothermal for 0.3 min, and then cooled to -10 °C at 10 °C.min^{-1}. The melting temperature, T_m, and enthalpy of fusion, ΔH_m, were determined from the first heating cycle (since any slow crystallising components of PHBV blends will not crystallise in time for the second heating scan[133]). The melt crystallisation temperature, T_{mc}, was determined from the cooling cycle. The crystallinity of the PHBV and PCL components was estimated assuming an enthalpy of fusion of the crystalline

regions of 146 J.g^{-1} and 139.5 J.g^{-1}, as determined by Barham et al.[134] and Crescenzi et al.[135], respectively. Given that the HV content of PHBV was only ~1%, the enthalpy of fusion of a theoretically 100% crystalline PHB was appropriate in this case. For the blended materials, the crystallinity for each phase was estimated based on ratio of PHBV to PCL, accounting for the DCD loadings. Experiments were run in duplicate.

4.7.2 *Gel permeation chromatography (GPC)*

GPC was used to compare the molecular weight of the biopolymer blends before and after extrusion and after release in Chapter 8. Samples were dissolved in high performance liquid chromatography (HPLC) grade chloroform at 25 °C for 30 min for PCL and at 70 °C for 2 hours for the blends containing PHBV, at a concentration of 2.5 mg/mL in a Teflon-lined capped glass tube. An Agilent 1260 Infinity Multi Detector Suite system (Cheshire, UK) was used for the analysis, calibrated with narrowly distributed molecular weight polystyrene standards. A column set consisting of a guard column (Agilent PLgel Guard (5 µm, 7.5 mm × 50 mm)) followed by three columns in series kept at 30 °C: Agilent PLgel 105 A (5 µm, 7.5 mm × 300 mm), Agilent PLgel 103 A (5 µm, 7.5 mm × 300 mm) and Agilent PLgel 100 A (5 µm, 7.5 mm × 300 mm). A refractometer, at 30 °C, was used to quantify the biopolymers. A chloroform flow rate of 1 mL/min was used.

CHAPTER 5

Understanding the mobilisation of a nitrification inhibitor from novel slow-release pellets, fabricated through extrusion processing with PHBV biopolymer

Ian Levett, Steven Pratt, Bogdan C. Donose, Richard Brackin, Chris Pratt, Matthew Redding & Bronwyn Laycock

Abstract

Dicyandiamide (DCD) has been studied as a stabiliser for nitrogen fertilisers for over 50 years. Its efficacy is limited at elevated temperatures but this could be addressed by encapsulation to delay exposure. Here, poly(3-hydroxybutyrate-*co*-3-hydroxyvalerate) (PHBV) was investigated as a biodegradable matrix for the encapsulation of DCD. Cylindrical ~3×3 mm pellets were fabricated through extrusion processing with 230 g.kg^{-1} DCD. Release kinetics were monitored in water, sand and both active and γ-irradiated agricultural clay loam soils. Raman maps showed a wide particle size distribution of DCD crystals and indicated that Hitachi's classic moving front theory did not hold for this formulation. The inhibitor release kinetics were mediated by four distinct mechanisms:

i)   initial rapid dissolution of surface DCD

ii) channelling of water through voids and pores in the PHBV matrix

iii) gradual diffusion of water and DCD through layers of PHBV

iv) biodegradation of the PHBV matrix

After ~6 months, 45-100% release occurred, depending on the release media. PHBV is shown to be an effective, biodegradable matrix for the long-term slow release of nitrification inhibitors.

5.1   Introduction

Conventional nitrogen (N) fertilisers are remarkably inefficient. Lassaletta et al.[136] note that more than half of N applied is lost to the environment. Moreover, this poor efficiency rate has been continually decreasing since the inception of the Haber–Bosch process, providing farmers with inexpensive and readily available N fertiliser.[137] Nitrogen loss pathways include the direct volatilisation of urea and ammonia (NH_3); microbial transformations to gaseous nitrogen oxides (NO_x) and nitrous oxide (N_2O) - a potent greenhouse gas; and leaching and runoff as ammonium (NH_4^+), nitrite (NO_2^-) and nitrate (NO_3^-).[6] Hence, poor N use efficiency is associated with both economic losses and considerable contamination of natural environments where N may naturally be scarce.

Nitrification inhibitors can decrease N losses and increase plant uptake. Synthetic nitrification inhibitors, such as dicyandiamide (DCD), 3,4-dimethyl-1H-pyrazole phosphate (DMPP) and 2-chloro-6-(trichloromethyl)-pyridine (nitrapyrin) have been investigated for over 50 years.[73] These compounds target soil microbial enzymes that catalyse the multistep oxidation of ammonium through to nitrate. By retarding these N conversion processes, inhibitors have shown success in increasing crop yields[6] and mitigating environmental impacts.[138-139] The efficacy of nitrogen stabilisers is well-established for temperate and subtropical climates.[6] However, their persistence diminishes with soil

temperature,[73, 140] limiting their applicability in tropical agriculture.

In general, the lack of efficacy of DCD in tropical agriculture has been attributed to its rapid microbial degradation at high temperatures.[8] In theory, the encapsulation and slow release of DCD can extend its effective duration. There are few accounts in the literature for fabrication of slow release nitrification inhibitors. Minet et al.[78] reported the use of a glyoxal-crosslinked hydrogel for the slow release of DCD. For beads that were allowed to dry, 33% was released into soil after 7 days under high rainfall simulated conditions. However, the long-term release was not studied, with experiments limited to 7 days at 5 °C. Bishop[79] produced a reactive layer polyurethane-coated DCD product that had ~50% release over 40 days. However, the production process was complex and application results in a polymer that will persist in the soil.

Controlled release agrichemical formulations predominantly utilise polymers that persist in the environment, such as polyolefins, alkyd resins and polyurethanes.[28] This leads to the accumulation of plastic in agricultural soils. More recently, research has targeted fully degradable materials for the slow or controlled release of agrichemicals. Polyhydroxyalkanoates (PHAs) are a family of polyesters that are both naturally synthesised and metabolised by bacteria. PHAs have been studied for the slow release of pesticides,[98-99, 141] herbicides,[95-97, 100-102] fungicides[103] and urea fertilisers.[93-94, 142] Formulations were produced through various processes, including cold-pressing pellets, solvent casting of films and granules, and coating pellets.

Extrusion processing is an industrially relevant method for the production of controlled release formulations. This simple, high throughput technique allows tight control over processing conditions, including temperature, pressure, shear, and product composition. The pellets produced have a narrow particle size distribution and are suitable for subsequent film coating if desired.[143] However, only a few studies have investigated extrusion processing to fabricate controlled release agrichemicals.[144-145]

Here, novel slow release DCD-PHBV pellets were fabricated using a laboratory scale twin-screw extruder. To date, the relative contribution of diffusion and polymer degradation on release kinetics from biodegradable materials is unclear, limiting accurate and effective design. By conducting controlled experiments in water, sand and active and γ-irradiated soil, the relative contributions of diffusion and biodegradation of the PHBV matrix were elucidated. This provides generic, practical knowledge about release characteristics of active agents from PHBV matrices for an agricultural context.

5.2 Materials and Methods

5.2.1 Materials

Dicyandiamide (DCD), poly(3-hydroxybutyrate-*co*-3-valerate) (PHBV), wheat starch, deuterated water (D_2O) and a 20 kg soil sample from a sugarcane field in Wangan, QLD, Australia, were used for this study. Details on these materials can be found in Section 4.2.

5.2.2 Stability of DCD in soil

The stability of DCD was studied using a high organic content clay loam soil at 30 °C. 3 mg of DCD was added to 25 g of soil in 50 mL specimen containers. Each treatment (three replicates) was brought to 80% saturation water capacity with de-ionised (DI) water. Samples were covered with parafilm, with holes punched through to allow gas exchange, and incubated at 30 °C in dark conditions. DCD was quantified using a destructive sampling approach. DCD was extracted by adding the soil to 100 mL of DI water in a 250 mL Schott bottle and rolled for 30 min. A 20 mL aliquot was syringe filtered (0.45 µm) and DCD was quantified with ultra-pressure liquid chromatography (UPLC), see Section 4.5.4. Samples were taken at time zero and weekly thereafter, for 5 weeks. The saturation moisture content (SMC) of the sand and soil were 240 and 690 $g.kg^{-1}$, respectively, calculated using Eq. 4.1.

5.2.3 Extrusion processing of slow release DCD-PHBV formulations

A general description of the extrusion fabrication technique can be found in Section 4.3. Formulations were extruded at 180ºC with a 3 mm circular die. DCD powder was ground with a mortar and pestle and thoroughly mixed at 250 $g.kg^{-1}$ with the PHBV powder. Plasticised starch (PS) was also formulated with 250 $g.kg^{-1}$ DCD loading as a control. Starch is known to be highly hydrophilic and rapid and complete release - via diffusion - was hypothesised to occur. The starch formulations were extruded with a Eurolab Digital, using a screw profile that included 4 mixing sections. Water was injected at zone 2 with a peristaltic pump to plasticise the starch, calibrated manually to achieve a 60:40 water: starch weight ratio. DCD-PS was extruded at 120 °C to ensure plasticization of the starch. For details on the screw and temperature profiles used, see Figure A-1.

5.2.4 Characterisation of slow release formulations

5.2.4.1 Surface morphology and distribution of DCD

A JEOL6460 scanning electron microscope coupled with energy dispersive X-ray (SEM/EDX) spectroscopy provided surface morphology micrographs and surface inhibitor distribution maps for the transverse and longitudinal surfaces of a fresh DCD-PHBV pellet. See Section 4.6.1 for details.

Raman spectroscopy was used to map DCD crystal location in the centre a fresh DCD-PHBV pellet and for pellets after 4 and 26 weeks in sand. The pellets were embedded in resin (EPON 812) and cross-sectioned employing a Leica Ultracut T ultramicrotome to produce a flat surface roughly in the middle of the pellet (see Appendix A, Figure A-2, A and B). Figure A-2 (right) shows the characteristic Raman spectra for the PHBV compared to DCD. The stretching vibration of CN in DCD bond at 2154 cm^{-1} was used to create the map for DCD. Here, the DCD signal does not overlap with that of PHBV.[146] Twelve 85x85 µm scans were acquired for each pellet, starting from the outer edge and working progressively toward to centre (see Figure A-2, C). The maps were manually stitched in Adobe Photoshop. Details on the acquisition and processing of the Raman maps can be found in Section 4.6.2.

5.2.4.2   Monitoring mobilisation of DCD from the biopolymer matrices

Solution release kinetics

The release kinetics of DCD into water from PHBV and PS matrices were monitored at a controlled temperature of 30 °C (± 1 °C). A single pellet (~30-40 mg) was studied in each triplicate and samples of 0.75 mL were taken at 1 h, 2 h, 3 h, 4 h, 5 h, 10 h, 1 d, 2 d, 4 d, 8 d, 2 w, 4 w, 8 w, 16 w and 20 w. DCD was quantified using ultraviolet-visible (UV-Vis) spectroscopy. The DCD remaining in the pellets was quantified at the end of the experiment. Details on the experimental methods can be found in Section 4.4.1. The exact initial DCD loading and variability was found to be 229 ± 12 g.kg^{-1}.

Sand and soil release kinetics

Leaching columns (see Figure 4.1) were constructed to evaluate the relation between the rate of DCD mobilisation from DCD-PHBV pellets and:

i)   the tortuosity of the media. The use of ethanol sterilised fine-grained sand (<0.2 mm) allowed maximum recovery of the DCD and ensured low biological activity.

ii)   microbial degradation of the PHBV matrix. This was investigated by comparing the release profiles for active soil with that of sand and γ-irradiated soil (72 h exposure prior to the addition of the DCD-PHBV pellets at a dose rate of 0.6 kGy.hour^{-1}, giving a resultant dose of 120 kGy). Sterility of the soil was confirmed by a streak test over agar.

iii) the soil texture. For this, sand was mixed with the active clay loam soil in weight ratios of 1:3, 1:1 and 3:1.

In total, nine columns were studied. Sand, soil and γ-irradiated soil were studied in duplicate, while a single column was used for each sand:soil ratio (1:3, 1:1 and 3:1).

DCD was extracted from the columns after 5 h, 10 h, 1 d, 2 d, 4 d, 1 w, 2 w, 3 w, 4 w, 8 w, 12 w, 17 w, 23 w and 26 w.

DCD in the leachate was quantified with ultra-pressure liquid chromatography (UPLC). Flow injection analysis (FIA) was used to quantify the concentrations of ammonium, nitrite, nitrate and phosphate in the leachate. Results confirmed that the nutrient availability did not limit biological activity in the soil, see Figure A-3, Appendix A. Details on the construction and operation of the leaching columns is presented in Section 4.4.2.

After 26 weeks, the columns were decommissioned and the DCD remaining in the pellets was quantified. The amount of PHBV degradation was estimated using Equation 5.2, where M is mass and N is the number of pellets recovered from the leaching column.

$$PHBV\ degradation = \frac{M(recovered\ pellets) - \frac{M(DCD\ extracted\ from\ 4\ pellets)}{4} \times N}{Initial\ mass\ of\ pellets} \quad \text{Eq. 5.2}$$

5.2.5 *Analytical methods*

See Section 4.5.3 and 4.5.4 for details on the quantification of DCD using UV-Vis spectroscopy and UPLC, respectively. The thermal stability of DCD and compatibility with high temperature extrusion processing was assessed using thermogravimetric analysis (TGA) and carbon nuclear magnetic resonance (^{13}C-NMR)) spectroscopy, as described in Section 4.5.1 and 4.5.2, respectively.

5.2.6 *Modelling mobilisation*

The Korsmeyer-Peppas (power) model [128], Equation 5.3, was fitted to the experimental fractional DCD release curves for DCD-PHBV and DCD-St pellet into water.

$$F = kt^{n} \quad\quad\quad \text{Eq. 5.3}$$

where F is the fractional release, k is a kinetic constant that depends on the structure and geometry and n is a diffusional exponent, the value of which indicates the mechanism controlling release.

5.3 Results

5.3.1 *Stability of DCD in soil*

The degradation of DCD in a sugarcane soil from Wangan, QLD, Australia at 30 $^{\circ}$C was monitored over 5 weeks. After one week, 21.4 ± 1.0 wt.% of DCD was degraded. A first order decay model fitted the data well (Equation 4), from which the half-life of DCD was calculated to be 25 ± 2 days.

$$Fractional\ recovery\ of\ DCD = 0.96\ (\pm0.02) \times e^{-0.026\ (\pm0.001)\times t}, R^2 = 0.993 \qquad \text{Eq. 5.4}$$

5.3.2   Characterisation of the slow-release inhibitor formulations

5.3.2.1   Thermal stability of DCD and compatibility with extrusion processing

Thermo-gravimetric results indicate the onset of degradative mass loss at ~240 °C for DCD. This is comparable to results by Zhang et al.[147] who reported the onset of decomposition of DCD at 248 °C. Since the highest extrusion temperature was 180 °C, it was unlikely that thermal degradation of the DCD occurred during extrusion processing. However, shearing forces and interaction with the molten polymer could lead to chemical modifications. NMR spectroscopy was used to provide further confidence that the DCD in the extruded DCD-PHBV pellets was still in its active form.

The ^{13}C-NMR results (see Appendix A, Figure A-4) show that no new peaks were produced when comparing DCD extracted from extruded DCD-PHBV pellets to the pure DCD spectra. No odours or colour change were observed either. Therefore, no significant degradation of DCD occurred during extrusion processing at 180 °C.

The extrusion of both DCD with PHBV and DCD with PS formed relatively consistent cylindrical strands that were easily pelletised. DCD melts at ~210 °C so it is unlikely melting occurred during extrusion with PHBV at 180 °C.

5.3.2.2   Distribution of DCD on the surface and within the DCD-PHBV pellets

EDX maps (see Appendix A, Figure A-5A and B), show the distribution of DCD crystals on the surface of an extruded DCD-PHBV pellet. SEM (Figure A-5E and F) revealed significant quantities of DCD on or very near the surface of the pellet, including large exposed crystals, but overall the DCD appears randomly distributed.

Raman spectroscopy mapping of fresh DCD-PHBV embedded in resin was used to obtain a high-resolution distribution of DCD from the edge in to the middle of the DCD-PHBV pellets. This approach was replicated with a pellet that was left in sand for 4 and 26 weeks at 80% of saturation. The optical images and Raman maps are shown in Figure 5.1.

Image J processing of the Raman maps allowed qualitative assessment of the amount, distribution and particle size (Figure 5.1, right) of the DCD over time, within the region of interest. The fresh pellet had a DCD area coverage of 9.3%. The DCD crystals are randomly distributed within the pellet. There is initially a wide distribution of DCD crystal sizes, ranging from a few to >100 µm. This is typical of many heterogeneous macro filler composite materials, where ground solids are encapsulated in a polymer or resin. For example, traditional composite resins contain ground inorganic fillers ranging from 0.1 to 100 µm.[148] After 4 weeks and 26 weeks in sand, the Raman scans

had DCD area coverages of 3.8% and 2.5%, respectively. There is evidence from the Raman images that both the quantity and the size of the DCD crystals decrease over time. These results are not replicated and highly dependent on the specific regions that were scanned. However, there is clear evidence that some DCD crystals remain encapsulated by polymer very close to the outer edge of the pellet.
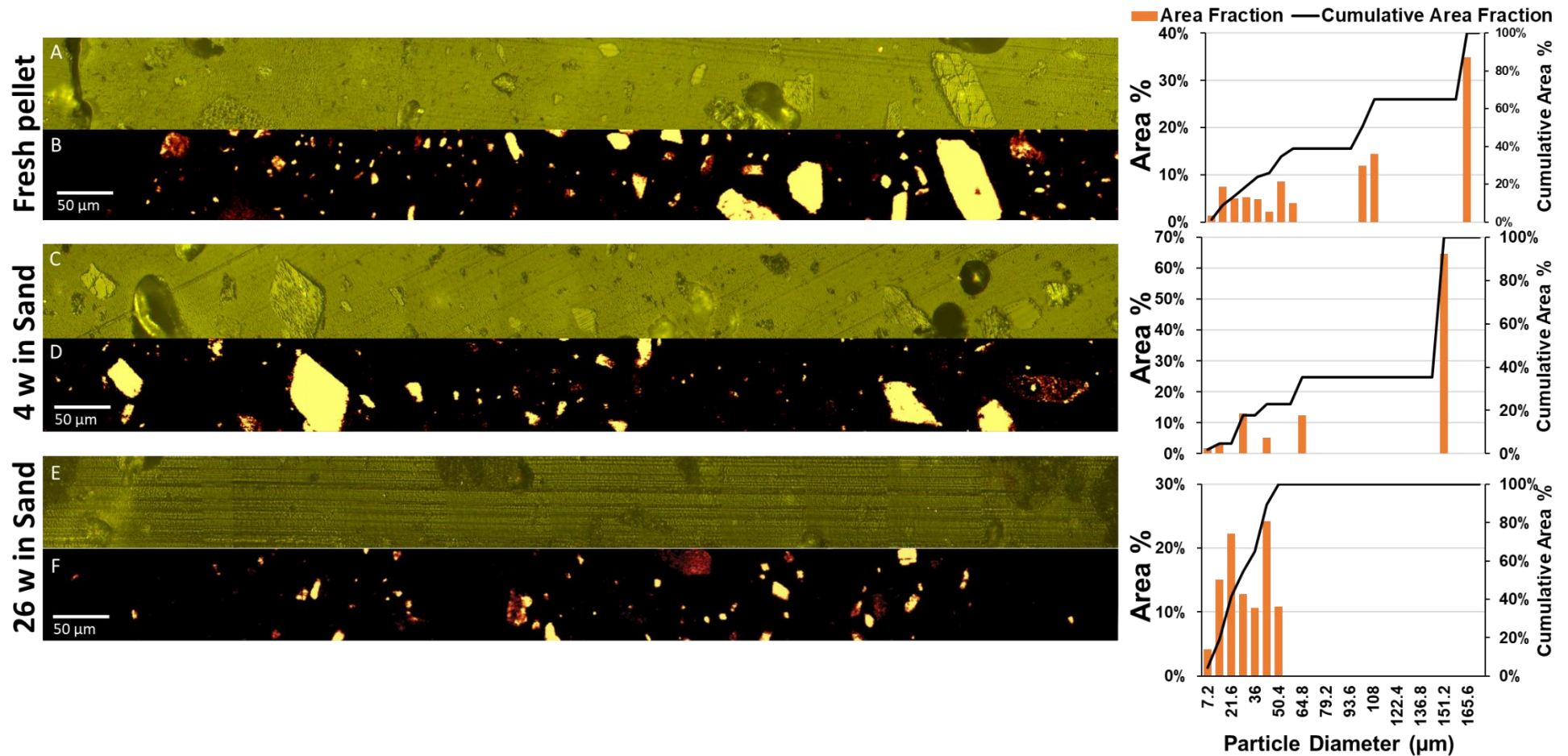
Figure 5.1: Left - stitched optical (A, C, and E) and Raman (B, D, and F) maps of the transverse microtomed cross-section of a fresh DCD-PHBV pellet (A and B); a DCD-PHBV pellet after 4 weeks in sand (C and D); and after 26 weeks in sand (E and F). Each stitch is 12 composited images, moving from the outer edge of the pellets (left hand side) and progressively moving into the centre of each pellet (right hand side). Right - particle size distributions, calculated using Image J processing of the Raman maps. Particle diameters were estimated assuming circular areas.

5.3.3   Mobilisation of DCD from a PHBV matrix

5.3.3.1   Release of DCD into water

The fractional release and release rates of DCD from the DCD-PS and DCD-PHBV pellets at 30 °C are shown in Figure A-6 and Figure 5.2, respectively. DCD-PS pellets released DCD into solution rapidly. Complete release of DCD occurred after 5 h, with 63.9 ± 1.3 wt.% mobilised within the first hour. A clear moving front of DCD was observed within the DCD-PS, with a white cylindrical core of undissolved DCD gradually reducing in size over time. Rapid swelling of the hydrophilic starch matrix was observed.

In contrast, PHBV is a hydrophobic polyester, and swelling was not observed. After 1 h in water 23.5 ± 1.3 wt.% of the DCD was mobilised, likely from the surface of the pellets. After ~3 weeks, the release rate of DCD plateaued significantly, to approximately 5.3 ± 2.1 µg.pellet^{-1}.day^{-1}, as shown by the straight line in Figure 5.2. The variation here is likely due to the random distribution of crystals within the pellet, and the wide spread of crystal sizes. However, this 23 w period contributes only 8% release, and some variability is expected for individual pellets over this long period.

Curve fitting results using the Korsmeyer-Peppas model, Eq. 5.3, are summarised in Table A-3. The exponent, n, provides an indication of the release mechanism. For the cylindrical pellets, n < 0.45 suggests Fickian diffusion controlled release, 0.45<n<0.89 indicates anomalous (non-Fickian) transport, n>0.89 suggests matrix swelling or relaxation. Since n was <0.45 for both PS and PHBV, release was likely mediated by Fickian diffusion processes. The exponent, n, for PHBV was 0.09 ± 0.02. This is considerably less than 0.45, suggesting that diffusion was significantly limited.

5.3.3.2   Effect of a tortuous media and PHBV degradation on DCD mobilisation

Sand, soil and γ-irradiated soil were used to investigate the effect of a tortuous media and the role of polymer degradation on the release kinetics of DCD from the DCD-PHBV pellets. In the first two weeks, there were seven leaching events. This intensive leaching regime was used to maximise the recovery of DCD. Beyond two weeks, leaching events were less frequent. In between the longer time points, DCD was vulnerable to microbial degradation or binding to soil organic matter. For this reason, a distinction should be noted here between fractional release from the pellet and the fraction of DCD quantified in the leachate. Figure 5.2 shows the cumulative fraction of DCD that was accounted for in the leachate for the sand, soil and γ-irradiated soil (left) and the three sand:soil mixtures (right). After 5 h the release into water is almost double that of sand, with 29.7 ± 2.7 wt.% and 16.8 ± 1.6 wt.% release, respectively. From 4 days onward, the rate of release in sand declines significantly. There was a roughly steady release rate of 1.9 ± 0.4 µg.pellet^{-1}.day^{-1} between 8 and

26 weeks. The steady release rate for water is 2.8 times higher than in sand, indicating a marked effect of a tortuous release media on release kinetics. For the active soil and γ-irradiated soil columns, 20.9 ± 2.2 wt.% and 20.2 ± 0.3 wt.% of DCD was accounted for in the first leach, respectively. After 26 weeks of incubation, the total fraction of DCD recovered in the leachate was 44.5 ± 0.9 wt.%, 57.7 ± 3.9 wt.% and 59.3 ± 1.1 wt.% for the sand, soil and γ-irradiated soil, respectively.

The effect of soil texture was investigated using three sand:soil ratios of 1:3, 1:1, and 3:1. These three columns gave markedly higher quantities of DCD collected in the leachate compared with the soil columns. After 5 h, 18.4 wt.%, 16.7 wt.% and 20.7 wt.% of the DCD was recovered from the 1:3, 1:1 and 3:1 sand:soil ratio columns, respectively. In the six leaching events between 4 weeks and 26 weeks, 15.4 wt.%, 32.1 wt.% and 21.1 wt.% of the initial DCD was recovered from the 1:3, 1:1 and 3:1 sand:soil ratio columns, respectively. In comparison, an average of 5.2 wt.%, 7.8 wt.% and 10.7 wt.% was accounted for over this period in the sand, soil and γ-irradiated soils. After 26 weeks, the cumulative fraction of DCD recovered in the leachate was 65.8 wt.%, 77.0 wt.% and 72.7 wt.% for the 1:3, 1:1 and 3:1 sand:soil ratio, respectively.

At the end of the 26 week incubation the pellets were recovered and the DCD remaining in the pellets was quantified. An estimate of the polymer remaining was then used to calculate an approximate degree of polymer degradation (see Figure 5.4). All six pellets were recovered from the sand and γ-irradiated columns, and the soil (replicate 1) column. However, for soil (replicate 2) and sand:soil mixtures of 3:1 and 1:3 only four pellets were recovered. In the column with sand:soil ratio of 1:1 no pellets were found. For the sand columns, the total mass of the initial pellets was accounted for. Therefore, the degradation of the polymer was assumed to be zero. For the γ-irradiated soil and active soil it was estimated that 25 ± 3 wt.% and 46 ± 3 wt.% of the polymer was degraded. In the sand:soil mixtures of 1:3, 1:1 and 3:1, PHBV degradation was estimated to be much higher, at 61 wt.%, 100 wt.% (since no pellets were recovered) and 57 wt.%, respectively.

Backscattered electron micrographs, Figure 5.3, confirm both the absence of biodegradation of the PHBV matrix in sand and significant degradation in other mixtures. Macroscopic differences in the porosity and density of the matrix between sand and soil environments were evident. The presence of fungal hyphae and euglyphid testate amoebae are shown growing on the surface of PHBV pellets when incubated in soil environments. Unexpectedly, in the γ-irradiated soil, both mass loss and SEM images confirm that the polymer was actively hydrolysed.
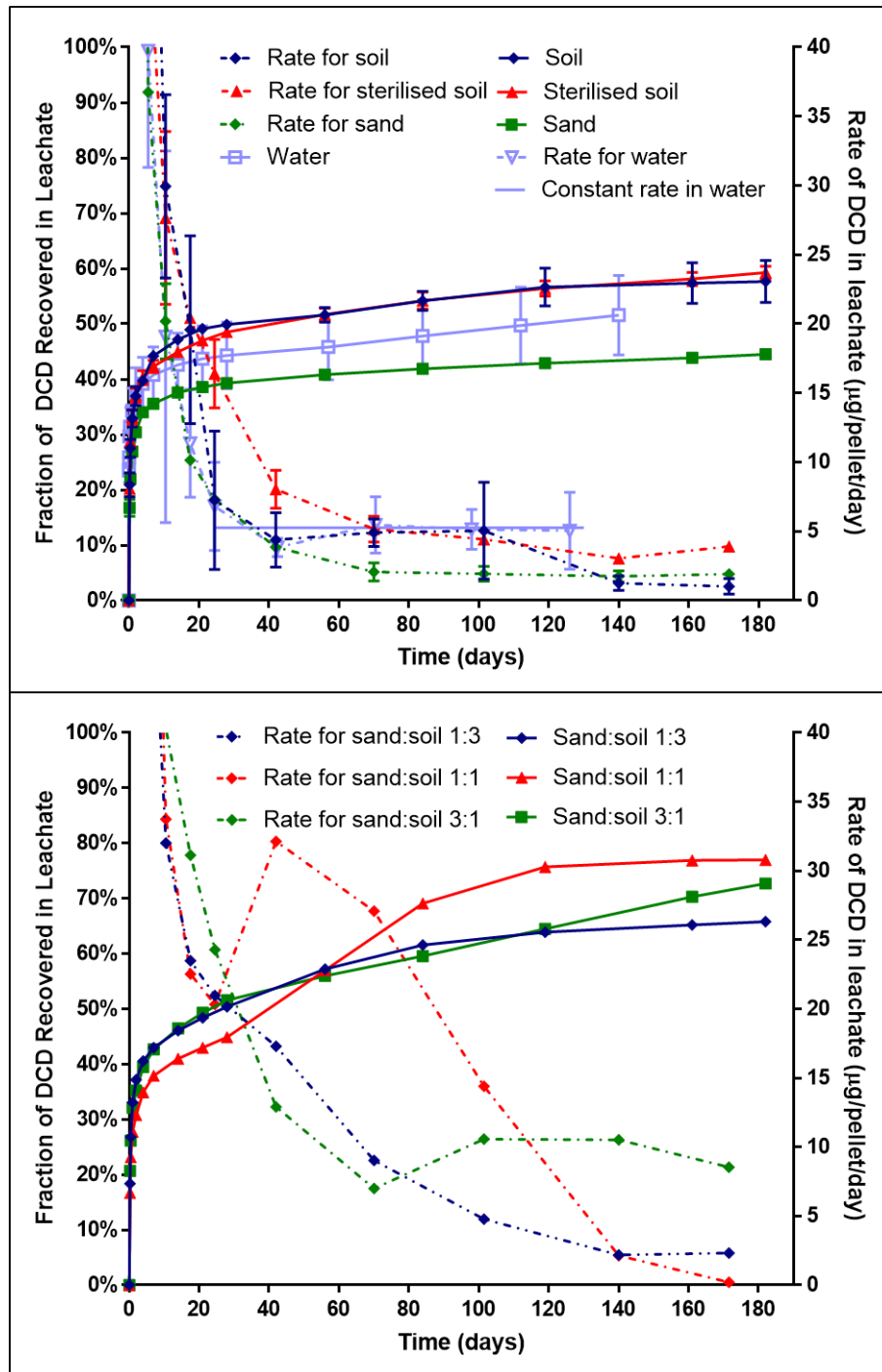
Figure 5.2: Fraction of DCD (wt.%) quantified in the leachateor fractional release for water (left y-axes, solid lines) and specific release rate (right y-axes, dotted lines) of DCD from DCD-PHBV pellets into water, sand, soil, and γ-irradiated soil (top) and sand:soil ratios of 1:3, 1:1 and 3:1 (bottom). Water release curve shows the average of three replicates. All columns were initially loaded with seven pellets. Data sets for sand, soil and γ-irradiated soil are the average of two incubation columns. Error bars show one standard deviation from the mean. Data sets for sand:soil ratios of 1:3, 1:1 and 3:1 are each from a single column.
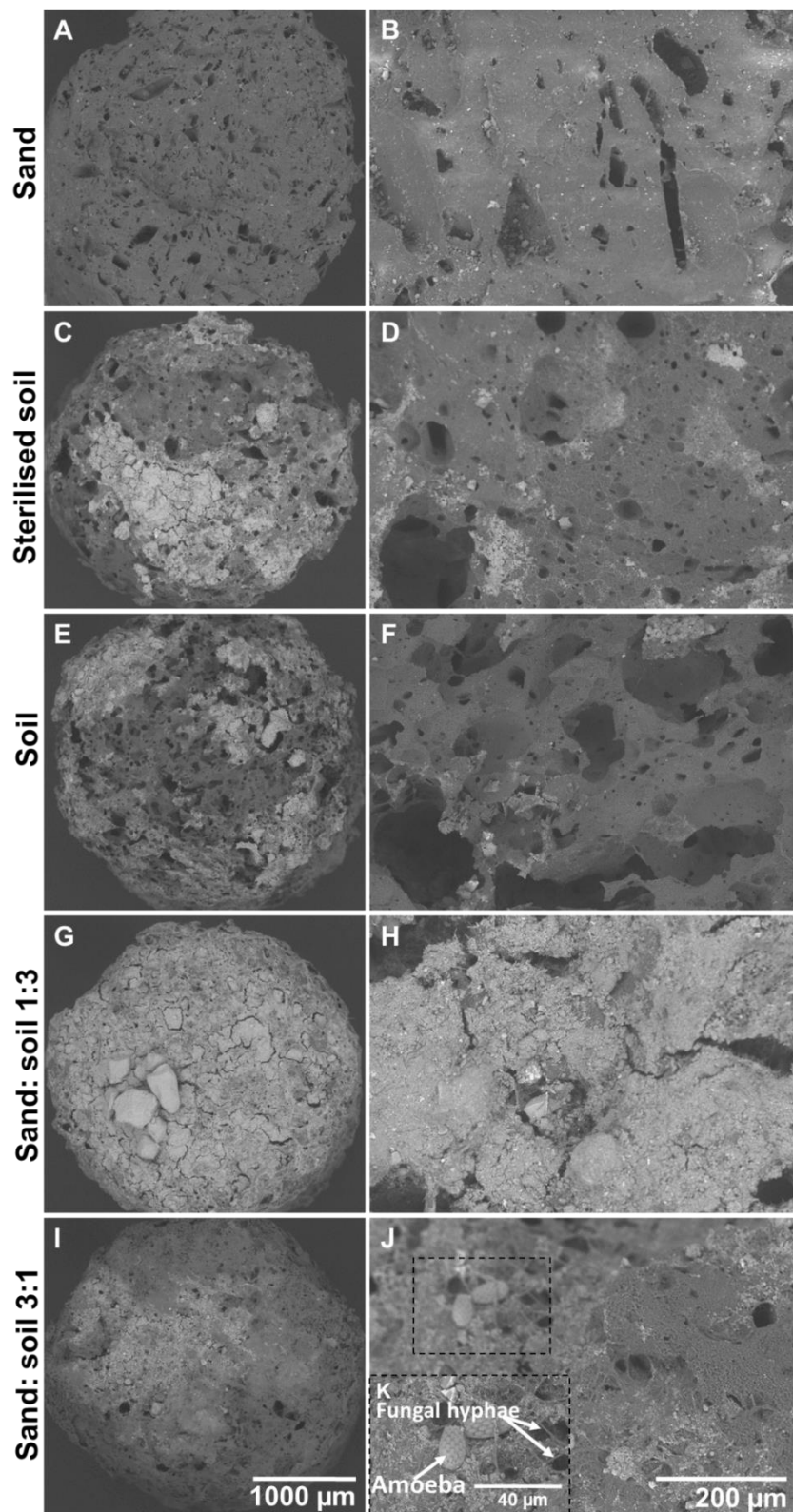
Figure 5.3: Backscattered electrons micrographs of DCD-PHBV pellets recovered after 26 weeks incubation in sand (A and B), γ-irradiated soil (C and D), soil (E and F), sand:soil 1:3 mixture (G and H) and sand:soil 3:1 mixture and (I and J). Insert K highlights the presence of fungal hyphae and euglyphid testate amoebae abound to the surface of the PHBV pellet.

5.4 Discussion

To provide confidence in the fractional release curves, the DCD remaining in the pellets was quantified for all experiments, with most of the DCD being recovered from water, sand and γ-irradiated soil (Figure 5.4). By comparison, 9-26 wt.% of the DCD was unaccounted for in the columns containing biologically active soil and was likely biologically degraded.
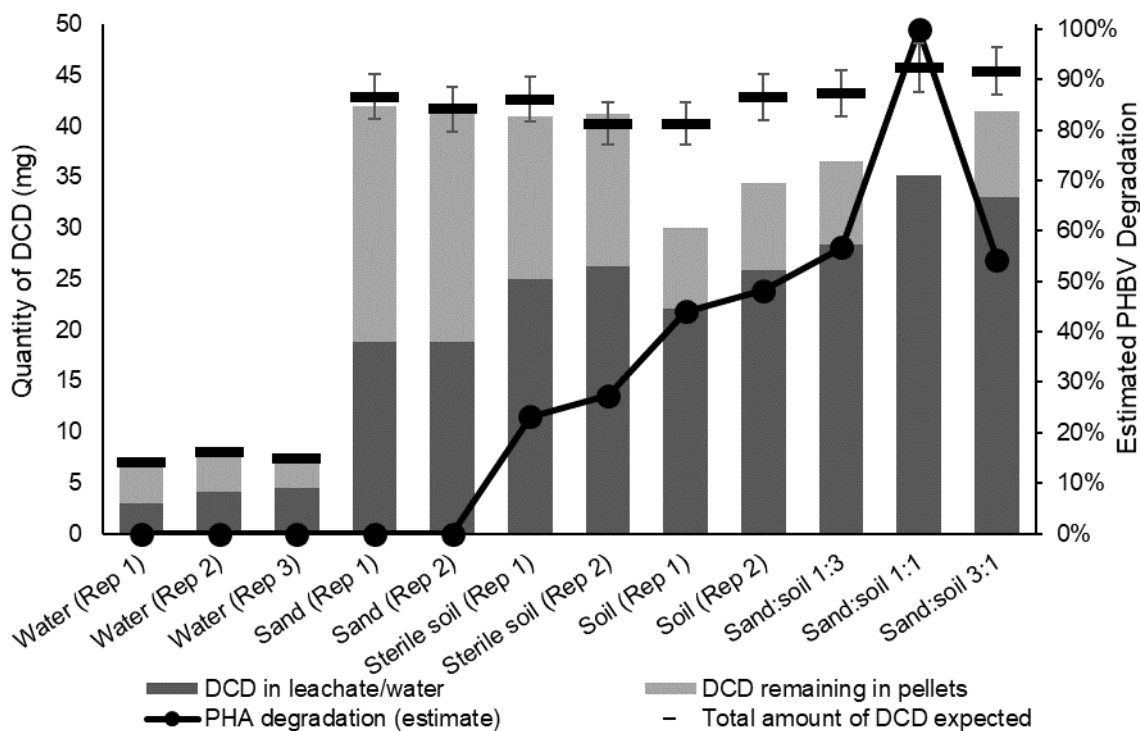
Figure 5.4: Summary of DCD quantified from each slow release experiment. The stacked columns show the DCD quantified in the water/leachate after 20 weeks (dark grey) and the DCD extracted from the pellet at the end of the experiment (light grey). The total amounts of DCD quantified were compared against the expected total DCD calculated based on an initial DCD loading of 229 ± 12 g.kg^{-1}.

From the DCD degradation study, the half-life of DCD in this soil was found to be 25 days. While this was rapid from an agricultural context, it was slow compared with other studies. Rajbanshi et al.[69] reported the half-life of DCD to be 12-15 days in a German silt loam incubated at 30 °C, while it was just 7 days at 30 °C in a silt loam from Alabama[140]. Temperature is a key determinant of the lifetime of DCD in soil,[8, 68, 149] with Kelliher et al.[8] finding that the half-life ($t_{1/2}$, days) exponentially declined with soil temperature (T, °C), according to $t_{1/2}(T) = 168e^{-0.084T}$. However, high organic matter content, lower moisture content and higher degree of aeration are also known to reduce the persistence of DCD.[150-151] The soil studied here was held at 80% saturation. The high water content

and low degree of aeration may have resulted in the comparatively low rates.

Both biotic and abiotic mechanisms contribute to DCD hydrolysis.[152] Metal oxides, particularly iron oxides in soil, catalyse the hydrolysis of the nitrile moiety of DCD. [150, 153] However, in agricultural soils degradation is more commonly attributed to *Rhodococcus* and *Pseudomonas sp*.[152] This is supported here, when comparing the γ-irradiated soil, where the majority of DCD was accounted for, and the biologically active soil, with 23 ± 4 wt.% DCD degradation.

Since all the DCD was recovered in water, sand or γ-irradiated soil, there is a high degree of confidence in the fractional release data. Intriguingly, the polymer degraded in the γ-irradiated soil. The mechanism is unknown, but this could be a result of microbial re-colonisation over the 6 month experiment. By studying the release profiles in different media, the contribution of different mechanisms could be analysed.

The release studies into water and sand show that DCD release can be driven by water diffusion alone, supported by an exponent value for the Peppas model of <0.45. These results are comparable to other studies for release from PHBV matrices.[154-155] Fickian diffusion was determined to be the driving mechanism for drug release from PHBV microspheres. Release of tetracycline fitted well to the Higuchi equation (exponent n = 0.5)[155] and daidzein release gave an exponent of 0.38,[154] both suggesting diffusion controlled release. In contrast, however, Boyandin et al.[100] found the release of the herbicide, metribuzin, from PHB pellets gave an exponent of 0.49, suggesting a non-Fickian release mechanism. This may be a result of the cold pressing fabrication technique used.

The rapid initial mobilisation of DCD from the surface of the pellet could be described as a surface wash phenomenon. This was higher in soils over sand, which may be a surface wetting effect of the release media - the SMC of the clay loam soil was three times higher than the sand and therefore had three times more water to begin with. The release after the first day of exposure follows the trend of water content, with water > soil > sand with 34 ± 4 wt.%, 33 ± 2 wt.% and 27 ± 0.4 wt.% release, respectively.

The SEM micrographs of the fresh pellet, Figure S6, show the rough topography of the pellet, exposed DCD crystals at the surface, and small pores on the transverse face of the pellet. Exposure to water led to the formation of voids and pores on the surface of the pellet, from where surface DCD crystals were eluted (Figure 5.3A and B). These voids allow water to migrate further into the pellet and access more DCD. The random distribution of the DCD crystals within the pellet results in some crystals encapsulated by thick layers of polymer. For others, there will only be a thin polymer sheet around them, or an incomplete covering, allowing channelling through voids in the matrix. Water diffusion through PHBV is slow, $\sim 1.5\text{-}2.2 \times 10^{-5}$ g.mm.m^{-2}.h^{-1}.Pa^{-1}.[156] However, water will gradually permeate the polymer, and dissolve the DCD crystals. In the aqueous phase, the DCD can then diffuse

back through the polymer and out of the pellet. This mechanism drives the very slow mobilisation of DCD seen between 4 and 12 weeks into water.

The Raman maps for the fresh and eluted pellets, Figure 5.1, show that there is:

i)   a large particle size distribution of DCD crystals within the PHBV matrix

ii)   roughly homogenous initial distribution of DCD through the PHBV matrix,

iii)   the presence of large DCD crystals toward the outer edge of the pellet, even after ~40 wt.% of the DCD had been released into the sand

The latter indicates the presence of void and pore channelling.

Fitting the Korsmeyer-Peppas model suggested that diffusion controlled the release in the absence of polymer degradation. However, the term 'diffusion' can be ambiguous. The classic concept of a moving front [124], where water ingress elutes the loaded agent gradually from the outer edge of the material inward, does not appear to hold here. While there seems to be more DCD removed from the outer regions, there was also significant amounts of DCD near the outer edge of the pellet that were inaccessible, or being accessed at a much lower rate. This is likely due to a thicker layer of the PHBV around these crystals, and a pore/void channelling effect around these crystals allowing access further into the pellet. While these are diffusive processes, they are in contrast to Higuchi's moving front theory, which is the basis for the Korsmeyer-Peppas model. Therefore, interpretation of the mechanisms derived from the exponent of this model may be challenging for these types of materials.

Figure 5.5 axis labels and data: Cumulative fraction of DCD in leachate over 26 weeks (y-axis, 40% to 100%) plotted against Polymer degradation after 26 weeks in release media (x-axis, 0% to 100%). Data points labelled: Sand, Soil, Sterilised soil, Sand:soil 3:1, Sand:soil 1:3, Sand:soil 1:1. Linear regression: y = 0.5719(± 0.04756)x + 48.6, r^2 = 0.954
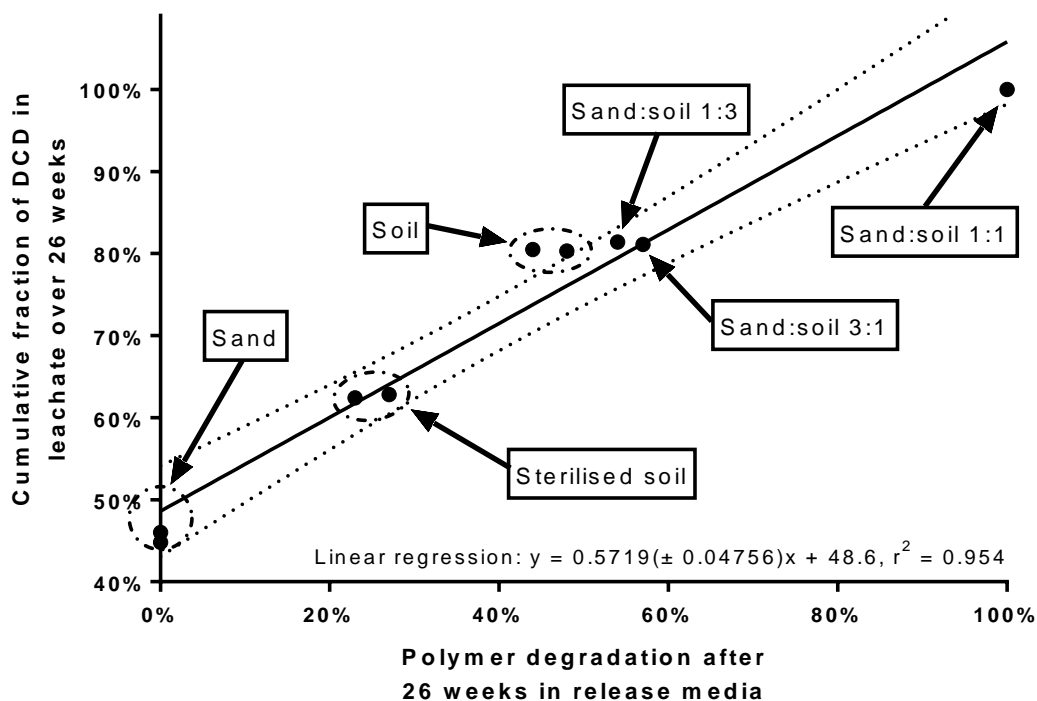
Figure 5.5: The cumulative fraction of DCD recovered in the leachate over the 26 week experiment plotted against the estimated polymer degradation based on the mass of pellets recovered from the columns.

The release rates were higher in all columns where polymer degradation occurred. Figure 5.5 shows the total cumulative fraction of DCD recovered in the leachate from each column plotted against the estimated PHBV degradation after 26 weeks. A linear regression shows a non-zero slope (p-value of <0.0001) of 0.57 ± 0.05. This confirms that greater polymer degradation correlates with higher amounts of DCD released by the end of the experiment.

Polyhydroxyalkanoates (PHAs) undergo an enzyme catalysed surface erosion degradation process in soil.[157] The monomeric composition, degree of crystallinity and crystal size influence the rate of enzymatic erosion.[106] Many PHA depolymerases have been isolated from bacteria and filamentous fungi. Fungal hyphae extensions were found covering the surface of the DCD-PHBV pellets that were embedded in soil. This suggests fungi played a key role here in the erosion of the PHBV matrices. Boyandin et al.[158] isolated fungi species in tropical soils containing PHA-depolymerases from the genera Gongronella, Penicillium, Acremonium, Paecilomyces, and Trichoderma. Fungal species are considered to be more efficient PHA degraders. This is attributed to the higher mobility of their PHA-depolymerases over bacteria's. A large number of bacterial isolates have also been identified from the surface of PHAs. The relative contribution from the two microbiological domains depends on the natural communities existing in the particular soil studied.

While layer-by-layer erosion occurs on the surface of the polymer, pores and the formation of voids formed allowed degradation to occur over a large surface area throughout the bulk of the 3 mm pellet.

To analyse the influence of a tortuous media, the fractional release from DCD-PHBV pellets in water was plotted against the release in sand (see Appendix A, Figure A-7 left). The first four time points, 5 h, 10 h, 1 d and 2 d, are considered release associated with the surface available DCD crystals. After 5 h, the release into water was almost double that of sand. The tortuous path through the bulk of the sand hindered the mass transfer of DCD away from the surface of the pellet. High concentrations of DCD at the surface of the pellet limited the driving force for mass transfer within the pellet. When a leaching event takes place, the DCD that accumulated at the surface of the pellet was removed. As a result, the release in sand approaches the release in water between 5 h and 2 d (the first four points). The surface wash phenomenon is therefore complete within the first few days of exposure. Between 4 d and 12 weeks the release of DCD into water and sand are roughly proportional. Interestingly, the Korsmeyer-Peppas model fits the post-wash data for the release into water (from 2 days onward) with an exponent value, n, of 0.43. This suggests a diffusion controlled post-wash release mechanism.

To investigate the timing of the effect of PHBV degradation further, the cumulative fraction of DCD recovered in the leachate in sand (where no PHBV degradation occurred) was plotted against γ-irradiated and active soil columns (Figure A-7, right). There is a small inflection in the curves around 4 days, suggesting that biodegradation may influence the release of DCD within the first week of exposure. However, it is from 4 weeks onward that the curves deviate from the midline most rapidly. Polymer biodegradation therefore played the most significant role between 4 and 26 weeks.

The schematic in Figure 5.6 depicts the four proposed mechanisms derived from the experimental evidence and their relative contribution to DCD mobilisation from a PHBV matrix. These include:

i) surface wash – exposed DCD crystals are mobilised rapidly (1-2 days) and independently of polymer degradation.

ii) voids and pore channelling through the polymer matrix, allowing water to access DCD crystals deeper in the PHBV matrix

iii) slow diffusion of water through layers of PHBV polymer followed by DCD dissolution and diffusion back through the polymer matrix

iv) enzyme catalysed hydrolysis of PHBV, opening up the matrix and allowing direct access of water to previously encapsulated DCD crystals. In the absence of polymer degradation ($\lambda=0$, such as the case in sand and water experiments), mobilisation was diffusion-controlled (mechanisms ii and iii). Where degradation does occur, higher surface erosion rates (λ) of the PHBV matrix further accelerates the mobilisation of DCD, as shown by the λ_1, λ_2, and

λ_3 curves where $\lambda_3 > \lambda_2 > \lambda_1$. The experiments showed that the texture of the soil influenced λ. It was evident that degradation rate and DCD release was highest with a 1:1 sand:soil ratio, and is depicted in Figure 5.6 by the λ_3 curve.

5.5 Conclusion

This study presents important findings on the fabrication of controlled release PHBV materials through extrusion processing. Results suggest that water ingress into these types of materials may be driven more rapidly through voids and pores. This finding may be relevant across various fields, including composite materials and could influence properties such as durability and the rate of biodegradation. Since >40 wt.% of the DCD remains encapsulated after 26 weeks in water, there is incomplete interconnectivity. From this work, further studies were designed to investigate the percolation threshold by fabricating materials at several loading and to determine how this threshold is affected by the DCD crystal size. That work is presented in Chapter 7. Access to DCD within the pellet through interconnected crystals is clearly important. Further understanding of the degree of interconnectivity and the controlling mechanisms are reported in Chapter 6, deploying high-resolution 3-D imaging using X-ray micro-computed tomography (μ-CT).
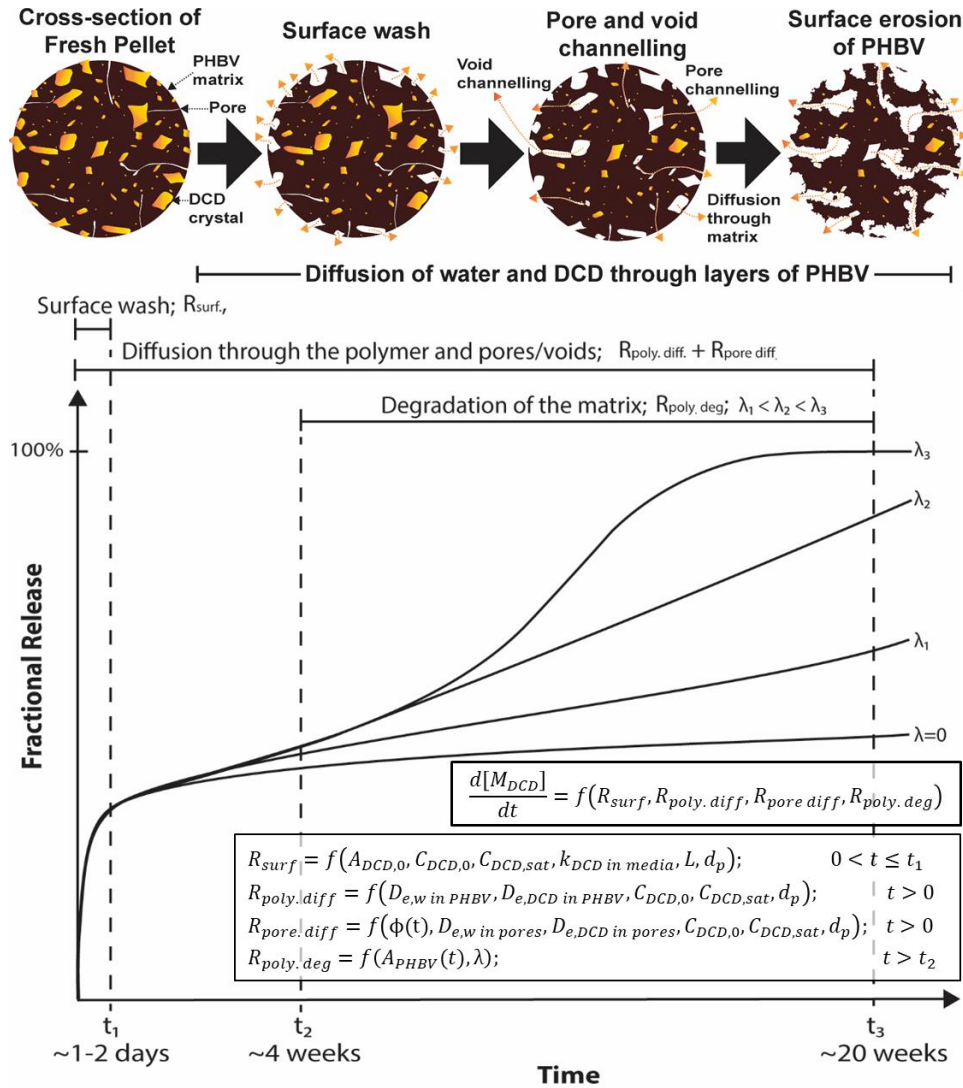
Figure 5.6: Top – a schematic showing the proposed mechanisms driving DCD mobilisation from the DCD-PHBV pellet. Bottom – plot and generalised equation describing the contribution and approximate timing of the mechanisms involved. $\frac{d[M_{DCD}]}{dt}$ is the overall rate of DCD release from the pellet, R_{surf} is the rate of DCD release from the surface wash, $R_{poly\ diff}$ is the rate of diffusion controlled release through layers of PHBV, $R_{pore\ diff}$ is the rate of release through pores and voids in the matrix, $R_{poly.\ deg}$ is the rate of PHBV degradation, $A_{DCD,0}$ is the initial surface area of exposure DCD, $C_{DCD,0}$ is the initial loading of DCD, $C_{DCD,sat}$ is the solubility of DCD, $k_{DCD\ in\ media}$ is the overall mass transfer coefficient of DCD through the release media (e.g., water or sand or soil), L is the length of diffusion layer and d_p is the particle size of the DCD crystals, $D_{e,w\ in\ PHBV}$ is the effective diffusivity of water or DCD through PHBV, $D_{e,DCD\ in\ PHBV}$ is the effective diffusivity of water or DCD through networks of pores or voids in the PHBV matrix, $\phi(t)$ is the porosity/void fraction of the matrix and λ is the rate of surface erosion of PHBV.

CHAPTER 6

High-resolution μ-CT reveals cracking in a hydrophobic composite: a new mechanism for mobilization in controlled release applications

Ian Levett, Bogdan C. Donose, Steven Pratt & Bronwyn Laycock
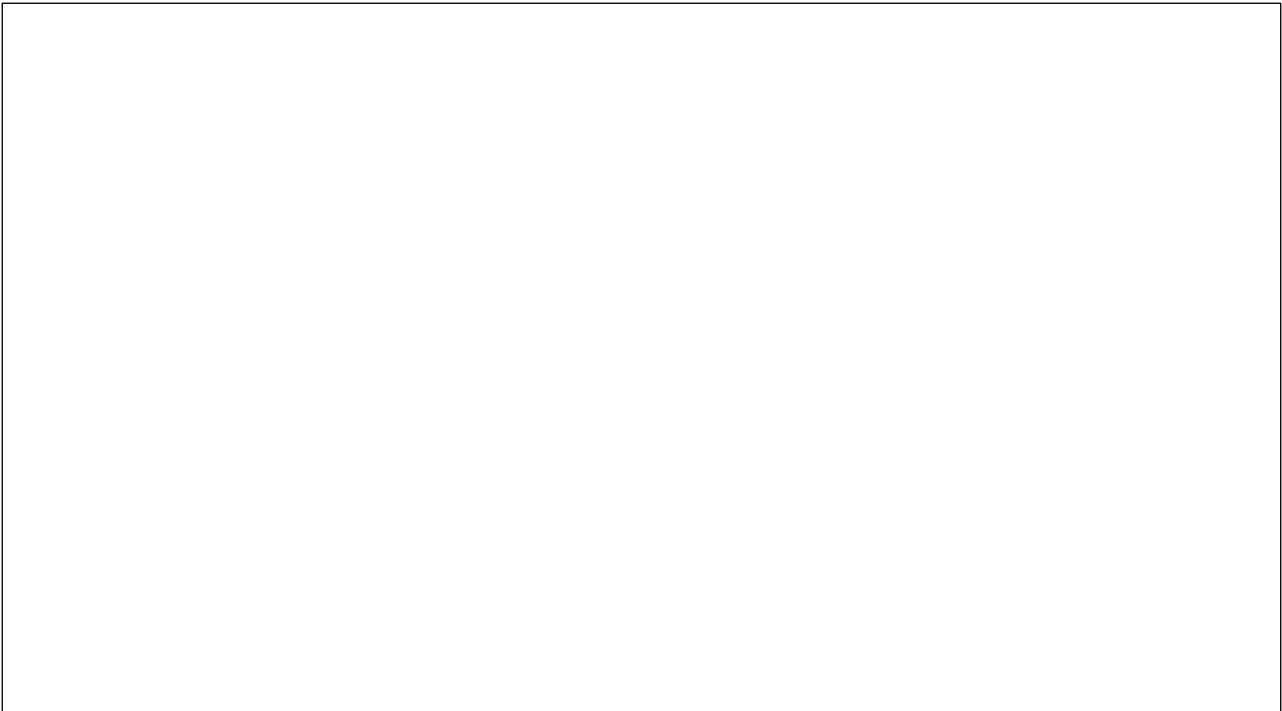
Abstract

High-resolution micro-computed tomography (μ-CT) provides new insights into the multi-mechanism release of water-soluble crystalline materials from hydrophobic polymer matrices. Here, this technique was applied to analyse the mechanisms underpinning the release of the agrichemical dicyandiamide (DCD), a common crystalline, water-soluble nitrification inhibitor, following encapsulation in a biodegradable poly(3-hydroxybutyrate-*co*-3-hydroxyvalerate) (PHBV) matrix at a loading of 250 g.kg^{-1}, as a mechanism for controlling its delivery and improving its stability in tropical cropping systems. The insights gained from the use of this advanced 3-D imaging technique deliver a new understanding of the processes driving release of active agents from composite materials and will aid the modelling and design of such tailored delivery formulations. These insights are generic in nature and will be relevant to the encapsulation and controlled release of soluble crystalline agrichemicals (fertilisers, pesticides, herbicides), drugs and medical implants alike.

DCD-PHBV pellets were fabricated through industrially relevant extrusion processing. The release rate was initially rapid, exponentially decaying over the first eight weeks. This was followed by a very gradual, linear release over the next 18 weeks. The characterization of the pellets before and after release using high-resolution μ-CT led to two important conclusions: i) the DCD that was rapidly mobilized existed within channels connected to the surface of the pellet, and ii) fine cracks present before and after release may at least in part explain the very slow mobilisation from the eighth week onward.

Understanding the microstructure of this type of composite material improves our current understanding of the mechanisms controlling the release of soluble crystalline materials encapsulated in a hydrophobic biodegradable polymer matrix. Further, there may be broader implication to understanding the biodegradation of polyhydroxyalkanoate-based composite materials.

6.1   Introduction

Slow- and controlled-release materials improve uptake of chemical agents by the target organism for a given dose. This concept applies to controlled release drugs and agrichemicals alike. Substantial research has been conducted to understand the mechanisms that regulate release from various polymeric matrices and coatings. Generally, these include the diffusion of water and the active agent through the polymer and voids in the matrix, the dissolution of the active agent and polymer swelling and degradation.[159] However, some highly hydrophobic polymers have very low water diffusivities, do not swell substantially, and degrade much slower, often through surface erosion.[106] For these materials, the controlling mechanisms are less clear.

In the study of sustained-action medications, Higuchi[124] proposed two mechanisms that may control release of granular drugs randomly dispersed in solid matrices: i) simple diffusion through and from a homogenous matrix following a moving front of drug dissolution within the matrix, and ii) leaching of the medication through water-filled pores, cracks and intergranular spaces. However, there is little physical evidence to support the proposed theory. Similarly, Brook and van Noort[160] proposed cracks and channels as the driver for release of antibiotics from acrylic resins without visual or other physical evidence to support the postulated mechanism. Modern characterization techniques are needed to verify if the theory accurately represents the controlling mechanisms. Warner et al.[161] employed scanning electron microscopy, atomic force microscopy and Raman spectroscopy to characterize strain induced crack formation in a polydimethylsiloxane–dexamethasone acetate (PDMS/DXA) drug collar used on cardiac leads. These techniques clearly showed microcracks on the collar surface and propagation between drug particles, which was hypothesized to accelerate drug elution. However, these are limited to surface characterization and rely on cryosectioning of the samples, which can alter the surface structure. Due to the contrast in density between void space and solid polymeric materials or solid active agents, X-ray techniques, such as micro-computed tomography (μ-CT), allow 3-D visualization and characterization of void space within a solid composite.

High-resolution μ-CT is a non-destructive technique that allows the visualization of fine internal features (down to 150 nm resolution[162]), without the need for laborious and skilled sectioning of the material. In addition to the visualization of fine cracks and channels, this technique allows quantification of porosity, pore size and spatial distribution, pore connectivity, plus the visualization and/or quantification of different components within a composite material. Markl et al.[163], for example, used μ-CT to characterize the architecture of 3-D printed single and multi-compartment slow-release pharmaceutical formulations. The technique allowed accurate quantification of porosity, pore volume and length, polymer shell thickness and drug loading. Further, it allowed qualitative assessment of the quality of the print and delivered an improved understanding of the mechanisms driving release to aid future design and optimization of the delivery system. Here, high-resolution μ-CT is employed to investigate the presence and role of cracks in the mobilisation of the nitrification inhibitor, dicyandiamide (DCD), from a biodegradable poly(3-hydroxybutyrate-*co*-3-hydroxyvalerate) (PHBV) matrix.

DCD is an agrichemical that can effectively inhibit the oxidation of ammonia to nitrate, reducing nitrogen losses through leaching, runoff and denitrification.[139] In our previous work,[164] we developed an extruded slow-release DCD-PHBV formulation, intended to extend the duration of nitrification inhibition for tropical agricultural applications. PHBV is an example of a highly hydrophobic

polymer, where mechanisms that control release are non-trivial and remain unclear from the literature. This semi-crystalline bacterial polyester has very low water diffusivity ($\sim 6 \times 10^{-14}\,\mathrm{m^2.s^{-1}}$)[165], minimal swelling and degrades through slow surface erosion ($<0.6\,\mathrm{mg.day^{-1}.cm^{-2}}$)[166]. PHBV is a fully degradable polymer within the family of polyhydroxyalkanoates (PHAs), naturally synthesized by numerous bacteria. In many applications, PHA is composited with a filler or active agent, such as tissue scaffolds,[167] wound dressings,[168] surgical implants, macro-, micro-[169] and nano[170]-encapsulation of drugs and controlled-release agrichemicals.[98, 171] Molecular migration within these composites is important, whether to understand release kinetics or the biodegradability and lifetime of the materials. Hobbs et al.[172] found fine circumferential cracks can develop as PHBV spherulites grow during crystallisation. However, the influence of such features on the material performance of PHBV composites is not clear. The purpose of this study was to characterize the microstructure of the slow-release DCD-PHBV composite and build mechanistic understanding of the release kinetics.

6.2   Materials and methods

6.2.1   Materials

Dicyandiamide (DCD) and poly(3-hydroxybutyrate-*co*-3-hydroxyvalerate) (PHBV) were used in this study, see Section 4.2 for details.

6.2.2   Extrusion processing and characterization of slow release DCD-PHBV formulations

DCD-PHBV pellets were fabricated through melt-compounding extrusion processing followed by pelletisation to produce $\sim 3 \times 3$ mm pellets. The procedure was the same as that presented in Chapter 5, Section 5.2.3, with further details provided in Section 4.3. The exact initial DCD loading was quantified by extracting the DCD from the pellets and was found to be $229 \pm 12\,\mathrm{g.kg^{-1}}$.

The release of DCD from the DCD-PHBV pellets was studied at 30 °C in sand using leaching columns. The setup of the columns was consistent with Section 5.2.4.2 and details on the construction and operation of the columns can be found in Section 4.4.2. DCD was extracted from the columns after 5 h, 10 h, 1 d, 2 d, 4 d, 1 w, 2 w, 3 w, 4 w, 8 w, 12 w, 17 w, 23 w and 26 w and quantified using ultra-pressure liquid chromatography (UPLC), see Section 4.5.4. After 26 weeks, the release media was washed through a 2 mm sieve to recover the pellets.

Micro-computed X-ray tomography (µ-CT) was used to characterize the extruded pellets before and after DCD release at low (4 µm) and high (0.5 µm) resolution. Data was attained using a ZEISS Xradia 520 Versa (ZEISS microscopy customer center, Shanghai), with acquisition parameters for each scan detailed in Table 6.1.

Table 6.1: Acquisition parameters for the ZEISS Xradia 520 μ-CT Versa μ-CT

Acquisition parameters	Before release		After release	
Voxel size (μm)	4×4×4	0.5×0.5×0.5	4×4×4	0.5×0.5×0.5
Field of view (mm)	4×4×4	0.5×0.5×0.5	4×4×4	0.5×0.5×0.5
Objective	0.4X	20X	0.4X	20X
Rotation	360°	180°	180°	180°
Exposure (ms)	1.5	2.5	1	2
Voltage (kV)	60	50	50	50
Power (W)	5	4	4	4
Scan time (h)	1.5	2	1	1.75

ZEISS OptiRecon was used for reconstruction and then CtVox and CTan software (Skyscan, Bruker, Belgium) were used for 2-D and 3-D analysis of the void space. The cross-sectional images were binarised, such that pores and void space were represented by black pixels and solid material (PHBV and DCD) as white pixels. The shrink-wrap algorithm was used to define the volume of interest (VOI) as the volume of the pellet. The 2-D analysis allowed investigation of where DCD had released from within the pellet, through slice-by-slice quantification of the void space in the cross-axial and coronal planes. The 3-D analysis was then run to find the total porosity (black voxels/total voxels within the VOI (Vt)), open porosity (black voxels with a connected path of black voxels to outside the VOI, i.e., to the surface of the pellet/ Vt), closed porosity (black voxels that are not connected to outside the VOI/ Vt) and the pore size distribution (defined by the largest sphere that can fit within a cluster of black voxels). To explore where the DCD released from further, the volume of the pellet was sectioned roughly into thirds, keeping a constant height to diameter ratio. Within the CT-An software, the VOI for the inner and middle thirds were defined as perfect cylinders, while the outer third was defined by the surface of the pellet through the shrink-wrap algorithm.

6.3   Results and Discussion

6.3.1   Mobilisation of DCD from the PHBV matrix

Release of DCD was monitored in sand at 30 °C over 182 days by periodically flushing the leaching columns. The fractional release profile and average rate of DCD release for each pellet are shown in Figure 6.1. The initial release was rapid, followed by a second phase of very gradual release. DCD dissolution from the surface of the pellet resulted in $17 \pm 2\%$ release within the first 5 h. Between 5 h and 8 wks a further $24 \pm 2\%$ of the DCD was mobilized from the pellets, after which the release rate slowed significantly. From 8 wks to 26 wks, only $4 \pm 1\%$ of the DCD released, at a roughly constant rate of 2 ± 0.4 μg DCD.pellet^{-1}.day^{-1}.
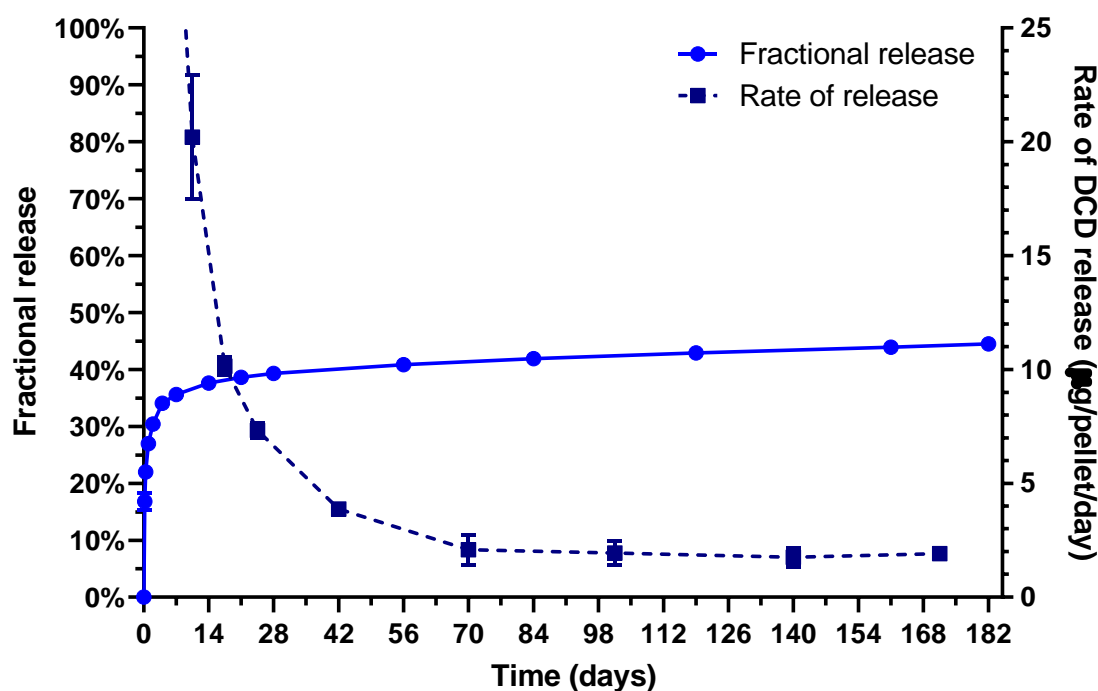
Figure 6.1: Release kinetics of DCD from the DCD-PHBV matrix into sand at 30 °Cwith the fractional release of the primary y-axis and the average rate of DCD mobilisation from each pellet on the secondary y-axis. Error bars show standard deviation (n = 2).

6.3.2   Characterisation of the pellets before and after release

DCD-PHBV pellets were imaged with SEM and μ-CT before and at the end of the release study in sand. The techniques have been invaluable in providing qualitative and quantitative knowledge of the mechanisms driving the mobilisation of DCD out of the matrix.

6.3.2.1   Burst release

The SEM micrographs (Figure 6.2) show the voids created when the DCD is released from the surface of the pellet. Several conclusions can be drawn from these images:

i)   DCD at the surface of the pellet is directly accessible, i.e., water does not need to penetrate the pellet and / or diffuse through PHBV to mobilise the surface DCD,

ii)   the distribution of DCD is random and homogeneous throughout the pellet, i.e., there is no clear clustering of crystals, separation of large and small crystals nor higher concentration of DCD at the edge or centre of the pellet, and

iii)   there is a wide spread of DCD crystal sizes, from tens of microns up to 500 μm in length.

The dissolution of DCD in water was tested and it was found that complete dissolution was achieved within two hours. Since the exposed surface area of the DCD is reduced when embedded in

the polymer, it is conservatively estimated that the surface available DCD will release within the first five hours of exposure to water.

| Before release | After release in sand |
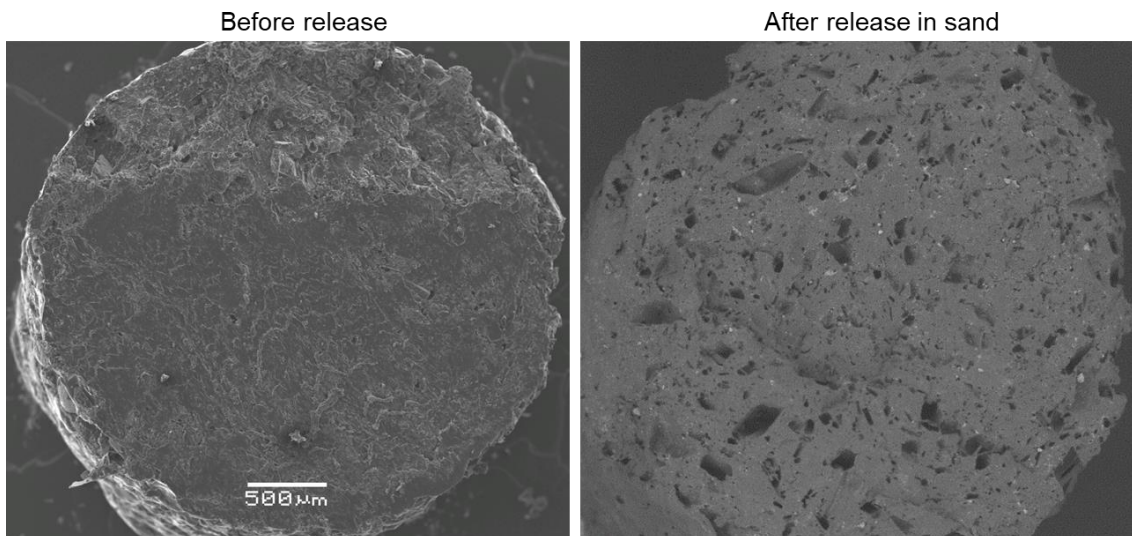
Figure 6.2: SEM of the surface of the DCD-PHBV pellet (left) and backscattered SEM of the DCD-PHBV after 26 weeks in sand (right).

6.3.2.2 The post-burst release mechanism

Micro-computed tomography (μ-CT) allows three-dimensional characterization of the pellets and visualization of the voids beneath the surface of the pellet (Figure 6.3). Within the CT-An software, the grey scale images were binarised and the speckle artifacts removed, generating slices where a black pixel represents void space and a white pixel represents solid material, i.e., PHBV or DCD. A shrink-wrap algorithm was run over the three-dimensional space to define the volume of pellet. This allows quantitative 2-D and 3-D analysis within the volume of the pellet, where black pixels/voxels represents void space and white pixels/voxels represent solid material, either PHBV or DCD. Key parameters were determined, including porosity, comparing open versus closed porosity, pore size distribution (Figure 6.4) and spatial distribution of the voids within the pellets (Figure 6.5).

The orthogonal slices of a pellet before and after release into sand (Figure 6.3) provide qualitative data on the distribution of voids at a resolution of 4 µm. Important findings include:

i)   randomly distributed spherical pores were present before release,

ii)   large voids formed from the dissolved DCD monoclinic clinopinacoid shaped crystals[173] near the surface of the pellet, but also toward the centre of the pellet, and

iii)   there was some alignment of the larger DCD crystals with the direction of flow within the extruder, particularly for crystals with higher aspect ratios.
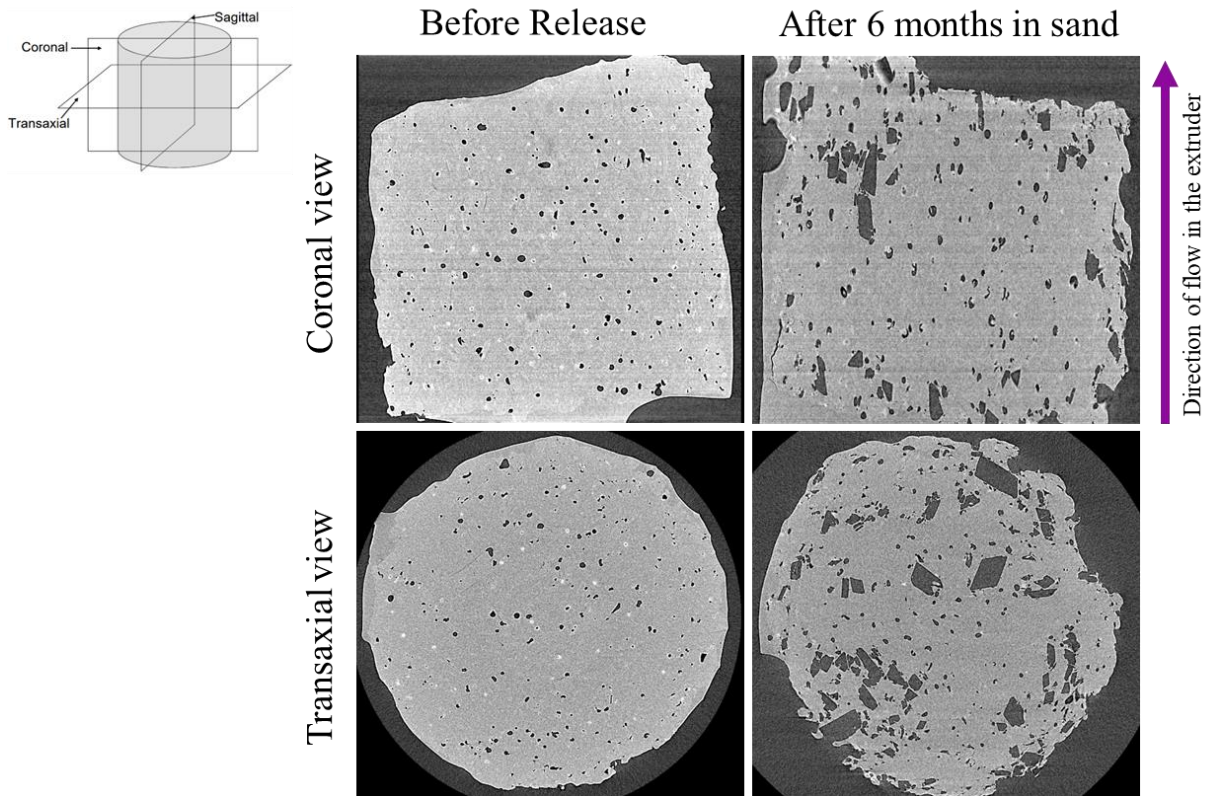
Figure 6.3: Grey-scale coronal and transaxial μ-CT slices at low resolution (4×4 μm pixel) through the middle of the pellets before and after release into sand for 6 months (45.1 ± 0.8% released).

The 3-D analysis results for the whole pellet at 4 μm resolution provides a quantitative comparison of the porosity and pore sizes before and after release. Initially the pellets had 2.4% porosity that existed predominantly as closed pores. The spherical shape of these ~20 μm pores (Figure 6.4A) suggest gaseous inclusions formed in the matrix during processing, possibly as pockets of air or water vapour. The porosity after 6 months in sand was ~11%, which is reasonable considering 45 wt.% of the DCD was mobilized and the initial loading was 250 g.kg^{-1}. Accounting for the density differences of DCD (1.4 g/cm^3) and PHA (1.25 g/cm^3) and the initial porosity (2.4%), we would expect a porosity of 12.7% for 45 wt.% release. This supports the quantitative nature of the μ-CT analysis results.

By inverting the binarised images, such that voids appear white and everything else is black, the quantification of the orientation of voids was possible. Figure 6.4B shows the angle between major axis of the voids from the vertical z-axis (θ °), which is the direction of flow in the extruder, as shown in Figure 6.3. Interestingly, the pores in the matrix before release appear to be ellipsoidal, with the major axis stretching in the radial direction of the cylindrical pellets (i.e., 90 ° to direction of flow), with a median angle of 61 °. In contrast, after release, the median angle was 20 °, indicating flow-

induced alignment of DCD crystals. This is important as it has implications on the connectivity between DCD crystals and likely contributes to the accessible fraction of DCD that was mobilized during the post-burst phase of the release profile. From the 2-D slices shown in Figure 6.3 it appears that many of the DCD crystals released were not connected to the outside of the pellet, i.e., the voids formed after dissolution appear to be encased in PHBV. However, the 3-D analysis results suggest otherwise, with the majority (74%) of the porosity after release existing as open voids, i.e., connected to the surface of the pellet. This explains the high release rate of DCD between 5 h and ~8 wks, with flow-induced crystal alignment possibly increasing the degree of contiguity. However, the closed porosity increased slightly from 2.3% to 2.8%, which may suggest that some DCD was mobilized from enclosed voids, i.e., through the polymer matrix. However, evidence from the high-resolution µ-CT suggest cracks, which could not be resolved at the lower resolution (4 µm), could connect to these "closed" voids. This small fraction could relate to the very slow release from ~8 weeks onward, discussed further in the following section.
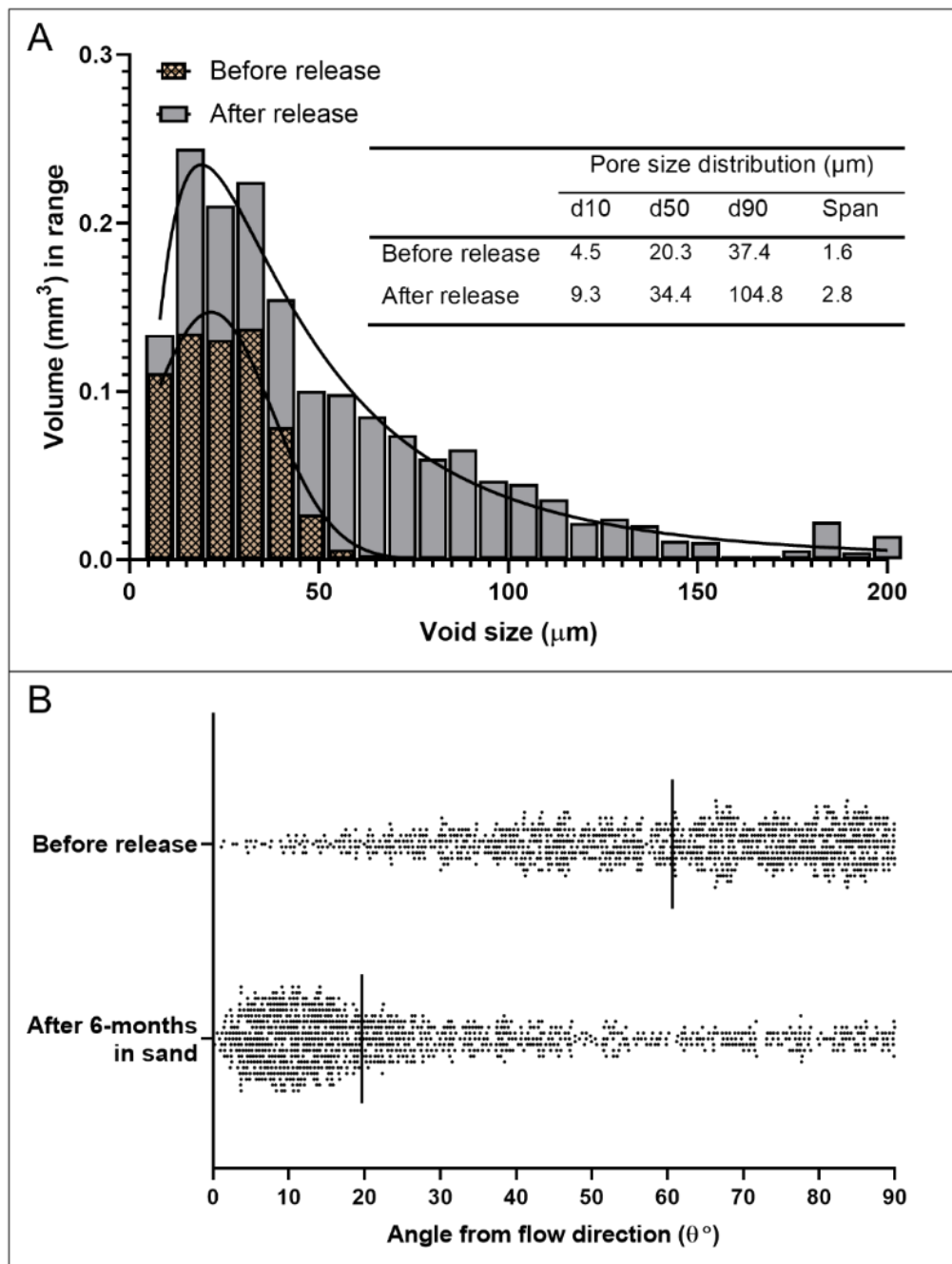
Figure 6.4: A) void size distribution before and after release, fit with a normal and a lognormal distribution, respectively and B) the angle (°) of the major axis of the largest 1000 'objects' of void space within the pellet before release and after 6-months in sand. The vertical lines represent the median values.

The porosity of each slice was calculated by running the 2-D analysis in the CT-An software. Figure 6.5 shows the distribution of porosity along the length and across the width of the DCD-PHBV pellet before and after release into sand. This analysis quantitatively supports the conclusion that the initial porosity of the pellet is homogeneous. As expected, the majority of the increase in porosity exists near the ends of the pellets, which were cut by the pelletiser, and around the curved surface of

74

the cylindrical pellet. There is 0.5-1 mm at either end of the pellet with greater void space than the center of the pellet. However, there is also evidence of DCD release from the center of the pellet.

The porosity at the center of the pellet was assessed by sectioning the volumes of the pellet into thirds, an outer third, a middle third and the inner third, as shown in Figure 6.5. The porosity of the inner, middle and outer third increase from 1.9% to 13.0%, 2.4% to 12.8% and 2.4% to 6.0%, respectively. The latter is surprising, since there was only ~45% DCD release, yet the inner 33% of the pellet volume accounted for ~11% of the increase in porosity, while the middle and outer thirds contributed ~46% and 43% of the increase in porosity, respectively.
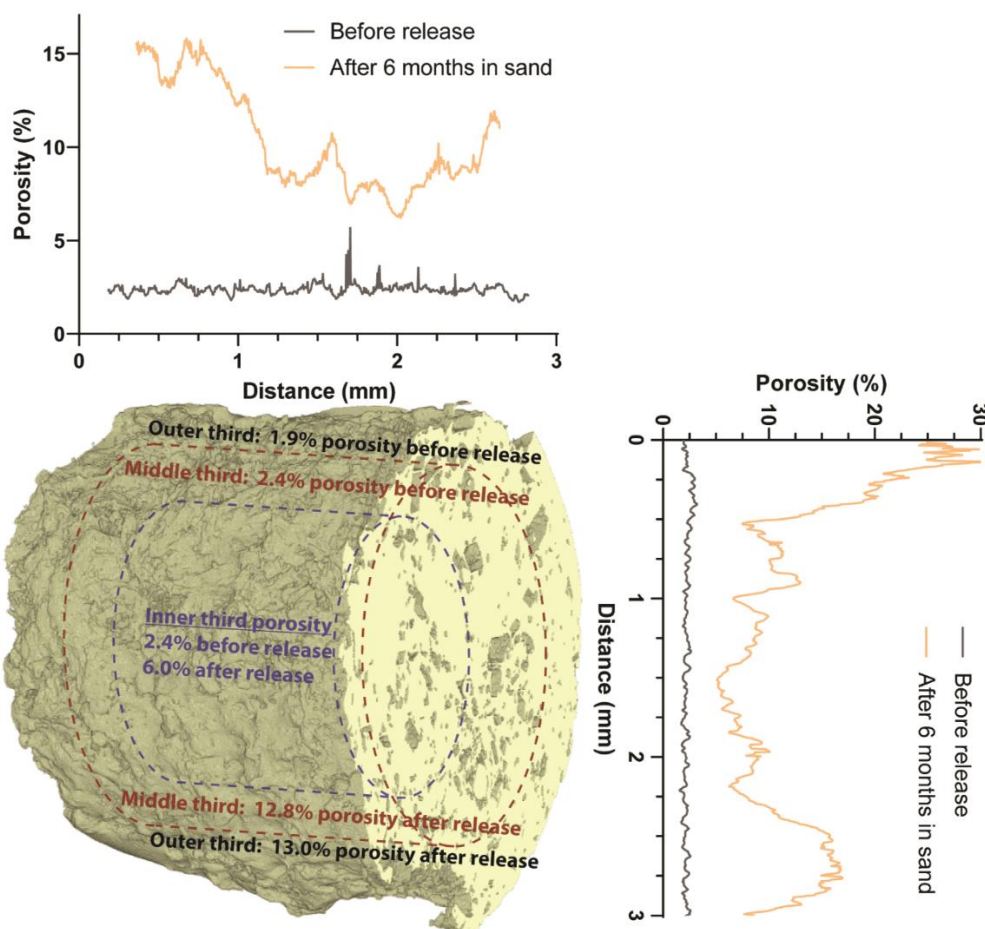
Figure 6.5: Spatial distribution of void space within the DCD-PHBV pellet before and after release. The line graphs were generated from 2-D analysis (i.e., slice by slice) in the transaxial and coronal directions. The porosities of the inner, middle and outer volumes were generated by the 3-D porosity analysis, keeping the height to diameter ratio constant.

6.3.2.3 A proposed mechanism for the slow phase of release

From four weeks until the end of the experiment, DCD is mobilized very gradually. The driving mechanism for this phase of release could be diffusion of DCD through the PHBV polymer, as proposed previously.[164] However, the high-resolution (0.5 µm) µ-CT images (Figure 6.6) show fine

cracks through the PHBV matrix, both before and after release, which were impossible to visualize at the 4 µm resolution. These images show:

i) the presence of very fine cracks in the matrix before and after release with widths up to 4-5 µm and down to 0.5-1 µm (limited by the resolution of the technique). An example of a relatively thick crack is shown in Figure 6.6B: crack width of 3.2 ± 0.7 µm;

ii) the preference for cracks to propagate through (or from) pores and edges of DCD crystals;

iii) cracking around the DCD crystals, particularly the large crystals; and

iv) small DCD crystals near the surface of the pellet without associated cracks that were not mobilized.

It is feasible that these fine cracks create a channel for the slow ingress of water to access DCD that was otherwise inaccessible over the six-month timescale of the experiment. These cracks may explain how the DCD was mobilized from the "closed" voids, as presented in Section 6.3.2.2. PHB and PHBV are known to undergo gradual secondary crystallisation, leading to increased brittleness.[174] This contraction may drive crack formation and propagation through the composite matrix.
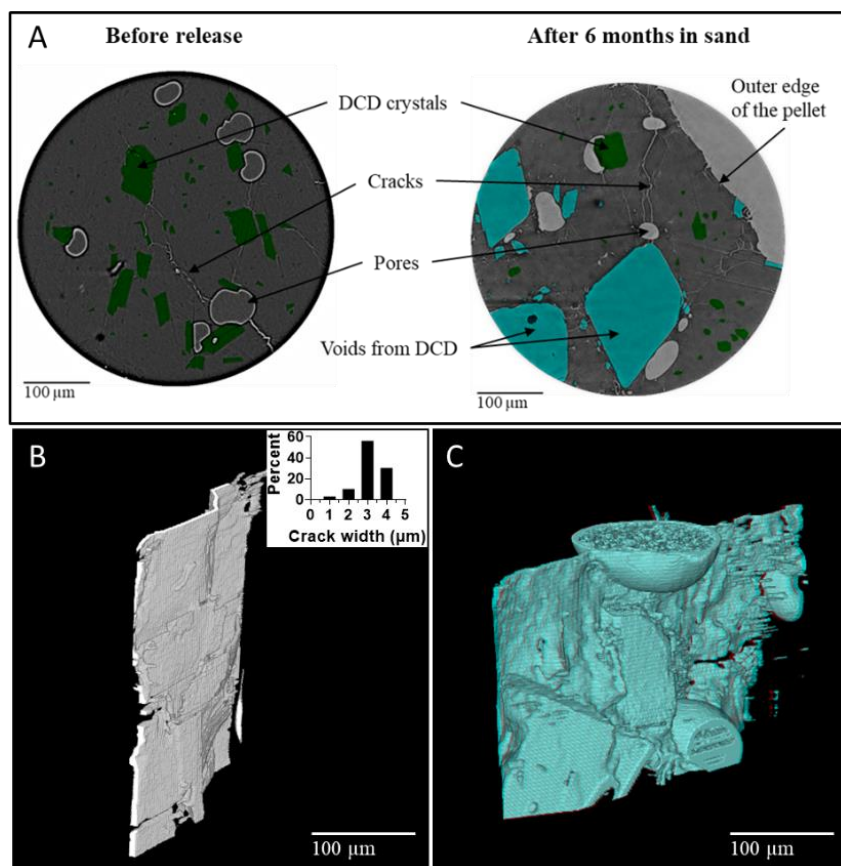
Figure 6.6: A) Colour-coded cross-sectional μ-CT slices from the high-resolution (0.5 µm) acquisition before (right) and after (left) release into water. Green indicates DCD crystals; blue represents voids generated when DCD crystals are released; light regions shown existing pore/void space and dark regions are the PHBV matrix. B) 3-D section highlighting a relatively thick transaxial planar crack with the crack size distribution. C) 3-D image of a crack passing straight through the middle of a spherical pore. Both B) and C) are isolated cracks from the pellet before release.

The role of cracks in controlled release from hydrophobic polymers has been speculated previously.[120] These authors suggested that microcracks or polymer chain reptation could be responsible for the slow phase of release of bovine serum albumin (BSA) from macroporous ethylene-vinyl acetate, though there was no evidence in support of either. In a following study, Siegel and Langer[175] proposed three models for the slow kinetics of BSA release: concentration-dependent diffusivity, random pore topology, and pore constriction, and concluded the latter was the only mechanism that could account for the extreme impedance on release. The constriction is described as narrow channels or throats with micron scale diameters that connect varicose pore bodies formed by drug particle aggregates during the casting process. Brook and van Noort[160] proposed that channels and cracks contribute to antibiotic drug release from acrylic resin, where serial rupturing of thin

polymer layers encapsulating hydrocortisone particles is suggested to create a pathway for drug mobilisation. It was proposed that the channels were created from the pressure induced from the dissolution of the osmotically active drug, however evidence of this was not provided. A three dimensional, non-destructive imaging technique, such as μ-CT could help support the conceptual and mathematical models proposed in the literature and provide quantitative input parameters, such as initial porosity, pore sizes and connectivity.

The presence of cracks within this composite material is an important discovery which improves our understanding of the mechanism controlling the latter phase of the release profile. This may extend to other composite materials that utilize a highly hydrophobic polymer matrix, such as other slow and controlled-release agrichemicals (fertilisers, pesticides, herbicides), drugs and medical implants alike. Further, such cracks in the matrix will contribute to the rate of release associated with the biodegradation of a biodegradable polymer matrix. The cracks found here are sufficiently large for extracellular enzyme migration, with the approximate size of PHB depolymerase around 4-5 nm,[176] around 1000 times smaller than the largest cracks in the matrix. Such enzymes will cleave the ester linkages of the PHBV backbone, further widening the channels, accelerating release, and creating new pathways for release. This presents an important consideration that is typically omitted from both biodegradation modelling and release kinetic modelling from hydrophobic biodegradable matrices.

These findings may also have implications for understanding brittle failure in composited materials. Polyhydroxyalkanoate (PHA) -based composites have received recent attention due to the environmentally friendly end-of-life biodegradation of such materials.[177] However, stiffness and brittleness due to their high crystallinity, and associated failure points at the interspherulitic interfaces as well as unfavorable embrittlement due to the slow interlamellar secondary crystallisation remain a challenge.[178] It is likely these processes lead to cracking in the composite matrices both initially and over time, but further investigation is needed. Beneficially, the presence of these channels may accelerate the rate of biodegradation, as discussed above, and reduce the time for breakdown of PHA-based biocomposites in landfill or natural environments.

6.4   Conclusions

The evidence presented here allows a clear understanding of the different mechanisms that control the mobilisation of a soluble crystalline material from a hydrophobic matrix over the relevant time frames. The release profiles of DCD crystals from a PHBV matrix can be summarized into three distinct phases of release:

i)   rapid release of surface available DCD (0-5 hours);

ii) fast release mediated by interconnected DCD crystals and pores (5 hours - ~8 weeks); and

iii) slow mobilisation likely mediated by diffusion along fine cracks within the matrix and diffusion through the polymer matrix (~4 weeks onward).

These mechanisms are supported by SEM and μ-CT characterization of the materials before and after release. Evidence of cracking in the matrix is a novel finding that could provide insights for controlled release materials based on hydrophobic polymers and for the performance and biodegradation of composite materials based on polyhydroxyalkanoates.

CHAPTER 7

Designing for effective controlled release in agricultural products: new insights into the complex nature of the polymer–active agent relationship and implications for use

Ian Levett, Minjie Liao, Chris Pratt, Matthew Redding, Bronwyn Laycock & Steven Pratt

Abstract

Various active chemical agents, such as soil microbial inhibitors, are commonly applied to agricultural landscapes to optimise plant yields or minimise unwanted chemical transformations. Dicyandiamide (DCD) is a common nitrification inhibitor. However, it rapidly decomposes under warm and wet conditions, losing effectiveness in the process. Blending DCD with an encapsulating polymer matrix could help overcome this challenge and slow its release. Here, we encapsulated DCD in a biodegradable matrix of poly(3-hydroxybutyrate-*co*-3-hydroxyvalerate) (PHBV) and investigated the effects of DCD crystal size and loading rates on release rates.

Three DCD crystal size fractions (0-106, 106-250 and 250-44µm) were blended with PHBV at 200, 400, 600 and 800 g.kg^{-1} loadings through extrusion processing and release kinetics were studied in water over eight weeks. For loadings $\geq$600 g.kg^{-1}, more than 95% release was reached within the first seven days. By contrast, at 200 g.kg^{-1} loading only 10%, 36% and 57% of the DCD was mobilized after eight weeks in water for 0-106 µm, 106-250 µm and 250-420 µm crystal size fractions, respectively.

The lower percolation threshold for this combination of materials lies between 200 and 400 g.kg^{-1} DCD loading. The grind size fraction of DCD significantly affects the quantity of burst release from the surface of the pellet, particularly below the lower percolation threshold. The results presented here are likely translatable to the encapsulation and release of other crystalline materials from hydrophobic polymer matrixes used in controlled release formulations, such as fertilisers, herbicides and pesticides.

7.1   Introduction

Over the last century, humans have more than doubled the total global flow of nitrogen (N).[4] Synthetic N fertilisers contribute ~46% of the 210 million tonnes (Tg) of N cycling the Earth system due to anthropological activities. Of this 96 Tg N, more than half is lost directly to the environment from agricultural soils.[136] Applied N is lost through direct volatilisation of urea and ammonia (NH$_3$), or transformed by microbes to gaseous nitrogen oxides (NO$_x$) and nitrous oxide (N$_2$O), a potent greenhouse gas, or to highly soluble forms, including ammonium (NH$_4^+$), nitrite (NO$_2^-$) and especially nitrate (NO$_3^-$), which are lost through leaching and runoff. These losses lead to major environmental harm and human health implications.[27] Retention of reactive N in the soil can be improved using nitrification inhibitors (NIs).[6] Synthetic NIs, such as dicyandiamide (DCD), 3,4-dimethyl-1H-pyrazole phosphate (DMPP) and 2-chloro-6-(trichloromethyl)-pyridine (nitrapyrin) have been studied extensively, predominantly in temperate climates.[73] These compounds bind to microbial

enzymes in the soil that rapidly oxidise ammonium to nitrate. By retarding this N transformation, inhibitors have shown success in reducing N loses to the environment and increasing crop N use efficiency and crop yields.[6, 138-139, 179] However, the persistence of NIs diminishes exponentially with soil temperature[73, 140] and they are therefore typically not effective in tropical agriculture. If the duration of inhibition could be extended, their potential in tropical agriculture could be realised.

One approach to achieve this is through slow release formations, where the NI is protected from degradation within a polymer matrix and gradually mobilises into the soil profile.[78-79, 164, 180] The present study builds on our previous work,[164] where DCD was extruded as a composite material within a biodegradable polymer matrix, namely poly(3-hydroxybutyrate-*co*-3-hydroxyvalerate) (PHBV). This bacterial polyester has been studied extensively for the controlled release of drugs,[181-183] food packaging additives[184] and agrichemicals[93, 100-101, 103, 105] due to its ability to slow the rate of water diffusion, biocompatibility and biodegradability in almost any environment, including soils, fresh water systems and oceans. Our previous study revealed that, at loading of 250 g.kg^{-1} mobilisation of DCD from the PHBV matrix occurs via four distinct mechanisms: (i) initial rapid dissolution of surface available DCD, (ii) channelling of water through voids and pores in the PHBV matrix, (iii) gradual diffusion of water and DCD through layers of PHBV, and (iv) biodegradation of the PHBV matrix.[164] However, the work did not consider mobilisation from highly loaded materials, and associated highly interconnected DCD pathways. High loadings minimise the amount of polymer required and are therefore commercially attractive.

This current study investigates the interconnectivity between DCD crystals within a PHBV matrix as a function of DCD crystal size and loading. As the loading is increased, a threshold concentration will be reached, known as the percolation threshold, where DCD crystals will become interconnected, rather than being encapsulated in polymer, and complete release will be rapid.[185] Percolation theory is a statistical method of characterising interconnectivity within disordered materials, developed by Broadbent and Hammersley[186] to determine the probability of a fluid percolating through a porous stone. It was first adopted by Leuenberger et al.[117] for slow/controlled release studies to improve understanding of pharmaceutical solid dosage forms. Two percolation thresholds, the upper and lower thresholds, were defined in the context of slow/controlled release materials. The lower threshold relates to the percolation of the solid active component throughout the material. Below the lower threshold, a loaded compound is considered to be encapsulated in polymer, and incomplete release may be observed. When the loading reaches the lower percolation threshold, clusters of particles and voids begin to span the matrix, forming an infinite connected path (percolation) and complete release is observed. The upper percolation threshold relates to the point at which there is no longer a continuous network of the polymer that ensures matrix integrity.[117]

Here, both the upper and the lower percolation thresholds were determined for three DCD crystal size fractions. To determine the upper percolation threshold, loadings were increased to the point where a continuous strand could no longer be extruded, i.e., a loss of matrix integrity was observed. The lower percolation thresholds, the primary focus of this work, were determined by studying the release kinetics in water and imaging the pellets in 3-D using micro-computed tomography (μ-CT) to determine the period for complete release and the degree of connected channels, respectively. To our knowledge, this is the first account for the investigation of percolation in controlled release materials using μ-CT.

Developments presented here provide broad insights into the design of matrix-type materials for the controlled release of crystalline agrichemicals. Knowledge of the degree of interconnectivity between crystals and of the percolation thresholds for materials produced under a range of crystal sizes allows for the sensible design of long-term release materials produced through industrially relevant extrusion processing.

7.2 Materials and Methods

7.2.1 Materials

Dicyandiamide (DCD) and poly(3-hydroxybutyrate-*co*-3-hydroxyvalerate) (PHBV) were used in this study, see Section 4.2 for details.

7.2.2 Extrusion processing of slow release DCD-PHBV formulations

As received DCD powder was pulverized using a SPEX SamplePrep Freezer/Mill™ model 6870. The ground DCD was then sieved using a Retsch AS200 analytical sieve shaker (Merck) into 0-106 µm, 106-250 µm and 250-420 µm size fractions. The ground DCD fractions were thoroughly mixed with PHBV powder in three mass ratios to generate mass loadings of 200, 400, 600 and 800 g.kg^{-1} DCD for each of the three size fractions. Formulations were then melt compounded through extrusion processing at 180°C, as detailed in Section 4.3. A vent was used at Zone 8 of the extruder to remove any vapours produced and to minimize product porosity. Extruded strands were pelletised to produce ~3×3 mm cylindrical pellets.

7.2.3 Characterisation of the slow release formulations

7.2.3.1 Monitoring the mobilisation of DCD from the PHBV matrices

The release kinetics of DCD into water from the PHBV composites were monitored at a temperature of 23 ± 1 °C, with five pellets (~30-40 mg each) in each container (see Section 4.4.1 for details). 1 mL samples were taken at 1 min, 30 min, 1 h, 2 h, 5 h, 10 h, 1 d, 2 d, 4 d, 7 d, 14 d, 28 d,

42 d and 56 d. The DCD was quantified using ultraviolet-visible (UV-Vis) spectroscopy (see Section 4.5.3).

The initial DCD loadings (Table 7.1) were estimated based on the nitrogen content of each material. Approximately 1 g of each material was cryogenically milled to a fine powder using a SPEX SamplePrep Freezer/Mill™ model 6870. The nitrogen content was then quantified using a LECO TruMac DUMAS combustion analyser, following methods reported in Walsh[187]. All five pellets from two of the three repeats were then used to quantify the DCD remaining in the pellets after eight weeks in water (see Section 4.4.1).

Table 7.1: The measured DCD loadings for each of the materials fabricated.

Size fractions Target Loadings	0-106 µm	106-250 µm	250-420 µm
200 g.kg^{-1}	190 g.kg^{-1}	190 g.kg^{-1}	199 g.kg^{-1}
400 g.kg^{-1}	390 g.kg^{-1}	387 g.kg^{-1}	391 g.kg^{-1}
600 g.kg^{-1}	589 g.kg^{-1}	584 g.kg^{-1}	601 g.kg^{-1}
800 g.kg^{-1}	793 g.kg^{-1}	n/a	n/a

7.2.3.2 Porosity analysis

Micro-computed tomography (µ-CT) was used to investigate the starting porosity and pore size distribution of the extruded pellets. The pellets were also scanned after eight weeks exposure in water to investigate the change in void space throughout the pellets. The µ-CT images were acquired over 360° with a Skyscan 1272 (Skyscan, Bruker, Belgium), as detailed in Section 4.6.3.

Images were binarised, with the threshold determined manually to best represent pores as black pixels and solid material (PHBV and DCD) as white pixels. The threshold varied due to the differences in acquisition parameters used and the differences in density of each pellet, which changed depending on the amount of DCD remaining in the pellet. A shrink-wrap algorithm was used to define the volume of interest (VOI) as the volume of the pellet. The 3-D analysis was then run to find the total porosity (black voxels/total voxels within the VOI (V_t)), open porosity (black voxels with a connected path of black voxels to outside the VOI, i.e., to the surface of the pellet/ V_t), closed porosity (black voxels that are not connected to outside the VOI/ V_t) and the pore size distribution (defined by the largest circle that can fit within a cluster of black voxels).

7.2.4 Statistical comparison of release profiles

To determine if two release profiles are statistically different from one another, a dissolution profile comparison test was conducted by calculating the similarity factor, f_2[188]

$$f_2 = 50 \log \left\{ \left[1 + \frac{1}{n} \sum_{t=1}^{n} W_t (R_t - T_t)^2 \right]^{-0.5} \times 100 \right\} \qquad \text{Eq. 7.1}$$

where n is the number of the sampling points, R_t and T_t are the mean reference and test fractional release (up to first point >85%) at time point t, and W_t is a weight factor, considered here to be one, meaning each time point was treated equally. For f_2 values greater than 50, release profiles are considered equivalent or similar. An f_2 factor that is less than 50 represents an average difference between the means of greater than 10%. Values of f_2>50 confer statistical similarity between the release profiles. Bootstrap 90% confidence intervals[189] were generated using the DDsolver Excel plugin[190] using a bootstrap number of 5000.

7.2.5   *Parameterisation of characteristic phases of release*

Fitting empirical models to the release data allows for quantitative comparisons of the data sets and the prediction of release profiles for materials not studied here. Release curves were divided into three distinct phases of release, based on the mechanisms for release presented in Levett et al.[164]. The initially rapid or 'burst' release from the surface of the pellet was modelled using a power law correlation, Eq. 7.2. The second phase of release was mediated through channelling through connected paths of DCD crystals. This phase was simulated using a first order exponential decay, Eq. 7.3. For materials that did not release 100% of the DCD through connected pathways, a very gradual mobilisation occurred from three weeks onward, possibly being accessed through polymer diffusion, or diffusion along cracks in the matrix. This phase of release was fitted to a zero-order model, Eq. 7.4. The fourth mechanism presented in Levett et al.[164], associated with biodegradation of the matrix, was not considered for these water-based release experiments where there was no evidence of significant biodegradation over the elution period.

Surface wash:	$F_1 = A t^B$	$for\ t < 5h$	Eq. 7.2
Connected paths:	$F_2 = F_{1\ @\ t=5\ h} + C\left(1 - e^{-D(t-0.208)}\right)$	$for\ 5\ h < t < 21\ d$	Eq. 7.3
Polymer/crack diffusion:	$F_3 = F_{2\ @\ t=21\ d} + E(t - 21)$	$for\ 21\ d < t < 56\ d$	Eq. 7.4

where F is the fractional release over time, t, and A, B, C, D and E are constants.

7.3   Results

7.3.1   *Upper percolation threshold*

Loadings of 200, 400, 600 and 800 g.kg^{-1} were extruded under the same conditions for the three

DCD crystal size fractions. For the smallest DCD crystals, 0-106 µm, the composite material integrity was maintained, even at 800 g.kg^{-1} DCD. Therefore, the upper percolation threshold lies somewhere between 800 and 1000 g.kg^{-1} DCD loading, where the latter is simply pure DCD. For 106-250 µm and 250-420 µm size fractions, the extruded strand lost integrity at 800 g.kg^{-1}. For these crystal sizes, the upper percolation threshold lies between 600 and 800 g.kg^{-1}.

7.3.2   Characterisation of slow release inhibitor formulations

7.3.2.1   Mobilisation of DCD from a PHBV matrix

For each material, five pellets were added to water at 23 °C and the concentration of DCD in the water was monitored over eight weeks. The release profiles are shown in Figure 7.1. The release data show that both DCD and crystal size and loadings markedly influence DCD mobilisation from the pellets.
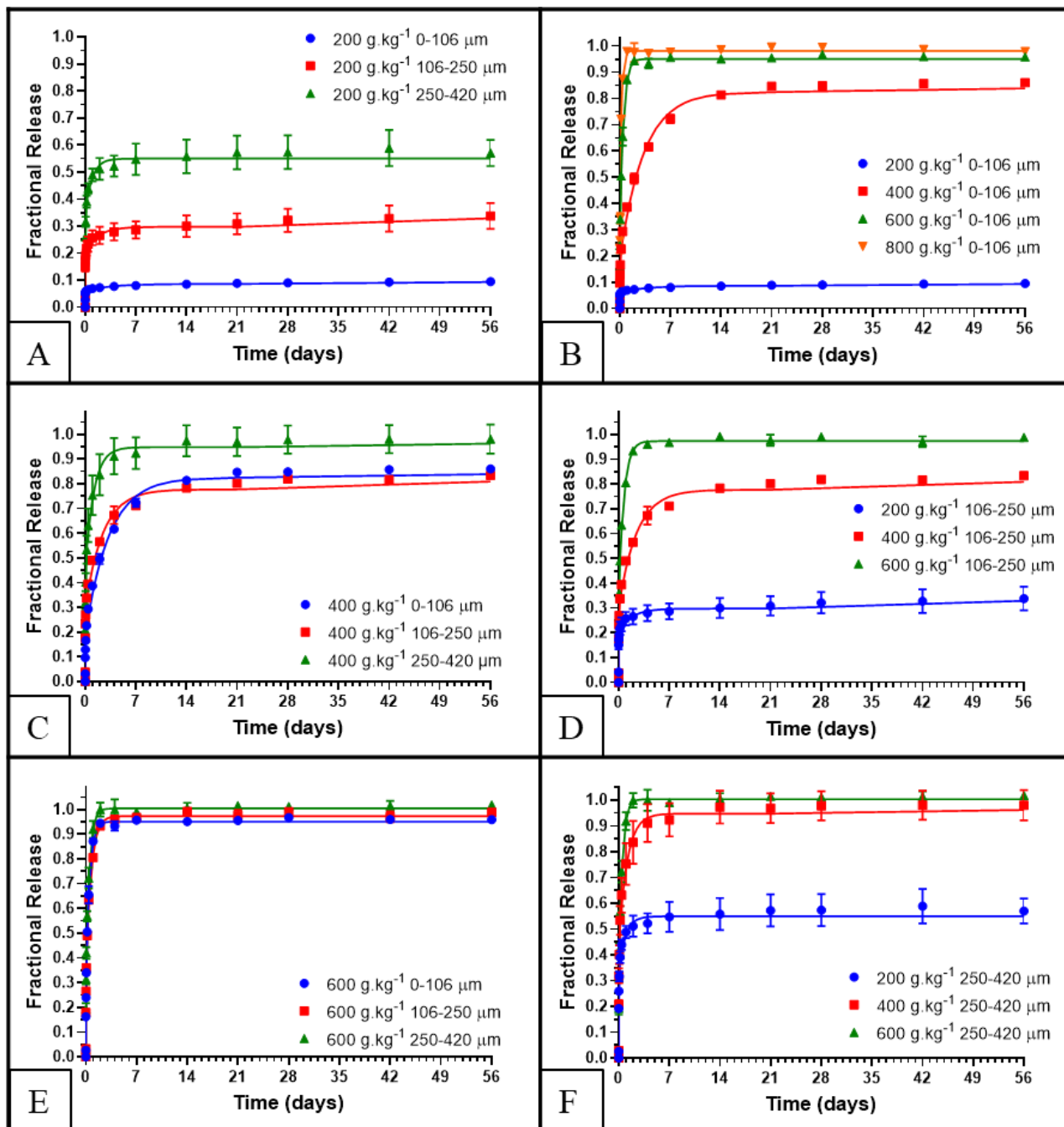
Figure 7.1: Fractional release of DCD into water at 23 °C from the ten DCD-PHBV materials. The left column (A, C, E) show the effect of DCD crystal size for each leading (200, 400 and 600 g.kg⁻¹, respectively) and the right column (B, D, F) show the effect of loading for particle size (0-106 μm, 106-250 μm, 250-420 μm). Error bars indicate the standard deviation of the triplicate data sets.

Five of the materials showed complete release of the DCD (>95% release) within the eight-week experiment. These were 400 g.kg⁻¹ 250-420 μm, 600 g.kg⁻¹ 0-106 μm, 600 g.kg⁻¹ 106-250 μm, 600 g.kg⁻¹ 250-420 μm and 800 g.kg⁻¹ 0-106 μm, with times to >90% release of 4 d, 2 d, 2 d, 1 d, and 1 d, respectively. The other five materials contained a significant amount (>10%) of

encapsulated DCD after eight weeks. The 200 g.kg^{-1} 0-106 µm, 200 g.kg^{-1} 106-250 µm, 200 g.kg^{-1} 250-420 µm, 400 g.kg^{-1} 0-106 µm and 400 g.kg^{-1} 106-250 µm materials contained 90.5 ± 0.04%, 66.2 ± 2.8%, 42.9 ± 2.8%, 14.0 ± 0.3% and 16.7 ± 0.3% of the initial DCD at the end of the experiment, respectively. Release curves were compared quantitatively using the similarity factors (f$_2$ values), shown in Table 7.2. These results allow individual profiles to be compared to determine whether they are statistically similar (f$_2$>50) or not (f$_2$<50). Further, the values show trends in the effect of DCD crystal size and loading, discussed further in Section 7.3.2.3 and 7.3.2.2, respectively, where decreasing f$_2$ values show greater differences between release profiles.

Table 7.2: Results for similarity factors (f$_2$) and the bootstrap 95% confidence intervals (CIs) for the comparison of release profiles. Values of f$_2$>50 confer statistical similarity between the release profiles.

Pairs of release profiles	f$_2$ values (95% CIs)	Pairs of release profiles	f$_2$ values (95% CIs)
Effect of DCD crystal size		**Effect of DCD loading**	
$f_{2(200\ \text{g.kg}^{-1}\ 0\text{-}106\ \mu\text{m},\ 200\ \text{g.kg}^{-1}\ 106\text{-}250\ \mu\text{m})}$	36.6 (34.2-39.3)	$f_{2(200\ \text{g.kg}^{-1}\ 0\text{-}106\ \mu\text{m},\ 400\ \text{g.kg}^{-1}\ 0\text{-}106\ \mu\text{m})}$	15.5 (15.3-15.7)
$f_{2(200\ \text{g.kg}^{-1}\ 0\text{-}106\ \mu\text{m},\ 200\ \text{g.kg}^{-1}\ 250\text{-}420\ \mu\text{m})}$	20.2 (18.8-21.8)	$f_{2(400\ \text{g.kg}^{-1}\ 0\text{-}106\ \mu\text{m},\ 600\ \text{g.kg}^{-1}\ 0\text{-}106\ \mu\text{m})}$	28.8 (28.3-29.2)
$f_{2(200\ \text{g.kg}^{-1}\ 106\text{-}250\ \mu\text{m},\ 200\ \text{g.kg}^{-1}\ 250\text{-}420\ \mu\text{m})}$	33.9 (30.3-38.4)	$f_{2(600\ \text{g.kg}^{-1}\ 0\text{-}106\ \mu\text{m},\ 800\ \text{g.kg}^{-1}\ 0\text{-}106\ \mu\text{m})}$	44.5 (42.5-46.0)
$f_{2(400\ \text{g.kg}^{-1}\ 0\text{-}106\ \mu\text{m},\ 400\ \text{g.kg}^{-1}\ 106\text{-}250\ \mu\text{m})}$	**56.6 (55.1-57.7)**	$f_{2(200\ \text{g.kg}^{-1}\ 106\text{-}250\ \mu\text{m},\ 400\ \text{g.kg}^{-1}\ 106\text{-}250\ \mu\text{m})}$	23.4 (21.9-25.0)
$f_{2(400\ \text{g.kg}^{-1}\ 0\text{-}106\ \mu\text{m},\ 400\ \text{g.kg}^{-1}\ 250\text{-}420\ \mu\text{m})}$	28.8 (26.0-32.0)	$f_{2(400\ \text{g.kg}^{-1}\ 106\text{-}250\ \mu\text{m},\ 600\ \text{g.kg}^{-1}\ 106\text{-}250\ \mu\text{m})}$	34.7 (34.3-35.2)
$f_{2(400\ \text{g.kg}^{-1}\ 106\text{-}250\ \mu\text{m},\ 400\ \text{g.kg}^{-1}\ 250\text{-}420\ \mu\text{m})}$	37.0 (33.0-42.1)	$f_{2(200\ \text{g.kg}^{-1}\ 250\text{-}420\ \mu\text{m},\ 400\ \text{g.kg}^{-1}\ 250\text{-}420\ \mu\text{m})}$	37.9 (32.8-43.9)
$f_{2(600\ \text{g.kg}^{-1}\ 0\text{-}106\ \mu\text{m},\ 600\ \text{g.kg}^{-1}\ 106\text{-}250\ \mu\text{m})}$	**74.9 (71.6-77.0)**	$f_{2(400\ \text{g.kg}^{-1}\ 250\text{-}420\ \mu\text{m},\ 600\ \text{g.kg}^{-1}\ 250\text{-}420\ \mu\text{m})}$	**56.5 (47.4-67.6)**
$f_{2(600\ \text{g.kg}^{-1}\ 0\text{-}106\ \mu\text{m},\ 600\ \text{g.kg}^{-1}\ 250\text{-}420\ \mu\text{m})}$	**61.4 (54.9-68.6)**		
$f_{2(600\ \text{g.kg}^{-1}\ 106\text{-}250\ \mu\text{m},\ 600\ \text{g.kg}^{-1}\ 250\text{-}420\ \mu\text{m})}$	**58.0 (53.3-63.1)**		

The mass balances for the water release experiments are shown in Figure 7.2. The amount of DCD accounted for in the water plus the quantity of DCD remaining in the pellet after the eight-week experiment were within ±10% of the total expected DCD for all trials, except for the 400 g.kg^{-1} 250-420 µm replicate 2, where 115% of the expected DCD was accounted for. We are comfortable with this variance considering these are materials fabricated through extrusion processing, resulting in some variability in the loading from pellet to pellet, especially for materials with the largest DCD crystals.
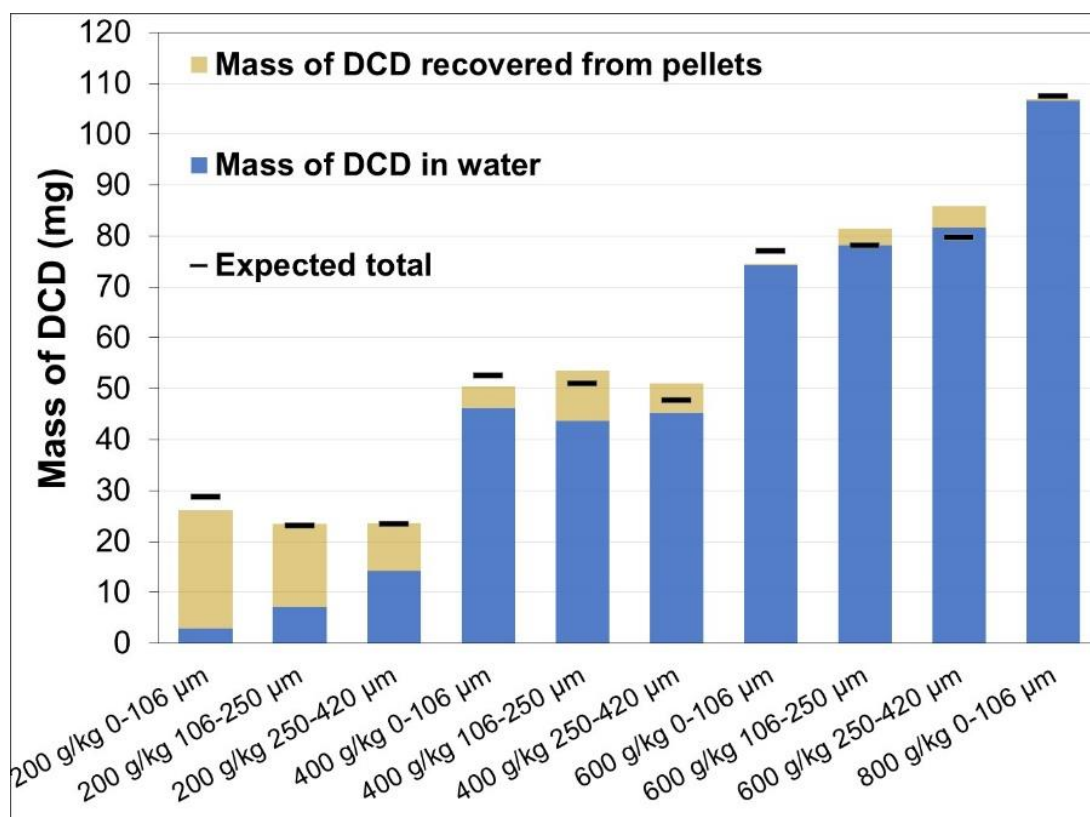
Figure 7.2: Mass balance for DCD for one of the three replicate trials for each of the ten materials studied. The stacked columns show the DCD quantified in the water after eight weeks (blue) and the DCD extracted from the pellets at the end of the experiment (orange). The total amounts of DCD quantified were compared against the expected total DCD based on the initial DCD loadings (Table 7.1) calculated from the elemental N assays.

7.3.2.2   Effect of DCD loading

A comparison of the release profiles from materials with the same DCD crystal size fractions is shown in the right column of Figure 7.1 (B, D and F). The most significant change in release rate occurred when the loading was increased from 200 to 400 g.kg^{-1}. For materials with 0-106 µm DCD crystals, the fraction released after eight weeks jumped from $9.1 \pm 0.1\%$ at a 200 g.kg^{-1} loading to $86.0 \pm 0.5\%$ for a 400 g.kg^{-1} loading. Similarly, for materials with 106-250 µm and 250-420 µm DCD crystal size fractions, the amount released jumped from $34 \pm 5\%$ and $57 \pm 5\%$ for 200 g.kg^{-1} loadings to $83.3 \pm 0.5\%$ and $95 \pm 5\%$ at 400 g.kg^{-1} loadings, respectively, after eight weeks.

The effect of loading was greater for the smaller DCD crystal sizes, shown by the reduction in f_2 values (Table 7.2). For all materials with 600 and 800 g.kg^{-1} loadings, release was rapid, with >90% released within the first two days and >95% within the first seven days for all DCD size fractions.

In most cases, higher loadings resulted in a significantly higher release rate and fractional release, except when comparing 600 g.kg^{-1} 0-106 µm to 800 g.kg^{-1} 0-106 µm, and 400 g.kg^{-1} 250-420 µm to

600 g.kg^{-1} 250-420 µm, where the f$_2$ values were greater than 50 and therefore these profiles were considered similar.

7.3.2.3   Effect of DCD crystal size

A comparison of the release profiles from materials with the same DCD loading is shown in the left column of Figure 7.1. Generally, the amount of release and release rates increased with larger DCD crystal size fractions. The effect of particle size was most pronounced at the lowest loading of 200 g.kg^{-1}. This is supported by the decreasing similarity factors with lower loadings (Table 7.2), which numerically shows that the curves are further apart as the loading is reduced. At 200 g.kg^{-1}, the majority of release was associated with DCD exposed at the surface of the pellet. The amount of DCD mobilised increased linearly with DCD crystal size. For the higher loadings of 400 g.kg^{-1} and 600 g.kg^{-1}, the release was rapid and the DCD crystal size had less effect on the release profiles. At 400 g.kg^{-1} loading, the amount of release was statistically similar for 0-106 µm and 106-250 µm fractions, with 72.3 ± 1.7% and 71.1 ± 1.6%, respectively, compared to 92.4 ± 6.4% for the 250-420 µm fraction. At 600 g.kg^{-1} loading, all size fractions reached >95% release within the first week with statistically similar release profiles, since f$_2$ > 50.

In addition to increasing rates of release with larger DCD particle size, there was also a higher spread of the data. The average standard deviation for all the data over the eight-week experiment was 0.7%, 1.5% and 3.4% for 0-106 µm, 106-250 µm and 250-420 µm fractions, respectively. This increased spread is a result of more heterogeneous composites being produced with larger crystals in terms of DCD distribution and the size and shape of the DCD crystals (see Figure 7.4 and Table 7.3).

7.3.2.4   Distribution of DCD within the DCD-PHBV pellets

The ten materials studied here were characterized using µ-CT before and after release at 5-7 µm resolution. The 2-D slices were converted to binary maps, making void space appear as black pixels and any material (DCD or PHBV) as white pixels. The binary images were used for 3-D analysis within the CTAn software. A summary of the analysis is shown in Figure 7.3 and Table 7.3. Transaxial and coronal slides taken roughly through the middle of the pellets after release are shown in Figure 7.4A and B, respectively.

The µ-CT scans after release provided information on the mechanisms driving DCD release. Further, they provide information about the distribution of DCD within the pellet, the DCD particle size distribution and the volume of DCD mobilized. The expected porosity (Table 7.3) was calculated by adding the amount of DCD quantified in the water to the initial porosity. Results were comparable to the total porosity calculated by the CTAn 3-D analysis (Table 7.3), with the exception of 600 g.kg^{-1} 0-106 µm. This material was found to have large dense inclusions in the images, possibly because of

entrapped water within the pellet.

The open porosity after release represented >98% of the total porosity for all materials, except for those with a loading of 200 g.kg^{-1}. For these materials, the open porosity made up 30%, 84% and 88% of the total porosity for 0-106 µm, 106-250 µm and 250-420 µm DCD crystals, respectively.
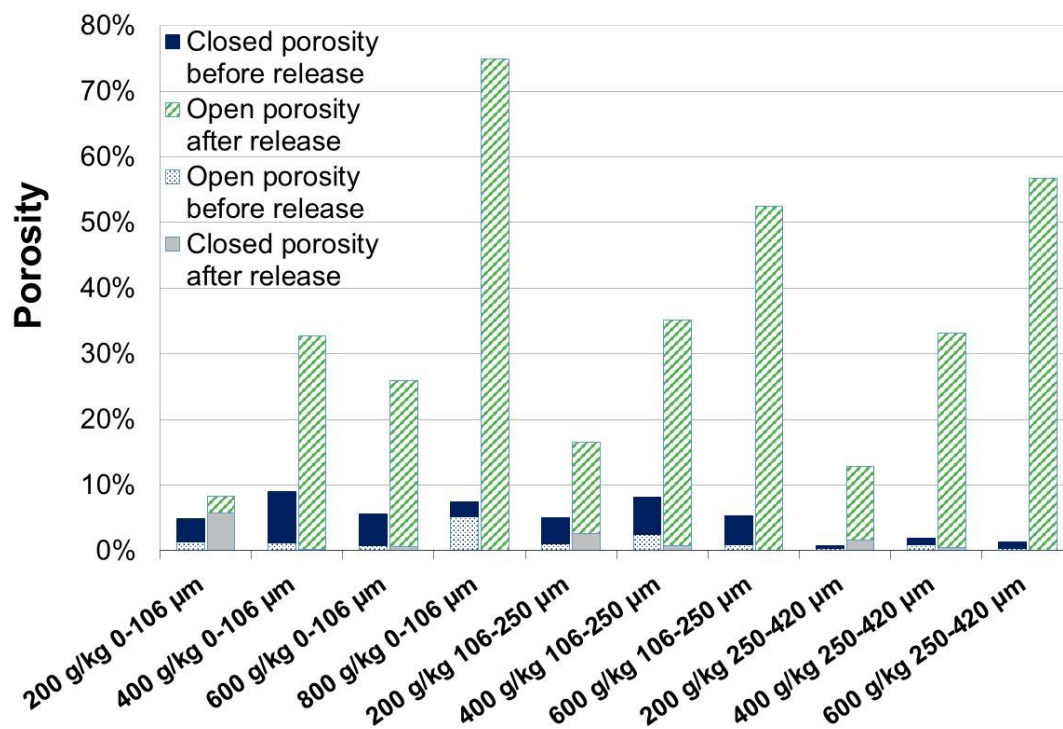
Figure 7.3: Stacked bar graphs showing the open and closed porosity quantified using 3D analysis of the µCT data before and after release.

The initial porosity of the extruded materials increased with decreasing DCD crystal size. It seems that the number of pores was proportional to the number of DCD particles present. However, there was no clear trend of initial porosity with loading. For all materials, initial porosity increased from 200 to 400 g.kg^{-1} loading, but decreased or stabilized from 40 to 600 g.kg^{-1} loading. Interestingly, the pore size decreased with loading for all materials and was significantly smaller for the 250-420 µm crystals compared to the smaller crystal sizes. The initial pores predominantly existed as closed spherical pores. An exception was the 0-106 µm 800 g.kg^{-1} loading material, where 70% of the initial porosity was connected to the surface of the pellet (i.e., open porosity).

Table 7.3: 2-D and 3-D analysis results from the binarised u-CT data using CTAn software.

Material		Pore/void distribution (µm)		Porosity			
		d50	Span	Closed	Open	Total	Expected †
200 g.kg⁻¹ 0-106 µm	Initial	28.4	1.4	3.5%	1.4%	4.9%	
	After release	30.9	1.3	5.7%	2.5%	8.3%	6.6%
400 g.kg⁻¹ 0-106 µm	Initial	22.5	1.3	7.8%	1.2%	9.0%	
	After release	22.3	1.6	0.1%	32.6%	32.7%	41.1%
600 g.kg⁻¹ 0-106 µm	Initial	17.4	1.3	4.8%	0.8%	5.6%	
	After release	20.6	1.7	0.6%	25.3%	25.9%	61.0%
800 g.kg⁻¹ 0-106 µm	Initial	12.5	1.8	2.3%	5.2%	7.5%	
	After release	29.0	1.2	0.0%	74.9%	74.9%	84.0%
200 g.kg⁻¹ 106-250 µm	Initial	34.8	1.1	3.9%	1.1%	5.0%	
	After release	41.5	2.3	2.6%	13.9%	16.5%	12.1%
400 g.kg⁻¹ 106-250 µm	Initial	21.9	1.4	5.7%	2.4%	8.1%	
	After release	47.8	1.9	0.7%	34.5%	35.2%	39.4%
600 g.kg⁻¹ 106-250 µm	Initial	17.6	1.3	4.3%	1.0%	5.3%	
	After release	48.6	2.1	0.1%	52.4%	52.5%	62.5%
200 g.kg⁻¹ 250-420 µm	Initial	19.9	1.8	0.4%	0.4%	0.8%	
	After release	155.0	1.6	1.6%	11.3%	12.9%	11.5%
400 g.kg⁻¹ 250-420 µm	Initial	18.3	1.6	0.9%	0.9%	1.9%	
	After release	125.2	2.0	0.6%	32.5%	33.1%	36.0%
600 g.kg⁻¹ 250-420 µm	Initial	12.8	1.8	0.9%	0.4%	1.3%	
	After release	124.5	2.2	0.1%	56.6%	56.8%	60.0%

† Calculated based on the volume of DCD released and the starting porosity

The transaxial and coronal images through the middle of the pellets after release (Figure 7.4) clearly illustrate the difference in heterogeneity between materials with very fine DCD powder (0-106 µm) compared to a coarse powder (250-420 µm). This is supported by the span of the void distribution increasing with increasing DCD crystal size (Table 7.3) and a decrease in the circularity of the voids.
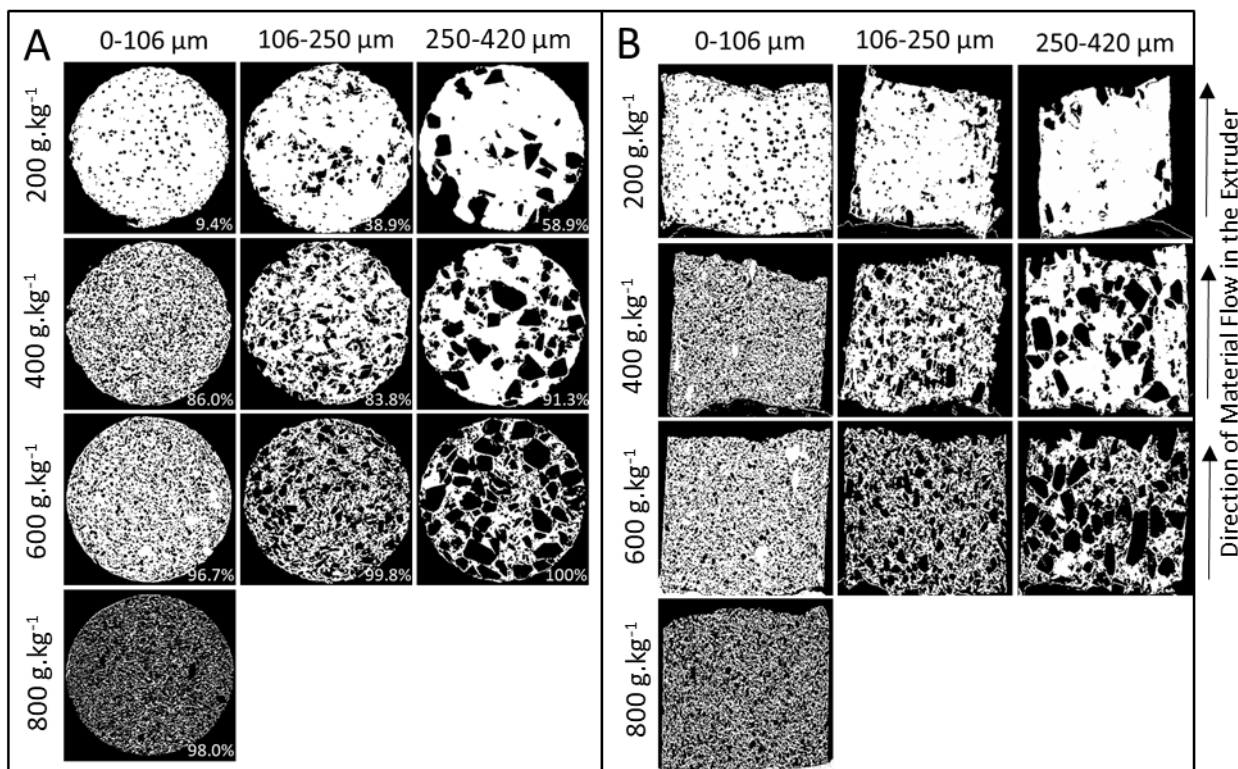
Figure 7.4: Transaxial (A) and coronal (B) binarised cross-sectional μ-CT images for each material after eight weeks exposure to water. The amount of DCD release from these pellets is provided in the bottom right of each transaxial cross-section and the direction of flow within the extruder is shown adjacent to the sagittal cross-sections.

7.3.3 Modelling results

Fitting mathematical equations to the curves allows both the quantitative comparison of experimental runs, and the potential for the prediction of materials that were not fabricated here. The parameters for the curve fits are given in Table 7.4. Depending on the location of the DCD within the pellet, the mechanism and pathway for release will vary. DCD exposed on the surface of the pellet will contact water with dissolution beginning immediately and rapidly. Thus, a power law fitted the first five hours of data well. Data for release from five hours to three weeks fitted a first order exponential decay well. This is reasonable since there will be a diminishing source of DCD within the pellet as release proceeds. The final phase of release (three weeks onwards) is only relevant for materials with a significant amount of DCD remaining within the pellet after three weeks, that is, materials with 200 and 400 g.kg^{-1} loadings. Due to the very slow release during this phase, the shape of the data looks roughly linear, though it would decay over a very long time frame as DCD reserves deplete. This zero-order phase of release can be attributed to dissolution-controlled release, where aqueous DCD concentrations reach saturation or close to it within the fine cracks and voids in the

pellet. Under these conditions, DCD dissolution becomes slow and rate limiting.[191] Only the zero-order fits where the slope was statistically greater than zero are reported in Table 7.4. Otherwise, the slope was considered zero.

Table 7.4: Parameters for the curve fit using the method of least squares.

Materials	Surface wash [Power law]			Connected paths [Exponential decay]			Polymer/crack diffusion [Linear regression]	
	A	B	R^2	C	D	R^2	E	R^2
200 g.kg^{-1} 0-106 μm	0.076	0.14	0.971	0.025	0.29	0.946	2.0×10^{-4}	0.956
400 g.kg^{-1} 0-106 μm	0.39	0.36	0.998	0.60	0.30	0.988	4.0×10^{-4}	0.449
600 g.kg^{-1} 0-106 μm	1.1	0.48	0.998	0.45	2.1	0.992	0	
800 g.kg^{-1} 0-106 μm	1.9	0.61	0.978	0.26	4.3	0.958	0	
200 g.kg^{-1} 106-250 μm	0.31	0.23	0.941	0.080	0.54	0.801	9.0×10^{-4}	0.709
400 g.kg^{-1} 106-250 μm	0.54	0.30	0.986	0.44	0.40	0.978	9.0×10^{-4}	0.705
600 g.kg^{-1} 106-250 μm	0.94	0.42	0.995	0.48	1.4	0.994	0	
200 g.kg^{-1} 250-420 μm	0.66	0.33	0.976	0.16	1.1	0.822	0	
400 g.kg^{-1} 250-420 μm	0.98	0.39	0.973	0.42	0.85	0.887	0	
600 g.kg^{-1} 250-420 μm	1.1	0.43	0.985	0.44	2.1	0.985	0	

For the surface wash (0-5 h), there is a clear trend, with higher loadings resulting in greater values for the power law parameters, A and B. In fact, multilinear regressions (Eq. 7.5 and 7.6) give a reasonable fit for the parameters A and B against the square of the loading and the square of the d_{50} of the DCD crystals and pores obtained from the μ-CT results.

$$A = \alpha_0 + \alpha_1 \times L^2 + \alpha_2 \times d_{50}{}^2 \qquad \text{Eq. 7.5}$$

$$B = \beta_0 + \beta_1 \times L^2 + \beta_2 \times d_{50}{}^2 \qquad \text{Eq. 7.6}$$

Table 7.5: Results for the multivariate linear regression for surface wash curve fit parameters.

Regression Parameters for A	Values (95% CI)	Significantly different from zero?	Regression Parameters for B	Values (95% CI)	Significantly different from zero?
α_0	0.07 (-0.15-0.29)	ns	β_0	0.19 (0.12-0.27)	***
α_1	0.26 (0.20-0.32)	****	β_1	0.06 (0.04-0.09)	***
α_2	24 (7-41)	*	β_2	4 (-2-11)	ns
R^2	0.934		R^2	0.871	

ns = not significantly different from zero (p>0.05), * = p<0.05, **=p<0.01, ***=p<0.001, ****=p<0.0001

The regression shows that the scaling factor, A, is significantly dependent on both loading and DCD crystal size. The exponent, B, however, is only significantly dependent on DCD loading. While there is a positive correlation of B with the square of the crystal size, it was not statistically significant (p=0.137), likely a result of having just three crystal sizes. Still, this regression allows reasonable prediction of the surface wash for loadings not studied experimentally here.

The amount of release in the surface wash largely affects the parameters for fitting the connected pathways (5 h to 21 d). As a result, the exponential decay parameters do not follow a simple trend with loading and/or DCD crystal size. There was also no clear trend for the very gradual diffusion driven release (21 d to 56 d). For this reason, parameters for loadings not studied experimentally were estimated using linear interpolation between loadings for each crystal size fraction independently. The resulting model curve fits are shown in Figure 7.5, along with profiles generated from the interpolated parameter estimation.
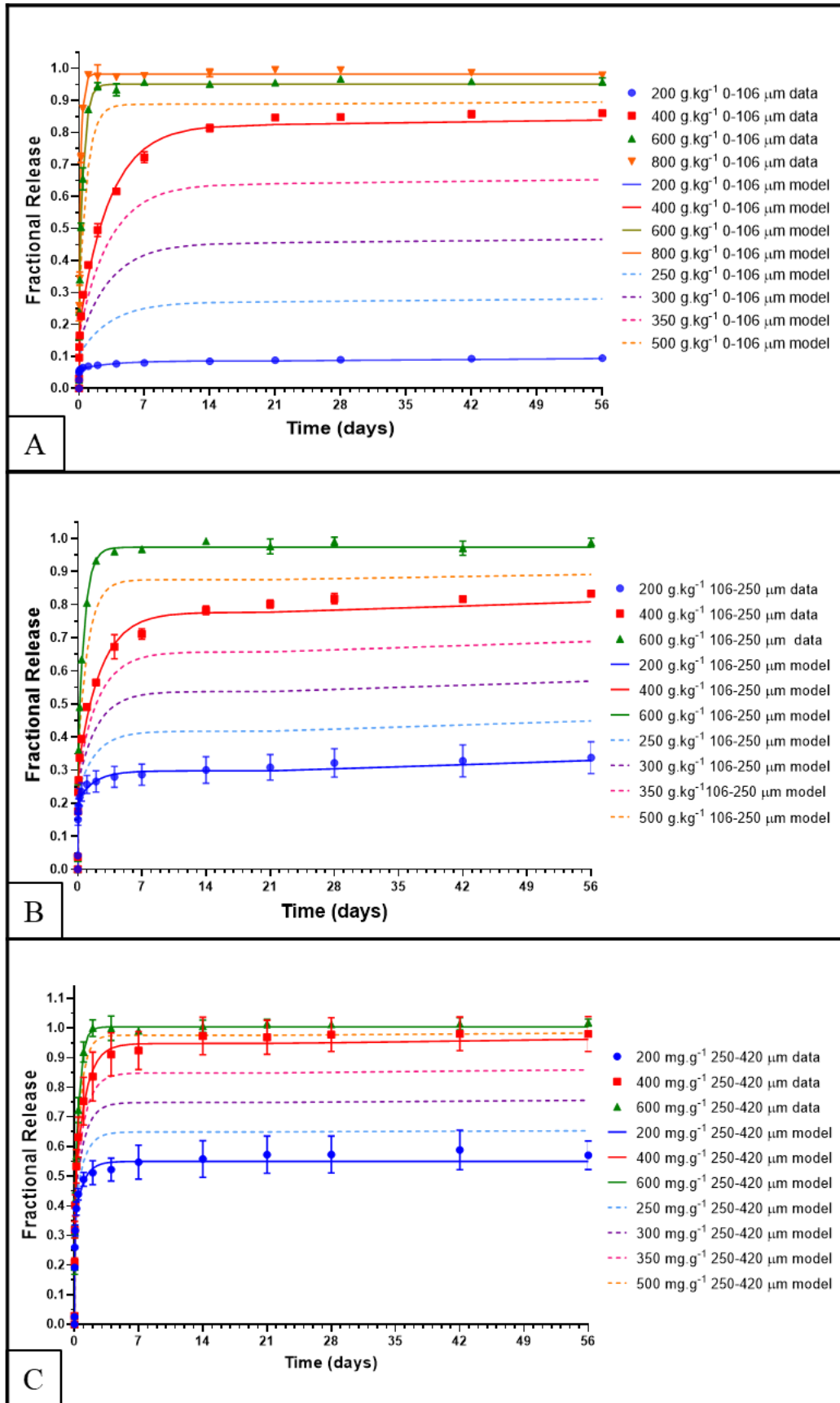
Figure 7.5: Combined curve fits (Eq. 1, 2 and 3) and predicted curves for interpolated loadings for DCD crystal size fractions of 0-106 µm (A), 106-250 µm (B), 250-420 µm (C).

7.4 Discussion and conclusions

In agriculture, controlled release products are able to increase the uptake of agrichemicals by the target organisms, whether it is nutrient uptake by the crop or pesticide uptake by the target pest. Here, we explore slow release as a means of protecting the active nitrification inhibitor, DCD, from microbial attack, to extend its effective lifetime, particularly for tropical agricultural applications. Few studies have explored this concept. Minet et al.[78] encapsulated DCD in glyoxal-crosslinked chitosan hydrogels. Release was significantly slower for beads with higher glyoxal polymerization, but, unfortunately, the encapsulation efficiency was reduced by 75%. Bishop[79] fabricated coated DCD micro-granules using a reactive polyurethane coating process. First, DCD was agglomerated with carboxyl methylcellulose (CMC), followed by drying and screening. Then the micro-granules were sealed with a DCD/CMC solution in a pan coater, before finally coating the granules with either three or four layers of polyurethane. Three layers did not slow the release significantly. However, four layers showed gradual release, with 50% mobilized from the granules after ~40 days. Extrusion processing offers a much simpler encapsulation method to these arduous and complex fabrication techniques.

Extrusion processing is a simple, scalable and industrially relevant fabrication technique for matrix-type slow release formulations. The active component and the polymer can simply be fed to the extruder, which melts the polymer and mixes the components. However, knowledge is limited on the encapsulation and controlled release of active solid agrichemicals fabricated this way. One challenge is the typical high temperatures required to melt the polymer(s). The high thermal stability of DCD (stable up to ~240 °C) allows melt extrusion with the bacterial polymer, PHBV, at 180 °C, without degrading or deactivating the DCD.[164] The results of this study highlight the importance of two fabrication parameters, loading and DCD crystal size, on the degree of interconnected DCD crystals with the composite DCD-PHBV material and the subsequent effect on release kinetics.

7.4.1 Effect of DCD loading on percolation

When exposed to water, DCD at the surface of the pellet dissolves and diffuses into the surrounding solution. If the next layer of DCD contacts the voids created at the surface, the direct path allows water to access the next layer, without permeating any PHBV. The likelihood of interconnected DCD crystals is directly dependent of the ratio of DCD to PHBV within the composite material. When the loading becomes high enough an interconnected path of DCD spans the entire matrix and rapid mobilisation of all the DCD is observed. This loading is known as the lower percolation threshold.[117]

In the multi-mechanism materials studied here, precise determination of the lower percolation

threshold is unrealistic. Still, percolation holds relevance, since clusters of DCD connected to the surface were mobilised rapidly. As Siegel et al.[120] describes, the concept of a percolation threshold should be replaced by the notion of a "critical porosity range", where the lower bound represents a small amount of release and the upper bound is where virtually all the material is mobilised through a percolating network. Here, this has been demonstrated from the release kinetics and µ-CT results. Both data sets indicate that a 200 g.kg^{-1} loading is below the lower percolation threshold, where the majority of release is from the surface of the pellet, and 400 g.kg^{-1} sits above the threshold, where >80% is released, for all DCD crystal sizes. Therefore, the critical porosity range exists between 200 and 400 g.kg^{-1}. This finding is comparable with other drug release studies that have reported percolation thresholds of 35.5%[192], 20-50%[120], 28.0-42.5%[121] and 18.3-34.5%.[193]

Above 400 g.kg^{-1}, connected paths form, where DCD crystals contact each other throughout the matrix and the polymer does not form a barrier for release, but simply acts as a binder. This interconnectivity is confirmed by the 3-D analysis of the µ-CT data. For loadings ≥400 g.kg^{-1}, the open porosity after release represented >98% of the total porosity. This confirms that the released DCD had a connected pathway to the outside of the pellet.

At 200 g.kg^{-1}, the amount of release was significantly lower and the open porosity was highly dependent on the crystal size. For the smallest DCD size fraction, the open porosity after release represented just 30% of the total porosity. Therefore, 200 g.kg^{-1} is below the lower percolation threshold, since the majority of DCD was not released as a result of interconnectivity between DCD crystals and/or pores.

Below the lower percolation threshold, a significant amount of DCD remained encapsulated after eight weeks in water, suggesting a very slow rate of diffusion through the PHBV matrix. A similar result was reported by Siegel et al.[120] who studied the effect of particle size and loading on the release of bovine serum albumin (BSA) from ethylene acetate copolymer matrices. At and above 450 g.kg^{-1}, complete release was realised. At loadings below 450 g.kg^{-1}, the amount of BSA entrapped in the polymer matrix increases, following a sigmoidal response with loading. Following the initial surface release and crystals connected to the surface layer, a very gradual release is reported, with release attributed to either polymer diffusion or matrix imperfections, such as cracking. This is likely the case here, since PHBV is a highly hydrophobic and brittle matrix. For Siegel et al.[120] the fraction not released was considered wasted drug. In our case, at low loadings, it is important to consider the role of polymer degradation on release, since the material will be exposed to a soil environment in practice. Our previous work,[164] showed that for a material with 250 g.kg^{-1} DCD in PHBV, microbial biodegradation of the PHBV matrix accelerated the rate of release into soil from ~28 days onward. The rate of polymer degradation in soil is a complex parameter that depends largely on the soil type,

texture, microbial population present, soil moisture content and temperature.[158, 164] The effect of polymer degradation on release will depend on the thickness of polymer encapsulating the DCD crystals. This thickness will in turn be a function of the initial loading and crystal size. The relationship between polymer degradation and crystal size and/or loading requires further investigation.

7.4.2   Effect of DCD crystal size on percolation

A few studies investigated the influence of drug particle size on the release kinetics and percolation threshold for controlled drug delivery. Millán et al.[121] studied KCl release from Eudragit® RS PM with five KCl particle size fractions and at least eight different drug loadings for each particle size. A positive linear relation was found between the drug percolation threshold and the drug particle size. This indicates that for larger particles, a higher loading is required to generate connected clusters. This aligns with classic percolation theory, where smaller particles are more likely to form an infinite cluster. However, this is in contrast to the results presented here, with more DCD entrapped in the PHBV matrix when the crystal size is smaller. We hypothesised that smaller crystals would be better encapsulated by the PHBV matrix based on our previous work,[164] where large DCD crystals appeared to be mobilised preferentially over smaller crystals. This discrepancy from classic percolation theory is likely due to the irregular shape of the large DCD crystals, the relative size of the crystals to the pellet, the higher aspect ratio (length/width) of larger crystals[194] and the potential alignment of large crystals during extrusion.[195]

This also relates to the upper limit of DCD loading within an extruded PHBV matrix, known as the upper percolation threshold. The results show that finer DCD crystals allow the fabrication of materials with higher loadings. Crystals >106 µm prevent the formation of a continuous strand at loadings at and above 800 g.kg⁻¹. The larger crystals disrupt flow at the extruder die, preventing PHBV from forming a continuous network within the material. As a result, a crumbly, discontinuous strand formed.

The influence of DCD crystal size on release kinetics was most pronounced at loadings below the lower percolation threshold. The significance of this is the ability to tailor the amount of surface wash using the DCD particle size. For example, for a 200 g.kg⁻¹ loading, in tropical regions where microbial activity is higher, a lower amount of surface wash may be desired to protect the majority of the DCD from degradation, so 0-106 µm DCD would be recommended, since only $8.0 \pm 0.1\%$ release was released in the first week. In subtropical regions, 106-250 µm may be more appropriate, where $29 \pm 3\%$ release was observed within the first week. For temperate climates, where microbial activity is lower 250-420 µm would be recommended, since $55 \pm 6\%$ of the DCD was initially

mobilized from the surface. The balance is then mobilised gradually through the biodegradation of the polymer matrix, and via diffusion along cracks and through the polymer matrix.

7.4.3   Modelling and tailoring formulations

At low loadings there are three distinct mechanisms driving release: i) release of surface available DCD; ii) release mediated by interconnected DCD crystals and pores; and iii) release mediated by other processes including diffusion along fine cracks within the matrix. For this reason, no single empirical or semi-empirical model (such as Higuchi, Peppas-Korsmeyer, Peppas and Sahlin, first order etc.) can be utilized to fit the release data for these materials. Hence, the three phases of release are proposed here, each with its own governing empirical model. For materials above the lower percolation threshold, complete release was realized and only the first two mechanisms substantially contributed to release. Parameterising of the data sets allowed interpolation between loadings, providing reasonable prediction of release profiles not studied experimentally (Figure 7.5). This shows the strong ability to tailor the material fabrication process to the desired release profile, without the need to study all the combinations experimentally.

This ability to tailor release is relevant for the broader field of controlled release of crystalline agents from polymer matrices fabricated through extrusion processing. Simple processing metrics, such as the particle size of the active agent, or the ratio of active agent to polymer are cost effective methods of tailoring release. For agricultural applications, target release periods tend to be long (several months). It is therefore recommended from this study, that loadings of <400 g.kg^{-1} be utilised by the encapsulation of crystalline agrichemicals in matrix-type controlled release materials. For long-term release profiles (up to 6-months), loadings of 20-35% would be most appropriate. The fraction of material accessible from the surface of the pellet for a given loading can be controlled by varying the crystal size of the agrichemical.

However, this work is limited to a single polymer of interest. Furthermore, the effect of temperature on release kinetics remains unclear and this knowledge would further aid material design for different climatic conditions. Chapter 8 presents the effect of blending PHBV with a more hydrophilic polymer, polycaprolactone (PCL), on the release rate into water at 10 °C, 23 °C and 40 °C.

CHAPTER 8

Tailoring agrichemical release kinetics through material design: understanding the counterintuitive effect of matrix hydrophobicity

Ian Levett, Minjie Liao, Chris Pratt, Matthew Redding, Steven Pratt & Bronwyn Laycock

Abstract

Nitrification inhibitors (NIs), such as dicyandiamide (DCD), can improve the nitrogen uptake efficiency by plants and reduce environmental losses. Unfortunately, DCD degrades rapidly through microbial action in warm and wet conditions, limiting its efficacy in tropical agriculture. Here, the encapsulation and controlled release of DCD as a model crystalline agrichemical was studied within biodegradable matrices composed of blends of poly(3-hydroxybutyrate-co-3-hydroxyvalerate) (PHBV) and poly(ε-caprolactone) (PCL). DCD was mixed at 400 mg.g^{-1} and extruded with PHBV:PCL blends at mass ratios of 1:0, 3:1, 1:1, 1:3 and 0:1 to produce ~3×3 mm cylindrical pellets. Release into water was monitored over 12 weeks at 15 °C, 23 °C and 40 °C.

The release kinetics demonstrate the ability to control DCD release from a biopolymer composite through material design, with complete release taking from just a few days to several months. Interestingly, the hydrophobic PHBV matrix released DCD the fastest. Release kinetics decreased as the PCL content increased, with the exception of the neat PCL matrix, which released the second fastest after PHBV, likely due to its high initial porosity. A Fickian diffusion model fit the data well and the diffusivities followed an Arrhenius dependence on temperature.

We conclude that the lower affinity between the hydrophobic PHBV and hydrophilic DCD led to rapid release through a connected network of voids and DCD crystals within the matrix and at the interfaces between the polymer phases, delivering a pathway for water access to these crystals. In contrast, the higher affinity between PCL and DCD likely led to PCL-coated DCD crystals, which reduces direct water access to the DCD crystals, and instead forces it to diffuse through layers of PCL. Therefore, as the content of PCL increases, the layers of PCL through which water and solubilised DCD must diffuse also increases, slowing release.

8.1   Introduction
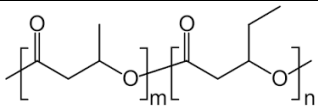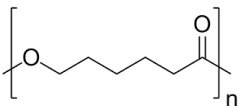
Globally, environmental losses of fertiliser-derived nitrogen (N) are so significant that they were classified as being at high risk of destabilizing the Earth system.[3] One approach to minimize N losses from agricultural fields is the use of nitrification inhibitors (NIs). These chemical entities, such as dicyandiamide (DCD), 3,4-dimethyl-1H-pyrazole phosphate (DMPP) and 2-chloro-6-(trichloromethyl)-pyridine (nitrapyrin), bind to the bacterial membrane-bound ammonium monooxygenase (AMO) enzyme. This enzyme is responsible for the rapid oxidation of ammonium to nitrate in soil following amendment with ammonium or urea-based N fertilisers. The high concentration of nitrate is then vulnerable to direct leaching and runoff during irrigation and rainfall events, and also gaseous emissions, through denitrification to nitrous oxide (N_2O) and nitric oxide

(NO).[179] Deactivating AMO with NIs has been shown to be effective at reducing all of these N loss pathways.[6, 138-139] The low cost of NIs compared to controlled release fertilisers offers agronomic benefits for broad acre agriculture. However, NIs degrade in soil at rates that increase exponentially with soil temperature,[73, 140] limiting their efficacy in tropical agriculture. The encapsulation and slow release could protect the encapsulated inhibitor from degradation, through shielding it from soil microbes, thereby extending the duration of an effective concentration in the soil, and thus increasing the overall efficacy of a given equivalent dose. DCD is used here as a model NI that is effective in temperate climates,[6] but degrades rapidly at higher temperatures (<20 days above 25 °C[8]).

In terms of the selection of matrix for encapsulation, several commercially available slow- and controlled-release agrichemical products utilize polymers that degrade very slowly in the soil. Polymers such as polyethylene and other polyolefins, polyurethanes and synthetic rubbers can accumulate in the soil as hazardous micro-plastics.[28] Here, we propose the use of fully biodegradable blends of poly(3-hydroxybutyrate-*co*-3-hydroxyvalerate) (PHBV) and poly(ε-caprolactone) (PCL) as matrices to control the release of DCD. Both polymers degrade through slow hydrolysis of ester linkages, catalyzed by soil microbial enzymes.[106] In our previous work,[164] PHBV degradation was shown to accelerate release of DCD from ~28 days onward in a soil environment. The present study investigates the effect of PHBV:PCL ratio on DCD release into water, where biological degradation of the matrices does not contribute to the release kinetics.

The nominated polymers, PHBV and PCL, were selected for their biodegradability, hydrophobicity and ease of melt processing. Both are semi-crystalline linear aliphatic polyester thermoplastics. PHBV is natural polyester belonging to the family of polyhydroxyalkanotes (PHAs) that are synthesized by numerous bacteria for intracellular carbon storage. In contrast, PCL is a synthetic polymer, derived from the ring opening polymerization of ε-caprolactone. Table 8.1 shows the molecular structure, Hildebrand solubility parameter δ_T and water diffusivity of each polymer. The higher δ_T of PHBV indicates higher hydrophobicity over PCL, which is reflected by the reported diffusion coefficient of water (D_w) through these polymers, with D_w of PHBV being ~15 times lower than that of PCL.[196] Therefore, we hypothesized that DCD release could be tailored using different blends of PHBV and PCL, with expected higher release rate for materials with higher PCL content.

Table 8.1: Molecular structure, Hildebrand solubility parameter (δ_T) and water diffusivity (D_W) for PHBV and PCL.

Component	Molecular structure	δ_T	D_W (cm^2.s^{-1})
PHBV		19.1[197]	1.54×10$^{-8,}$ [a] at 36.5 °C[196]
PCL		16.1[198]	22.9×10$^{-8,}$ [a] at 36.5 °C[196]

[a] Measured at external water vapour pressure of 0.072 atm

The use of PHBV/PCL blends has been demonstrated in the literature to effectively control the release of agrichemicals, such as fertilisers[105], herbicides[100], pesticides[141] and various orally administered drugs.[199-201] Due to the difference in chemical and physical properties, varying the ratio of these biodegradable polymers provides some control over the release rate. Examples in the literature typically use a cold tablet press or simple emulsion/solvent evaporation technique to prepare microparticles. Here, we present extrusion processing as a simple, inexpensive, and industrially relevant technique for the fabrication of macro-particle composites (as 3×3 mm pellets) for the controlled release of agrichemicals from biopolymer matrices.

The objective of this study was therefore to understand how the release of the model crystalline agrichemical, DCD, could be controlled by varying the ratio of PHBV to PCL using an extrusion process. We present the extrusion processing conditions for the fabrication of five DCD-PHBV/PCL materials initially composed of 400 mg/g DCD and 600 mg/g polymer with PHBV:PCL ratios of 1:0, 3:1, 1:1, 1:3 and 0:1. The mechanisms controlling the release kinetics were studied through mechanistic mathematical modelling and high-resolution characterization of the pellets, including mapping the distribution of DCD, PHBV and PCL with Raman spectroscopy, three-dimensional imaging through micro-computed tomography (μ-CT), analysis of the crystallinity and thermal properties of the polymer blends and assessment of polymer chain scission.

8.2 Materials and Methods

8.2.1 Materials

Dicyandiamide (DCD), poly(3-hydroxybutyrate-*co*-3-hydroxyvalerate) (PHBV) and polycaprolactone (PCL) were used in this study, see Section 4.2 for details.

8.2.2   Extrusion processing of slow release DCD-PHBV/PCL formulations

The PCL pellets and the DCD powder were separately pulverized using a SPEX SamplePrep Freezer/Mill™ model 6870. The ground DCD was sieved using a Retsch AS200 analytical sieve shaker (Merck), collecting material <106 µm. Five mixtures of PHBV and PCL powders were combined with PHBV:PCL mass ratios of 1:0, 3:1, 1:1, 1:3 and 0:1. The ground DCD was then mixed with the PHBV/PCL blends to produce mass loadings of 400 g DCD per kg of final composite. Formulations were then melt compounded through extrusion processing at 60-180 °C, as detailed in Table 8.2, and pelletised. Details on the extruder configuration and operation are reported in Section 4.3.

8.2.3   Water release kinetics

The release kinetics of DCD into water from the PHBV, PHBV:PCL 3:1, 1:1 and 1:3 and PCL biopolymer matrices was monitored at temperatures of 10±1 °C (in a temperature-controlled refrigerator), 23±1 °C (room temperature, benchtop) and 40±1 °C (temperature-controlled, heated chamber) over 12 weeks. Five pellets (~30-40 mg each) were selected at random and photographed with a 0.5 mm graduated ruler for measuring the length and diameter of each pellet in ImageJ, which was required for modelling the release kinetics. 1 mL samples were taken at 1 min, 30 min, 1 h, 2 h, 5 h, 10 h, 1 d, 2 d, 4 d, 7 d, 14 d, 28 d, 42 d and 56 d. DCD was quantified using ultraviolet-visible (UV-Vis) spectroscopy (see Section 4.5.3).

All five pellets from two of the three repeats were then used to quantify the DCD remaining in the pellets at the end of the experiment, as described in Section 4.4.1. This method has been previously shown to recover 100 ± 5% of the expected DCD from the pellets based on the known initial loadings.[164]

8.2.4   Materials characterisation

Raman spectroscopy was used to map DCD crystal location and investigate the blending of the PHBV and PCL polymers within the materials. The pellets were cross-sectioned using a surgical blade and mounted with Blu-Tack on a metal pill. Raman maps (30x30 µm, 100x100 pixels, 100x objective) were acquired and processed following the procedure described in Section 4.6.2.

Micro-computed tomography (µ-CT) was used to investigate the initial porosity and pore size distribution of the extruded pellets. The pellets were also scanned after eight weeks of exposure in water to investigate the change in pore distribution. The µ-CT images were acquired over 360° with a Skyscan 1272 (Skyscan, Bruker, Belgium) as detailed in Section 4.6.3.

A differential scanning calorimeter (DSC) Q2000 (TA Instruments) was used to determine the

thermal properties of the DCD-polymer composites, as described in Section 4.7.1 For the blended materials, the crystallinity for each phase was estimated based on ratio of PHBV to PCL, accounting for the actual DCD loadings (see Table 8.2).

Gel permeation chromatography (GPC) was used to compare the molecular weight of the biopolymer blends before and after extrusion and after release, following the procedure outlined in Section 4.7.2.

8.2.5 *Mathematical modelling of release profiles*

The kinetics of DCD mobilisation from the pellets was modelled over two distinct phases of release. The release in the first day from the surface of the pellet was modelled using a power law relation:

$$\frac{M_t}{M_\infty} = At^B \qquad\qquad for\ 0 < t < 1\ day \qquad\qquad \textbf{Eq. 8.1}$$

where M_t and M_∞ denote the absolute cumulative amounts of DCD released at time t, and infinite time, respectively, and A and B are constants.

The second phase of release, from 1 day onward, was modelled based on Fick's second law of diffusion, considering both radial and axial mass transfer from a cylinder.[202]

$$\frac{\partial c}{\partial t} = \frac{1}{r}\left\{\frac{\partial}{\partial r}\left(rD\frac{\partial c}{\partial r}\right) + \frac{\partial}{\partial z}\left(rD\frac{\partial c}{\partial z}\right)\right\} \qquad\qquad \textbf{Eq. 8.2}$$

where c is the concentration of DCD ($mg.cm^{-3}$); t is time (s); r and z represent the radial and axial coordinates relative to the centre of the pellet (cm) and D denotes the apparent diffusion coefficient ($cm^2.s^{-1}$), explained further in the discussion.

An analytical solution to this partial differential equation for the fractional release as a function of time was derived by Vergnaud[129] as an infinite series of exponential decay terms. Fick's law is solved according to the initial and boundary conditions of initially homogeneous distribution of DCD and perfect sink conditions, giving:[129]

$$\frac{M_t}{M_\infty} = F_B + P \times \left[1 - \frac{32}{\pi^2}\sum_{n=1}^{\infty}\frac{1}{q_n^2}exp\left(-\frac{q_n^2}{R^2}Dt\right)\sum_{p=0}^{\infty}\frac{1}{(2p-1)^2}\times exp\left(-\frac{(2p+1)^2\pi^2}{L^2}Dt\right)\right] \qquad \textbf{Eq. 8.3}$$

where F_B is the y-intercept, introduced to account for the burst release described above; q_n are the zero order roots of the Bessel function of the first kind, and R and L are the radius and length of the cylindrical pellet (cm), respectively. For some materials, incomplete release was realized, so P was

introduced to allow the theoretical plateau of the fractional release profiles to be less than unity, with a lower bound of 0.9-B.

The temperature dependence of the Fickian diffusion coefficient was defined according to the Arrhenius rate law:

$$D = D_0 \exp\left(-\frac{E_a}{RT}\right)$$ **Eq. 8.4**

where D_0 (cm^2.s^{-1}) is the permeability index, E_a (J.mol^{-1}) is the activation energy of the diffusion process, R is the universal gas constant (8.3145 J.mol^{-1}.K^{-1}), and T (K) is the absolute temperature of the release experiment.

8.3 Results

The five PHBV/PCL blends were successfully extruded, with DCD initially mixed at 400 mg DCD/g. This shows the immediate feasibility for industrial-scale fabrication of these controlled-release nitrification inhibitor formulations. Further, this shows the potential to encapsulate other crystalline agrichemicals in this fashion, provided they are thermally stable at the extrusion temperature (DCD is thermally stable up to ~240 °C)[164]. The produced pellets were consistent in size, at roughly 3×3 mm length×diameter, with slightly higher variability in sizes for DCD-PCL and DCD-PHBV:PCL 1:3 (Table 8.2). These two materials were tackier due to the very low crystallisation temperature of the PCL (~33 °C, see Figure 8.2), which also led to higher torque during processing (Table 8.2).

Table 8.2: Summary of extrusion parameters (maximum and die temperatures (T) and torque range) and sizing (diameter, D and length, L) of the produced pellets and the actual DCD loadings. The standard deviations (±) given for D and L are based on the 15 pellets used for each material in the release studies (5 pellets for each of the three temperatures studied), while the DCD loadings represent the triplicate data based, one data set for each temperature.

Material	Max./Die T (°C)	Torque (N.m)	D (mm)	L (mm)	DCD loading (mg DCD/g)
DCD-PHBV	180/160	2.5-5	3.1 ± 0.1	3.0 ± 0.2	395 ± 6
DCD-PHBV:PCL 3:1	180/150	2.5-5	2.9 ± 0.1	2.9 ± 0.1	351 ± 10
DCD-PHBV:PCL 1:1	180/150	2.5-5	2.9 ± 0.2	3.0 ± 0.1	303 ± 7
DCD-PHBV:PCL 1:3	180/125	2.5-5	3.1 ± 0.4	3.0 ± 0.2	339 ± 8
DCD-PCL	80/60	2.5-10	2.8 ± 0.3	3.0 ± 0.3	356 ± 16

Some DCD was lost during the fabrication process, likely due to the high moisture content of the

cryoground PCL. Use of an apparatus that ensured a dry feed to the extruder could potentially prevent these losses. The actual DCD loadings, Table 8.2, were calculated based on the amount of DCD released from the pellet and the amount remaining in the pellet at the end of the release experiment (see Figure 8.5). There was effectively no DCD loss during processing for DCD-PHBV. The amount of loss increased with PCL content until DCD-PHBV:PCL 1:3, where the die temperature was dropped to 125 °C, likely reducing the amount of DCD lost with steam during processing. Similarly, DCD-PCL showed further reduction in DCD losses since the extrusion temperature was reduced to 80 °C, with the die at 60 °C.

8.3.1 Characterisation of slow release inhibitor formulations

8.3.1.1 The distribution of DCD, PHA and PCL

Raman mapping of each component (DCD, PHBV and PCL) allowed the visualisation of the DCD crystals and the micro-phase separation between PHBV and PCL (Figure 8.1). The size and distribution of the phases varied depended on the polymer blend. DCD-PHBV:PCL 3:1 shows PHBV and PCL are extensively intermixed such that the separate phases are hard to distinguish and appear to be co-continuous. PCL possibly exists as inclusions within the PHBV spherulites, as observed by Kim and Woo[203] and Lovera et al.[204] through polarizing optical microscopy. For the PHBV:PCL 1:1 and 1:3 blends, small isolated crystals of PHBV can be visualised, but still the signal is mixed at 300 nm resolution, suggesting PCL incorporation into PHBV spherulites and vice-versa. For these two materials, the PHBV rich regions appear as isolated spherulites, held together by the PCL rich phase, due to the higher crystallisation temperature of PHBV (Figure 8.2). The size of the PHBV-rich regions reduces from ~820 ± 360 nm to 630 ± 200 nm for PHBV:PCL 1:1 and 1:3, respectively, as determined from manual measurement within the ImageJ image processing program.
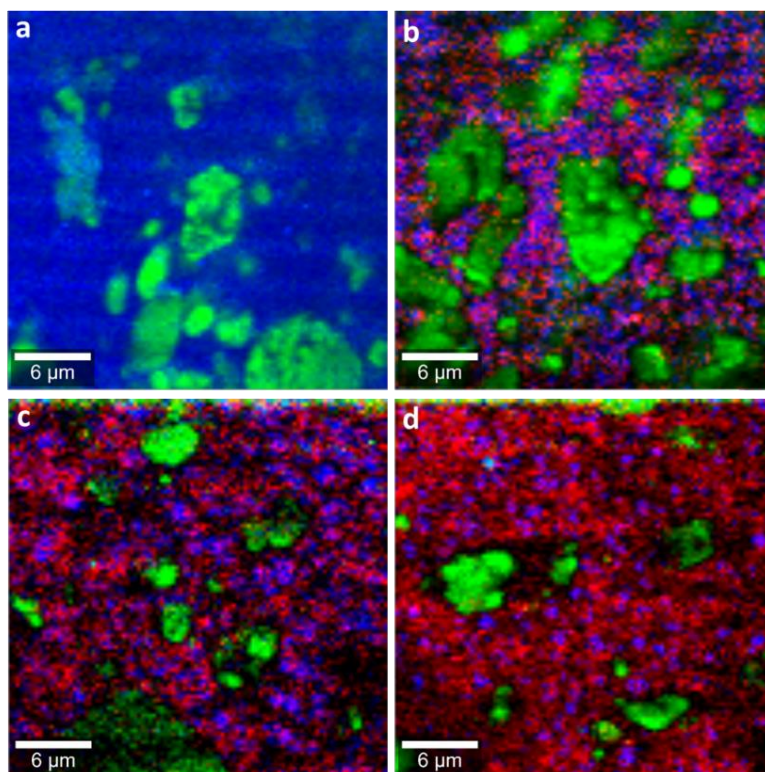
Figure 8.1: Raman maps showing the distribution of phases separation of DCD (green), PHBV (blue) and PCL (red) in a) DCD-PHBV b) DCD-PHBV:PCL 3:1 c) DCD-PHBV:PCL 1:1 and d) DCD-PHBV:PCL 1:3 pellets.

8.3.1.2   Crystallinity and thermal properties of DCD-PHA/PCL composites

DSC thermograms of the first heating and first cooling cycles are shown in Figure 8.2A and B, respectively. For all blends, the PCL phase crystallised and melted at ~33 °C and ~60 °C, respectively. In contrast, the PHBV phase was significantly influenced by the composition of the blend. The DCD-PHBV composite showed a broad melting endotherm with two major peaks, indicative of two or more crystal phases. This was potentially a result of the disruption of the crystallisation process during extrusion due to the presence of DCD crystals, leading to less perfect and/or smaller PHBV crystals. However, such multiple peaks are common for PHAs and can also be a result of physical aging, different molar mass species, orientation effects, and so on.[205] As the PCL content increases, the width of the melting endotherm decreases and one crystal type becomes more dominant until a single melting peak is seen for the DCD-PHBV:PCL 1:3 composite. The crystallisation temperature of the PHBV phase decreases substantially with increasing PCL content, from 107 °C for DCD-PHBV, to 80 °C for DCD-PHBV:PCL 1:3. The melting temperature of the PHBV phase was not significantly influenced by the PCL content, in line with results of Lovera et al.[204] for high molecular weight (M_w 120 000 g.mol^{-1}) PCL blended with PHBV, though the span of the melting temperature is reduced.
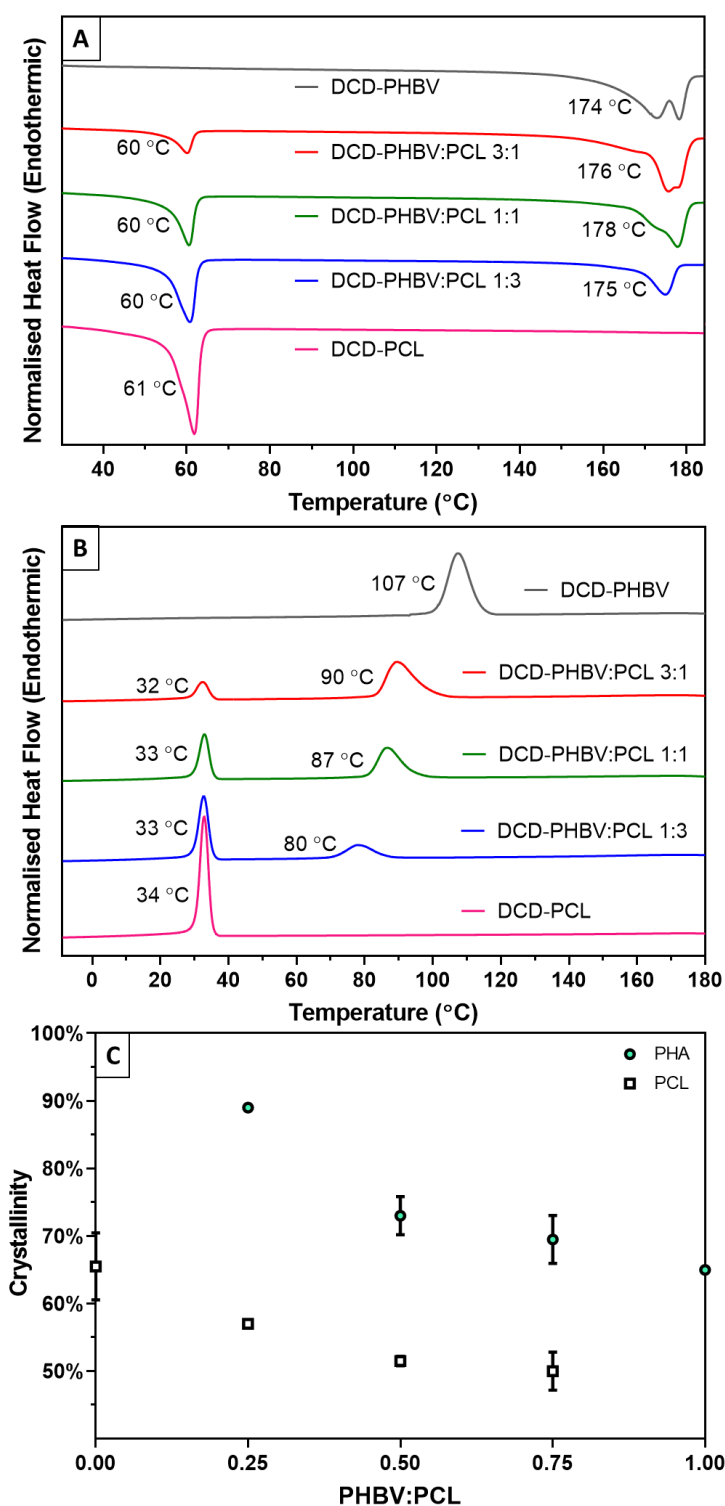
Figure 8.2: (A) First heating scan and (B) first cooling scan from DSC of the extruded DCD with PHA and PCL polymer blends. The melting and crystallisation temperatures are indicated in the respective figures. (C) Crystallinity of the PHA and PCL phases as a function of the PCL content within the polymer blend as determined from the heat of fusion for each component upon first heating, accounting for the actual DCD loadings as presented in Table 8.2. Errors bars show the standard deviation (n=2).

Integration of the first DSC heating scan allowed the estimation of the crystallinity of the PHBV and PCL phases. DCD-PHBV showed PHBV crystallinity of 65%, which is comparable to reports of 68% crystallinity by Chan et al.[206] who characterized ENMAT Y1000 using wide angle X-ray scattering (WAXS). For DCD-PCL, the PCL crystallinity was 65.5%, which is slightly higher than that reported by Blázquez-Blázquez et al.[207] who reported 54% crystallinity for extruded PCL, melt pressed into films.

Interestingly, as the PCL content increased, both the PHBV and the PCL phases increased in crystallinity. This was unexpected as crystallinity of PHBV in PHBV/PCL has been reported to be independent of,[208] or inversely correlated with[209] PCL content, albeit these studies used solvent-based fabrication techniques, leading to co-crystallization of the PHBV and PCL phases. The extrusion fabrication technique used here facilitates initial crystallization of PHBV followed by the crystallization of PCL, on cooling from the melt. At lower PHBV contents in the blend, e.g., at 25 wt.% PHBV, this results in smaller spherulites that solidify first with a well-defined structure (Figure 8.1). Since the crystalline lamellar fibrils grow radially outward from the site of nucleation, a higher proportion of smaller spherulites results in a higher degree of crystallinity,[210] at ~89% in this case. In that same system, the lower amounts of PHBV means the matrix structure is not defined until the PCL has crystallised. This allows more freedom for the PCL phase to form larger, better-defined PCL crystallites, giving the PCL phase a high degree of crystallinity. Conversely, for DCD-PHBV:PCL 3:1, larger PHBV spherulites are formed first, creating more interlamellar space of amorphous polymer and therefore lower PHBV crystallinity. In this case, the higher PHBV content results in a scaffold that defines the matrix dimensions and distribution, resulting in physically confined and disrupted PCL crystallisation, reducing the PCL crystallinity. Confined crystallisation is known to reduce crystallinity. For example, Ho et al.[211] reported a reduction of PCL crystallinity of ~30% when crystallisation was confined between lamellar microstructure of polystyrene-*b*-poly(ethylenepropylene) (PS-PEP).

8.3.1.3   Hydrolysis of the polyester chains

Gel permeation chromatography (GPC) was used to quantify molecular weights of the polymers at day 0 and day 84, allowing assessment of both the degree of polymer degradation during the extrusion process and the amount of polymer chain hydrolysis over the 12-week water release experiment. A comparison of the as-received molecular weight of the PHBV and PCL with the initial molecular weight of DCD-PHBV and DCD-PCL indicates that there was no degradation of PCL during extrusion, but significant degradation of PHBV, with a 27 ± 9% reduction in the weight average molecular weight.
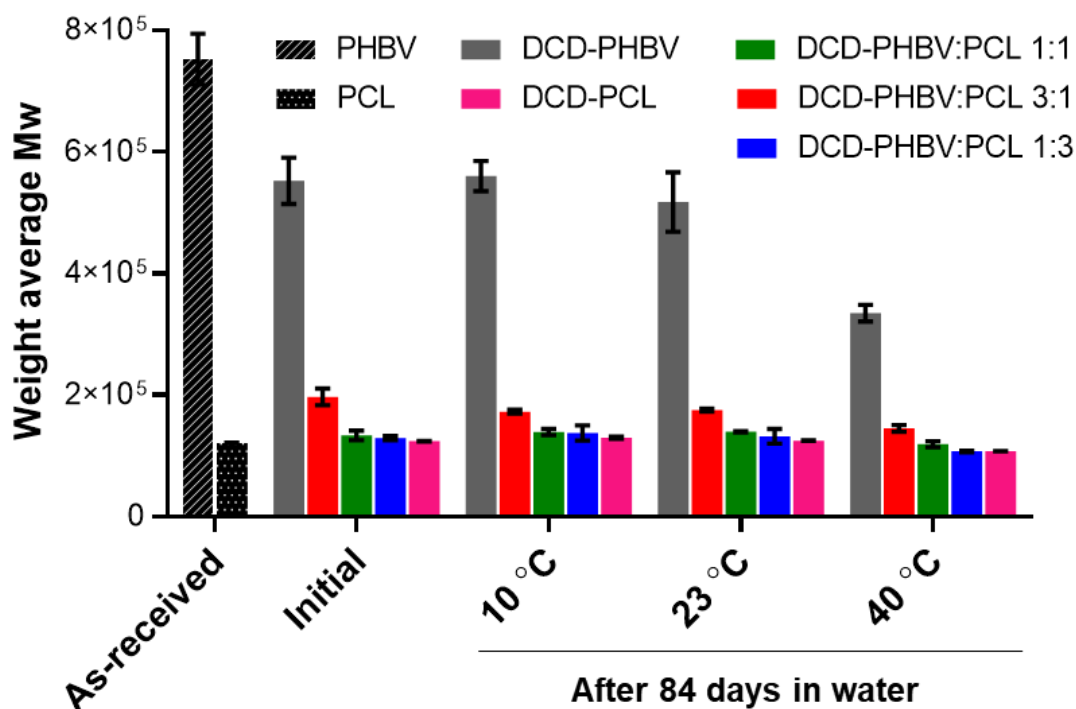
Figure 8.3: GPC results showing the weight average molecular weight (Mw) of PHBV and PCL as received (before extrusion) and the five DCD-PHBV:PCL blends after extrusion (initial) and after the 12-week water release experiments at 10 °C, 23 °C and 40 °C.

The amount of hydrolysis of the polyesters over the 12-week water release experiment was negligible at 10 °C and 23 °C, while at 40 °C all materials showed some reduction in molecular weight. At 40 °C, DCD-PHBV showed the most degradation, with a ~40% reduction in molecular weight from the starting material. DCD-PHBV:PCL 3:1, 1:1 and 1:3 dropped by $26 \pm 8\%$, $10 \pm 9\%$ and $17 \pm 1\%$, respectively, while DCD-PCL showed a $13 \pm 0.05\%$ decrease. Therefore, both PHBV and PCL were susceptible to hydrolysis at 40 °C, but the rate of degradation of PHBV was higher.

8.3.1.4   Voids and porosity

Micro-computed tomography (μ-CT) allowed visualization and quantification of the void space distribution within the pellets in three-dimensions. Pellets imaged before release allow the quantification of the initial porosity. This initial porosity (Table 8.3) increases exponentially with PCL content within the blend, with the exception of DCD-PHBV (i.e., 0% PCL). There are competing processes here, with PCL acting as a compatibiliser between DCD and PHBV, reducing porosity, while also holding more moisture prior to extrusion, which likely increases porosity in the extruded product. For DCD-PHBV:PCL 3:1 and 1:1, the starting porosity is low, existing almost exclusively near the curved surface of the pellet, which was in contact with the extruder die (see Figure 8.4).

Some large pores were found in the centre of DCD-PHBV:PCL 1:1, but significantly more can be seen for DCD-PHBV:PCL 1:3, distributed throughout the pellet, reflected by the increase in pore size (Table 8.3). DCD-PCL had the highest starting porosity at 16%, seen distributed throughout the pellet. This was surprising, since the extrusion temperature was ≤80 °C for this material. These pores may be formed by both water vapour and air pockets included into the matrix during extrusion due to the increased die pressure caused by the high viscosity and tackiness of the PCL.[212]

Table 8.3: The porosity and pore size distribution of the extruded DCD-PHBV/PCL pellets determined through 3-D analysis of the binarised μ-CT images.

Material	Porosity (%)	d50 (μm)	Span
DCD-PHBV	9	22	1.3
DCD-PHBV:PCL 3:1	1	11	2.0
DCD-PHBV:PCL 1:1	2	14	1.8
DCD-PHBV:PCL 1:3	4	26	1.4
DCD-PCL	16	19	1.1

For the pellets imaged after release, the void space represents both the starting porosity as well as the void spaces created from dissolved/released DCD crystals. For pellets where incomplete release occurred, a clear front was found between the region from which DCD had been released and the remaining core of non-dissolved DCD. This evidence supports the classical Higuchi's theory of drug release, derived assuming a sharp diffusion front.[123] In addition, these microtomographs indicate that the rate of axial diffusion is similar to that of the radial diffusion. Since the length of the pellets was roughly double the radius, the radius of the pellet therefore controls the amount of time until complete release. This will be true for all materials with length>radius, while, conversely, for materials with length<radius, the length of the pellet will control the time for complete release. Of course, the length of the pellet will still affect the shape of the curve, i.e., increasing the length of the pellet would not affect the time to complete release, but would increase the time to 50% and 80% release.

Generally, the fractional release determined from the mass of DCD released into water (shown in the bottom right of each μ-CT slice within Figure 8.4) aligned with the μ-CT images. However, in some cases they did not. For example, for DCD-PCL at 10 °C, the μ-CT images indicate ~40% release compared to 72% release calculated from the solution concentrations for that replicate. At 40 °C, the fractional release of DCD was found to be ~85% for DCD-PHBV:PCL 3:1, 1:1 and 1:3, while the μ-CT show ~100%, ~85% and ~98% release, respectively (calculated based on the volume of the remaining undissolved core compared to the total volume of the pellet). These discrepancies likely

result from pellet to pellet variability, since the solution data is an average of the five pellets in each container. This could result from variability in the pellet heights and diameters, starting porosities or DCD loadings, as well as some randomness in the distribution of DCD, PHBV and PCL phases within the pellet. The large inclusion within the DCD-PHBV materials is believed to be trapped water within the hydrophobic matrix.
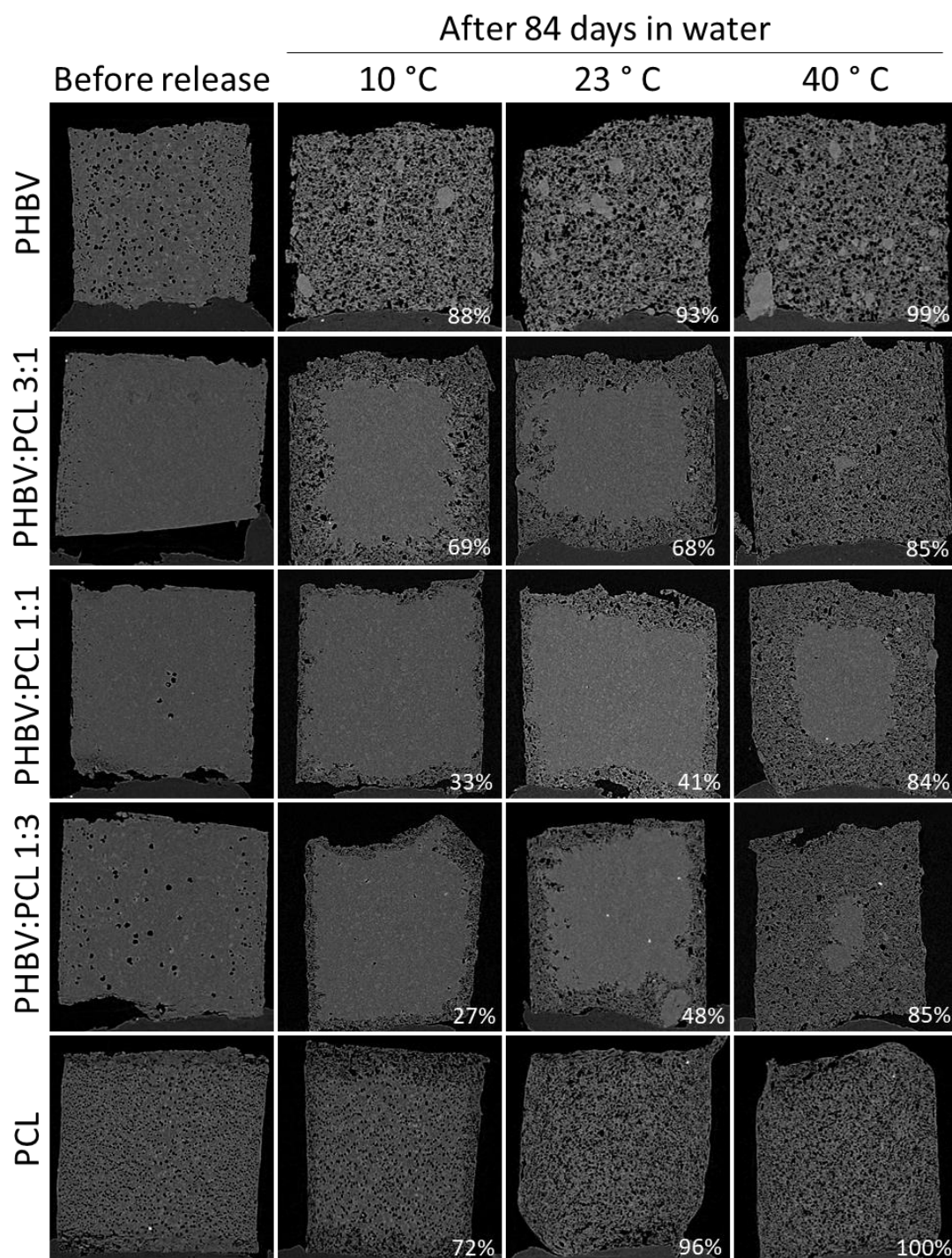
Figure 8.4: Coronal μ-CT slices of DCD-PHBV/PCL pellets scanned after extrusion and after release in water for 84 days at 10 °C, 23 ° C and 40 °C, with the fractional release .

8.3.2 DCD mobilisation

The release of DCD into temperature-controlled water at 10 °C, 23 °C and 40 °C was monitored over 12 weeks using UV-Vis spectroscopy. A mass balance of the DCD mobilized into the water compared to the DCD remaining encapsulated after 12 weeks is shown in Figure 8.5 for two of the three replicate experiments.
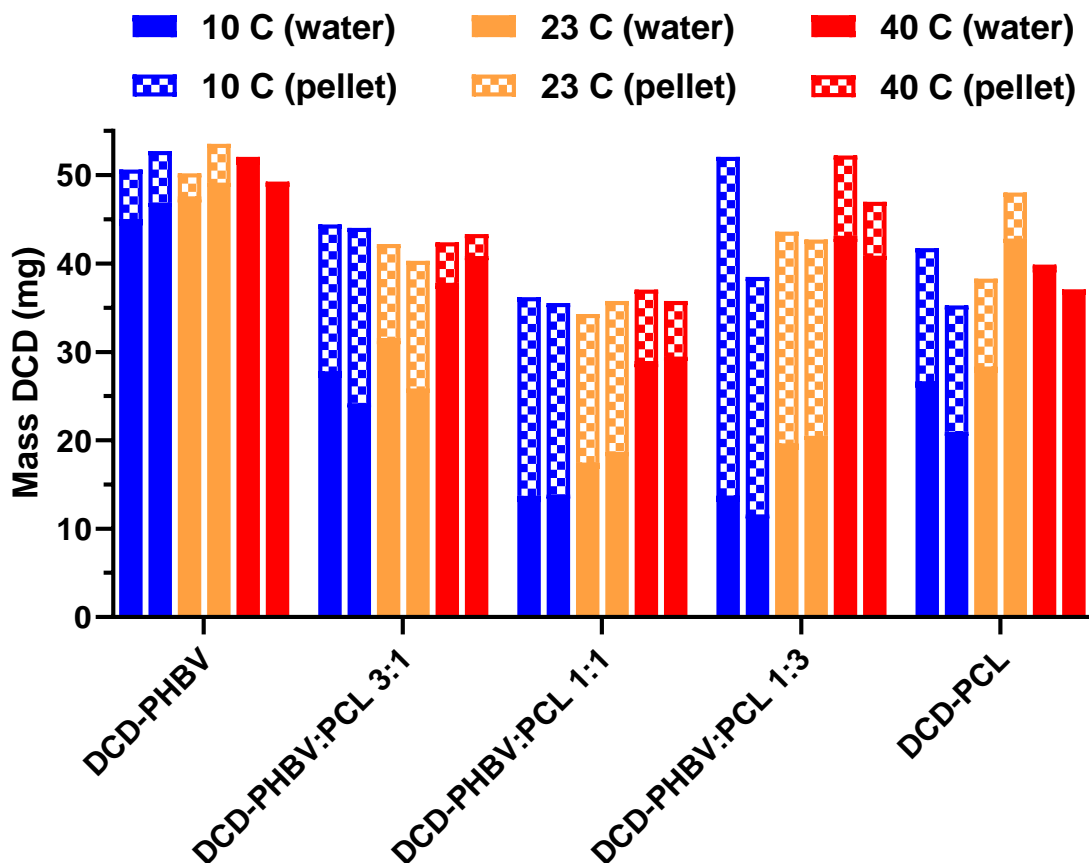
Figure 8.5: Mass balance for two of the three replicates from each 12-week water release experiment. The solid fill shows the cumulative amount of DCD quantified in the water, while the checkered fill represents amount of DCD extracted from the pellets at the end of the release study. The dashes show the calculated DCD loading for each replicate based on the total mass of DCD quantified and the starting mass of the pellets.

This gives a snapshot at the 12-week time point, showing the amount of DCD mobilized for each material and the influence of temperature. Figure 8.5 shows the relative proportion of DCD release into water compared to that remaining encapsulated in the pellet after 84 days in water, with reasonable agreement between the replicates.

8.3.2.1 Mathematical modelling

The modelling results for the least-squares parameter estimation from the release kinetic study are presented in Table 8.4. There was good agreement between the model fit and experimental data, suggesting diffusion processes controlled the rate of DCD mobilisation from the biopolymer matrices from day one onward. The fit parameters for the diffusion model, A, B and D, are an average of the best fit for each replicate within the experimental set, using the average pellet radius and length for each replicate as model inputs.

Table 8.4: Summary of modelling parameters from non-linear regressions.

T	Material	A	B	F_B	P	D (cm.s^{-1})	R^2
10 °C	PHBV	0.32	0.35	0.32	0.68	2.0×10^{-9}	0.990
	PHBV:PCL 3:1	0.20	0.29	0.20	0.70	2.9×10^{-10}	0.983
	PHBV:PCL 1:1	0.12	0.23	0.12	0.78	4.3×10^{-11}	0.970
	PHBV:PCL 1:3	0.08	0.23	0.08	0.84	2.4×10^{-11}	0.988
	PCL	0.11	0.38	0.11	0.85	2.9×10^{-10}	0.999
23 °C	PHBV	0.40	0.37	0.40	0.60	3.0×10^{-9}	0.971
	PHBV:PCL 3:1	0.24	0.30	0.24	0.66	6.2×10^{-10}	0.991
	PHBV:PCL 1:1	0.15	0.26	0.15	0.75	1.1×10^{-10}	0.972
	PHBV:PCL 1:3	0.11	0.27	0.12	0.78	1.2×10^{-10}	0.989
	PCL	0.18	0.45	0.18	0.82	1.0×10^{-9}	0.999
40 °C	PHBV	0.60	0.35	0.59	0.41	4.2×10^{-9}	0.933
	PHBV:PCL 3:1	0.34	0.31	0.34	0.66	1.3×10^{-9}	0.989
	PHBV:PCL 1:1	0.24	0.26	0.23	0.75	1.0×10^{-9}	0.977
	PHBV:PCL 1:3	0.19	0.33	0.19	0.81	9.4×10^{-10}	0.994
	PCL	0.37	0.44	0.36	0.64	2.1×10^{-9}	0.977

8.3.2.2 Effect of matrix composition

Using the loadings calculated from each experimental run (Figure 8.5), the fractional release profiles of DCD were determined for the five different PHBV/PCL matrices at 10 °C, 23 ° C and 40 °C, shown in Figure 8.6. The composition of the biopolymer controlled-release matrix had a significant effect on the rate of release and the amount of burst release from the surface of the pellet. Figure 8.6 highlights the ability to control the rate of release by varying the amount of PCL in the matrix, allowing the tailoring of material design to specific applications and climate conditions. For

example, at 23 °C, the fraction of DCD mobilized over 12 weeks varied from $48 \pm 4\%$ for DCD-PHBV:PCL 1:3 to $93\% \pm 1\%$ for DCD-PHBV, with the other materials lying between these.

The amount of DCD mobilized from the surface of the pellet can be considered as the DCD release within the first five hours of exposure to water. Again, considering conditions at 23 °C, the amount of surface release reduces with increasing PCL content, with the exception of 100% PCL: reducing from $23.2 \pm 0.2\%$ for PHBV to $15 \pm 0.5\%$, $10 \pm 0.5\%$ and $8 \pm 0.2\%$ for PHBV:PCL 3:1, 1:1 and 1:3, respectively, while PCL released $9 \pm 1\%$.

Similarly, PHBV released the fastest over the 12-week experiment out of all the materials studied. Counter-intuitively, increasing the content of the more hydrophilic PCL in the PHBV/PCL blends resulted in a slower release. In some cases, the effect of the composition of the polymer matrix was dependent on the temperature of the release media. For example, DCD-PHBV:PCL 1:1 and 1:3 released at similar rates at 23 °C and 40 °C, while at 10 °C DCD-PHBV:PCL 1:1 released significantly faster, with 37 ± 2 wt.% of the DCD mobilized over the 12 week experiment compared to 28 ± 1 wt.% for DCD-PHBV:PCL 1:3. DCD-PCL stands as an exception to the trend of higher PCL content slowing release. This material displayed the greatest variability for DCD mobilisation, likely as a result of the high porosity (Table 8.3) and variable loading (Table 8.2). DCD-PCL had a similar release profile to DCD-PHBV:PCL 3:1 at 10 °C, while at 23 °C, the fractional release was on average 17% higher than DCD-PHBV:PCL 3:1 after 12 weeks. At 40 °C, DCD-PCL reached 80% release within 14 days, compared to 42 days for DCD-PHBV:PCL 3:1.
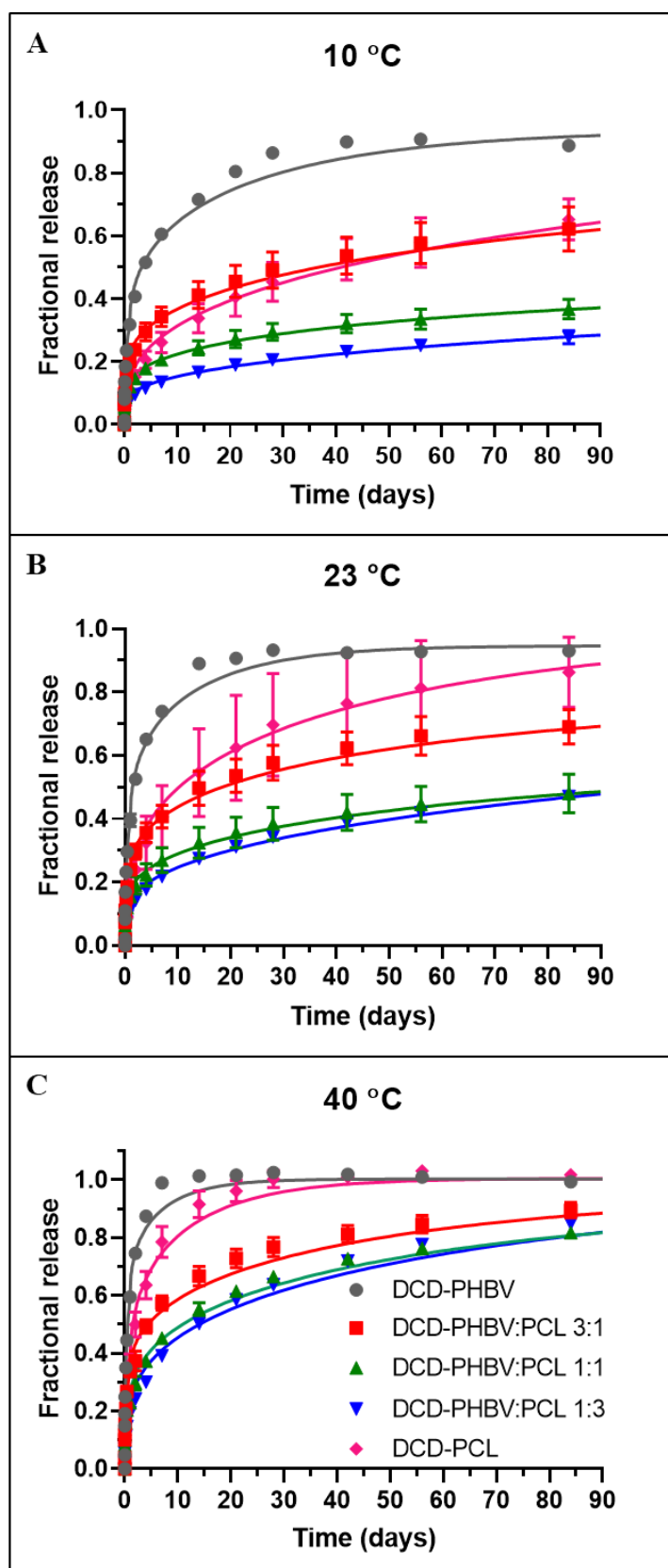
Figure 8.6: Fractional release curves for DCD from matrices composed of PHBV/PCL blends at 10 °C (A), 23 ° C (B) and 40 °C (C). Error bars represent the standard deviation of the triplicate data.

8.3.2.3 Effect of temperature on release kinetics
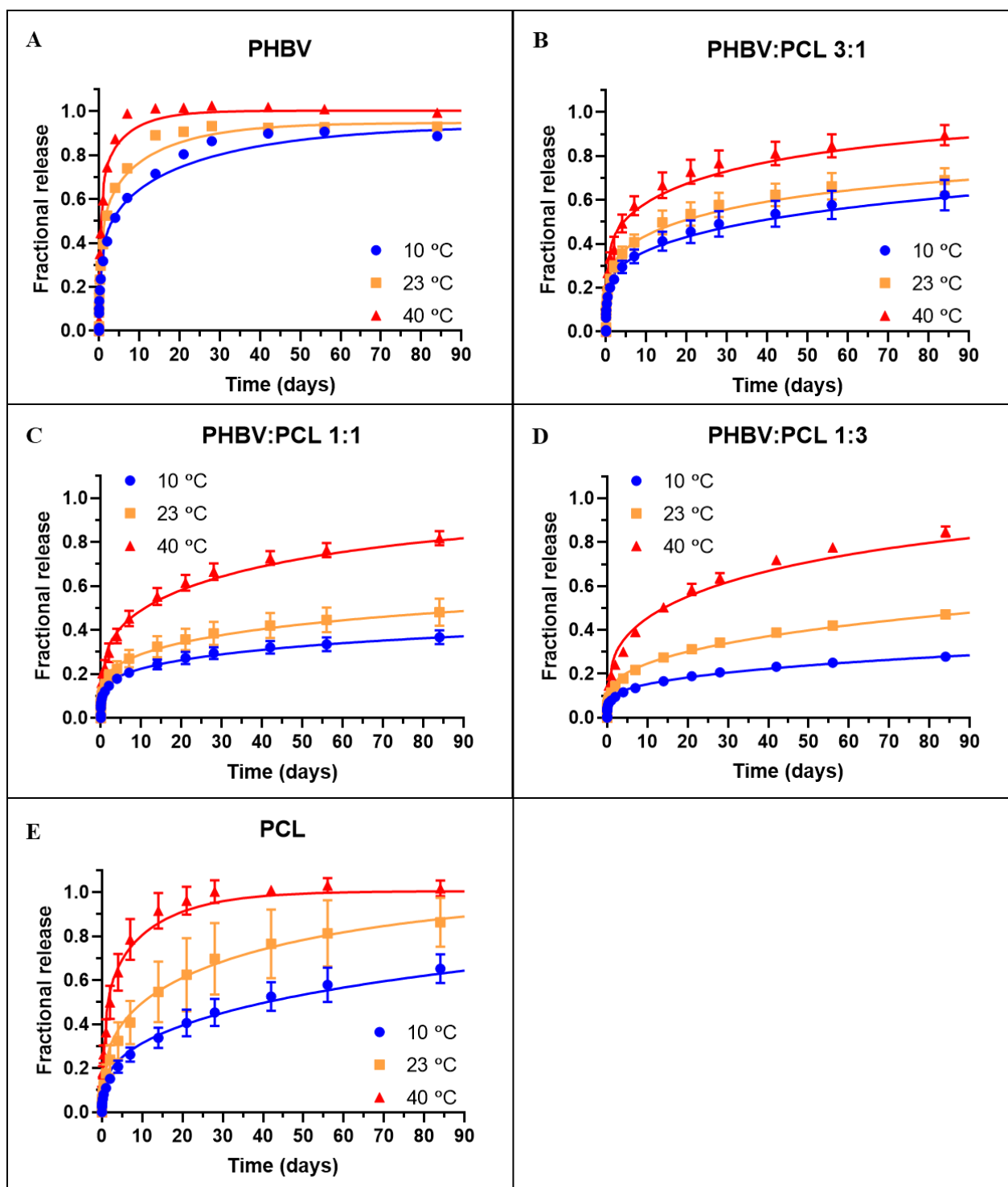
Figure 8.7: Fractional release curves of DCD at 10 °C, 23 ° C and 40 °C from matrices composed of PHBV (A) PHBV:PCL 3:1 (B) PHBV:PCL 1:1 (C) PHBV:PCL 1:3 (D) and PCL (E). Error bars represent the standard deviation of the triplicate data.

The effect of temperature on the fractional release of DCD from the five biopolymer matrices, with the fit diffusion model is shown in Figure 8.7. The diffusion coefficients from the best fit (Table

8.4) follow an Arrhenius dependence on temperature as seen in Figure 8.8. The values of the activation energy determine the responsiveness to temperature. Temperature has the lowest effect on release from DCD-PHBV, with increasing responsiveness as the PCL content within the PHBV/PCL blends increased. DCD-PCL was an anomaly to the trend with a temperature responsiveness sitting between DCD-PHBV:PCL 3:1 and DCD-PHBV 1:1.
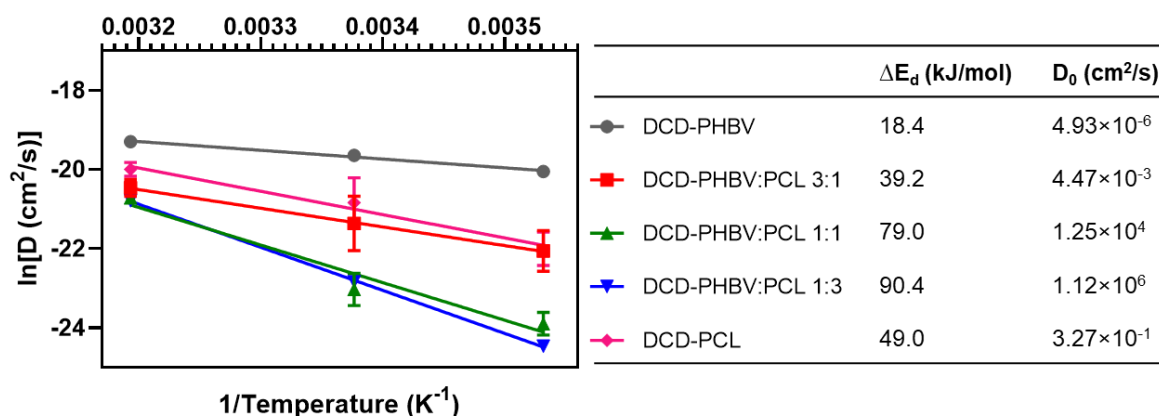
Figure 8.8: Arrhenius relation between diffusivity and temperature for DCD release from matrices of the five different PHA/PCL blends , along with the Arrhenius parameters calculated from the linear regression of ln(D) against T^{-1}. Error bars represent the standard deviation from the triplicate release experiments.

	ΔE_d (kJ/mol)	D_0 (cm^2/s)
DCD-PHBV	18.4	4.93×10^{-6}
DCD-PHBV:PCL 3:1	39.2	4.47×10^{-3}
DCD-PHBV:PCL 1:1	79.0	1.25×10^{4}
DCD-PHBV:PCL 1:3	90.4	1.12×10^{6}
DCD-PCL	49.0	3.27×10^{-1}

8.4   Discussion and conclusions

8.4.1   *Mechanisms controlling mobilisation and interpretation of 'diffusivity'*

The mechanisms controlling the rate of DCD mobilisation from the biopolymer matrices depend on the composition of the matrix. Interestingly, PHBV released the fastest into water, and higher PCL contents led to slower DCD mobilisation, which is counter-intuitive, since PHBV is significantly more hydrophobic than PCL (Table 8.1). It is therefore likely that the DCD did not diffuse through layers of PHBV. Rather, it seems that DCD existed as a connected network, as described by Levett et al.[213] In this case, the rate-limiting step is likely the diffusion of DCD along a tortuous path within the PHBV matrix, created by the pores and voids formed as DCD crystals dissolved. In this case, the apparent diffusivity reported represents a lumped parameter of the tortuosity (τ) and the diffusivity of DCD in water.

Interestingly, the plateau of the fractional release from a PHBV matrix was dependent on temperature. At 10 °C, 23 °C and 40 °C the plateau was 90%, 91% and 100%, respectively. This correlates with the amount of PHBV degradation, with 0%, 6 ± 2% and 39 ± 2% reduction in

molecular weight after 12 weeks (Figure 8.3). Hydrolysis of PHBV chains can cause microscopic changes in the matrix structure, opening channels, such as cracks, as reported by Levett et al.[214], or provides more free space and/or voids between the polymer chains since the lower molecular weight fractions have more mobility. This enables increased internal water access, accelerating the release of the previously inaccessible fraction of DCD. Hydrolytic degradation of PHBV was unexpected under these abiotic conditions. However, since DCD has three amine groups, this may be evidence of base catalyzed hydrolysis of the ester linkages in both PHBV and PCL.

Addition of PCL to the PHBV appears to reduce the connectivity between DCD crystals. For DCD-PHBV:PCL 3:1, the mechanism controlling DCD release is likely a combination of DCD diffusion through water along a tortuous path within the matrix, and diffusion through thin layers of PCL. Adding more PCL into the blend likely increased the thickness of the PCL layer through which the DCD diffused, slowing the rate of DCD release. For DCD-PCL, the higher starting porosity means the path for DCD release will occur through diffusion through thin layers of PCL and the more rapid diffusion of DCD through water-filled pores. Intriguingly, DCD-PHBV:PCL 1:1 and 1:3 released at similar rates, particularly at 23 °C and 40 °C. The characterization of these materials suggests competing processes influence the release kinetics. Following the theory proposed above, the higher PCL content of DCD-PHBV:PCL 1:3 should result in thicker layers of PCL for DCD to diffuse through. Furthermore, DSC results indicated that both the PCL and the PHBV phases had a higher degree of crystallinity, which slows diffusion.[215] However, the μ-CT results show a higher starting porosity for this material, which accelerates release. In addition, the DCD loading for DCD-PHBV:PCL 1:3 was ~12% higher than DCD-PHBV:PCL 1:1. The significantly faster release from DCD-PCL pellets over DCD-PHBV:PCL 1:1 and 1:3 is certainly related to the much higher initial porosity of this material. However, the incorporation of PHBV in the blends will result in a more hydrophobic matrix,[216] which may be responsible for the lower diffusivities seen in the blends compared to DCD-PCL.

Following the proposed theory, it is reasonable that the blends with higher PCL contents showed the highest dependence on temperature. The diffusion of DCD through the layers of PCL will be more dependent on temperature, compared to the diffusion of DCD through water. This can be explained by the multi-factorial effect of increased temperature, affecting:

i) the rate of diffusion of water in the polymer matrix, due to increased kinetic energy of water and polymer chain mobility;

ii) the rate of DCD diffusion in water, due to higher kinetic energy of the DCD molecules;

iii) the rate of DCD diffusion back through the biopolymers, due to higher kinetic energy of the DCD molecules and increased polymer chain mobility;

iv) the solubility of DCD within the biopolymers and in water;

v)   the rate of DCD dissolution, likely related to or limited by the rate of DCD diffusion away from DCD crystals; and

vi) the rate of hydrolysis of ester linkages in the PHBV and PCL (as evidenced from the GPC results, Figure 8.3).

For materials where DCD diffuses through layers of PCL, all of the above are relevant and affected by temperature. Whereas, for DCD-PHBV, where DCD diffuses along a tortuous path of water filled channels, only ii) and iv) are relevant.

In a field environment, soil microbes will metabolise both PHBV and PCL as a carbon source.[106] Both polymers degrade via an enzymatic surface erosion mechanism, while PCL also undergoes abiotic hydrolysis through the bulk of the material. Our previous study,[164] showed for a material with 250 g.kg^{-1} DCD in PHBV, biodegradation of the PHBV matrix accelerated release into soil from~28 days onward. The rate of polymer degradation in soil is a complex parameter that depends largely on the soil type, texture, microbial population present, soil moisture content and temperature.[158, 164] Surface erosion of the polymers will likely open pathways for encapsulated DCD and reduce the diffusion path length, while the bulk hydrolysis of PCL would accelerate the rate of diffusion through the matrix. Further investigation is required to improve our understanding of the role of degradation on release from matrices composed of PHBV/PCL blends.

8.4.2   *The importance of polymer-agent affinity*

This counter-intuitive response of release to the hydrophobicity of the matrix may be explained by the increased affinity of DCD to PCL over PHBV. The interaction between DCD and the polymer matrix occurs during extrusion processing and the subsequent crystallisation of the matrix. If the polymer-DCD interaction is weak, it is more likely that the polymer will pull away during the crystallisation process, leaving voids and channels for direct water access to the DCD within the matrix. In contrast, all else being equal (including initial porosity), if a stronger interaction exists, contact between the DCD crystals and the polymer matrix minimizes the formation of voids and as a result forces DCD to diffuse through layers of polymer along the release pathway.

8.4.3   *Material design for tailoring release*

This work uses DCD as a model crystalline material. However, these results are relevant to the encapsulation of any soluble crystalline agrichemical within the studied polymeric matrices. These results show the rate of release of a crystalline agrichemical can be easily tailored to the climatic conditions and crop or soil-specific requirements, bearing in mind that the relative affinity of different

chemicals for the different polymer matrixes will likely affect the relative release rates. Take the example of moderate soil temperatures around 23 °C. If 50% release is desired within the first week, month or 3 months, the recommended polymer matrix would be PHBV, PHBV:PCL 3:1, or PHBV:PCL 1:1, respectively. Alternatively, if the rate of DCD degradation was known for a specific soil in a specific climate, the modelling results presented here could be used to determine which material would sustain an active concentration of DCD within the soil profile for the longest period of time. This tailoring of release kinetics is pertinent to the effective delivery of agrichemicals and minimization of harmful environmental losses. Further work is needed to confirm the efficacy of these materials in pot and field-based experiments.

CHAPTER 9

Discussion & recommendations

Nitrification inhibitors (NIs) have been widely recognised for their ability to reduce environmental nitrogen losses, thereby reducing the agricultural carbon footprint and impact on local fresh and coastal aquatic environments, while also increasing the nitrogen uptake efficiency of the crop and potentially improving crop performance. However, evidence of efficacy is limited to temperate climates, with the rate of inhibitor degradation in tropical soils a key limitation. As such, the objectives of this project were to:

1. Design controlled-release nitrification inhibitors (CRNIs) to prolong their activity for tropical agricultural applications.

2. Determine the feasibility of extrusion processing as a simple, industrially relevant technique for the fabrication of controlled-release crystalline agrichemicals distributed in biodegradable matrices.

3. Develop a detailed understanding of the mechanisms that control release of soluble, crystalline agrichemicals distributed within a biodegradable polymer matrix.

4. Advance the knowledge on some of the key design parameters that modulate release kinetics.

This chapter synthesises the conclusions from the research on these topics and presents a model of how some of the materials developed might perform in tropical agricultural soils, along with a preliminary economic feasibility assessment, and recommendations for future work.

9.1 Knowledge gained

9.1.1 Feasibility of extrusion processing

The studies herein investigated the controlled-release of the nitrification inhibitor dicyandiamide (DCD) from thermoplastic wheat starch (TPS), poly(3-hydroxybutyrate-*co*-3-hydroxyvalerate) (PHBV) and synthetic polycaprolactone (PCL). The thermal stability of DCD up to 240 °C allowed extrusion with these polymers, since the highest melting polymer, PHBV, melts at 176 °C. The lack of DCD degradation during processing was confirmed with NMR spectroscopy, establishing extrusion as a viable technique for the fabrication of controlled-release nitrification inhibitors, as a drop-in technology of commercial relevance. Other agrichemicals that could be formulated this way can similarly be screened with thermogravimetric analysis (TGA), followed by the selection of a polymer with a crystallisation temperature (T_c) below the onset temperature (T_0) of thermal degradation for the agrichemical. Figure 9.1 shows a simple decision tree. For simplicity, it is best to select a polymer with a melting temperature (T_m) that is well below (>10 °C below) the T_0 of the agrichemical. This allows the polymer(s) and agrichemical to be fed together in the feed zone of the extruder, where the polymer melts in zone 1 and 2, while the agrichemical remains crystalline. In the

case that T_0 and T_m are similar, extrusion can still be used, but the agrichemical needs to be fed down the barrel, after the polymer has melted and cooled to well below T_0 of the agrichemical but above T_c of the polymer, which is commonly the die temperature.
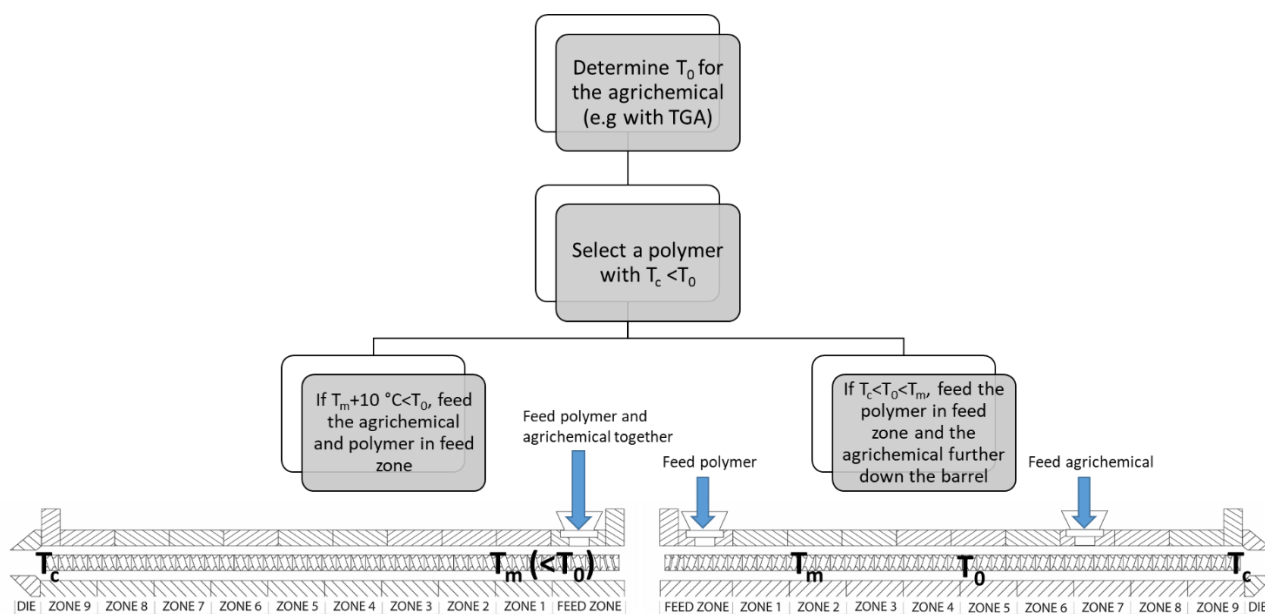
Figure 9.1: Decision tree for the feasibility of extrusion processing for the fabrication of controlled-release crystalline agrichemicals.

9.1.2 Polymer selection and release mechanisms

Once the range of feasible polymers has been identified based on the T_0 of the agrichemical and the T_c or T_m of the polymer, the next step is to consider the physical and chemical properties of the polymer, as these will determine the release kinetics. An ideal polymer would also be low cost, biodegradable in natural environments and easily processed.

As shown in Chapter 5, the release rate can range from 100% mobilisation in just 1 day to ~50% release over 140 days depending on the chemistry of the polymers selected. Thermoplastic starch (TPS) has five oxygen atoms per monomer unit resulting in a hydrophilic matrix that swells upon contact with water. The low packing density of the pyran rings, along with the branched nature of the amylopectin component also aid rapid migration of water and other small molecules through this polymer. In contrast, PHBV is a tightly packed, non-swelling, linear, semi-crystalline polymer with just two oxygen atoms per monomeric unit, resulting in extremely limited diffusion of both water and agrichemicals through the polymer. As such, agrichemical release is mediated through other pathways, including percolating networks of agrichemical crystals and pores, cracks and imperfections in the matrix, and in soil environments through erosion of the polymer matrix by soil microbes. The latter could influence release in several ways. Erosion of layers of polymer could

directly expose crystals, allowing water to dissolve and release the agrichemical, or the erosion process changes the properties of the polymer. Enzyme-catalysed chain scission decreases the molecular weight of the polymer and also preferentially erodes the amorphous portions of the polymer, making it more brittle, possibly leading to further cracking of the matrix, creating channels for release. Polymer hydrolysis also increases the number of hydrophilic carboxyl and hydroxyl end groups, leading to increased hydrophilicity and therefore higher rates of diffusion through the polymer. Further investigation is needed to understand this mechanism fully.

These two polymers represent the extreme ends of the spectrum in terms of hydrophilicity/hydrophobicity, with most other biodegradable polymers lying between these. As shown in Chapter 8, increasing the hydrophilicity through polymer blending can increase the rate of diffusion through the polymer matrix. However, this may not translate into a higher rate of release. Highly hydrophobic polymers, like PHBV, have a low affinity for soluble crystalline agrichemicals, leading to more interconnection between agrichemical crystals, resulting to a rapid release through percolation. A limitation of this thesis is the limited number of polymers evaluated. The characterisation of release from a broader range of biodegradable polymers, e.g. other types of PHA, polyethylene glycol (PEG), polybutylene adipate terephthalate (PBAT), poly(vinyl alcohol) (PVA), along with food waste polymers, such as cellulose, lignin or chitosan, would be useful to tailor formulations further and potentially lower production costs.

9.2   Tailoring release through material design

This section synthesises the results and learnings presented in Chapters 5 through 8 through a combined model to assess controlled-release DCD in field applications. The model helps to explore how tailoring material design can optimise the duration of active DCD in agricultural soils. The model developed is a simple mass balance, with the mass of DCD at any point in time equal to the cumulative mass released from the pellets minus the cumulative mass of DCD degraded at that time, as shown in Figure 9.2A. The model assumes that DCD degrades via first order kinetics, which accounts for all loss pathways – biotic and abiotic degradation, leaching/runoff, volatilisation etc. and the diffusion of DCD in the soil is rapid compared to the release rate, resulting in a homogenous DCD concentration in the soil. The release kinetics from Chapter 8 were used to model the mass of DCD mobilised into the soil. This is, of course, a simplification. That study was in pure water, so the effect of the release media and the influence of microbial metabolism of the matrix is not accounted for here. Assuming the effect of these factors is similar for all materials, this model allows the comparison of the different materials at different soil temperatures, application rates and pellet sizes.

In soil the half-life ($t_{1/2}$) of DCD exponentially declines with increasing soil temperature (°C):[8]

$$t_{1/2} = 168 \times e^{-0.084T}$$ **Eq. 9.1**

From Eq. 9.1, for a given soil temperature, the first order decay constant (k) can be estimated:

$$k = \frac{ln(2)}{t_{1/2}}$$ **Eq. 9.2**

Using a finite element approach for a first order decay and assuming quasi-steady state, the mass of DCD degraded in the soil (ΔM_{deg}) over a very short time frame (Δt) can be estimated:

$$\Delta M_{deg,t} = k \times M_t \times \Delta t$$ **Eq. 9.3**

Where M_t is the mass of active DCD in the soil at time, t. Assuming the release kinetics of DCD from the controlled-release formulation is diffusion driven, the fractional release can be estimated from a modified diffusion model,[129] to account for the fractional burst release (F_B), as described in Chapter 8:

$$F_{R,t} = F_B + (1 - F_B) \times \left[1 - \frac{32}{\pi^2} \sum_{n=1}^{\infty} \frac{1}{q_n^2} exp\left(-\frac{q_n^2}{R^2} Dt\right) \sum_{p=0}^{\infty} \frac{1}{(2p-1)^2} \times exp\left(-\frac{(2p+1)^2\pi^2}{L^2} Dt\right) \right]$$ **Eq. 9.4**

where F_R is the fractional release at time t, D denotes the apparent diffusion coefficient, q_n are the zero order roots of the Bessel function of the first kind, and R and L are the radius and length of the cylindrical pellet, respectively. The mass released into the soil at any point in time ($M_{R,t}$) can be easily estimated from the fractional release multiplied by the application rate of DCD (AR):

$$M_{R,t} = F_{R,t} \times AR$$ **Eq. 9.5**

From Eq. 9.3 and Eq. 9.5, the mass of active DCD in the soil can be estimated stepwise:

$$M_{t=0} = M_{R,t=0}$$ **Eq. 9.6**

$$M_t = M_{t-1} + (M_{R,t} - M_{R,t-1}) - \Delta M_{deg,t-1}$$ **Eq. 9.7**

For this modelling exercise, the materials of interest relate to Chapter 8, with pellets composed of 400 g.kg^{-1} DCD in PHBV, PHBV:PCL 3:1, PHBV:PCL 1:1 and PHBV:PCL 1:3 and PCL. The Arrhenius parameters reported in Figure 8.8 were used to calculate the diffusivity at a given temperature using Eq. 8.4, and the release after 10 h at 10 °C was taken as the fractional burst release, F_B, since at 10 °C the change in mechanisms from surface wash to matrix-controlled release was most apparent.

The outcomes from the model are summarised in Figure 9.2, with the relevant material(s), soil temperature, pellet size(s) and application rate(s) summarised in the table above each plot. Plot A is

an example of the model construction, using DCD-PCL as an example, showing the cumulative mass of DCD released into the soil, the cumulative mass of DCD degraded and the net mass of active DCD in the soil on a kg DCD per hectare basis. DCD without encapsulation decays with a half-life of 21 days at 25 °C (and 48 days at 15 °C), as shown by the solid black line in each of the plots. Field application rates of DCD are typically between 5 and 15 kg.ha^{-1},[139] with 10 kg.ha^{-1} chosen as the application rate of DCD without encapsulation for comparison with the controlled-release DCD formulations. The dotted line at 5 kg.ha^{-1} is the assumed content required for effective nitrification inhibition. Further research is required to determine this value accurately for various soil types. Plot B highlights the need for significantly higher DCD application to prolong inhibition significantly, using DCD-PCL as an example. At 10 kg DCD.ha^{-1} (i.e., 25 kg of DCD-PCL), the soil content will never reach 5 kg DCD.ha^{-1}. Increasing the application rate to 15 kg DCD.ha^{-1} could prolong the duration of effective inhibition from 21 days to 36 days, while further increases to 20 and 25 kg DCD.ha^{-1} may extend this period out to 52 days and 63 days, respectively. DCD-PCL was selected for this example as this material theoretically performs the best at both 25 °C and 15 °C, as shown in plot C and D, respectively, with DCD-PHBV:PCL 3:1 performing equally well at both temperatures. DCD-PHBV released too quickly, shortening the effective period at 25 °C to 55 days at 25 kg DCD.ha^{-1}, whereas DCD-PHBV:PCL 1:1 and DCD-PHBV:PCL 1:3 release too slowly, extending the effective period to 42 days and 38 days, respectively.

One approach to increasing the rate of release is to reduce the size of the pellet. Plot E shows the effect of reducing the mass of the DCD-PHBV:PCL 1:1 pellet by a half and a quarter of the size of pellets studied in this thesis, from 3×3 mm (H×D) to 2.4×2.4 mm and 1.9×1.9 mm, respectively. Halving and quartering the pellet size could theoretically increase the effective period from 42 days to 52 days and 58 days, respectively, with the latter getting close to the performance of DCD-PCL. Reducing the pellet size increases the release rate firstly by an increase in the surface wash (increasing F_B from 8% to 10% and 13%, respectively) and secondly by the reduced diffusion distance within the pellet and increased surface area of the moving front for a given mass of applied pellets. The increase in burst release was estimated by determining the specific surface wash (mg DCD.cm^{-2}) for each material from the release data in Chapter 8. An additional benefit of reducing the pellet mass is the proportional increase in the number of pellets for a given application rate (e.g., halving the mass doubles the number of pellets). This will improve the homogeneity of inhibitor concentration in the soil profile and increase the likelihood of the inhibitor molecules binding to AMO enzymes. Reducing the pellet size further has diminishing improvements, with release becoming too rapid at ~1.6×1.6 mm. This model predicts that DCD-PCL as 3×3 mm pellets outperforms DCD-PHBV:PCL 1:1 as 1.9×1.9 mm pellets in terms of the duration of soil content above 5 kg.ha^{-1}.

However, it would be recommended to use DCD-PHBV:PCL 1:1 as 1.9×1.9 mm pellets due to both the improved distribution of DCD in the soil and the lower peak concentration, slowing the rate of degradation, leading to higher soil content from ~80 days onward and reducing the likelihood of leaching losses during rainfall or irrigation events.

With 1.9×1.9 mm pellets of DCD-PHBV:PCL 1:1 preferred at 25 °C, plot F explores the effect of field application rates of this material at the lower soil temperature of 15 °C. Under these conditions, this material could potentially extend the effective DCD content from 48 days to ~125 days at 25 kg DCD.ha^{-1} application rate. This is likely longer than required, meaning the application rate could be reduced to 20 kg DCD.ha^{-1} while still achieving ~90 days above 5 kg.ha^{-1}.

This simple modelling exercise aids the design of optimal materials for different climatic conditions, though it is limited to inputs from experimental data of materials fabricated at 400 g.kg^{-1}. A universal model that can account for the loading and particle size of the inhibitors provides more flexibility and power for the design of controlled-release agrichemicals. The results here provide a reasonable idea of the range of inputs and processing conditions required for effective release. However, it is clear that significantly more inhibitor is required to prolong inhibition. This leads to concerns about the economic viability of the proposed field application rates.
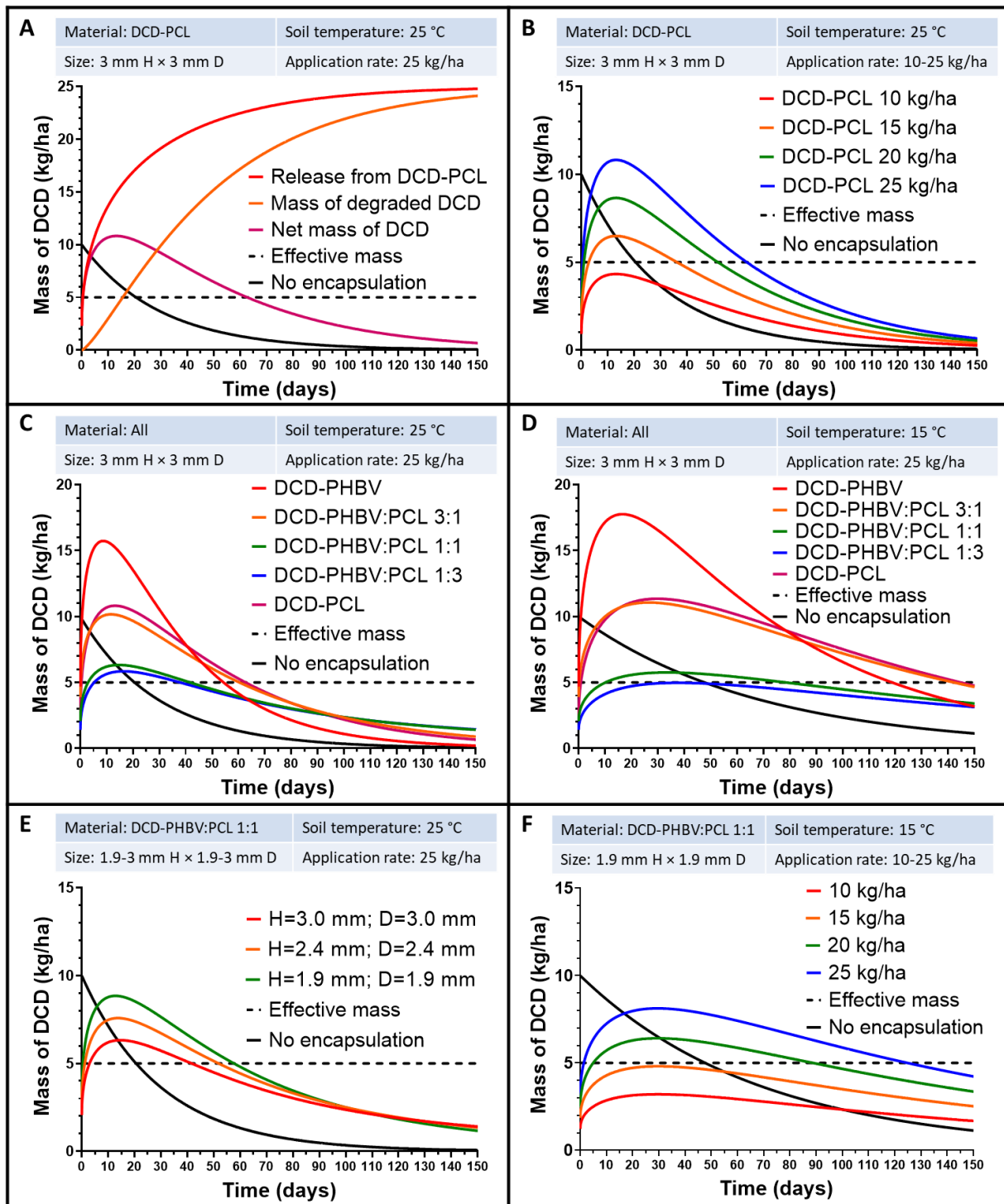
Figure 9.2: Field model results showing A) the model components using DCD-PCL as an example, with the net mass of DCD in the soil calculated from the cumulative mass released minus the cumulative mass degraded, **B)** the effect of application rate, using DCD-PCL as an example, **C)** and **D)** a comparison of performance of the different materials (PHBV, PHBV:PCL 3:1, PHBV:PCL 1:1, PHBV:PCL 1:3 and PCL) at 25 °C and 15 °C, respectively, **E)** the effect of pellet size, with DCD- PHBV:PCL 1:1 as an example and **F)** the effect of field application rates of 1.9×1.9 mm pellets of DC D- PHBV:PCL 1:1 at 15 °C.

9.3 Cost benefit analysis

What is the cost of a controlled-release nitrification inhibitor?

Assuming the cost of DCD is $1.50 kg^{-1}, the costs of PHBV and PCL are around $6 kg^{-1} and a conservative extrusion processing cost of $1 kg^{-1} [217] - *though this could be much less at large scale* - the cost to produce 1 kg of controlled-release DCD at a loading of 400 g DCD.kg^{-1} is around $5.2 kg^{-1}. In comparison, the cost of the competitor nitrification inhibitor, DMPP, is much higher, around $23.50 kg^{-1} DMPP. As such, a controlled-release DMPP formulation might cost closer to $14 kg^{-1} (Figure 9.3). However, typically field application rates differ by an order of magnitude, from 5-15 kg.ha^{-1} for DCD compared to 0.5-1.5 kg.ha^{-1} for DMPP. [139]

Controlled-release DMPP $14.0 kg^{-1}

Controlled-release DCD $5.2 kg^{-1}
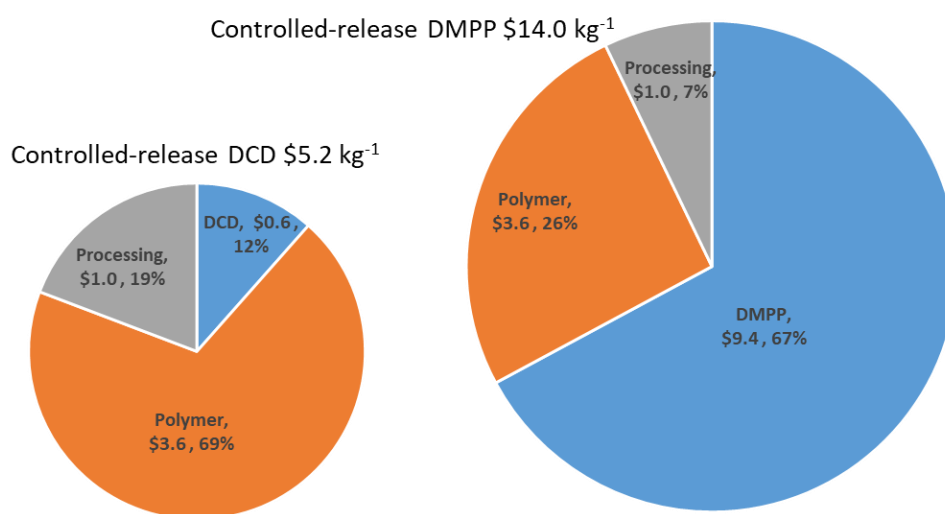
Figure 9.3: Cost breakdown for controlled-release nitrification inhibitors.

How effective does the controlled-release nitrification inhibitor need to be for economic viability?

The sugarcane industry (part funders of this work) will be taken as an example to assess the economic viability of these products, as sugarcane is a tropical crop of global significance with poor nitrogen uptake efficiency (NUE). Reports of NUE for sugarcane vary from 30-50% [218] (i.e., 30-50% of the applied N can be accounted for in the plant matter, the rest is assumed lost to the environment). Here, in Australia, closer to 50% is more commonly reported [218] and will be used for this assessment. In theory, any improvement in NUE should mean that less N fertiliser needs to be applied, saving fertiliser costs, and/or the increased N uptake should result in improved crop performance. Furthermore, any increase in improved NUE is beneficial to the local and global environment as it reduces N pollution and GHG emissions, however, a there is currently no financial incentive to reduce N losses in Australia. Following the work Di Bella et al. [219], the cost of urea is ~$500 t^{-1}, applied at

~200 kg N.ha⁻¹, and the revenue from sugar sales is ~\$420 t⁻¹, with average sugar yields around 7.9 t.ha⁻¹. This gives a base return of \$3,041 ha⁻¹, accounting for harvesting costs of \$7.50 per tonne of harvested sugar. The modelling results suggest as much as 25 kg DCD.ha⁻¹ controlled-release DCD is required to prolong the effective period of inhibition, 2.5 times the typical application rate used in temperate climates. Similarly, for the comparison to DMPP, an application rate of 2.5 kg DMPP.ha⁻¹ was assumed.
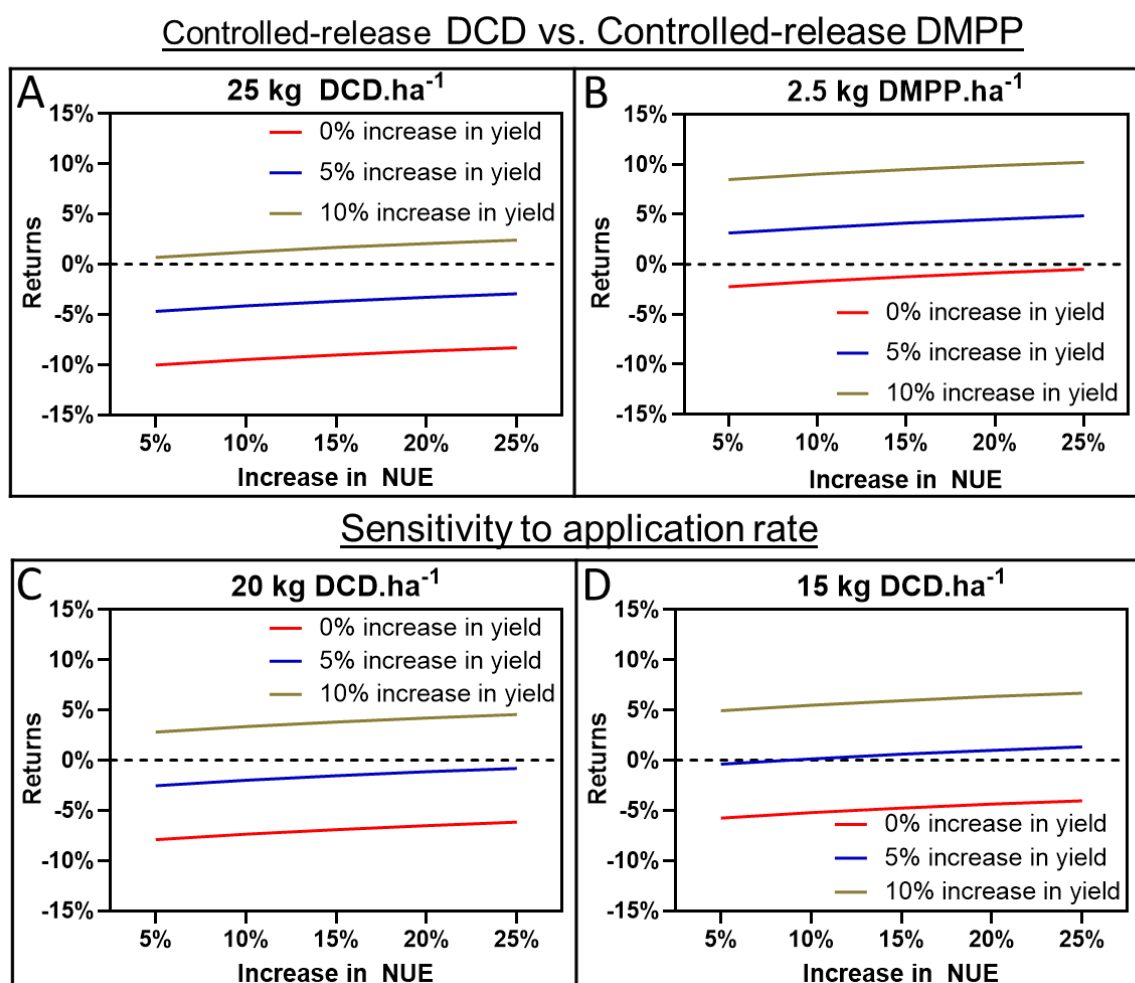
Figure 9.4: Summary of the back-of-the-envelope economic feasibility assessment for controlled-release DCD applied at 25 kg DCD.ha⁻¹ (A), 20 kg DCD.ha⁻¹ (C) and 15 kg DCD.ha⁻¹ (D), compared to controlled-release DMPP applied at 2.5 kg DMPP.ha⁻¹ (B).

The potential cost benefit of using controlled-release nitrification inhibitors is summarised in Figure 9.4. The results highlight the economic importance of achieving a yield increase compared to improving NUE. Here, the cost benefit of a 400 g DCD.kg⁻¹ controlled-release DCD formulation applied at 25 kg DCD.ha⁻¹ is challenging, with a ~10% yield increase required to break even compared with urea application alone. In comparison, if controlled-release DMPP formulated with 400 g DMPP.kg⁻¹ was applied at 2.5 times the typical application rate, i.e., 2.5 kg DMPP.ha⁻¹, an

increase in yield of <5% would see economic benefits to the farmer. While the cost of controlled-release DMPP would be almost three times higher than for DCD (Figure 9.3), the lower application rates of DMPP reduce the polymer input cost from \$225 ha^{-1} for controlled-release DCD to just \$22.50 for controlled-release DMPP. It is possible the lower application rates of controlled-release DCD could be effective, but would still require an increase in productivity and NUE of at least 7.5% and 5%, respectively, at 20 kg DCD.ha^{-1} and 5% and 10%, respectively at 15 kg DCD.ha^{-1}.

As shown in Figure 2.3 of the literature review (Chapter 2), realistic improvements in NUE and crop productivity when DCD is applied range from 11-27% and 2.5-10%, respectively.[6] That same meta-data study suggests DMPP was less effective, with changes in NUE and crop productivity ranging from 2 to 15% and -1 to 4%, respectively. This shows that the economics for controlled-release DCD are feasible, but challenging. There are two economically feasible paths to commercialisation of a controlled-release nitrification inhibitor:

1. fabricate controlled-release DMPP at 400 g DMPP.kg^{-1} using extrusion processing or

2. reduce the amount of polymer required, e.g., by fabricating coated DCD materials with <10 wt.% polymer in which case only a 5% increase in both NUE and crop productivity would result in agronomic benefits.

9.4   Recommendations for future developments

While the work presented in this thesis has largely answered the core research objectives, it has also highlighted a number a key outstanding knowledge gaps, including:

1. How much does polymer degradation contribute to release for different formulations? While the effect of polymer degradation is presented in Chapter 5, further research is needed to fully understand how this mechanism affects release kinetics at different loadings, inhibitor crystal sizes, and across different biodegradable polymers. Further, the exact mechanism through which release occurs is still not clear, i.e., opening of channels, cracks formation etc.

2. Is the understanding gained universal for controlled-release crystalline agrichemicals? Much of the knowledge gained here around polymer cracking, percolation, crystal size and polymer blends will be relevant to many crystalline agrichemicals and could aid the design of controlled-release fertilisers, pesticides, herbicides, fungicides etc. However, each agrichemical will have differing physical and chemical properties. Particularly water solubility/hydrophilicity and molecular weight/size will affect the rate of diffusion in both water-filled voids and through polymer matrices. The former property will also determine the degree of intermolecular interactions between the polymer and agrichemical, an important phenomenon as highlighted in Chapter 8.

3. Could a 3-D simulation be developed to model the various mechanisms reported here, i.e., surface release, diffusion through the polymer, pores and along cracks and polymer degradation and its influence on release kinetics? Simulation packages continue to improve in both complexity but also user-friendliness. For example, Comsol Multiphysics™ allows the building of complex structures (e.g., distributed objects, such as crystals or pores, within a given volume), to which properties can be linked, e.g., density, diffusivity, solubility etc. The software can couple reaction and transport processes to simulate transient release profiles. Packages of this nature may allow the development of a universal model in which the size, shape, distribution and loading of the crystalline additive form the inputs to the simulation. A model of this nature would be a powerful tool to guide the design of effective controlled-release materials.

4. Would other polymers within the PHA family improve release performance? The monomeric composition of this bacterial polymer alter its physical and chemical properties. PHB and PHBV have high crystallinity and brittle polymers, with high melting temperature (T_m), low water diffusivity and slow biodegradation. However, there are several other commercially available homo- and co-polymers of PHA which are commercially available, including poly(3-hydroxybutyrate-co-3-hydroxyhexanoate) (P(3HB-co-3HHx)) and poly(3-hydroxybutyrate-co-4-hydroxybutyrate) (P(3HB-co-4HB)).[177] These co-polymers have lower crystallinity, resulting in a softer more flexible polymer with lower T_m and higher water diffusivity.[174] As such, release characterisation from these polymers may outperform the PHBV used in the studies presented here. However, the availability and cost of these polymers limit their applicability at present.

The modelling and economic exercises highlight a path forward for the research and ultimate commercialisation of controlled-release nitrification inhibitors (CRNIs). The modelling highlights the need for significantly higher inhibitor application rates over those typically reported for temperate climates (approximately 2.5 times higher). As such, the economic viability becomes challenging. DMPP offers clear economic advantages over DCD when fabricated with extrusion processing; however, the agronomic benefits in terms of crop yield as well as environmental N losses are typically poorer than those of DCD[6-7, 139] and the lower application rates mean the number of pellets in the soil will be approximately ten times less. The efficacy of DMPP is being trialled by Queensland Department of Agriculture and Fisheries (QDAF). As mentioned in Chapter 1, this project was conducted in collaboration with the QDAF, who have tested the efficacy the materials developed in this project. As such, the scope here was confined to the fabrication, testing and characterisation of the controlled-release DCD pellets. The efficacy of these materials at inhibiting nitrification and the resulting impact on plant growth and environmental N loss is being tested at pot, plot and field-scale

by QDAF. Those results will be reported elsewhere when the outcomes have been finalised. Those studies are investigating a wider range of NI-polymer combinations than reported here and the results will isolate which materials work best in tropical cropping systems. Beyond those results, a number of other knowledge gaps remain:

1. What is the effect of pellet size on field application of CRNIs? This parameter needs to be explored experimentally to verify the modelled release kinetics, but also to investigate the effect of pellet size on distribution in the soil and the efficacy of the formulation. Based on the theory presented above, this could be a critical design parameter to achieve the desired release profile.

2. What is the effective nitrification inhibitor dose in field applications? In order to design effective materials, the effective inhibitor concentration in the soil and its dependency on soil properties and climatic conditions needs to be determined experimentally. Combining this knowledge with field efficacy testing will further aid material design through optimisation of the release kinetics.

3. What is the rate of migration of the inhibitors in the soil once they are released from the pellet? This is an important question that needs to be answered to understand what spacing between CRNI pellets is feasible, and could therefore determine the optimal pellet size and/or loading.

4. What is the best way to apply CRNIs in the field? Spherical pellets of the size studied here (~3 mm) could be mixed with fertilisers and spread together. However, as discussed, one concern is the spacing separation between pellets leading to poor NI distribution in the soil profile. This question may be crop specific. For example, sugarcane can be fertilised through stool splitting, concentrating the fertiliser in furrows. Compared to surface spreading, stool splitting reduces the distance the inhibitor would need to migrate in the soil to co-locate with the N fertiliser. Both DCD and DMPP migrate within the soil at similar rates with NH_4^+-N.

9.5   Conclusions

This project confirms extrusion as a viable production method for controlled-release crystalline agrichemicals, with a wide range of biodegradable polymers available. The release rate from such products can be tailored through material design:

1. Polymer(s) selection – depending on the physical and chemical properties of the polymer, release can range from 1 day to 6+ months and determines the mechanisms controlling release. PHBV shows promise for long-term release profiles (6+ months), but diffusion through this polymer is so slow that release occurs initially via surface release, percolation and cracks, while a large portion (~50%) of the agrichemical remains encapsulated until the polymer matrix degrades. To increase the rate of matrix diffusion, other more hydrophilic polymers can be

incorporated.

2. The agrichemical loading – this determines the degree of percolation within the matrix, with a threshold between 200 and 400 g.kg^{-1}. Below the percolation threshold, this parameter controls the thickness of polymer between agrichemical crystals.

3. Agrichemical crystal size – below the percolation threshold, the fractional release from the surface of the pellet can be modulated through the grind size of the agrichemical.

4. Pellet size – as identified through mathematical modelling, this parameter can control the fractional release rate and has consequences on the distribution within the soil.

As with most research projects, the key research questions have been addressed, leading to many new questions still outstanding.

REFERENCES

References

1.   Rockstrom, J.; Steffen, W.; Noone, K.; Persson, A.; Chapin, F. S.; Lambin, E. F.; Lenton, T. M.; Scheffer, M.; Folke, C.; Schellnhuber, H. J.; Nykvist, B.; de Wit, C. A.; Hughes, T.; van der Leeuw, S.; Rodhe, H.; Sorlin, S.; Snyder, P. K.; Costanza, R.; Svedin, U.; Falkenmark, M.; Karlberg, L.; Corell, R. W.; Fabry, V. J.; Hansen, J.; Walker, B.; Liverman, D.; Richardson, K.; Crutzen, P.; Foley, J. A., A safe operating space for humanity. *Nature* **2009,** *461* (7263), 472-475.

2.   Erisman, J. W.; Galloway, J. N.; Seitzinger, S.; Bleeker, A.; Dise, N. B.; Petrescu, A. M. R.; Leach, A. M.; de Vries, W., Consequences of human modification of the global nitrogen cycle. *Philosophical Transactions of the Royal Society B: Biological Sciences* **2013,** *368* (1621), 20130116.

3.   Steffen, W.; Richardson, K.; Rockström, J.; Cornell, S. E.; Fetzer, I.; Bennett, E. M.; Biggs, R.; Carpenter, S. R.; de Vries, W.; de Wit, C. A.; Folke, C.; Gerten, D.; Heinke, J.; Mace, G. M.; Persson, L. M.; Ramanathan, V.; Reyers, B.; Sörlin, S., Planetary boundaries: Guiding human development on a changing planet. *Science* **2015,** *347* (6223).

4.   Fowler, D.; Coyle, M.; Skiba, U.; Sutton, M. A.; Cape, J. N.; Reis, S.; Sheppard, L. J.; Jenkins, A.; Grizzetti, B.; Galloway, J. N.; Vitousek, P.; Leach, A.; Bouwman, A. F.; Butterbach-Bahl, K.; Dentener, F.; Stevenson, D.; Amann, M.; Voss, M., The global nitrogen cycle in the twenty-first century. *Philosophical Transactions of the Royal Society B: Biological Sciences* **2013,** *368* (1621), 20130164.

5.   Galloway, J. N.; Aber, J. D.; Erisman, J. W.; Seitzinger, S. P.; Howarth, R. W.; Cowling, E. B.; Cosby, B. J., The Nitrogen Cascade. *BioScience* **2003,** *53* (4), 341-356.

6.   Abalos, D.; Jeffery, S.; Sanz-Cobena, A.; Guardia, G.; Vallejo, A., Meta-analysis of the effect of urease and nitrification inhibitors on crop productivity and nitrogen use efficiency. *Agriculture, Ecosystems & Environment* **2014,** *189*, 136-144.

7.   Akiyama, H.; Yan, X.; Yagi, K., Evaluation of effectiveness of enhanced-efficiency fertilizers as mitigation options for N2O and NO emissions from agricultural soils: meta-analysis. *Global Change Biology* **2010,** *16* (6), 1837-1846.

8.   Kelliher, F. M.; Clough, T. J.; Clark, H.; Rys, G.; Sedcole, J. R., The temperature dependence of dicyandiamide (DCD) degradation in soils: A data synthesis. *Soil Biology and Biochemistry* **2008,** *40* (7), 1878-1882.

9.   Apodaca, L., Nitrogen Statistics and Information. In *National Minerals Information Center*, Survey, U. S. G., Ed. United States of America, 2020.

10.   Erisman, J. W.; Sutton, M. A.; Galloway, J.; Klimont, Z.; Winiwarter, W., How a century of ammonia synthesis changed the world. *Nature Geoscience* **2008,** *1* (10), 636-639.

11.   Lubkowski, K., Environmental impact of fertilizer use and slow release of mineral nutrients

as a response to this challenge. In *Polish Journal of Chemical Technology*, 2016; Vol. 18, p 72.

12.   Townsend, A. R.; Howarth, R. W.; Bazzaz, F. A.; Booth, M. S.; Cleveland, C. C.; Collinge, S. K.; Dobson, A. P.; Epstein, P. R.; Holland, E. A.; Keeney, D. R.; Mallin, M. A.; Rogers, C. A.; Wayne, P.; Wolfe, A. H., Human health effects of a changing global nitrogen cycle. *Frontiers in Ecology and the Environment* **2003,** *1* (5), 240-246.

13.   Gruber, N.; Galloway, J. N., An Earth-system perspective of the global nitrogen cycle. *Nature* **2008,** *451* (7176), 293-296.

14.   Galloway, J. N.; Dentener, F. J.; Capone, D. G.; Boyer, E. W.; Howarth, R. W.; Seitzinger, S. P.; Asner, G. P.; Cleveland, C. C.; Green, P. A.; Holland, E. A.; Karl, D. M.; Michaels, A. F.; Porter, J. H.; Townsend, A. R.; Vöosmarty, C. J., Nitrogen Cycles: Past, Present, and Future. *Biogeochemistry* **2004,** *70* (2), 153-226.

15.   Galloway, J. N.; Townsend, A. R.; Erisman, J. W.; Mateete, B.; Cai, Z.; Freney, J. R.; Martinelli, L. A.; Seitzinger, S. P.; Sutton, M. A., Transformation of the Nitrogen Cycle: Recent Trends, Questions, and Potential Solutions. *Science* **2008,** *320* (5878), 889-892.

16.   Krajewska, B.; van Eldik, R.; Brindell, M., Temperature- and pressure-dependent stopped-flow kinetic studies of jack bean urease. Implications for the catalytic mechanism. *Journal of Biological Inorganic Chemistry* **2012,** *17* (7), 1123-1134.

17.   Coskun, D.; Britto, D. T.; Shi, W.; Kronzucker, H. J., Nitrogen transformations in modern agriculture and the role of biological nitrification inhibition. *Nature Plants* **2017,** *3*, 17074.

18.   Liu, J.; You, L.; Amini, M.; Obersteiner, M.; Herrero, M.; Zehnder, A. J. B.; Yang, H., A high-resolution assessment on global nitrogen flows in cropland. *Proceedings of the National Academy of Sciences* **2010,** *107* (17), 8035-8040.

19.   Billen, G.; Garnier, J.; Lassaletta, L., The nitrogen cascade from agricultural soils to the sea: modelling nitrogen transfers at regional watershed and global scales. *Philosophical transactions of the Royal Society of London. Series B, Biological sciences* **2013,** *368* (1621), 20130123.

20.   Selman, M.; Greenhalgh, S.; Diaz, R.; Sugg, Z. *Eutrophication and hypoxia in coastal areas: a global assessment of the state of knowledge*; World Resources Institue: Washington, DC, USA, 2008.

21.   IPCC *Climate Change 2007: Mitigation. Contribution of Working Group III to the Fourth Assessment Report of the Intergovernmental Panel on Climate Change*; Cambridge, United Kingdom and New York, NY, USA., 2007; pp 497-540.

22.   Sutton, M. A.; Schjorring, J. K.; Wyers, G. P.; Duyzer, J. H.; Ineson, P.; Powlson, D. S., Plant-Atmosphere Exchange of Ammonia [and Discussion]. *Philosophical Transactions: Physical Sciences and Engineering* **1995,** *351* (1696), 261-278.

23.   Follett, R. F., *Nitrogen in the environment : sources, problems, and management / edited by R.F. Follett and J.L. Hatfield.* 1st ed.. ed.; Amsterdam ; New York : Elsevier: Amsterdam ; New York, 2001.

24.   Smil, V., *Feeding the world : a challenge for the twenty-first century.* The MIT Press: Cambridge, London, 2000.

25.   Hu, F. B.; Willett, W. C., Optimal diets for prevention of coronary heart disease. *Jama* **2002,** *288* (20), 2569-78.

26.   Kampa, M.; Castanas, E., Human health effects of air pollution. *Environmental Pollution* **2008,** *151* (2), 362-367.

27.   Timilsena, Y. P.; Adhikari, R.; Casey, P.; Muster, T.; Gill, H.; Adhikari, B., Enhanced efficiency fertilisers: a review of formulation and nutrient release patterns. *Journal of the science of food and agriculture* **2015,** *95* (6), 1131-1142.

28.   Trenkle, M. E. *Slow- and Controlled-Release and Stabilized Fertilizers: An Option for Enhancing Nutrient Efficiency in Agriculture*; International Fertilizer Industry Association: Paris, France, 2010.

29.   Shaviv, A., Advances in controlled-release fertilizers. In *Advances in Agronomy*, Academic Press: 2001; Vol. s71, pp 1-49.

30.   Sempeho, S. I.; Kim, H. T.; Mubofu, E.; Hilonga, A., Meticulous overview on the controlled release fertilizers. *Advances in Chemistry* **2014,** *2014*, 1-16.

31.   Majeed, Z.; Ramli Nur, K.; Mansor, N.; Man, Z., A comprehensive review on biodegradable polymers and their blends used in controlled-release fertilizer processes. In *Reviews in Chemical Engineering*, 2015; Vol. 31, p 69.

32.   Slangen, J. H. G.; Kerkhoff, P., Nitrification inhibitors in agriculture and horticulture: A literature review. *Fertilizer Research* **1984,** *5* (1), 1-76.

33.   Bronson, K. F.; Mosier, A. R., Effect of encapsulated calcium carbide on dinitrogen, nitrous oxide, methane, and carbon dioxide emissions from flooded rice. *Biology and Fertility of Soils* **1991,** *11* (2), 116-120.

34.   Johnson, J. M. F.; Franzluebbers, A. J.; Weyers, S. L.; Reicosky, D. C., Agricultural opportunities to mitigate greenhouse gas emissions. *Environmental Pollution* **2007,** *150* (1), 107-124.

35.   Weiske, A.; Benckiser, G.; Herbert, T.; Ottow, J. C. G., Influence of the nitrification inhibitor 3,4-dimethylpyrazole phosphate (DMPP) in comparison to dicyandiamide (DCD) on nitrous oxide emissions, carbon dioxide fluxes and methane oxidation during 3 years of repeated application in field experiments. *Biology and Fertility of Soils* **2001,** *34* (2), 109-117.

36.   Shrestha, R. K.; Strahm, B. D.; Sucre, E. B., Greenhouse gas emissions in response to nitrogen fertilization in managed forest ecosystems. *New Forests* **2015**, *46* (2), 167-193.

37.   Pasda, G.; Hähndel, R.; Zerulla, W., Effect of fertilizers with the new nitrification inhibitor DMPP (3,4-dimethylpyrazole phosphate) on yield and quality of agricultural and horticultural crops. *Biology and Fertility of Soils* **2001**, *34* (2), 85-97.

38.   Elgala, A.; Amberger, A., Factors Affecting Solubilization of Rock Phosphates in Soils. *International Journal of Plant & Soil Science* **2017**, *14* (1).

39.   Phongpan, S.; Freney, J. R.; Keerthisinghe, D. G.; Chaiwanakupt, P., Use of phenylphosphorodiamidate and N-(n-butyl)thiophosphorictriamide to reduce ammonia loss and increase grain yield following application of urea to flooded rice. *Fertilizer research* **1995**, *41* (1), 59-66.

40.   Modolo, L. V.; de Souza, A. X.; Horta, L. P.; Araujo, D. P.; de Fátima, Â., An overview on the potential of natural products as ureases inhibitors: A review. *Journal of Advanced Research* **2015**, *6* (1), 35-44.

41.   Mohanty, S.; Patra, A. K.; Chhonkar, P. K., Neem (Azadirachta indica) seed kernel powder retards urease and nitrification activities in different soils at contrasting moisture and temperature regimes. *Bioresource Technology* **2008**, *99* (4), 894-899.

42.   Suescun, F.; Paulino, L.; Zagal, E.; Ovalle, C.; Muñoz, C., Plant extracts from the Mediterranean zone of Chile potentially affect soil microbial activity related to N transformations: A laboratory experiment. *Acta Agriculturae Scandinavica Section B: Soil and Plant Science* **2012**, *62* (6), 556-564.

43.   Subbarao, G. V.; Ito, O.; Sahrawat, K. L.; Berry, W. L.; Nakahara, K.; Ishikawa, T.; Watanabe, T.; Suenaga, K.; Rondon, M.; Rao, I. M., Scope and Strategies for Regulation of Nitrification in Agricultural Systems—Challenges and Opportunities. *Critical Reviews in Plant Sciences* **2006**, *25* (4), 303-335.

44.   Topp, E.; Knowles, R., Effects of Nitrapyrin [2-Chloro-6-(Trichloromethyl) Pyridine] on the Obligate Methanotroph Methylosinus trichosporium OB3b. *Appl Environ Microbiol* **1984**, *47* (2), 258-62.

45.   Singh, S.; Verma, A., The Potential of Nitrification Inhibitors to Manage the Pollution Effect of Nitrogen Fertilizers in Agricultural and Other Soils: A Review. *Environmental Practice* **2007**, *9* (4), 266-266.

46.   Sahrawat, K. L.; Keeney, D. R., Perspectives for research on development of nitrification inhibitors. *Communications in Soil Science and Plant Analysis* **1985**, *16* (5), 517-524.

47.   Hyman, M. R.; Wood, P. M., Ethylene oxidation by Nitrosomonas europaea. *Archives of*

References

Microbiology **1984,** *137* (2), 155-158.

48.   Marsden, K. A.; Marín-Martínez, A. J.; Vallejo, A.; Hill, P. W.; Jones, D. L.; Chadwick, D. R., The mobility of nitrification inhibitors under simulated ruminant urine deposition and rainfall: a comparison between DCD and DMPP. *Biology and Fertility of Soils* **2016,** *52* (4), 491-503.

49.   Upadhyay, R. K.; Patra, D. D.; Tewari, S. K., Natural nitrification inhibitors for higher nitrogen use efficiency, crop yield, and for curtailing global warming. *Journal of Tropical Agriculture* **2011,** *49*, 19-24.

50.   Subbarao, G. V.; Yoshihashi, T.; Worthington, M.; Nakahara, K.; Ando, Y.; Sahrawat, K. L.; Rao, I. M.; Lata, J. C.; Kishii, M.; Braun, H. J., Suppression of soil nitrification by plants. *Plant Science* **2015,** *233*, 155-164.

51.   Paavolainen, L.; Kitunen, V.; Smolander, A., Inhibition of nitrification in forest soil by monoterpenes. *An International Journal on Plant-Soil Relationships* **1998,** *205* (2), 147-154.

52.   Ward, B. B.; Courtney, K. J.; Langenheim, J. H., Inhibition of Nitrosomonas europaea by Monoterpenes from Coastal Redwood (Sequoia sempervirens) in Whole-Cell Studies. *Journal of Chemical Ecology* **1997,** *23* (11), 2583-2598.

53.   Wood, S. E.; Gaskin, J. F.; Langenheim, J. H., Loss of monoterpenes from Umbellularia californica leaf litter. *Biochemical Systematics and Ecology* **1995,** *23* (6), 581-591.

54.   Adamczyk, S.; Adamczyk, B.; Kitunen, V.; Smolander, A., Monoterpenes and higher terpenes may inhibit enzyme activities in boreal forest soil. *Soil Biology and Biochemistry* **2015,** *87*, 59-66.

55.   White, C. S., Nitrification Inhibition by Monoterpenoids: Theoretical Mode of Action Based on Molecular Structures. *Ecology* **1988,** *69* (5), 1631-1633.

56.   White, C., The role of monoterpenes in soil nitrogen cycling processes in ponderosa pine. *Biogeochemistry* **1991,** *12* (1), 43-68.

57.   Subbarao, G.; Rondon, M.; Ito, O.; Ishikawa, T.; Rao, I.; Nakahara, K.; Lascano, C.; Berry, W., Biological nitrification inhibition (BNI)—is it a widespread phenomenon? *An International Journal on Plant-Soil Relationships* **2007,** *294* (1), 5-18.

58.   Byrnes, B.; Vilsmeier, K.; Austin, E.; Amberger, A., Degradation of the urease inhibitor phenyl phosphorodiamidate in solutions and floodwaters. *Journal of Agricultural and Food Chemistry* **1989,** *37* (2), 473-477.

59.   Barth, G.; Von Tucher, S.; Schmidhalter, U., Influence of soil parameters on the effect of 3,4-dimethylpyrazole-phosphate as a nitrification inhibitor. *Biology and Fertility of Soils* **2001,** *34* (2), 98-102.

60.   Shi, X.; Hu, H.-W.; Müller, C.; He, J.-Z.; Chen, D.; Suter, H. C., Effects of the Nitrification

Inhibitor 3,4-Dimethylpyrazole Phosphate on Nitrification and Nitrifiers in Two Contrasting Agricultural Soils. *Appl Environ Microb* **2016,** *82* (17), 5236-5248.

61.   Zhu, G.; Ju, X.; Zhang, J.; Müller, C.; Rees, R. M.; Thorman, R. E.; Sylvester-Bradley, R., Effects of the nitrification inhibitor DMPP (3,4-dimethylpyrazole phosphate) on gross N transformation rates and N2O emissions. *Biology and Fertility of Soils* **2019,** *55* (6), 603-615.

62.   Shi, Y.-F.; Zhang, L.-L.; Zhao, M.-Q., Nitrification inhibitor DMPP adsorption behavior on soils and the effects of pH, Cu(II) and Cd(II). In *Advanced Materials and Energy Sustainability*, 2017; pp 554-561.

63.   Zhao, M. Q.; Zhang, L. L.; Shi, Y. F., Effects of Incubation Temperature, Repeated Application, and Heavy Metal Addition on Degradation of Nitrification Inhibitor 3,4-Dimethylpyrazole Phosphate (DMPP) in Burozem with Model Experiments. *Applied Mechanics and Materials* **2017,** *858*, 348-353.

64.   Merino, P.; Menéndez, S.; Pinto, M.; González-Murua, C.; Estavillo, J. M., 3,4-Dimethylpyrazole phosphate reduces nitrous oxide emissions from grassland after slurry application. *Soil Use and Management* **2005,** *21* (1), 53-57.

65.   Mahmood, T.; Ali, R.; Lodhi, A.; Sajid, M., 4-Amino-1,2,4-triazole can be more effective than commercial nitrification inhibitors at high soil temperatures. *Soil Research* **2017,** *55* (7), 715-722.

66.   Amberger, A., Research on dicyandiamide as a nitrification inhibitor and future outlook. *Communications in Soil Science and Plant Analysis* **1989,** *20* (19-20), 1933-1955.

67.   Irigoyen, I.; Muro, J.; Azpilikueta, M.; Aparicio-Tejo, P.; Lamsfus, C., Ammonium oxidation kinetics in the presence of nitrification inhibitors DCD and DMPP at various temperatures. *Australian Journal of Soil Research* **2003,** *41* (6), 1177-1183.

68.   Kelliher, F. M.; van Koten, C.; Kear, M. J.; Sprosen, M. S.; Ledgard, S. F.; de Klein, C. A. M.; Letica, S. A.; Luo, J.; Rys, G., Effect of temperature on dicyandiamide (DCD) longevity in pastoral soils under field conditions. *Agriculture, Ecosystems and Environment* **2014,** *186*, 201-204.

69.   Rajbanshi, S. S.; Benckiser, G.; Ottow, J. C. G., Effects of concentration, incubation temperature, and repeated applications on degradation kinetics of dicyandiamide (DCD) in model experiments with a silt loam soil. *Biology and Fertility of Soils* **1992,** *13* (2), 61-64.

70.   Lammel, J. In *Cost of the different options available to the farmers: Current situation and prospects*, IFA International Workshop on Enhanced-Efficiency Fertilizers, Frankfurt, Paris, France, International Fertilizer Industry Association: Paris, France, 2005.

71.   Morgan, K. T.; Cushman, K. E.; Sato, S., Release Mechanisms for Slow- and Controlled-release Fertilizers and Strategies for Their Use in Vegetable Production. *HortTechnology* **2009,** *19*

References

(1), 10-12.

72.   Shoji, S.; Delgado, J.; Mosier, A.; Miura, Y., Use of controlled release fertilizers and nitrification inhibitors to increase nitrogen use efficiency and to conserve air and water quality. *Communications in Soil Science and Plant Analysis* **2001,** *32* (7-8), 1051-1070.

73.   Prasad, R.; Power, J. F., Nitrification Inhibitors for Agriculture, Health, and the Environment. *Advances in Agronomy* **1995,** *54*, 233-281.

74.   Ruser, R.; Schulz, R., The effect of nitrification inhibitors on the nitrous oxide (N2O) release from agricultural soils—a review. *Journal of Plant Nutrition and Soil Science* **2015,** *178* (2), 171-188.

75.   Cai, Y.; Akiyama, H., Effects of inhibitors and biochar on nitrous oxide emissions, nitrate leaching, and plant nitrogen uptake from urine patches of grazing animals on grasslands: a meta-analysis. *Soil Science and Plant Nutrition* **2017,** *63* (4), 405-414.

76.   Oenema, O.; Wrage, N.; Velthof, G. L.; van Groenigen, J. W.; Dolfing, J.; Kuikman, P. J., Trends in Global Nitrous Oxide Emissions from Animal Production Systems. *Nutrient Cycling in Agroecosystems* **2005,** *72* (1), 51-65.

77.   Otey, F. H.; Trimnell, D.; Westhoff, R. P.; Shasha, B. S., Starch matrix for controlled release of urea fertilizer. *Journal of Agricultural and Food Chemistry* **1984,** *32* (5), 1095-1098.

78.   Minet, E. P.; O'Carroll, C.; Rooney, D.; Breslin, C.; McCarthy, C. P.; Gallagher, L.; Richards, K. G., Slow delivery of a nitrification inhibitor (dicyandiamide) to soil using a biodegradable hydrogel of chitosan. *Chemosphere* **2013,** *93* (11), 2854-2858.

79.   Bishop, P. A. Polymer Coated Controlled Release Agrichemicals as Mitigation Tools in Pastoral Farming. Massey University, Palmerston North, New Zealand, 2010.

80.   Göpferich, A., Mechanisms of polymer degradation and erosion. *Biomaterials* **1996,** *17* (2), 103-114.

81.   Naz Muhammad, Y.; Sulaiman Shaharin, A., Attributes of natural and synthetic materials pertaining to slow-release urea coating industry. In *Reviews in Chemical Engineering*, 2017; Vol. 33, p 293.

82.   Chen, J.; Lü, S.; Zhang, Z.; Zhao, X.; Li, X.; Ning, P.; Liu, M., Environmentally friendly fertilizers: A review of materials used and their effects on the environment. *Science of The Total Environment* **2018,** *613–614*, 829-839.

83.   Jin, S.; Wang, Y.; He, J.; Yang, Y.; Yu, X.; Yue, G., Preparation and properties of a degradable interpenetrating polymer networks based on starch with water retention, amelioration of soil, and slow release of nitrogen and phosphorus fertilizer. *Journal of Applied Polymer Science* **2013,** *128* (1), 407-415.

84.   Han, X.; Chen, S.; Hu, X., Controlled-release fertilizer encapsulated by starch/polyvinyl alcohol coating. *Desalination* **2009,** *240* (1), 21-26.

85.   Rychter, P.; Kot, M.; Bajer, K.; Rogacz, D.; Šišková, A.; Kapuśniak, J., Utilization of starch films plasticized with urea as fertilizer for improvement of plant growth. *Carbohydrate Polymers* **2016,** *137*, 127-138.

86.   Azeem, B.; KuShaari, K.; Man, Z., Effect of Coating Thickness on Release Characteristics of Controlled Release Urea Produced in Fluidized Bed Using Waterborne Starch Biopolymer as Coating Material. *Procedia Engineering* **2016,** *148*, 282-289.

87.   Naz, M. Y.; Sulaiman, S. A., Testing of starch-based carbohydrate polymer coatings for enhanced urea performance. *Journal of Coatings Technology and Research* **2014,** *11* (5), 747-756.

88.   Cao, Y.; Huang, L.; Chen, J.; Liang, J.; Long, S.; Lu, Y., Development of a controlled release formulation based on a starch matrix system. *International Journal of Pharmaceutics* **2005,** *298* (1), 108-116.

89.   Lü, S.; Feng, C.; Gao, C.; Wang, X.; Xu, X.; Bai, X.; Gao, N.; Liu, M., Multifunctional Environmental Smart Fertilizer Based on l-Aspartic Acid for Sustained Nutrient Release. *Journal of Agricultural and Food Chemistry* **2016,** *64* (24), 4965-4974.

90.   Ni, B.; Liu, M.; Lü, S.; Xie, L., Multifunctional slow-release organic-inorganic compound fertilizer. *Journal of agricultural and food chemistry* **2010,** *58* (23), 12373-12378.

91.   Ni, B.; Liu, M.; Lü, S.; Xie, L.; Zhang, X.; Wang, Y., Novel Slow-Release Multielement Compound Fertilizer with Hydroscopicity and Moisture Preservation. *Industrial & Engineering Chemistry Research* **2010,** *49* (10), 4546-4552.

92.   Ni, B.; Lü, S.; Liu, M., Novel Multinutrient Fertilizer and Its Effect on Slow Release, Water Holding, and Soil Amending. *Industrial & Engineering Chemistry Research* **2012,** *51* (40), 12993-13000.

93.   Volova, T. G.; Prudnikova, S. V.; Boyandin, A. N., Biodegradable poly-3-hydroxybutyrate as a fertilizer carrier. *Journal of the science of food and agriculture* **2016**.

94.   Costa, M. M. E.; Cabral-Albuquerque, E. C. M.; Alves, T. L. M.; Pinto, J. C.; Fialho, R. L., Use of Polyhydroxybutyrate and Ethyl Cellulose for Coating of Urea Granules. *Journal of Agricultural and Food Chemistry* **2013,** *61* (42), 9984-9991.

95.   Grillo, R.; de Melo, N. F. S.; de Lima, R.; Lourenço, R. W.; Rosa, A. H.; Fraceto, L. F., Characterization of Atrazine-Loaded Biodegradable Poly(Hydroxybutyrate-Co-Hydroxyvalerate) Microspheres. *Journal of Polymers and the Environment* **2010,** *18* (1), 26-32.

96.   Grillo, R.; Pereira, A. d. E. S.; de Melo, N. F. S.; Porto, R. M.; Feitosa, L. O.; Tonello, P. S.; Filho, N. L. D.; Rosa, A. H.; Lima, R.; Fraceto, L. F., Controlled release system for ametryn using

References

polymer microspheres: Preparation, characterization and release kinetics in water. *Journal of Hazardous Materials* **2011,** *186* (2–3), 1645-1651.

97.   Lobo, F. A.; de Aguirre, C. L.; Silva, M. S.; Grillo, R.; de Melo, N. F. S.; de Oliveira, L. K.; de Morais, L. C.; Campos, V.; Rosa, A. H.; Fraceto, L. F., Poly(hydroxybutyrate-co-hydroxyvalerate) microspheres loaded with atrazine herbicide: screening of conditions for preparation, physico-chemical characterization, and in vitro release studies. *Polymer Bulletin* **2011,** *67* (3), 479-495.

98.   Voinova, O. N.; Kalacheva, G. S.; Grodnitskaya, I. D.; Volova, T. G., Microbial polymers as a degradable carrier for pesticide delivery. *Applied Biochemistry and Microbiology* **2009,** *45* (4), 384-388.

99.   Volova, T. G.; Voinova, O. N.; Kalacheva, G. S.; Grodnitskaya, I. D., The prospects of the use of resorbable polyesters for designing safe pesticides. *Doklady Biological Sciences* **2008,** *419* (1), 100-103.

100.   Boyandin, A. N.; Zhila, N. O.; Kiselev, E. G.; Volova, T. G., Constructing Slow-Release Formulations of Metribuzin Based on Degradable Poly(3-hydroxybutyrate). *Journal of Agricultural and Food Chemistry* **2016,** *64* (28), 5625-5632.

101.   Zhila, N.; Murueva, A.; Shershneva, A.; Shishatskaya, E.; Volova, T., Herbicidal activity of slow-release herbicide formulations in wheat stands infested by weeds. *Journal of Environmental Science and Health, Part B* **2017**, 1-7.

102.   Prudnikova, S. V.; Boyandin, A. N.; Kalacheva, G. S.; Sinskey, A. J., Degradable Polyhydroxyalkanoates as Herbicide Carriers. *Journal of Polymers and the Environment* **2013,** *21* (3), 675-682.

103.   Volova, T.; Zhila, N.; Vinogradova, O.; Shumilova, A.; Prudnikova, S.; Shishatskaya, E., Characterization of biodegradable poly-3-hydroxybutyrate films and pellets loaded with the fungicide tebuconazole. *Environmental Science and Pollution Research* **2016,** *23* (6), 5243-5254.

104.   Volova, T.; Prudnikova, S.; Boyandin, A.; Zhila, N.; Kiselev, E.; Shumilova, A.; Baranovskiy, S.; Demidenko, A.; Shishatskaya, E.; Thomas, S., Constructing Slow-Release Fungicide Formulations Based on Poly(3-hydroxybutyrate) and Natural Materials as a Degradable Matrix. *Journal of Agricultural and Food Chemistry* **2019,** *67* (33), 9220-9231.

105.   Boyandin, A. N.; Kazantseva, E. A.; Varygina, D. E.; Volova, T. G., Constructing Slow-Release Formulations of Ammonium Nitrate Fertilizer Based on Degradable Poly(3-hydroxybutyrate). *Journal of Agricultural and Food Chemistry* **2017,** *65* (32), 6745-6752.

106.   Laycock, B.; Nikolić, M.; Colwell, J. M.; Gauthier, E.; Halley, P.; Bottle, S.; George, G., Lifetime prediction of biodegradable polymers. *Progress in Polymer Science* **2017,** *71*, 144-189.

107.   Grassi, M.; Grassi, G., Application of mathematical modeling in sustained release delivery systems. *Expert Opinion on Drug Delivery* **2014,** *11* (8), 1299-1321.

108.   Lin, C.-C.; Metters, A. T., Hydrogels in controlled release formulations: Network design and mathematical modeling. *Advanced Drug Delivery Reviews* **2006,** *58* (12–13), 1379-1408.

109.   Ford Versypt, A. N.; Pack, D. W.; Braatz, R. D., Mathematical modeling of drug delivery from autocatalytically degradable PLGA microspheres — A review. *Journal of Controlled Release* **2013,** *165* (1), 29-37.

110.   Irfan, S. A.; Razali, R.; KuShaari, K.; Mansor, N.; Azeem, B.; Ford Versypt, A. N., A review of mathematical modeling and simulation of controlled-release fertilizers. *Journal of Controlled Release* **2018,** *271*, 45-54.

111.   Siepmann, J.; Göpferich, A., Mathematical modeling of bioerodible, polymeric drug delivery systems. *Advanced Drug Delivery Reviews* **2001,** *48* (2–3), 229-247.

112.   Siepmann, J.; Siepmann, F., Mathematical modeling of drug delivery. *International Journal of Pharmaceutics* **2008,** *364* (2), 328-343.

113.   Siepmann, J.; Siepmann, F., Modeling of diffusion controlled drug delivery. *J Control Release* **2012,** *161* (2), 351-62.

114.   De, A.; Bose, R.; Kumar, A.; Mozumdar, S., *Targeted Delivery of Pesticides Using Biodegradable Polymeric Nanoparticles*. Springer India, New Delhi: New Delhi, 2014.

115.   Trinh, T. H.; Shaari, K. Z. K.; Basit, A.; Azeem, B., Effect of Particle Size and Coating Thickness on the Release of Urea Using Multi-Diffusion Model. *International Journal of Chemical Engineering and Applications* **2014,** *5* (1), 6.

116.   Shaviv, A.; Raban, S.; Zaidel, E., Modeling Controlled Nutrient Release from Polymer Coated Fertilizers: Diffusion Release from Single Granules. *Environmental Science & Technology* **2003,** *37* (10), 2251-2256.

117.   Leuenberger, H.; Rohera, B. D.; Haas, C., Percolation theory — a novel approach to solid dosage form design. *International Journal of Pharmaceutics* **1987,** *38* (1), 109-115.

118.   Bajpai, A. K.; Giri, A., Swelling dynamics of a ternary interpenetrating polymer network (ipn) and controlled release of potassium nitrate as a model agrochemical. *Journal of Macromolecular Science, Part A* **2002,** *39* (1-2), 75-102.

119.   Volova, T. G.; Prudnikova, S. V.; Zhila, N. O.; Vinogradova, O. N.; Shumilova, A. A.; Nikolaeva, E. D.; Kiselev, E. G.; Shishatskaya, E. I., Efficacy of tebuconazole embedded in biodegradable poly-3-hydroxybutyrate to inhibit the development of Fusarium moniliforme in soil microecosystems. *Pest management science* **2017,** *73* (5), 925-935.

120.   Siegel, R. A.; Kost, J.; Langer, R., Mechanistic studies of macromolecular drug release from

macroporous polymers. I. Experiments and preliminary theory concerning completeness of drug release. *Journal of Controlled Release* **1989,** *8* (3), 223-236.

121.   Millán, M.; Caraballo, I.; Rabasco, A. M., The Role of the Drug/Excipient Particle Size Ratio in the Percolation Model for Tablets. *Pharmaceutical Research* **1998,** *15* (2), 216-220.

122.   Jarrell, W. M.; Boersma, L., Release of urea by granules of sulfur-coated urea. *Release of urea by granules of sulfur-coated urea.* **1980,** *44* (2), 418-422.

123.   Higuchi, T., Rate of release of medicaments from ointment bases containing drugs in suspension. *Journal of Pharmaceutical Sciences* **1961,** *50* (10), 874-875.

124.   Higuchi, T., Mechanism of sustained-action medication. Theoretical analysis of rate of release of solid drugs dispersed in solid matrices. *Journal of Pharmaceutical Sciences* **1963,** *52* (12), 1145-1149.

125.   Roseman, T. J., Release of steroids from a silicone polymer. *Journal of Pharmaceutical Sciences* **1972,** *61* (1), 46-50.

126.   Roseman, T. J.; Higuchi, W. I., Release of medroxyprogesterone acetate from a silicone polymer. *Journal of Pharmaceutical Sciences* **1970,** *59* (3), 353-357.

127.   Peppas, N. A., Analysis of Fickian and non-Fickian drug release from polymers. *Pharm Acta Helv* **1985,** *60* (4), 110-1.

128.   Ritger, P. L.; Peppas, N. A., A simple equation for description of solute release I. Fickian and non-fickian release from non-swellable devices in the form of slabs, spheres, cylinders or discs. *Journal of Controlled Release* **1987,** *5* (1), 23-36.

129.   Vergnaud, J. M., *Controlled drug release of oral dosage forms*. E. Horwood: New York, 1993.

130.   Chan, C. M.; Vandi, L.-J.; Pratt, S.; Halley, P.; Ma, Y.; Chen, G.-Q.; Richardson, D.; Werker, A.; Laycock, B., Understanding the effect of copolymer content on the processability and mechanical properties of polyhydroxyalkanoate (PHA) / wood composites. *Manuscript submitted to: Composites Part A: applied science and manufacturing* **2019**.

131.   Medina, L. C.; Sartain, J. B.; Obreza, T. A.; Hall, W. L.; Thiex, N. J., Evaluation of a soil incubation method to characterize nitrogen release patterns of slow- and controlled-release fertilizers. *Journal of AOAC International* **2014,** *97* (3), 643-60.

132.   Ge, X.; Wu, X.; Liang, S.; Su, M.; Sun, H., Trace residue analysis of dicyandiamide, cyromazine, and melamine in animal tissue foods by ultra-performance liquid chromatography. *Journal of Food and Drug Analysis* **2016,** *24* (3), 579-585.

133.   Laycock, B.; Arcos-Hernandez, M. V.; Langford, A.; Pratt, S.; Werker, A.; Halley, P. J.; Lant, P. A., Crystallisation and fractionation of selected polyhydroxyalkanoates produced from

mixed cultures. *New Biotechnology* **2014,** *31* (4), 345-356.

134.   Barham, P. J.; Keller, A.; Otun, E. L.; Holmes, P. A., Crystallization and morphology of a bacterial thermoplastic: poly-3-hydroxybutyrate. *Journal of Materials Science* **1984,** *19* (9), 2781-2794.

135.   Crescenzi, V.; Manzini, G.; Calzolari, G.; Borri, C., Thermodynamics of fusion of poly-β-propiolactone and poly-ϵ-caprolactone. comparative analysis of the melting of aliphatic polylactone and polyester chains. *European Polymer Journal* **1972,** *8* (3), 449-463.

136.   Lassaletta, L.; Billen, G.; Grizzetti, B.; Anglade, J.; Garnier, J., 50 year trends in nitrogen use efficiency of world cropping systems: the relationship between yield and nitrogen input to cropland. *Environmental Research Letters* **2014,** *9* (10), 105011.

137.   Verzeaux, J.; Hirel, B.; Dubois, F.; Lea, P. J.; Tétu, T., Agricultural practices to improve nitrogen use efficiency through the use of arbuscular mycorrhizae: Basic and agronomic aspects. *Plant Science* **2017,** *264*, 48-56.

138.   Liu, C.; Wang, K.; Zheng, X., Effects of nitrification inhibitors (DCD and DMPP) on nitrous oxide emission, crop yield and nitrogen uptake in a wheat–maize cropping system. *Biogeosciences* **2013,** *10* (4), 2427-2437.

139.   Yang, M.; Fang, Y.; Sun, D.; Shi, Y., Efficiency of two nitrification inhibitors (dicyandiamide and 3, 4-dimethypyrazole phosphate) on soil nitrogen transformations and plant productivity: a meta-analysis. *Scientific Reports* **2016,** *6*, 22075.

140.   Bronson, K. F.; Touchton, J. T.; Hauck, R. D., Decomposition rate of dicyandiamide and nitrification inhibition. *Communications in Soil Science and Plant Analysis* **1989,** *20* (19-20), 2067-2078.

141.   Suave, J.; Dall'Agnol, E. C.; Pezzin, A. P. T.; Meier, M. M.; Silva, D. A. K., Biodegradable microspheres of poly(3-hydroxybutyrate)/poly(ε-caprolactone) loaded with malathion pesticide: Preparation, characterization, and in vitro controlled release testing. *Journal of Applied Polymer Science* **2010,** *117* (6), 3419-3427.

142.   Harmaen, A. S.; Harmaen, A. S.; Khalina, A.; Ali, H. M.; Azowa, I. N., Thermal, Morphological, and Biodegradability Properties of Bioplastic Fertilizer Composites Made of Oil Palm Biomass, Fertilizer, and Poly(hydroxybutyrate-co-valerate). *Journal of Controlled Release* **2016,** *2016* (1), 1-8.

143.   Gandhi, R.; Lal Kaul, C.; Panchagnula, R., Extrusion and spheronization in the development of oral controlled-release dosage forms. *Pharmaceutical Science & Technology Today* **1999,** *2* (4), 160-170.

144.   Doane, W. M., Encapsulation of pesticides in starch by extrusion. *Industrial Crops and*

Products **1992,** *1* (2), 83-87.

145.   Pereira, E. I.; Minussi, F. B.; da Cruz, C. C. T.; Bernardi, A. C. C.; Ribeiro, C., Urea–Montmorillonite-Extruded Nanocomposites: A Novel Slow-Release Material. *Journal of Agricultural and Food Chemistry* **2012,** *60* (21), 5267-5272.

146.   Sato, H.; Dybal, J.; Murakami, R.; Noda, I.; Ozaki, Y., Infrared and Raman spectroscopy and quantum chemistry calculation studies of C–H⋯O hydrogen bondings and thermal behavior of biodegradable polyhydroxyalkanoate. *Journal of Molecular Structure* **2005,** *744-747*, 35-46.

147.   Zhang, J.-B.; Tan, Z.-C.; Meng, S.-H.; Li, S.-H.; Zhang, L.-M., Heat capacity and thermal decomposition of dicyandiamide. *Thermochimica Acta* **1997,** *307* (1), 11-15.

148.   Lang, B. R.; Jaarda, M.; Wang, R. F., Filler particle size and composite resin classification systems. *Journal of oral rehabilitation* **1992,** *19* (6), 569-84.

149.   Di, H. J.; Cameron, K. C., Effects of temperature and application rate of a nitrification inhibitor, dicyandiamide (DCD), on nitrification rate and microbial biomass in a grazed pasture soil. *Australian Journal of Soil Research* **2004,** *42* (8), 927-932.

150.   Amberger, A.; Vilsmeier, K., Breakdown of dicyandiamide in quartz sand and soils. *Zeitschrift für Pflanzenernährung und Bodenkunde* **1979,** *142* (6), 778-785.

151.   Balaine, N.; Clough, T. J.; Kelliher, F. M.; Van Koten, C., Soil aeration affects the degradation rate of the nitrification inhibitor dicyandiamide. *Soil Research* **2015,** *53* (2), 137-143.

152.   Hallinger, S.; Wallnöfer, P. R.; Goldbach, H.; Amberger, A., Several aspects of bacterial dicyandiamide degradation. *Naturwissenschaften* **1990,** *77* (7), 332-334.

153.   Rathsack, K., Über Umsetzungsprodukte des Cyanamids im Boden. *Landwirtsch. Forsch* **1955,** *7*, 116-123.

154.   Macías-Andrés, V. I.; Li, W.; Aguilar-Reyes, E. A.; Ding, Y.; Roether, J. A.; Harhaus, L.; León-Patiño, C. A.; Boccaccini, A. R., Preparation and characterization of 45S5 bioactive glass-based scaffolds loaded with PHBV microspheres with daidzein release function. *Journal of Biomedical Materials Research Part A* **2017,** *105* (6), 1765-1774.

155.   Li, W.; Jan, Z.; Ding, Y.; Liu, Y.; Janko, C.; Pischetsrieder, M.; Alexiou, C.; Boccaccini, A. R., Facile preparation of multifunctional superparamagnetic PHBV microspheres containing SPIONs for biomedical applications. *Scientific Reports* **2016,** *6*, 23140.

156.   Dilkes-Hoffman, L. S.; Pratt, S.; Lant, P. A.; Levett, I.; Laycock, B., Polyhydroxyalkanoate coatings restrict moisture uptake and associated loss of barrier properties of thermoplastic starch films. *Journal of Applied Polymer Science* **2018,** *135* (25), 46379.

157.   Luo, S.; Netravali, A. N., A study of physical and mechanical properties of poly(hydroxybutyrate-co-hydroxyvalerate) during composting. *Polymer Degradation and Stability*

2003, *80* (1), 59-66.

158.   Boyandin, A. N.; Prudnikova, S. V.; Karpov, V. A.; Ivonin, V. N.; Đỗ, N. L.; Nguyễn, T. H.; Lê, T. M. H.; Filichev, N. L.; Levin, A. L.; Filipenko, M. L.; Volova, T. G.; Gitelson, I. I., Microbial degradation of polyhydroxyalkanoates in tropical soils. *International Biodeterioration & Biodegradation* **2013,** *83*, 77-84.

159.   Siepmann, J.; Peppas, N. A., Mathematical modeling of controlled drug delivery. *Advanced Drug Delivery Reviews* **2001,** *48* (2-3), 137-138.

160.   Brook, I. M.; van Noort, R., Drug release from acrylic polymers via channels and cracks: In vitro studies with hydrocortisone. *Biomaterials* **1985,** *6* (4), 281-285.

161.   Warner, J. A.; Polkinghorne, J. C.; Gonerka, J.; Meyer, S.; Luo, B.; Frethem, C.; Haugstad, G., Strain-induced crack formations in PDMS/DXA drug collars. *Acta Biomaterialia* **2013,** *9* (7), 7335-7342.

162.   Garcea, S. C.; Wang, Y.; Withers, P. J., X-ray computed tomography of polymer composites. *Composites Science and Technology* **2018,** *156*, 305-319.

163.   Markl, D.; Zeitler, J. A.; Rasch, C.; Michaelsen, M. H.; Müllertz, A.; Rantanen, J.; Rades, T.; Bøtker, J., Analysis of 3D Prints by X-ray Computed Microtomography and Terahertz Pulsed Imaging. *Pharmaceutical Research* **2017,** *34* (5), 1037-1052.

164.   Levett, I.; Pratt, S.; Donose, B. C.; Brackin, R.; Pratt, C.; Redding, M.; Laycock, B., Understanding the Mobilization of a Nitrification Inhibitor from Novel Slow Release Pellets, Fabricated through Extrusion Processing with PHBV Biopolymer. *Journal of Agricultural and Food Chemistry* **2019,** *67* (9), 2449-2458.

165.   Srubar Iii, W. V.; Frank, C. W.; Billington, S. L., Modeling the kinetics of water transport and hydroexpansion in a lignocellulose-reinforced bacterial copolyester. *Polymer* **2012,** *53* (11), 2152-2161.

166.   Dilkes-Hoffman, L. S.; Lant, P. A.; Laycock, B.; Pratt, S., The rate of biodegradation of PHA bioplastics in the marine environment: A meta-study. *Marine Pollution Bulletin* **2019,** *142*, 15-24.

167.   Diermann, S. H.; Lu, M.; Zhao, Y.; Vandi, L.-J.; Dargusch, M.; Huang, H., Synthesis, microstructure, and mechanical behaviour of a unique porous PHBV scaffold manufactured using selective laser sintering. *J Mech Behav Biomed* **2018,** *84*, 151-160.

168.   Shishatskaya, E. I.; Nikolaeva, E. D.; Vinogradova, O. N.; Volova, T. G., Experimental wound dressings of degradable PHA for skin defect repair. *Journal of Materials Science: Materials in Medicine* **2016,** *27* (11), 165.

169.   Valappil, S. P.; Misra, S. K.; Boccaccini, A. R.; Roy, I., Biomedical applications of

polyhydroxyalkanoates, an overview of animal testing and in vivo responses. *Expert Review of Medical Devices* **2006,** *3* (6), 853-868.

170.   Shrivastav, A.; Kim, H.-Y.; Kim, Y.-R., Advances in the Applications of Polyhydroxyalkanoate Nanoparticles for Novel Drug Delivery System. *BioMed Research International* **2013,** *2013*, 12.

171.   Levett, I.; Pratt, S.; Donose, B. C.; Brackin, R.; Pratt, C.; Redding, M.; Laycock, B., Understanding the Mobilization of a Nitrification Inhibitor from Novel Slow Release Pellets, Fabricated through Extrusion Processing with PHBV Biopolymer. *Journal of Agricultural and Food Chemistry* **2019**.

172.   Hobbs, J. K.; McMaster, T. J.; Miles, M. J.; Barham, P. J., Cracking in spherulites of poly(hydroxybutyrate). *Polymer* **1996,** *37* (15), 3241-3246.

173.   Stafford, T. G. R. R. W.; Davis, D. W.; Gilbert, R. L., Cyanamide, Dicyandiamide, And Melamine Optical and Crystallographic Properties. *Industrial & Engineering Chemistry* **1940,** *32* (9), 1187-1188.

174.   Li, Z.; Yang, J.; Loh, X. J., Polyhydroxyalkanoates: opening doors for a sustainable future. *Npg Asia Materials* **2016,** *8*, e265.

175.   Siegel, R. A.; Langer, R., Mechanistic studies of macromolecular drug release from macroporous polymers. II. Models for the slow kinetics of drug release. *Journal of Controlled Release* **1990,** *14* (2), 153-167.

176.   Hisano, T.; Kasuya, K.-i.; Tezuka, Y.; Ishii, N.; Kobayashi, T.; Shiraki, M.; Oroudjev, E.; Hansma, H.; Iwata, T.; Doi, Y.; Saito, T.; Miki, K., The Crystal Structure of Polyhydroxybutyrate Depolymerase from Penicillium funiculosum Provides Insights into the Recognition and Degradation of Biopolyesters. *Journal of Molecular Biology* **2006,** *356* (4), 993-1004.

177.   Chan, C. M.; Vandi, L.-J.; Pratt, S.; Halley, P.; Richardson, D.; Werker, A.; Laycock, B., Composites of Wood and Biodegradable Thermoplastics: A Review. *Polymer Reviews* **2017**, 1-51.

178.   Chan, C. M.; Vandi, L.-J.; Pratt, S.; Halley, P.; Richardson, D.; Werker, A.; Laycock, B., Mechanical performance and long-term indoor stability of polyhydroxyalkanoate (PHA)-based wood plastic composites (WPCs) modified by non-reactive additives. *European Polymer Journal* **2018,** *98*, 337-346.

179.   Qiao, C.; Liu, L.; Hu, S.; Compton, J. E.; Greaver, T. L.; Li, Q., How inhibiting nitrification affects nitrogen cycle and reduces environmental impacts of anthropogenic nitrogen input. *Global Change Biology* **2015,** *21* (3), 1249-1257.

180.   Minet, E. P.; Jahangir, M. M. R.; Krol, D. J.; Rochford, N.; Fenton, O.; Rooney, D.; Lanigan, G.; Forrestal, P. J.; Breslin, C.; Richards, K. G., Amendment of cattle slurry with the

nitrification inhibitor dicyandiamide during storage: A new effective and practical N2O mitigation measure for landspreading. *Agriculture, Ecosystems & Environment* **2016,** *215*, 68-75.

181.   Akhtar, S.; Pouton, C. W.; Notarianni, L. J., The influence of crystalline morphology and copolymer composition on drug release from solution cast and melt-processed P(HB-HV) copolymer matrices. *Journal of Controlled Release* **1991,** *17* (3), 225-233.

182.   Li, H.; Chang, J., Preparation, characterization and in vitro release of gentamicin from PHBV/wollastonite composite microspheres. *Journal of Controlled Release* **2005,** *107* (3), 463-473.

183.   Scheithauer, E. C.; Li, W.; Ding, Y.; Harhaus, L.; Roether, J. A.; Boccaccini, A. R., Preparation and characterization of electrosprayed daidzein–loaded PHBV microspheres. *Materials Letters* **2015,** *158*, 66-69.

184.   Requena, R.; Vargas, M.; Chiralt, A., Release kinetics of carvacrol and eugenol from poly(hydroxybutyrate-co-hydroxyvalerate) (PHBV) films for food packaging applications. *European Polymer Journal* **2017,** *92*, 185-193.

185.   Leuenberger, H.; Bonny, J. D.; Kolb, M., Percolation effects in matrix-type controlled drug release systems. *International Journal of Pharmaceutics* **1995,** *115* (2), 217-224.

186.   Broadbent, S. R.; Hammersley, J. M., Percolation processes: I. Crystals and mazes. *Mathematical Proceedings of the Cambridge Philosophical Society* **1957,** *53* (3), 629-641.

187.   Walsh, L. M., *Instrumental Methods for Analysis of Soils and Plant Tissue*. Soil Science Society of America: Madison, WI, 1971.

188.   Moore, J. W.; Flanner, H. H., Mathematical Comparison of Dissolution Profiles. *Pharmaceutical Technology* **1996,** *20*, 64-75.

189.   Shah, V. P.; Tsong, Y.; Sathe, P.; Liu, J.-P., In Vitro Dissolution Profile Comparison— Statistics and Analysis of the Similarity Factor, f2. *Pharmaceutical Research* **1998,** *15* (6), 889-896.

190.   Zhang, Y.; Huo, M.; Zhou, J.; Zou, A.; Li, W.; Yao, C.; Xie, S., DDSolver: an add-in program for modeling and comparison of drug dissolution profiles. *AAPS J* **2010,** *12* (3), 263-271.

191.   Gurny, R.; Doelker, E.; Peppas, N. A., Modelling of sustained release of water-soluble drugs from porous, hydrophobic polymers. *Biomaterials* **1982,** *3* (1), 27-32.

192.   Caraballo, I.; Fernández-Arévalo, M.; Holgado, M. A.; Rabasco, A. M., Percolation theory: application to the study of the release behaviour from inert matrix systems. *International Journal of Pharmaceutics* **1993,** *96* (1), 175-181.

193.   Caraballo, I.; Millan, M.; Rabasco, A. M., Relationship between drug percolation threshold and particle size in matrix tablets. *Pharm Res* **1996,** *13* (3), 387-90.

194.   Berhan, L.; Sastry, A. M., Modeling percolation in high-aspect-ratio fiber systems. I. Soft-core versus hard-core models. *Physical Review E* **2007,** *75* (4), 041120.

References

195.   Kale, S.; Sabet, F. A.; Jasiuk, I.; Ostoja-Starzewski, M., Effect of filler alignment on percolation in polymer nanocomposites using tunneling-percolation model. *Journal of Applied Physics* **2016,** *120* (4), 045105.

196.   Yoon, J.-S.; Jung, H.-W.; Kim, M.-N.; Park, E.-S., Diffusion coefficient and equilibrium solubility of water molecules in biodegradable polymers. *Journal of Applied Polymer Science* **2000,** *77* (8), 1716-1722.

197.   Terada, M.; Marchessault, R. H., Determination of solubility parameters for poly(3-hydroxyalkanoates). *International Journal of Biological Macromolecules* **1999,** *25* (1), 207-215.

198.   Adamska, K.; Voelkel, A.; Berlińska, A., The solubility parameter for biomedical polymers—Application of inverse gas chromatography. *Journal of Pharmaceutical and Biomedical Analysis* **2016,** *127* (Supplement C), 202-206.

199.   Barboza, F. M.; Machado, W. M.; Olchanheski Junior, L. R.; Padilha de Paula, J.; Zawadzki, S. F.; Fernandes, D.; Farago, P. V., PCL/PHBV Microparticles as Innovative Carriers for Oral Controlled Release of Manidipine Dihydrochloride. *The Scientific World Journal* **2014,** *2014*, 10.

200.   Riekes, M. K.; Barboza, F. M.; Vecchia, D. D.; Bohatch, M.; Farago, P. V.; Fernandes, D.; Silva, M. A. S.; Stulzer, H. K., Evaluation of oral carvedilol microparticles prepared by simple emulsion technique using poly(3-hydroxybutyrate-co-3-hydroxyvalerate) and polycaprolactone as polymers. *Materials Science and Engineering: C* **2011,** *31* (5), 962-968.

201.   Mendes, J. B. E.; Riekes, M. K.; de Oliveira, V. M.; Michel, M. D.; Stulzer, H. K.; Khalil, N. M.; Zawadzki, S. F.; Mainardes, R. M.; Farago, P. V., PHBV/PCL microparticles for controlled release of resveratrol: physicochemical characterization, antioxidant potential, and effect on hemolysis of human erythrocytes. *ScientificWorldJournal* **2012,** *2012*, 542937-542937.

202.   Crank, J., *The mathematics of diffusion*. 2d ed. ed.; Clarendon Press: Oxford, Eng, 1975.

203.   Kim, B. O.; Woo, S. I., Compatibilizing capability of poly(β-hydroxybutyrate-,co-ε-caprolactone) in the blend of poly(β-hydroxybutyrate) and poly(ε-caprolactone). *Polymer Bulletin* **1998,** *41* (6), 707-712.

204.   Lovera, D.; Márquez, L.; Balsamo, V.; Taddei, A.; Castelli, C.; Müller, A. J., Crystallization, Morphology, and Enzymatic Degradation of Polyhydroxybutyrate/Polycaprolactone (PHB/PCL) Blends. *Macromolecular Chemistry and Physics* **2007,** *208* (9), 924-937.

205.   Yoshie, N.; Inoue, Y., Cocrystallization and Phase Segregation in Blends of Two Bacterial Polyesters. *Macromol Symp* **2005,** *224* (1), 59-70.

206.   Chan, C. M.; Vandi, L.-J.; Pratt, S.; Halley, P.; Ma, Y.; Chen, G.-Q.; Richardson, D.; Werker, A.; Laycock, B., Understanding the effect of copolymer content on the processability and

mechanical properties of polyhydroxyalkanoate (PHA)/wood composites. *Composites Part A: Applied Science and Manufacturing* **2019,** *124*, 105437.

207.   Blázquez-Blázquez, E.; Pérez, E.; Lorenzo, V.; Cerrada, M. L., Crystalline Characteristics and Their Influence in the Mechanical Performance in Poly(ε-Caprolactone) / High Density Polyethylene Blends. *Polymers* **2019,** *11* (11), 1874.

208.   Chun, Y. S.; Kim, W. N., Thermal properties of poly(hydroxybutyrate-co-hydroxyvalerate) and poly(ε-caprolactone) blends. *Polymer* **2000,** *41* (6), 2305-2308.

209.   Chiono, V.; Ciardelli, G.; Vozzi, G.; Sotgiu, M. G.; Vinci, B.; Domenici, C.; Giusti, P., Poly(3-hydroxybutyrate-co-3-hydroxyvalerate)/poly(ε-caprolactone) blends for tissue engineering applications in the form of hollow fibers. *Journal of Biomedical Materials Research Part A* **2008,** *85A* (4), 938-953.

210.   Dingler, C.; Dirnberger, K.; Ludwigs, S., Semiconducting Polymer Spherulites—From Fundamentals to Polymer Electronics. *Macromolecular Rapid Communications* **2019,** *40* (1), 1800601.

211.   Ho, R.-M.; Chiang, Y.-W.; Lin, C.-C.; Huang, B.-H., Crystallization and Melting Behavior of Poly(ε-caprolactone) under Physical Confinement. *Macromolecules* **2005,** *38* (11), 4769-4779.

212.   Saldanha do Carmo, C.; Varela, P.; Poudroux, C.; Dessev, T.; Myhrer, K.; Rieder, A.; Zobel, H.; Sahlstrøm, S.; Knutsen, S. H., The impact of extrusion parameters on physicochemical, nutritional and sensorial properties of expanded snacks from pea and oat fractions. *LWT* **2019,** *112*, 108252.

213.   Levett, I.; Liao, M.; Pratt, C.; Redding, M.; Laycock, B.; Pratt, S., Designing for effective controlled release in agricultural products: new insights into the complex nature of the polymer–active agent relationship and implications for use. *Journal of the science of food and agriculture* **2020**.

214.   Levett, I.; Donose, B. C.; Laycock, B.; Pratt, S., High-resolution μ-CT reveals crazing in a hydrophobic composite - a new mechanism for mobilization in controlled release applications. *In press* **2020**.

215.   Vieth, W. R., *Diffusion in and through polymers : principles and applications*. Munich New York : Hanser: 1991.

216.   Liu, H.; Gao, Z.; Hu, X.; Wang, Z.; Su, T.; Yang, L.; Yan, S., Blending Modification of PHBV/PCL and its Biodegradation by Pseudomonas mendocina. *Journal of Polymers and the Environment* **2017,** *25* (2), 156-164.

217.   Suleiman, R.; Rosentrater, K., Techno-economic Analysis (TEA) of Extruded Aquafeeds. *Journal of Food Research* **2018,** *7* (5), 57.

References

218.   Bell, M. J. *A review of nitrogen use efficiency in sugarcane*; 2015.

219.   Di Bella, L. P.; Stacey, S. P.; Moody, P.; Benson, A.; Dowie, J.; Sluggett, R., An assessment of controlled release fertilisers in the Australian sugar industry. *Proceedings of the Australian Society of Sugar Cane Technologists* **2014,** *36*, 121-131.

APPENDIX A

Supplementary information for Chapter 5

Table A-1: Summary of the soil report provided by SWEP Analytical Laboratories, Keysborough, VIC, Australia for a soil supplied from a sugarcane field in Wangan, QLD, Australia

Cation Balance

ITEM			RESULT	DESIRABLE
pH(1:5 Water)			5.5	6.5-8.0
pH(1:5 0.01M CaCl$_2$)			4.91	
Electrical Conductivity EC µS/cm			298	< 780
TOTAL SOLUBLE SALT TSS ppm			983.4	< 2574
TOTAL ORGANIC MATTER %			4.44	4 - 6
TOTAL ORGANIC CARBON %			2.22	2 - 3

EXCHANGEABLE CATIONS			RESULTS	DESIRABLE LEVEL
CALCIUM	Ca	meq/100 of soil	3.08	8.05
MAGNESIUM	Mg	meq/100 of soil	1.05	1.86
SODIUM	Na	meq/100 of soil	0.05	< 0.62
POTASSIUM	K	meq/100 of soil	0.32	0.62
HYDROGEN	H	meq/100 of soil	10.1	
ADJ. EXCH. HYDROGEN	H	meq/100 of soil	7.88	< 1.86
CATION EXCHANGE CAPACITY	CEC	meq/100 of soil	14.6	
ADJUSTED CEC	Adj.CEC	meq/100 of soil	12.38	
SATURATION BASE PERCENTAGE	BSP		36	

EXCHANGEABLE CATION BALANCE	% OF ADJUSTED CEC	DESIRABLE
CALCIUM PERCENTAGE	24.9	65-70%
MAGNESIUM PERCENTAGE	8.5	12-15%
SODIUM PERCENTAGE ESP	0.4	0.5-5%
POTASSIUM PERCENTAGE	2.6	3-5%
ADJ. HYDROGEN PERCENTAGE	63.7	<20%
CALCIUM / MAGNESIUM RATIO Ca/Mg	2.95	2 - 4

Nutrient Balance

ITEMS			RESULTS	DESIRABLE LEVEL
AVAILABLE CALCIUM	Ca	ppm	778	1843
AVAILABLE MAGNESIUM	Mg	ppm	158.4	244
AVAILABLE SODIUM	Na	ppm	14.076	< 156
AVAILABLE NITROGEN	N	ppm	80.9	102
AVAILABLE PHOSPHORUS	P	ppm	15.8	75
AVAILABLE POTASSIUM	K	ppm	157.17	263
AVAILABLE SULPHUR	S	ppm	123	11 - 15
AVAILABLE COPPER	Cu	ppm	14.9	3
AVAILABLE ZINC	Zn	ppm	27.6	4 - 6
AVAILABLE IRON	Fe	ppm	10	> 30
AVAILABLE MANGANESE	Mn	ppm	6	> 20
AVAILABLE COBALT	Co	ppm	2.11	0.7-0.8
AVAILABLE MOLYBDENUM	Mo	ppm	0.13	0.3-0.4
AVAILABLE BORON	B	ppm	0.29	0.6-1.0
TOTAL PHOSPHORUS	TP	ppm	1080	
TOTAL NITROGEN	TN	%	0.18	

Biology Balance

ITEM		Result		% of TAP	Desirable	% Desirable
ACTIVE LACTIC ACID BACTERIA	cfu/g soil		120,000	38.7%	113,066	17.0%
Active Fungi	cfu/g soil	50,000				
Cellulose utilisers	cfu/g soil	70,000				
TOTAL ACTIVE FUNGI	cfu/g soil		120,000	38.7%	219,480	33.0%
ACTIVE YEASTS	cfu/g soil		100	0.0%	106,415	16.0%
ACTIVE ACTINOMYCETES	cfu/g soil		70,000	22.6%	139,669	21.0%
ACTIVE PHOTOSYNTHETIC BACTERIA	cfu/g soil		100	0.0%	86,462	13.0%
Total Active Population (TAP):	cfu/g soil		310,200		665,092	
CARBON/NITROGEN RATIO			12.3		10-15	

Table A-2: Nutrient media solution (NMS) used for leaching columns containing biologically active soil. The bulk nutrient media was diluted 1:100 with deionised water and pre-warmed to 30 °C before it was added to the column.

| Nutrient media solution		
Composition per liter		
Agar	12.5	g
$MgSO_4.7H_2O$	1.0	g
KNO_3	1.0	g
$Na_2HPO_4.H_2O$	0.7	g
KH_2PO_4	0.3	g
$CaCl_2.6H_2O$	0.2	g
Ferric ammonium EDTA	4.0	g
Trace elements solution	0.5	ml
pH 6.8 ± 0.2 at 25°C		
Trace elements solution		
Disodium EDTA	0.5	g
$FeSO_4.7H_2O$	0.2	g
H_3BO_3	0.03	g
$CoCl_2.6H_2O$	0.02	g
$ZnSO_4.7H_2O$	0.01	mg
$MnCl_2.4H_2O$	3.0	mg
$Na_2MoO_4.2H_2O$	3.0	mg
$NiCl_2.6H_2O$	2.0	mg
$CaCl_2.2H_2O$	1.0	mg
Preparation of trace elements solution:		
Add components to distilled/deionized water and bring volume to 1 L. Mix thoroughly.		
Preparation of medium:		
Add components to distilled/deionized water and bring volume to 1 L. Mix thoroughly. Gently heat and bring to boilling. Adjust pH to 6.8. Distribute into tubes or flasks. Autoclave for 15 min at 121°C. Pour into sterile Petri dishes or leave in tubes.		
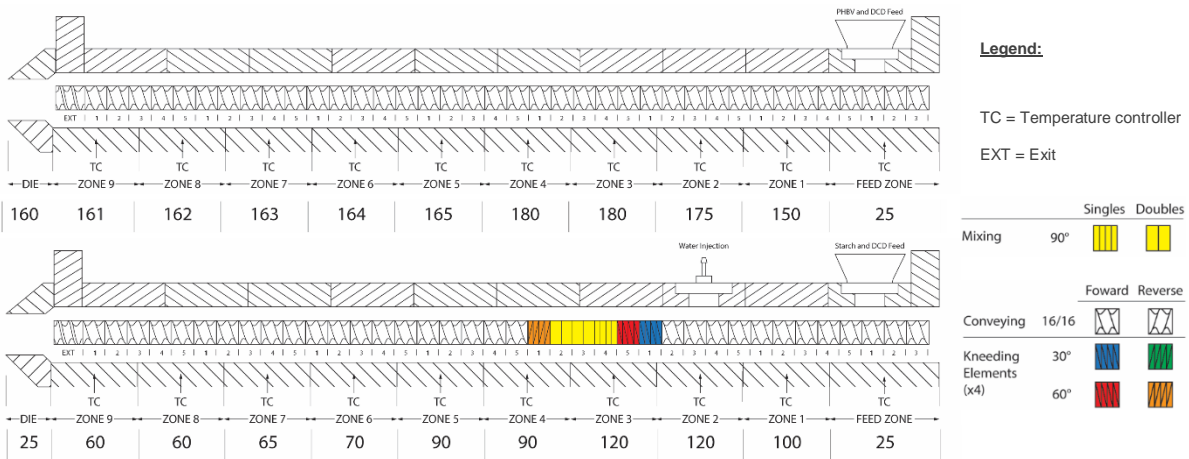
Figure A-1: Extruder schematic illustrating the screw profile and temperature for each zone (shown along the bottom) used during the processing of DCD with A) PHBV and B) PS. Material flows from right to left. The starch is plasticized within the extruder with water injected in zone 2 with a peristaltic pump to make a 60: 40 water: starch weight ratio. Kneading and mixing zones in zones 3, 4 and 5 aid the hydration and plasticization of the of the starch molecules. The mixing section included a 30º and a 60º kneading section, followed by four single and four double mixing screw elements and finally a 60º reverse kneading element.
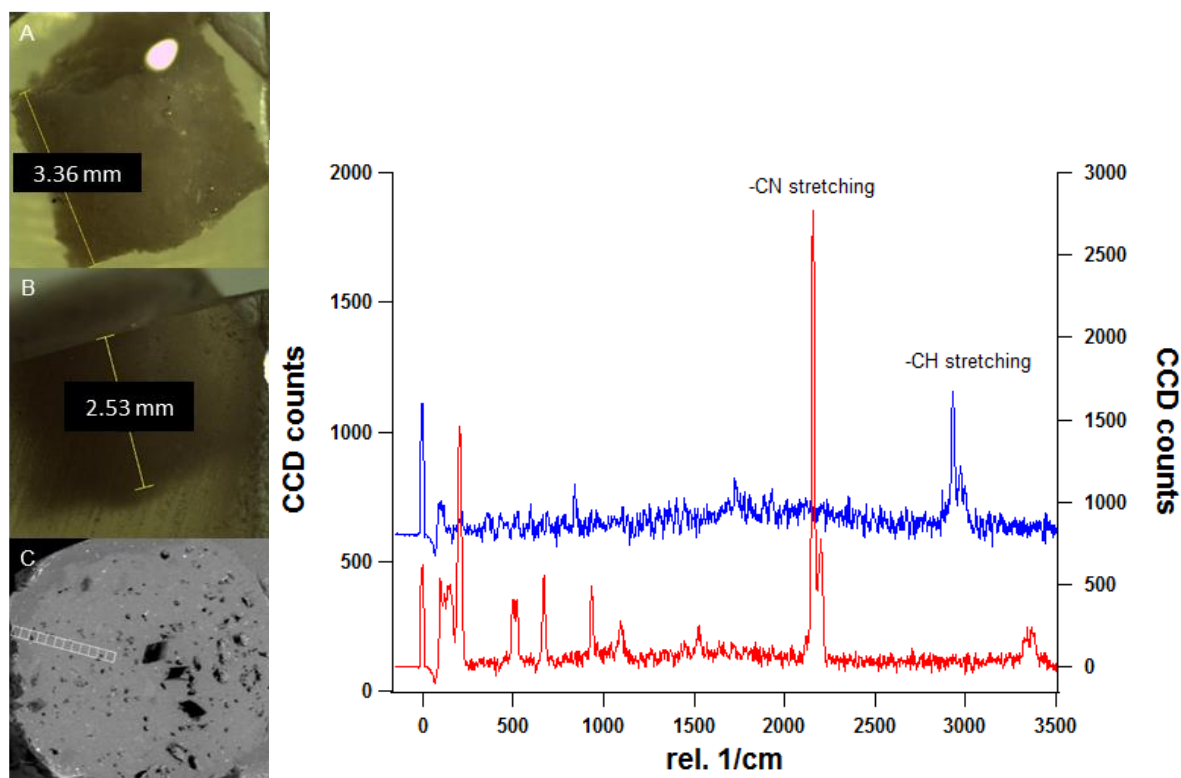
Figure A-2: Left - an example of a DCD-PHBV pellet embedded in resin A) before and B) after microtoming. C) is a top view backscattered SEM micrograph of the embedded, microtomed pellet, showing the region of interest (ROI) where the 12 optical images and Raman maps were acquired from. The ROI started at the outer edge and progressively moved toward the centre of the pellet. Right - Raman signature of DCD (red/lower spectrum, right y-axis) and PHBV (blue/upper spectrum, left y-axis) calculated from the microtomed pellet. Raman maps were acquired on an Alpha 300 Raman/AFM (WITec GmbH, Ulm, Germany) equipped with a frequency-doubled continuous-wave Nd:YAG laser to obtain a 532 nm excitation line through a collar corrected objective (Nikon 40X, N.A. 0.6, CFI S Plan Fluor ELWD objective). The back-scattered Raman signal was collected with a 100 μm optical fiber, employing an Andor Raman spectrometer (600 grooves per mm grating) with an electron-multiplier charge-coupled device (EMCCD) spectroscopic detector. Raman maps were generated by binning the CN vibration mode at 2154 rel. cm^{-1}.
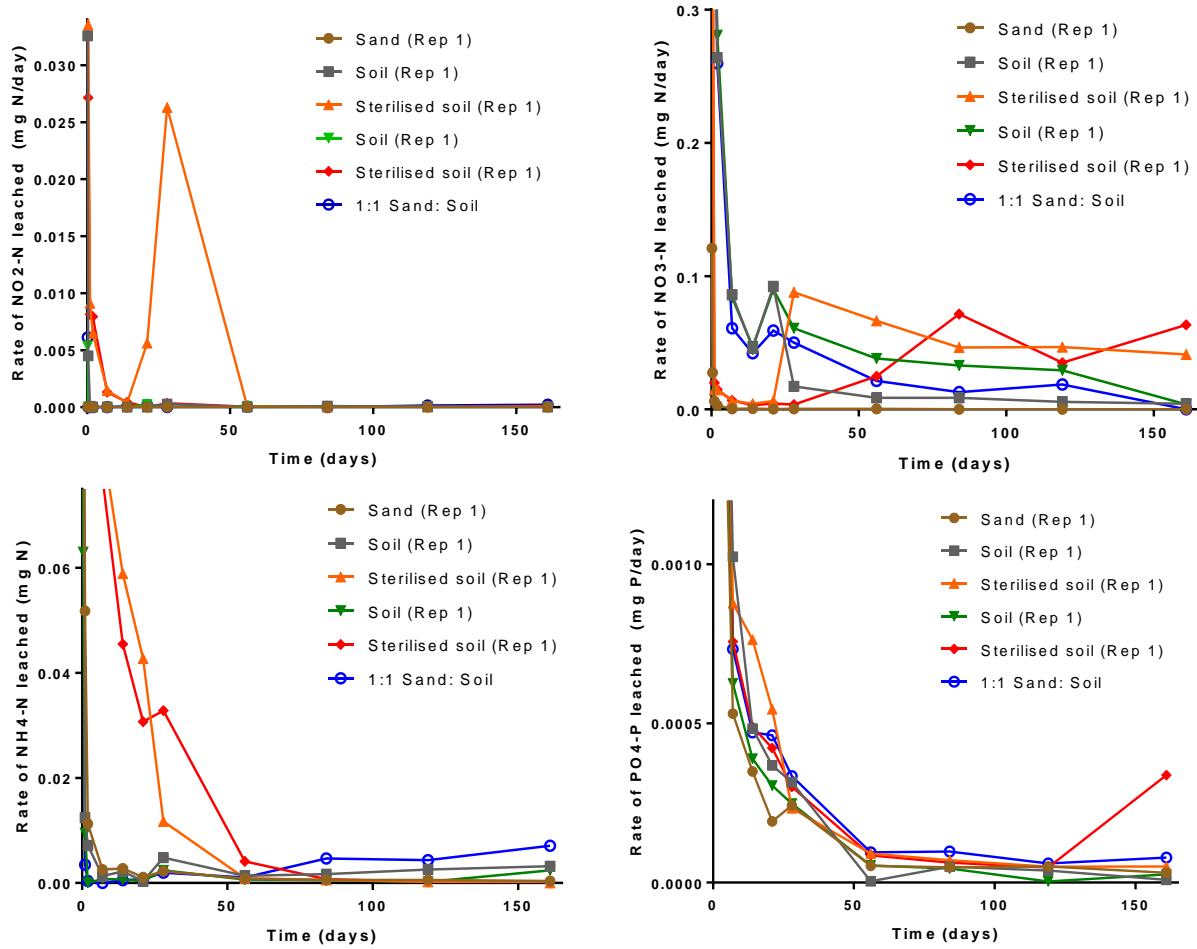
Figure A-3:The rate of leaching of nitrite (NO₂⁻), top left, nitrate (NO₃⁻), top right, ammonia (NH₄⁺), bottom left and phosphate (PO₄⁻), bottom right, from the incubation columns calculated from FIA results.
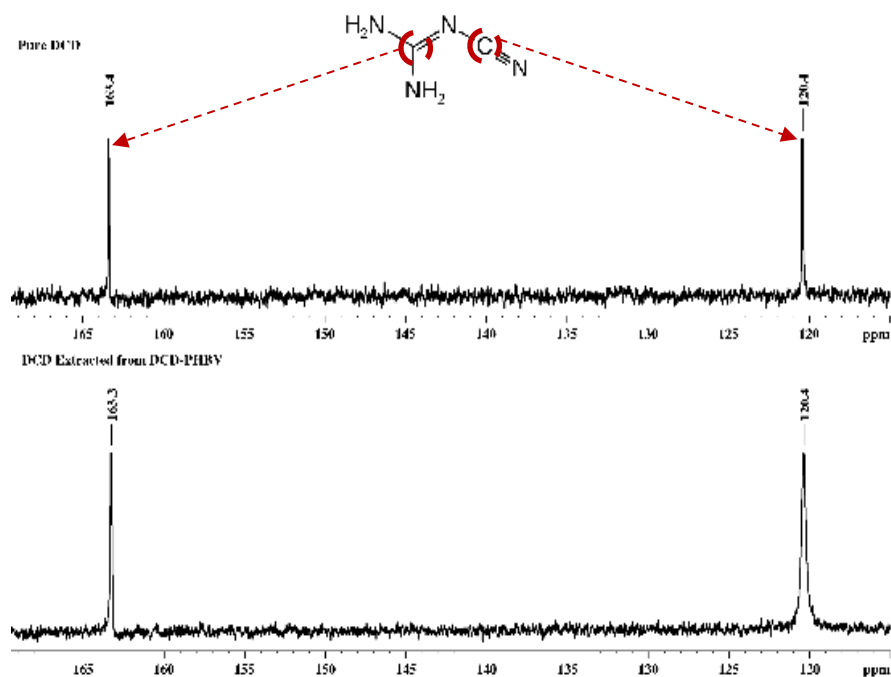
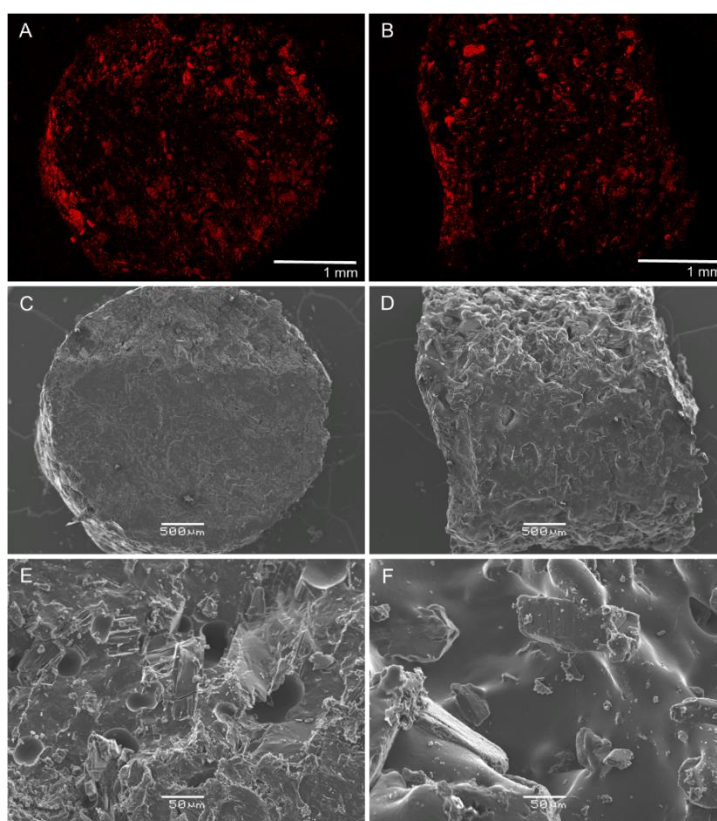**Figure A-4:** ^{13}C-NMR of pure DCD (top) and DCD extracted from an extruded DCD-PHBV pellet (bottom).

Figure A-5: EDX nitrogen map overlays (A and B) and SEM micrographs at 100X (C and D) and 300X (E and F) magnification of the transverse (A, C and E) and lateral (B, D and E) face of a DCD-PHBV pellet. Red regions on the EDX indicates domains rich in nitrogen associated with dicyandiamide crystals.

Table A-3: Results from fitting the Korsmeyer-Peppas equation to the aqueous release data.

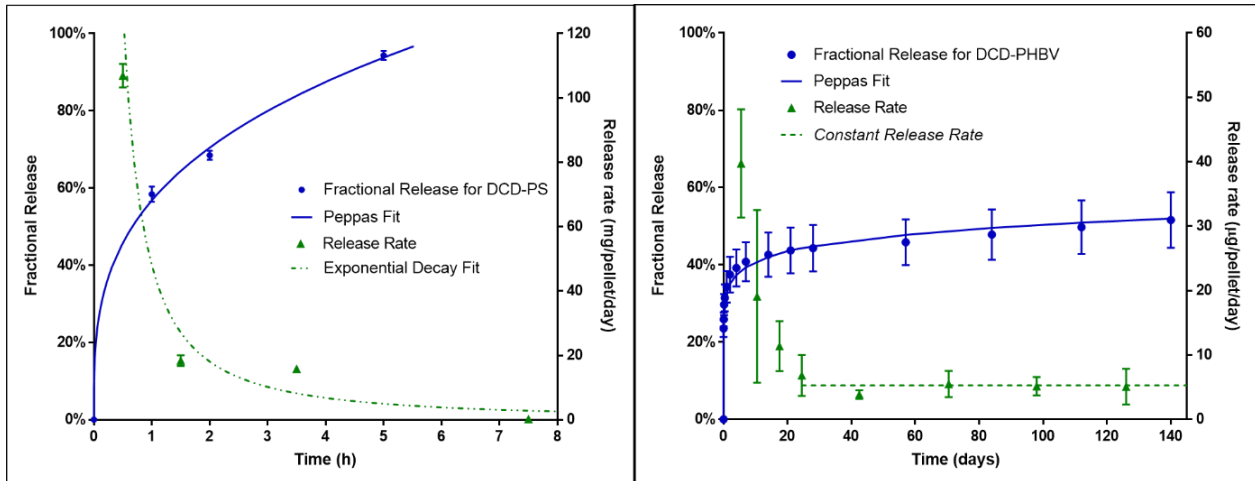|	k (d^{-n}) (± 95% confidence limits)	n (± 95% confidence limits)	R^2
DCD-PHBV	32.9 (± 1.7)	0.09 (± 0.02)	0.874
DCD-PS	153 (± 10)	0.31 (± 0.03)	0.997

Figure A-6: Fractional release and release rate of DCD from DCD-PS pellets (left) and DCD-PHBV (right) into DI water. Data points are the mean of three triplicates with error bars representing one standard deviation from the mean.
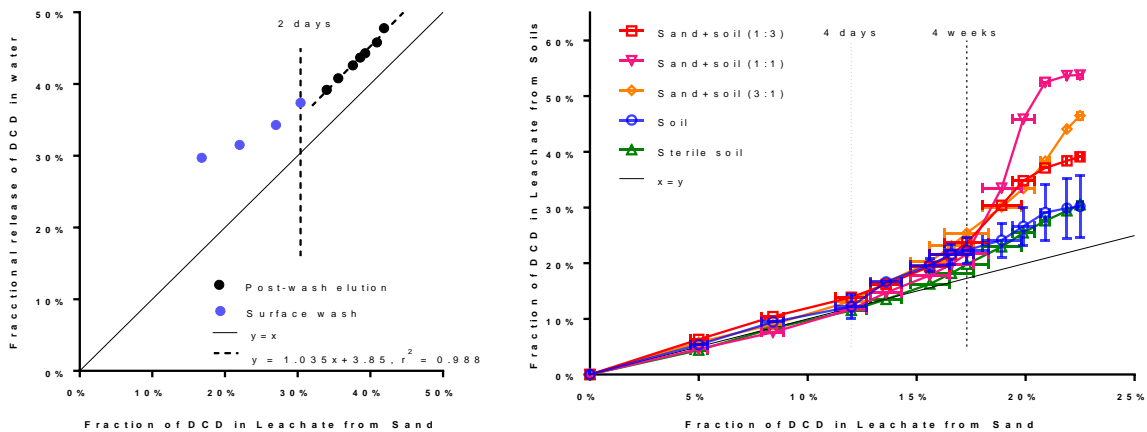

Figure A-7: Left - fractional release data for water plotted against sand, with a linear regression fitted to the post-surface wash data. Data points in blue represent time points of 5 h, 10 h, 1 d and 2 d, while data points in black correspond to time points from 4 d out to 12 weeks. Right - the post-surface wash (after 10 h incubation) fraction of DCD accounted for in the leachate for sand plotted against soil and sand: soil mixtures of 1:3, 1:1 and 3:1. Error bars show one standard deviation from the mean.